Biophysical and Functional Studies of Neurotensin Receptor 1



Steven Lavington

Magdalen College

Thesis submitted to the Board of the Medical Sciences Division in partial fulfilment of the requirements for the degree of *Doctor of Philosophy*.

Trinity Term 2019

Abstract

G protein coupled receptors (GPCRs) are a large family of membrane proteins that facilitate diverse cellular signalling processes and represent significant drug targets. There has been considerable progress in understanding the molecular process of GPCR activation, but structural, biophysical & functional studies of GPCRs typically make use of a small number of well-studied receptors, sometimes with heavily modified sequences and often in the absence of the lipid environments in which GPCRs have evolved to be functional. In this thesis, the neurotensin receptor 1 (NTS1) is used as a model GPCR to explore aspects of receptor dynamics and function, with emphasis on the use of minimally modified receptor sequences. Firstly, using site-specific cysteine mutants and an *E. coli* expression system, the conformational dynamics of the proximal C-terminus of NTS1 were defined for the receptor in a native-like lipid environment, resolving a literature dispute concerning the structure of 'helix 8' for NTS1. Secondly, production of NTS1 and the heterotrimeric G proteins G_q and G_{i1} was established using insect cell expression systems, and high-quality native mass spectra were obtained for NTS1 that demonstrate receptor palmitoylation, and pave the way for the study of post-translational modifications of GPCRs by native mass spectrometry. Thirdly, using a GTP turnover assay, lipids were identified which selectively enhanced NTS1-G_q over NTS1-G_{i1} coupling, suggesting a role for membrane composition in selectivity of NTS1 signalling. Finally, the novel polymethacrylate (PMA) amphipathic polymer was used to establish detergent-free purification of NTS1, representing the first detergent-free purification of any membrane protein using PMA. The work presented here thus progresses the field, both in terms of our molecular understanding of GPCR signalling and in terms of technical advances that will facilitate further studies.

Acknowledgements

First and foremost, I'd like to thank Professor Anthony Watts for his supervision. Tony gave me the freedom to pursue my own ideas, manage my own time and indulge myself in the science. He has always been optimistic and has shown me a great deal of kindness and generosity, for which I am very grateful.

Amongst members of the Watts lab past and present, I owe the greatest debt to Dr Patricia Dijkman. Patricia (very) patiently taught me the ways of the bench, got me started on the helix 8 project and was always happy to discuss ideas (and very occasionally gossip). Dr Marc Phillip Pfeil and Dr Daniel Yin were a considerable source of fun, support and ale-based therapy in my first couple of years in the lab, whilst Javier Vinals Camallonga has been a constant source of humour and positivity in the last few years. I am very grateful to the members of "team NTS1" for their help - thanks Ros, Rosana, Juan ("new") & Juan ("original"). I'd also like to thank Henry Sawcycz for assistance with polymers and ordering, Dr ("swiss") Juan Bada Juarez for his magic touch with various pieces of equipment and Dr Peter Judge for many helpful conversations and insights over the last four years. Finally, Claudia Cassidy gets a big thank you for her quality gossip and supply of baked goods.

Next, I'd like to thank the members of the Kobilka Lab in Stanford. Firstly, to Brian and Tong Sun, who showed enormous generosity in hosting me in the lab and welcomed me so warmly. Thanks to Dr Hideaki Kato for his help in all things NTS1, and Dr Daniel Hilger and Dr Matthieu Masureel for valuable insights on EPR, GPCRs and G proteins and scientific life in general. I must also express my sincere thanks to Foon Sun and Benghoe for making me feel so welcome.

I would also like to thank Dr Hsin-Yung (Jason) Yen of the Robinson lab in Oxford for all things native mass spectrometry, for his excitement and for some great discussions. I am grateful to members of the Newstead Lab in Oxford – Simon, Jo, Gurdeep, Gabriel, Phil and Oli - for helpful discussions, comic relief and generous use of their microplate reader.

For financial support, I thank the Medical Research Council for funding my Medical Sciences Graduate School Studentship, Magdalen College, COST action CM1207 & the Department of Biochemistry at Oxford for support with conference travel, and to Santander for an academic travel award.

My immense gratitude to my friends, who have given me the confidence, love and support necessary to navigate the last four years. There are too many individuals to list here, but special mentions are as follows. To the 103 Bullingdon Road crew - Harry, Kalina, Tim & James - thanks for the kitchen philosophy and sooty shenanigans. To my bandmates - Phil, James, Cres, Felix & Sam - thanks for the sweet jams, it's been an honour to play with such talented and sometimes organised musicians. Thanks to Annie, Grace & Saran for their support of the music. An extra-special mention to Sam Williams for being an all-round cracking person, who always had time for tea and Kamasi.

Finally, to my family. Thanks to my Nan for her old-fashioned but incredibly astute advice and for showing me how it is always possible to keep pushing on. Thanks to my Dad and Chris for love and support and a final enormous thank you to my Mum for the endless encouragement and love that has provided the foundation for all my achievements.

List of publications and presentations

Publications

1. P.M. Dijkman & J.C. Muñoz-García, **S. Lavington,** P.S. Kumagai, R.I. dos Reis, D. Yin, P.J. Stansfeld, A.J. Costa-Filho and A. Watts. Conformational dynamics of a G protein coupled receptor helix 8 in lipid membranes. *Manuscript submitted.*
2. **S. Lavington** & A. Watts. Detergent-free purification of a class A GPCR using a polymethacrylate co-polymer. *Manuscript in preparation.*
3. **S. Lavington** & A. Watts. Lipid determinants of NTS1-G protein coupling selectivity. *Manuscript in preparation.*

Oral and poster presentations

Invited oral presentations

1. 13th International School of Biophysics, Croatia, September 2016: "Conformational dynamics of NTS1 helix 8"
2. RTG Biomembranes group "Membrane Seminar" at Friedrich-Alexander-Universität Erlangen-Nürnberg, July 2018: "Conformational dynamics of NTS1 helix 8"

Poster presentations

Posters were presented at the following international conferences:

- British Biophysical Society meeting, Liverpool, July 2016
- 13th International School of Biophysics, Croatia, September 2016
- GLISTEN meeting, Prague, September 2016
- 11th EBSA congress, Edinburgh, July 2017

- GPCR workshop, Hawaii, December 2017

Awards

- Santander Academic Travel Award, 2018.

- Goodger and Schorstein Research Scholarship in Medical Sciences, 2018.

Contents

Abstract ..... **i**

Acknowledgements ..... **ii**

List of publications and presentations ..... **iv**

Publications iv

Oral and poster presentations iv

List of figures ..... **xii**

List of tables ..... **xv**

Abbreviations ..... **xvi**

1. Introduction **1**

1.1 Biological membranes **1**

1.1.1 Lipids 2

1.1.2 Membrane proteins 4

1.2 G protein coupled receptors (GPCRs) **5**

1.2.1 GPCR signalling 6

1.2.2 Advances in structural studies of GPCRs 9

1.2.3 Structural features of GPCRs 11

1.2.4 Biophysical and computational studies of GPCR activation 15

1.2.5 Receptor-G protein interactions and selectivity 17

1.2.6 Receptor-arrestin interactions and functional selectivity 19

1.2.7 Frontiers in understanding GPCR activation 21

1.2.8 Neurotensin Receptor 1 21

1.3 Solubilisation and reconstitution of membrane proteins 27

1.3.1 Detergents 27

1.3.2 Protein-based nanodiscs 29

1.3.3 Polymer-based nanodiscs 30

1.3.4 Liposomes 31

1.4. Electron paramagnetic resonance 32

1.4.1 Site-directed spin labelling (SDSL) 32

1.4.2 Basics of EPR 33

1.4.3 Anisotropy and motion in EPR 35

1.4.4 CW-EPR and protein dynamics 36

1.4.5 CW-EPR and protein secondary structure 38

1.4.6 CW-EPR & GPCRs 39

1.5 Native mass spectrometry 39

1.6 GTPase-Glo™ assay 42

1.7 Aims 43

2. Conformational dynamics of NTS1 helix 8 45

2.1. Introduction 45

2.1.1 Roles for helix 8 in GPCR function 45

2.1.2 NTS1 helix 8 48

2.2 Aims 51

2.3 Materials and methods 51

2.3.1 Constructs used 51

2.3.2 Expression & purification of NTS1 from *E. coli* 52

2.3.3 Preparation of NTS1 proteoliposomes 54

2.3.4. CW-EPR experiments and analysis 56

2.3.5 Acknowledgement 56

2.4. Results 57

2.4.1 Purification of NTS1 cysteine mutants 57

2.4.2 CW-EPR spectra 58

2.4.3 Secondary structure of the apo-receptor C terminus 60

2.4.4 Effects of agonist binding 60

2.4.5 Effects of $G\alpha_{i1}$ and β-arrestin$_1$ on rNTS1 helix 8 62

2.5 Discussion 64

2.5.1 The presence and extent of rNTS1 helix 8 64

2.5.2 Comparison of rNTS1 and rhodopsin helix 8 65

2.5.3 Interpreting effects of agonist binding 67

2.5.4 Interpreting effects of $G\alpha_{i1}$ and β-arrestin$_1$ 68

2.5.5 Roles for lipids in helix 8 stability 71

2.5.6 Conclusions 73

3. Expression, purification & characterisation of hNTS1 & heterotrimeric G proteins 74

3.1 Introduction 74

3.1.1 Limitations of *E. coli* as an expression host for NTS1 74

3.1.2 Limitations of *E. coli* as an expression host for G proteins 75

3.2 Aims 76

3.3 Materials & methods 77

3.3.1 Insect cell culture 77

3.3.2 Expression and purification of hNTS1 from Sf9 78

3.3.3 Expression & purification of G proteins 81

3.3.4 GTPase-Glo™ assays 82

3.3.5 Native mass spectrometry 83

3.4 Results 84

3.4.1 Purification of G protein heterotrimers 84

3.4.2 Purification of hNTS1 87

3.4.3 Activity of hNTS1 and G proteins 88

3.4.4 Native mass spectrometry of hNTS1 90

3.5 Discussion 93

3.5.1 Production and characterisation of G_{i1}, G_q and hNTS1 93

3.5.2 Native mass spectrometry 94

3.5.3 Conclusions 98

4. Lipid determinants of NTS1-G protein coupling 99

4.1 Introduction 99

4.1.1 Roles for lipids in GPCR function 99

4.1.2 Roles for lipids in NTS1 function 103

4.2 Aims 105

4.3 Materials & methods 105

4.3.1 Protein expression & purification 105

4.3.2 Lipid preparation 105

4.3.3 GTPase-Glo™ assays 107

4.3.4 Data processing 107

4.4 Results 108

4.4.1 Effects of BPL, PG & PS on hNTS1-G_{i1} coupling 108

4.4.2 Effects of BPL, PG & PS on hNTS1-G_q coupling 109

4.4.3 Effects of $MgCl_2$ & PIP_2 on hNTS1-G_{i1} protein coupling 111

4.5 Discussion 113

4.5.1 Effects of lipids on hNTS1-G_{i1} coupling 113

4.5.2 Effects of lipids on hNTS1-G_q coupling 116

4.5.3 Lipid determinants of hNTS1-G protein selectivity 117
4.5.4 Conclusions and future directions 120
5. Detergent-free purification of hNTS1 using a polymethacrylate polymer 121
5.1 Introduction 121
5.1.1 Limitations of detergent-based studies of GPCRs 121
5.1.2 Detergent-free studies of GPCRs with SMA 123
5.1.3 Other amphipathic co-polymers 124
5.1.4 Mechanism of polymer-nanodisc formation & practical considerations ... 126
5.2 Aims 128
5.3 Materials & methods 128
5.3.1 Receptor expression and membrane preparation 128
5.3.2 Polymer preparation 129
5.3.3 Solubilisation screens 129
5.3.4 Purification of receptor in PMA-nanoparticles 129
5.3.5 GTPase-Glo™ assays 130
5.3 Results 130
5.3.1 Solubilising hNTS1 from Sf9 membranes with the PMA co-polymer 130
5.3.2 Detergent-free purification of hNTS1 from Sf9 membranes 134
5.3.4 Characterisation of hNTS1-PMA-NPs 137
5.5 Discussion 140
5.5.1 Solubilisation of Sf9 membranes with PMA 140
5.5.2 Purification of PMA-NPs 143
5.5.3 hNTS1 activity in PMA vs detergent 144

5.6 Conclusions 145

6. Conclusions and future work 147

Appendix 152

A1 Receptors without helix 8 152

A1.1 Receptors with unusual helix 8 conformations 153

A2 Expression & purification of rNTS1BH$_6$ and mutants thereof 154

A3 Expression & purification of proteins for Chapters 3-5 156

A3.1 Expression & purification of G_q heterotrimer 156

A3.2 Expression & purification of myristoylated $G\alpha_{i1}$ 157

A4 Data sets for GTPase-Glo™ assay 158

Bibliography 162

List of figures

Figure 1.1: A biological membrane. 1

Figure 1.2: Structures of major mammalian lipids. 3

Figure 1.3: Lipid composition of mammalian membranes. 4

Figure 1.4: Overview of GPCR signalling. 7

Figure 1.5: Features of GPCR structure and activation. 12

Figure 1.6: A model of GPCR activation based on studies of the β_2AR. 17

Figure 1.7: GPCR-G protein interactions. 18

Figure 1.8: Rhodopsin-arrestin interactions. 20

Figure 1.9: NTS1 interactome. 23

Figure 1.10: NTS1 structural biology. 26

Figure 1.11: Structures of commonly used detergents. 28

Figure 1.12: MSP-nanodiscs and SMALPs. 29

Figure 1.13: Size and morphology of different lipid vesicles. 31

Figure 1.14. Site directed spin labelling of cysteine residues. 33

Figure 1.15: Basics of EPR. 34

Figure 1.16: Orientation-dependence of nitroxide EPR spectra. 35

Figure 1.17: Sensitivity of nitroxide spectra to dynamics. 36

Figure 1.18: EPR and protein dynamics. 37

Figure 1.19: EPR and secondary structure. 38

Figure 1.20: Electrospray ionisation. 40

Figure 1.21: GTPase-Glo™ assay set-up. 42

Figure 2.1: Helix 8 sequence & structural characteristics. 46

Figure 2.2: NTS1 helix 8 conformations. 49

Figure 2.3: Features of the NTS1 constructs used in chapter 2. 53

Figure 2.4: Purification of 20 cysteine mutants of rNTS1 57

Figure 2.5: CW-EPR spectra of apo-rNTS1. 59

Figure 2.6: Helicity of apo-rNTS1 C-terminus. 60

Figure 2.7: Helicity of the agonist-bound rNTS1 C-terminus 61

Figure 2.8: Agonist induced changes in helix 8 dynamics. 61

Figure 2.9: Effects of $G\alpha_{i1}$ on S382C spectral appearance. 63

Figure 2.10: Effects of β-arrestin on S382C spectral appearance. 64

Figure 2.11: Comparison of rNTS1 and rhodopsin helix 8 EPR data. 66

Figure 2.12: Helix 8 contacts to $G\alpha_{i1}$ and arrestin. 70

Figure 2.13: MD simulation of NTS1 in lipid bilayers. 71

Figure 3.1: Features of the hNTS1-GFP construct used in chapter 3. 79

Figure 3.2: Purification of G_q heterotrimer. 85

Figure 3.3: Purification and reconstitution of G_{i1} heterotrimer. 86

Figure 3.4: Purification of hNTS1. 87

Figure 3.5: Intrinsic GTPase activity of A) G_{i1} and B) G_q. 88

Figure 3.6: Activity of hNTS1 on A) G_{i1} and B) G_q. 89

Figure 3.7: Native mass spectrum for hNTS1 treated with PNGaseF. 90

Figure 3.8: Effects of PPT-1 treatment on the hNTS1 native mass spectrum. 91

Figure 3.9: Adducts of hNTS1 observed in native mass spectrum of the PPT-1 treated sample. 92

Figure 4.1: Modes of action by which lipids modulate GPCR activity. 100

Figure 4.2: Chemical structures of lipids used in chapter 4. 106

Figure 4.3: Effects of BPL, PG & PS on A) intrinsic G_{i1}-GTPase and B) hNTS1-stimulated G_{i1} activity. 109

Figure 4.4: Effects of the lipids BPL, PG & PS on A) intrinsic G_q-GTPase activity and B) hNTS1-stimulated G_q activity. 110

Figure 4.5: Effects of PIP_2 on the intrinsic and hNTS1-stimulated activities of G_{i1}. 111

Figure 4.6: Effects of BPL on the A) intrinsic GTPase activity of G_{i1} and B) hNTS1-stimulated activity of G_{i1} at low $MgCl_2$. 112

Figure 4.7: Effects of PIP_2 on NTS1-G_{i1} coupling. 115

Figure 4.8: Charge motifs in the HN helix of Gα. 118

Figure 4.9: Cartoon summary of the roles of lipids in hNTS1-G protein selectivity. 120

Figure 5.1: Synthesis of polymethacrylate co-polymers. 126

Figure 5.2: Mechanism of nanodisc formation by SMA. 127

Figure 5.3: Effects of temperature and incubation length on PMA solubilisation efficiency. 131

Figure 5.4: Effect of A) pH and B) NaCl concentration on PMA solubilisation efficiency. 132

Figure 5.5: Effect of varying A) polymer amount/concentration and B) membrane amount/concentration on PMA solubilisation efficiency. 133

Figure 5.6: Purification of hNTS1 in PMA-NPs or MNG/CHS detergent using Ni-NTA resin. 134

Figure 5.7: Purification of hNTS1 in PMA-NPs or DDM/CHS detergent using M1 anti-FLAG resin. 135

Figure 5.8: Purification of cleaved hNTS1 in PMA-NPs. 137

Figure 5.9: Estimation of PMA-hNTS1 amount relative to detergent-solubilised standards. 138

Figure 5.10: Control GTP turnover experiments with receptor in DDM or PMA. 139

Figure 5.11: Stimulation of A) G_{i1} and B) G_q by hNTS1 in DDM or PMA. 140

Figure A1. Data used to produce figure 4.3A and 4.3B. 158

Figure A2: Data used to produce figure 4.4. 159

Figure A3: Data used to produce figures 4.5 & 4.6. 160

Figure A4: Data used to produce figure 5.10 & 5.11 161

List of tables

Table 1.1: Class A receptors for which inactive & active structures are available. *14*

Table 1.2: Summary of constructs used to obtain crystal structures of rNTS1. *25*

Table 2.3: Lipid composition of Brain Polar Lipid Extract (Porcine). *54*

Table 3.1: Post-translational lipid modifications of G protein heterotrimers. *76*

Table 3.2: Accounting for the difference between theoretical hNTS1 mass and those observed by native mass spectrometry. *95*

Table 5.1: Summary of amphipathic polymers available for membrane solubilisation. *125*

Table A1: Receptors without helix 8. *153*

Abbreviations

$5HT_{1B}R$	Serotonin $5HT_{1B}$ receptor
A_1R	Adenosine A1 receptor
$A_{2A}R$	Adenosine A2A receptor
$AT_{II}R$	Angiotensin II type 2 receptor
AT_1R	Angiotensin II type 1 receptor
B_2R	Bradykinin B2 receptor
BLT_1R	Leukotriene B4 receptor 1
BPL	Brain polar lipid extract
BRET	Bioluminescence resonance energy transfer
cAMP	3',5'-cyclic adenosine monophosphate
CB1	Cannabinoid type 1 receptor
CCR5	Chemokine receptor type 5
CHAPS	3-[(3-Cholamidopropyl)dimethylammonio]-1-propanesulfonate
CHS	Cholesteryl hemisuccinate
CID	Collision-induced dissociation
CMC	Critical micellar concentration
Cryo-EM	Cryo-electron microscopy
CW-EPR	Continuous wave electron paramagnetic resonance
CXCR4	Chemokine receptor type 4
DAG	Diacylglycerol
DDM	n-Dodecyl-β-D-Maltopyranoside
DEER	Double electron electron resonance

DHA	Docoshexanoic acid
DLS	Dynamic light scattering
DMSO	Dimethyl sulfoxide
E. coli	*Escherichia coli*
ECL	Extracellular loop of a GPCR
EDTA	Ethylenediaminetetraacetic acid
eGFP	Enhanced green fluorescent protein
ESI	Electrospray ionisation
EtOH	Ethanol
FFAR1	Free fatty acid receptor 1
GDP	Guanosine-5'-diphosphate
GEF	Guanine nucleotide exchange factor
GPCR	G protein coupled receptor
GRK	GPCR kinase
GST	Glutathione S-transferase
GTP	Guanosine-5'-triphosphate
GTPγS	Guanosine-5'-O-(3-thiotriophosphate)
GUV	Giant unilamellar vesicle
Gα	Alpha subunit of heterotrimeric G protein
Gβγ	Beta-gamma heterodimer of heterotrimeric G protein
HCD	Higher-energy collisional dissociation
HEPES	4-(2-Hydroxyethyl)piperazine-1-ethanesulfonic acid
hNTS1	Human sequence of NTS1
ICL	Intracellular loop of GPCR
IMAC	Immobilised metal affinity chromatography

IPTG	Isopropyl-β-D-thiogalactoside
JNK	c-Jun N-terminal kinase
LDS	Lithium dodecyl sulfate
LMNG	Lauryl-maltose neopentyl glycol
LPA_6R	Lyosphosphatidic acid receptor 6
LUV	Large unilamellar vesicle
M_1R	M1 muscarinic receptor
M_2R	M2 muscarinic receptor
MAPK	Mitogen activated protein kinase
MBP	Maltose binding protein
MeOH	Methanol
MQ	Milli-Q® ultrapure water
MSP	Membrane scaffold protein
MST	Microscale thermophoresis
MT_1R	Melatonin-1 receptor
MTSL	2,2,5,5-tetramethyl-l-oxyl-3- methyl methanethiosulfonate
Ni-NTA	Ni^{2+}-Nitrilotriacetic acid resin
NMR	Nuclear magnetic resonance
nMS	Native mass spectrometry
NMT-1	N-myristoyltransferase 1
NN	Neuromedin N
NT	Neurotensin
NT_{8-13}	Neurotensin residues 8-13
NTS1	Neurotensin receptor 1
NTS2	Neurotensin receptor 2

NTS3	Neurotensin receptor 3 /Sortilin
ON	Overnight
P_2Y_1R	Purinergic P_2Y_1 receptor
PA	Phosphatidic acid
PAFR	Platelet-activating factor receptor
PAR1	Protease-activated receptor 1
PC	Phosphatidylcholine
PE	Phosphatidylethanolamine
PG	Phosphatidylglycerol
PhS	Phenyl Sepharose
PI	Phosphatidylinositol
PIP_2	Phosphatidylinositol 4,5-bisphosphate
PKA	Protein kinase A
PKC	Protein kinase C
PLC-β	Phospholipase C-β
PMA	Polymethacrylate polymer
PMA-NP	PMA-nanoparticle
POPG	1- palmitoyl-2-oleoyl-*sn*-phosphatidylglycerol
POPS	1-palmitoyl-2-oleoyl-*sn*-phosphatidylserine
PPT-1	Palmitoyl-Protein Thioesterase 1
PS	Phosphatidylserine
RFU	Relative fluorescence units
RMSD	Root mean squared deviation
rNTS1	Rat NTS1 sequence
RT	Room temperature

SDS	Sodium dodecyl sulfate
SDS-PAGE	SDS-polyacrylamide gel electrophoresis
SDSL	Site-directed spin labelling
SEC	Size exclusion chromatography
Sf9	*Spodoptera frugiperda* clonal isolate
SM	Sphingomyelin
SMA	Styrene maleic acid polymer
SMALP	Styrene maleic acid lipid particle
SPR	Surface plasmon resonance
SUV	Small unilamellar vesicle
T4L	T4 lysozyme
TCEP	Tris(2-carboxyethyl)phosphine
TEV	Tobacco etch virus
TM	Transmembrane helix
Tris	Tris(hydroxymethyl)aminomethane
TrxA	Thioredoxin A
$V_{1A}R$	Vasopressin 1A receptor
V_2R	Vasopressin 2 receptor
w/v	Weight by volume
XFEL	X-ray free electron laser
XRC	X-ray crystallography
β_1AR	β_1-adrenergic receptor
β_2AR	β_2-adrenergic receptor
κOR	κ-opioid receptor
μOR	μ-opioid receptor

1. Introduction

1.1 Biological membranes

Biological membranes are fundamental to all life. For mammalian cells, the plasma membrane provides an interface with the extracellular environment, whilst organelle membranes facilitate compartmentalisation of the cell (Van Meer *et al*, 2008).

The main components of a biological membrane are lipids and proteins, and the structure and behaviour of these components are described by the fluid mosaic model (Singer & Nicolson, 1972; Nicolson, 2014). In this model, the membrane is fundamentally a bilayer of two lipid leaflets, whereby amphipathic lipid molecules with hydrophobic acyl chains and polar "headgroups" are driven into the bilayer structure by the hydrophobic effect (figure 1.1). In addition to lipids, the membrane is associated with membrane proteins (section 1.1.2). Both lipid and protein components can diffuse laterally in the fluid mosaic model.

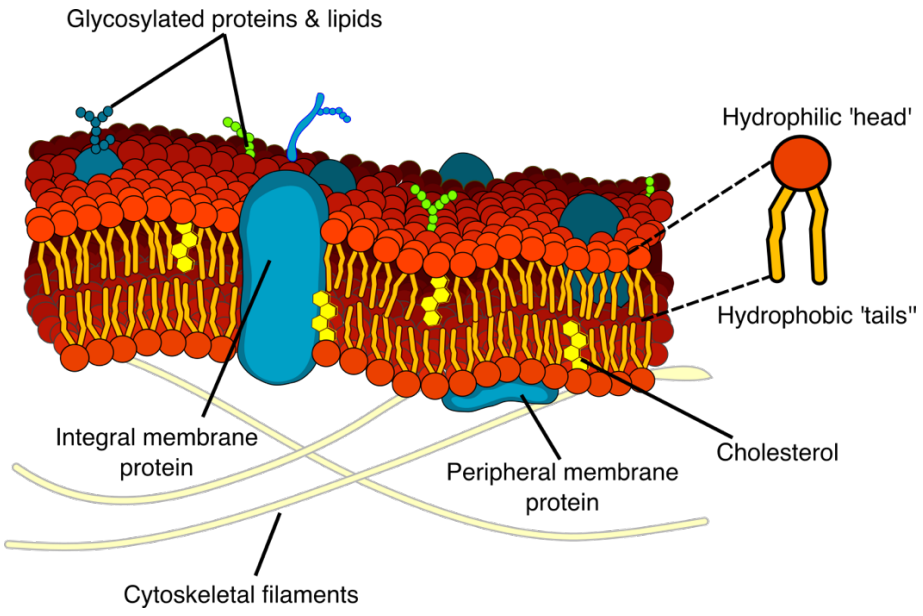


Figure 1.1: A biological membrane. Shown is a lipid bilayer, consisting of amphipathic lipids, with associated integral and peripheral membrane proteins. Adapted from a diagram obtained from Wikipedia.

1.1.1 Lipids

Most lipids found in mammalian biological membranes can be broadly classified into three groups: glycerophospholipids, sphingolipids and sterols (Van Meer *et al*, 2008) (figure 1.2). Glycerophospholipids (figure 1.2A) consist of a diacylglycerol esterified with a phosphoric acid group. In the simplest case, this gives phosphatidic acid (PA). However, the phosphoric acid "headgroup" can be decorated with a variety of additional chemical groups to give lipids such as phosphatidylcholine (PC), phosphatidylserine (PS), phosphatidylethanolamine (PE), phosphatidylinositol (PI) and phosphatidylglycerol (PG), all of which differ in terms of headgroup size and net charge. In addition, for each "headgroup", the fatty acyl chains of the diacylglycerol can have different lengths and degrees of unsaturation (figure 1.2D). Sphingolipids are ceramides, which in turn consist of sphingosine linked to a fatty acyl chain through an amide linkage (figure 1.2B). Here, again there is diversity in the chemistry of the fatty acyl chain, and in the chemistry of the ceramide "headgroup". Finally, sterols feature a steroid nucleus linked to a hydroxy group, and cholesterol is by far the most abundant of these in mammalian membranes (Van Meer *et al*, 2008) (figure 1.2C).

The diverse structures and chemistries of the lipids shown in figure 1.2 means that different lipids can confer different physicochemical properties on a biological membrane. The fluidity of a membrane is regulated by acyl chain packing and so longer, more unsaturated acyl chains produce a more fluid membrane. The steroid nucleus of cholesterol is rigid in comparison with flexible fatty acyl chains, and so tends to pack against saturated chains, increasing order and decreasing fluidity (Ikonen, 2008). The differing properties of individual lipids may also lead to lateral heterogeneities or 'microdomains' in the membrane. This process is still somewhat controversial and may occur as a result of preferential acyl chain packings, specific headgroup interactions (e.g. sphingolipid-

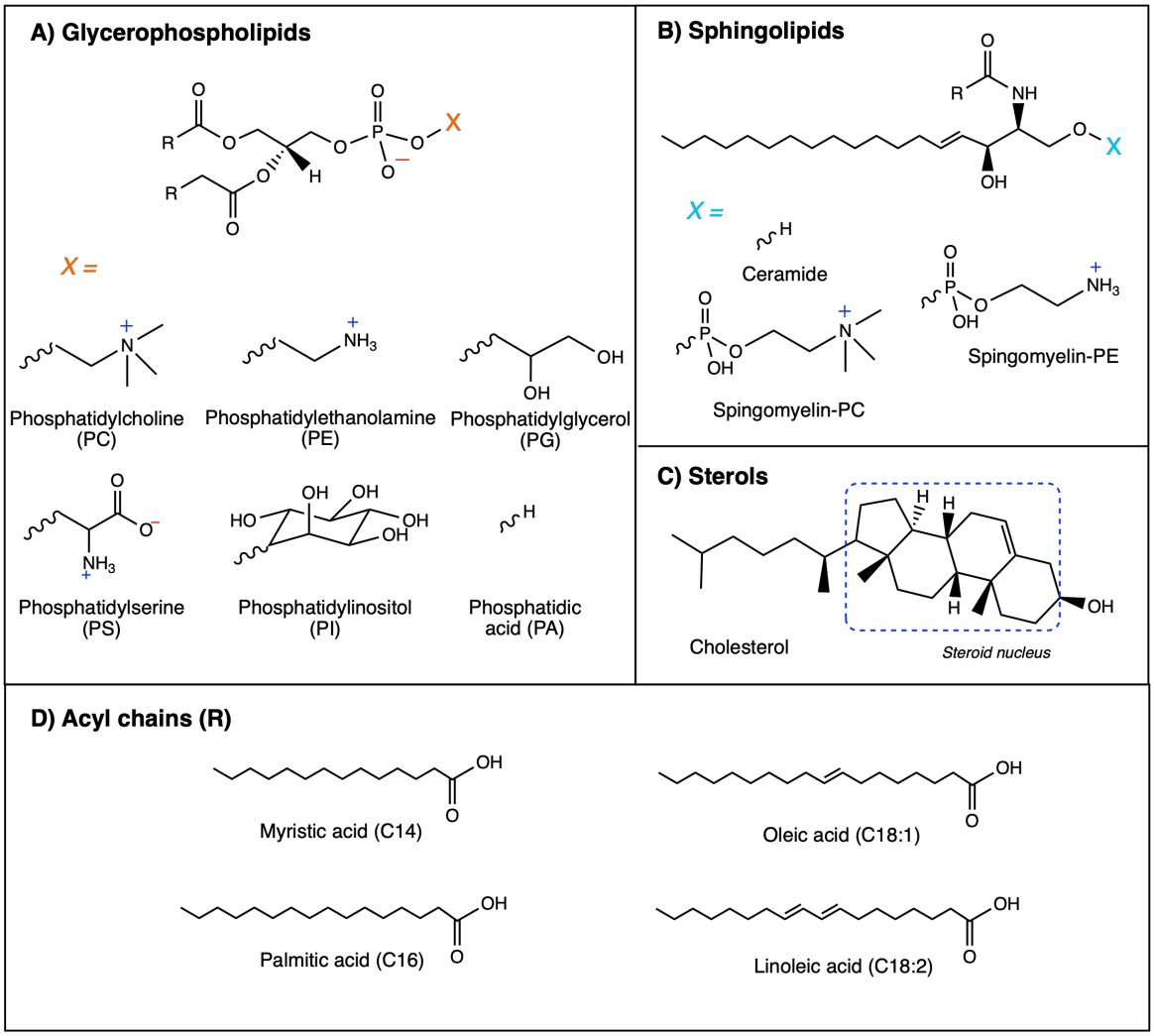


Figure 1.2: Structures of major mammalian lipids. Structures of A) glycerophospholipids, B) sphingolipids and C) cholesterol are given, alongside D) common acyl chain structures.

cholesterol hydrogen bonds) or through organisation of lipids by proteins (Harayama & Riezman, 2018). One type of frequently invoked domain is the 'lipid raft', a transient domain of 10-200 nm which is enriched in sphingolipids and cholesterol (Pike, 2006). In addition, several lipids found in biological membranes will, in pure form, tend to form non-bilayer structures. PE, for example, tends to form highly curved inverted-hexagonal phases, and so its presence in biological bilayer membranes can create a curvature stress that may play a role in regulating membrane protein function (Botelho *et al*, 2002) or in processes such as membrane fusion (Zick *et al*, 2014).

The compositions of three different mammalian membranes are outlined in figure 1.3. For the plasma membrane, the different headgroup and acyl chain compositions of the inner and outer leaflets are also indicated, demonstrating the considerable asymmetry of this membrane.

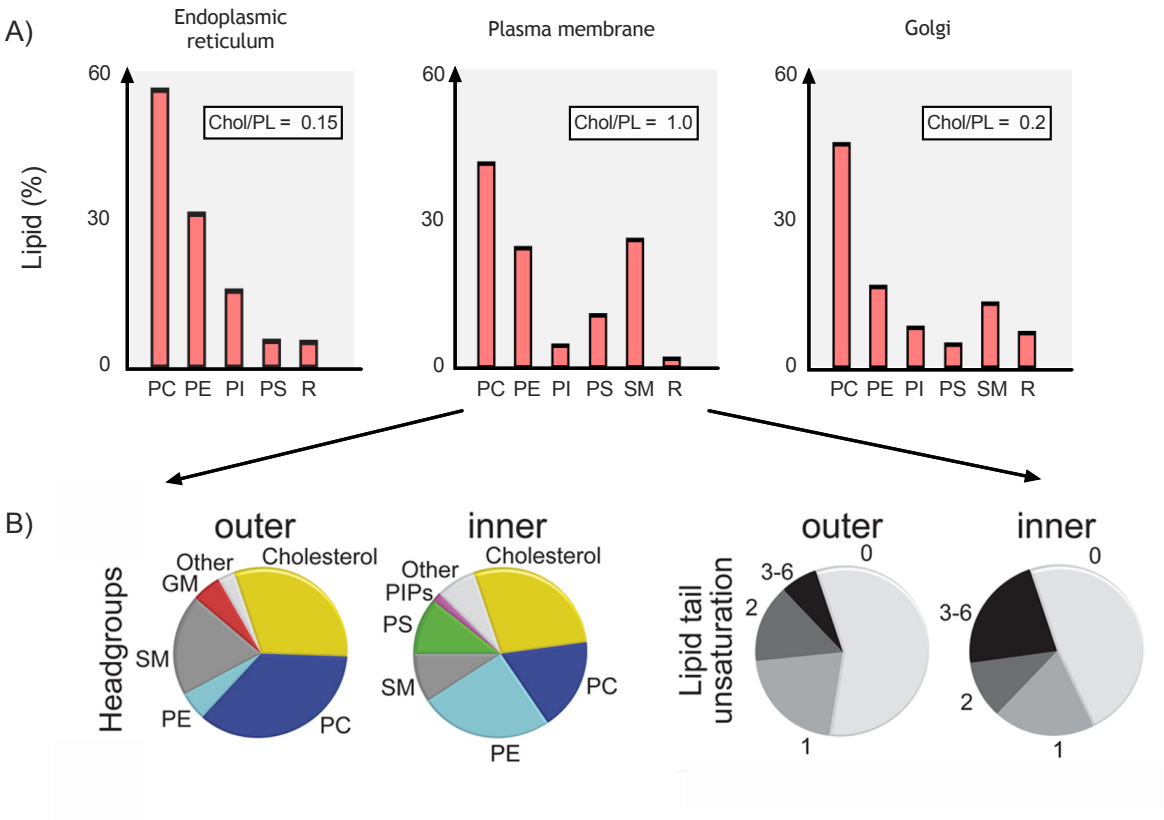


Figure 1.3: Lipid composition of mammalian membranes. A) The composition of three mammalian membranes is given, adapted from diagrams and information in (Van Meer et al, 2008). Chol/PL = ratio of cholesterol to phospholipids (glycerophospholipids + sphingomyelins). R = remaining lipids to give 100%, SM = sphingomyelins. B) The lipid compositions of the two leaflets of the plasma membrane are given in terms of both headgroup (left) and acyl chain unsaturation (right), reproduced from (Ingólfsson et al, 2014). PIPs = phosphatidylinositol-phosphates, GM = gangliosides (a class of glycosylated sphingolipid).

1.1.2 Membrane proteins

Membrane proteins can be broadly separated into two classes; peripheral and integral membrane proteins (figure 1.1) (Singer & Nicolson, 1972). Peripheral membrane proteins are those which can be dissociated from the membrane by changes in ionic strength, reflecting a primarily hydrophilic association with the membrane. Integral membrane

proteins, by contrast, can only be removed from the membrane by agents that disrupt the bilayer structure (namely detergents – see section 1.3), reflecting the hydrophobic interactions these proteins make with lipids. Typically, integral membrane proteins are composed of transmembrane α-helices (TMs) (Hedin *et al*, 2011), although there are notable examples of β-sheet structures (e.g. the β-barrels of bacterial outer membranes (Fairman *et al*, 2011)), and of helices that do not cross the membrane (e.g. the prostaglandin endoperoxide H synthases (Spencer *et al*, 1999)).

Integral membrane proteins fulfil a wide range of crucial functions that underpin communication, energy transduction and transport across biological membranes. Accordingly, alpha helical transmembrane proteins account for around 30% of the human proteome (Almén *et al*, 2009) and membrane proteins represent 40-60% of all drug targets (Overington & Hopkins, 2006; Santos *et al*, 2017). Despite the fundamental importance of these proteins, our understanding of their structure and function lags behind that of soluble proteins considerably (Hendrickson, 2016). Membrane proteins are notoriously difficult to obtain in sufficient amounts and of sufficient quality for structural and biophysical studies, not least because they typically express at low levels in heterologous expression hosts and they typically require detergents for purification which may denature them (Bill *et al*, 2011; Reis & Moraes, 2018; Zhang & Cherezov, 2019).

1.2 G protein coupled receptors (GPCRs)

G protein-coupled receptors (GPCRs) constitute a large family of integral membrane proteins, with more than 800 receptors encoded in the human genome (Fredriksson *et al*, 2003) grouped into five classes according to sequence similarity: class A receptors (Rhodopsin-like), class B receptors (Secretin), class C receptors (Glutamate), adhesion receptors & frizzled/taste 2 receptors (Schiöth & Fredriksson, 2005). The class A family is

by far the best studied (Weis & Kobilka, 2018) and will be given primary consideration in this thesis.

Collectively, GPCRs are involved in an enormous diversity of physiological processes, being activated by ligands as diverse as photons, peptides, amines, nucleotides, lipids & other proteins (Dorsam & Gutkind, 2007). Given their involvement in cellular responses to such stimuli, it is not surprising that their dysfunction is implicated in a plethora of pathologies, not least obesity (Riddy *et al*, 2018), diabetes (Sebastiani *et al*, 2018), cancer (Dorsam & Gutkind, 2007) and neurodegenerative diseases (Huang *et al*, 2017). GPCRs are also of considerable importance as drug targets, since they account for around 34% of drugs approved by the FDA in the United States, with these 475 drugs targeting 108 receptors (Hauser *et al*, 2017). Consequently, a large proportion of currently marketed drugs target a small fraction of receptors, leaving a great deal of potential for further design of drugs targeted at GPCRs (Fang *et al*, 2015). Despite being activated by diverse ligands, reviews of biophysical and structural studies (Manglik & Kruse, 2017; Weis & Kobilka, 2018), alongside bioinformatics approaches (Flock *et al*, 2015; Venkatakrishnan *et al*, 2016; Flock *et al*, 2017), suggest most GPCRs are activated by a conserved mechanism.

Understanding GPCR activation and signalling is therefore of fundamental biological and biomedical importance, with significant opportunities for advances in understanding to translate into new and better drugs to improve human health. In the following section, a summary of our current understanding of these processes at the molecular level is provided.

1.2.1 GPCR signalling

A simple, canonical scheme for GPCR signalling is given in figure 1.4. A GPCR is activated by extracellular binding of a ligand (typically a diffusible molecule), which leads

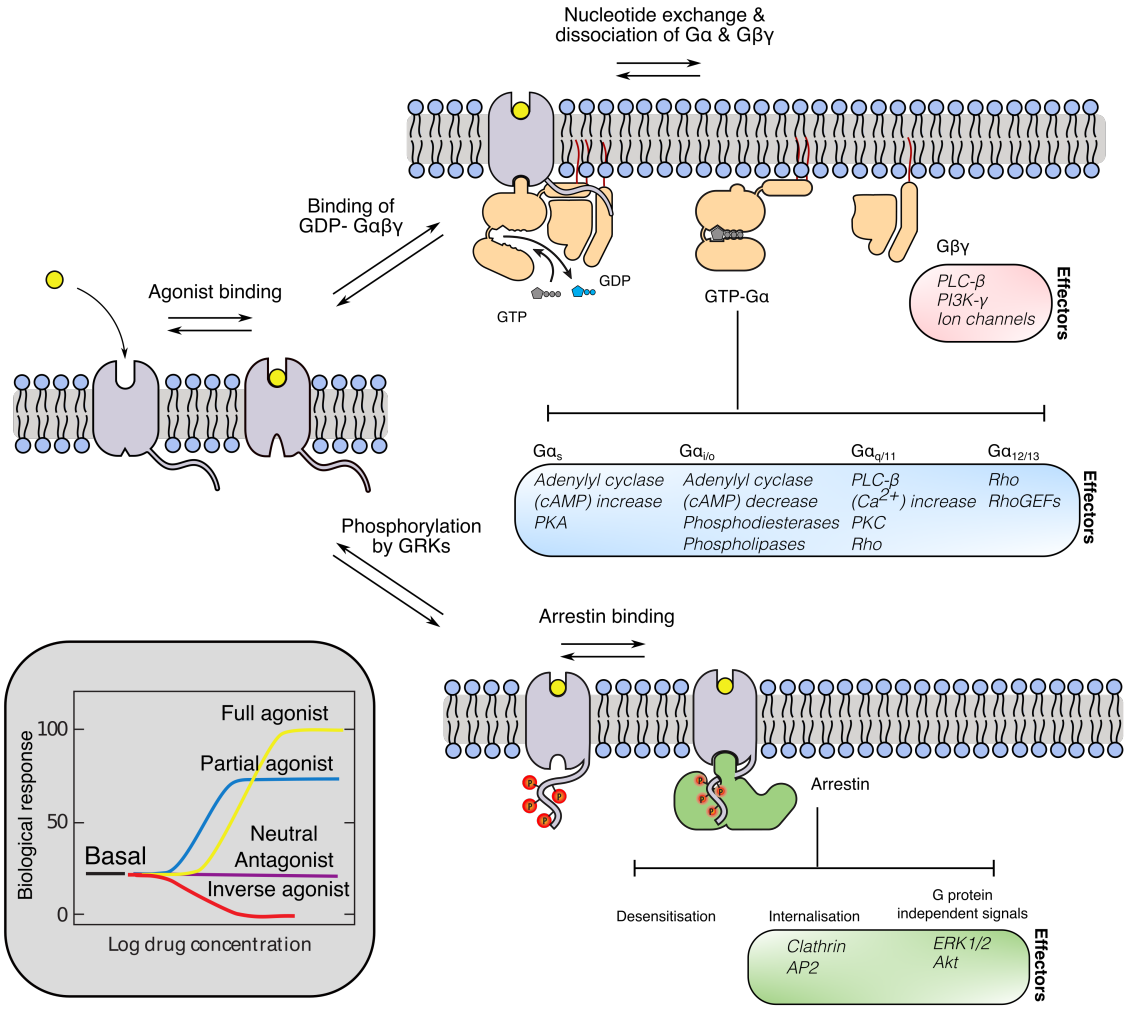


Figure 1.4: Overview of GPCR signalling. Top: engagement of the GDP-bound heterotrimer by the receptor leads to signals from Gα and Gβγ. The four families of Gα are shown. Bottom: phosphorylation of the receptor by GRKs leads to arrestin binding, which in turn can cause several different outcomes. Shown in the red, blue & green boxes are examples of downstream effector proteins involved in the various processes. Shown in the grey box is a definition of ligand efficacy. cAMP = cyclic AMP, PKA = protein kinase A, PLC-β = phospholipase C- β, PKC = protein kinase C, PI3K-γ = phosphoinositide 3-kinase γ, JNK3 = c-Jun N-terminal kinase, Akt = protein kinase B. This figure is adapted from (Weis & Kobilka, 2018) with additional information from (DeWire et al, 2007; Dorsam & Gutkind, 2007).

to the establishment of intracellular signals through coupling to heterotrimeric G proteins and arrestins.

GPCR ligands are classified according to their efficacy – that is, the degree to which they activate a particular pathway. The unliganded GPCR may show basal activity, which can

be lowered by inverse agonists, or increased by agonists (figure 1.4, inset) (Kenakin, 2004; Weis & Kobilka, 2018). The efficacy of a full agonist is defined as 100%, whilst that of a partial agonist is less. Neutral antagonists bind the receptor and compete for binding of other ligands without modulating basal activity.

Heterotrimeric G proteins consist of an alpha subunit (Gα), which binds guanine nucleotides and possesses GTP-hydrolysing enzymatic activity (GTPase activity), and a beta-gamma heterodimer (Gβγ) (Milligan & Kostenis, 2006). 16 Gα genes produce at least 21 distinct protein isoforms, which can be classified into four subtype families – G_s, $G_{i/o}$, $G_{q/11}$ & $G_{12/13}$ (Strathmann & Gautam, 1991; Downes & Gautam, 1999) and which determine the downstream signalling partners that are activated (figure 1.4, blue box) (Neves *et al*, 2002).

Mechanistically, an agonist-bound GPCR engages the GDP-bound, signalling-inactive Gαβγ heterotrimer and stimulates the exchange of GDP for GTP at Gα (figure 1.4, top). This leads to dissociation of Gαβγ into Gα & Gβγ, both of which can go on to effect downstream processes, before the intrinsic GTPase activity in Gα terminates the signal and promotes reformation of the GDP-bound heterotrimer. Hence an agonist-bound GPCR acts as a guanine nucleotide exchange factor (GEF) on the heterotrimeric G protein. When considering the scheme outlined in figure 1.4, it should be noted that in many cases, a specific GPCR may show selectivity for a specific G protein subtype (Okashah *et al*, 2019). For example, the μ-opioid receptor (μOR) is considered to couple exclusively to the $G_{i/o}$ subtype (Connor & Christie, 2006). However, one GPCR may signal via more than one G protein, and in some cases receptors are able to signal to almost all tested G protein subtypes (Inoue *et al*, 2019; Okashah *et al*, 2019; Masuho *et al*, 2015).

In addition to this G-protein dependent signalling, a second cascade of events can be initiated by an agonist-bound GPCR, involving arrestin proteins (figure 1.4, bottom).

Visual arrestin and cone arrestin are both expressed in the eye & specialised for interaction with light activated receptors, whilst β-arrestin$_1$ and β-arrestin$_2$ are expressed in a wide range of cell types (Attramadal *et al*, 1992; Reiter & Lefkowitz, 2006). Canonically, recruitment of arrestins to an activated GPCR involves phosphorylation of the activated GPCR by GPCR kinases (GRKs) on the GPCR C-terminus and/or third intracellular loop (ICL3) (Luttrell & Lefkowitz, 2002). Arrestin binding can sterically inhibit G protein binding and thus arrest G protein-dependent signalling (desensitisation), can target the receptor to clathrin-coated pits (internalisation), and can initiate G-protein independent signals through proteins such as mitogen-activated protein kinase (MAPK or ERK) (Reiter & Lefkowitz, 2006; Reiter *et al*, 2012). It should be noted that additional mechanisms of receptor-desensitisation involving second-messenger dependent kinases (e.g. protein kinase A) also exist, which do not require arrestins for desensitisation (Luttrell & Lefkowitz, 2002).

There is considerable interest in studying & developing ligands which display selectivity between different signalling proteins and so signalling outcomes. These so called "biased ligands" display efficacy profiles in which there is selectivity for one signalling pathway over another, compared to a reference ligand that is comparatively "balanced" (Violin *et al*, 2014; Reiter *et al*, 2012). Such bias may manifest itself as selectivity for arrestin signalling over G protein signalling, or selectivity towards one subtype of G protein over another.

1.2.2 Advances in structural studies of GPCRs

Characterisation of GPCRs at the molecular level has undergone a revolution in the last decade (Ghosh *et al*, 2015). Until 2007, rhodopsin was the sole GPCR for which crystal structures existed. At the time of writing in mid-2019, well over 300 structures representing more than 60 unique receptors exist, solved by both X-ray crystallography (XRC) and cryo-electron microscopy (cryo-EM) and complemented by an ever-growing suite of

biophysical and computational studies. Several developments have converged to allow such progress.

Firstly, robust systems have been developed and optimised for heterologous overexpression of GPCRs in eukaryotic hosts, most notably Sf9 insect cells but increasingly HEK293 cells (Milic & Veprintsev, 2015; Maeda & Schertler, 2013; Ghosh *et al*, 2015; Munk *et al*, 2019).

Secondly, there have been significant advances in protein engineering to produce constructs that are more thermostable in detergent and/or amenable to crystallographic & biophysical studies. Pioneering work by the labs of Brian Kobilka and Raymond Stevens established the fusion of well folded soluble proteins such as T4 lysozyme (T4L) to GPCRs (mostly at ICL3 or the N-terminus) to produce a greater hydrophilic surface area for crystallogenesis (Cherezov *et al*, 2007; Rosenbaum *et al*, 2007; Chun *et al*, 2012). Complementary techniques involving mutagenesis to improve receptor thermostability in detergents were developed by Christopher Tate and colleagues, initially for the β_1-adrenergic receptor (β_1AR) through alanine scanning (Warne *et al*, 2008; Tate & Schertler, 2009; Warne *et al*, 2009). Work in Andreas Plückthun's lab has produced additional directed evolution approaches to thermostabilisation (Sarkar *et al*, 2008; Dodevski & Plückthun, 2011) and subsequently crystal structures of several receptors (Egloff *et al*, 2014; Schöppe *et al*, 2019; Ehrenmann *et al*, 2018). Whilst protein engineering has facilitated structural studies, and it is clear that the structures of thermostabilised and non-thermostabilised receptors are broadly similar (Heydenreich *et al*, 2015), these approaches can nonetheless impair receptor function in terms of G protein and/or arrestin signalling.

Lastly, several technical developments have assisted GPCR structural biology in recent years.). The development of lipidic cubic phases as a crystallisation medium for GPCRs has been of significant utility (Cherezov *et al*, 2007; Cherezov, 2009). Likewise, the development of microfocus beamlines and rastering techniques that can handle the small,

fragile crystals typically produced for GPCRs has allowed considerable progress (Ghosh *et al*, 2015; Smith *et al*, 2012). X-ray free electron laser (XFEL) sources for crystallography have also produced GPCR structures, including the angiotensin II type 1 receptor (AT_1R) (Zhang *et al*, 2015c), rhodopsin-arrestin complexes (Zhou *et al*, 2017; Kang *et al*, 2015) and the glucagon receptor (Zhang *et al*, 2017b). These developments have been accompanied by the rapid maturation of single particle cryo-EM into a technique capable of producing structures <4Å of proteins smaller than 100 kDa (this size limit is approximate and rapidly improving). This cryo-EM "resolution revolution" (Kuhlbrandt, 2014) was brought about by synergistic advances in detector technology and data processing (Bai *et al*, 2015; Fernandez-Leiro & Scheres, 2016).

1.2.3 Structural features of GPCRs

All class A GPCRs share a structure of seven transmembrane helices (TMs) linked by a series of intracellular and extracellular loops (ICLs and ECLs) and typically accompanied by an eighth, non-transmembrane helix (helix 8) (figure 1.5A, left) (Manglik & Kruse, 2017; Weis & Kobilka, 2018). In order to describe and compare conserved residues across different GPCR sequences and structures in this thesis, the Ballesteros-Weinstein nomenclature is used; here, the most conserved residue on a TM is denoted as residue 50 (Ballesteros & Weinstein, 1995). For example, the highly conserved Asparagine in TM1 would be labelled generically $Asn^{1.50}$, and residue 1.49 would be the residue on the N-terminal side of 1.50.

Class A GPCR structures can be divided into "inactive" and "active" states, based on whether that GPCR conformation is capable of coupling with downstream signalling partners. Active and inactive state structures of the prototypical β_2-adrenergic receptor (β_2AR) are used to illustrate key features of GPCR structure and activation in figure 1.5.

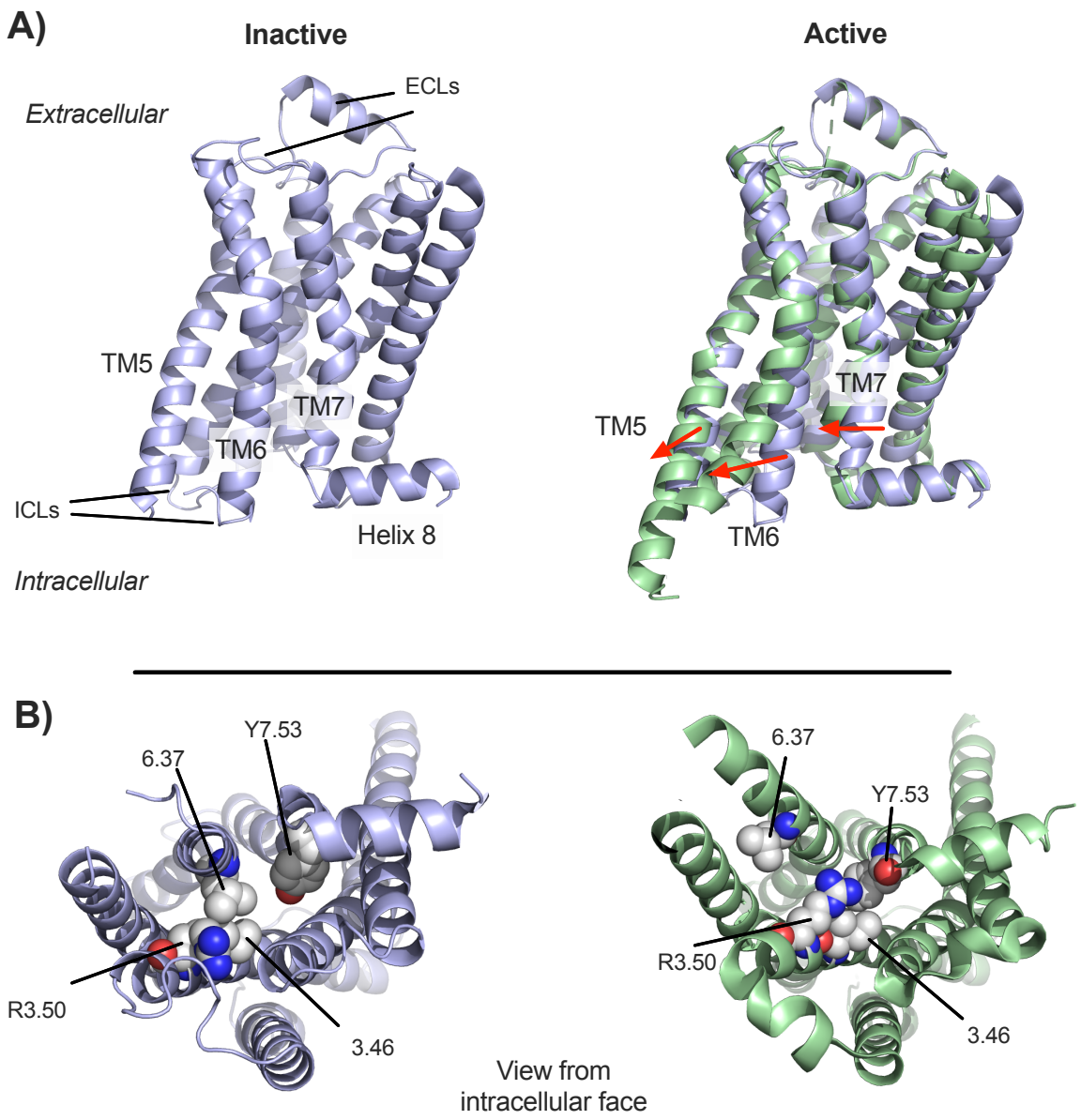


Figure 1.5: Features of GPCR structure and activation. A) Left: structure of the inactive, inverse-agonist bound β_2AR (PDB ID 2RH1, (Cherezov et al, 2007)), demonstrating the TM, ICL, ECL and helix 8 elements of GPCR structure. Right: an active β_2AR structure (PDB ID 3SN6, (Rasmussen et al, 2011b)) aligned to the inactive structure, with red arrows highlighting the movements of TM5/6/7 upon GPCR activation. B) Intracellular views of the receptor inactive and active states, demonstrating the rearrangements of conserved residues at the intracellular receptor face.

The main conformational changes on the intracellular face of the receptor upon activation are conserved across all active state GPCR structures solved to date and were first demonstrated by structures of the photoreceptor rhodopsin (Park *et al*, 2008; Scheerer *et al*, 2008). Most significant is the movement of TM6, which rotates and translates away from

the transmembrane core of the receptor (figure 1.5A, right). This is accompanied by an outwards movement of TM5 and an inwards movement of TM7 with respect to the protein core. These conformational changes are facilitated by changes in contacts between conserved residues at the receptor intracellular face (figure 1.5B). These residues include conserved hydrophobic residues at positions 3.46 & 6.37, and the highly conserved $Y^{7.53}$ and $R^{3.50}$ residues (Venkatakrishnan *et al*, 2016; Manglik & Kruse, 2017; Weis & Kobilka, 2018). Together, these changes create a cavity that accommodates the C-terminal alpha-5 helix (α5) of the G protein α subunit (Scheerer *et al*, 2008) or finger loop of arrestin (Szczepek *et al*, 2014; Kang *et al*, 2015). Moving from the intracellular receptor face towards the orthosteric ligand-binding pocket on the extracellular receptor face, the changes in receptor conformation upon activation become more diverse – necessarily so, given the differing identities of the agonist distinct receptors engage (Venkatakrishnan *et al*, 2016).

A summary of the class A receptors for which both inactive and active state structures are available is given in table 1.1, along with an indication of the methodology used to obtain the active structure. The majority of structures solved to date are of inactive states (Munk *et al*, 2019) and obtaining active-state structures of GPCRs has generally required the presence of a protein bound to the intracellular face of the receptor to stabilise the active conformation (Manglik & Kruse, 2017). Successful approaches include the use of nanobodies, which are fragments of antibodies produced by camelid species such as Llamas (Manglik *et al*, 2016). Nanobodies have a compact structure that allows them to recognise conformational epitopes that may be hidden to conventional antibodies (Pardon *et al*, 2014) and have been shown to mimic the effects of a G protein pharmacologically (Manglik *et al*, 2016). A second approach is to use "mini-G proteins": engineered forms of the Ras-like GTPase domain of Gα, which bind to GPCRs in the absence of Gβγ subunits

Receptor	Method to obtain active structure	Reference
Adenosine A1 (A_1R)	Cryo EM with G_{i2} heterotrimer	(Draper-Joyce *et al*, 2018)
Adenosine A2A ($A_{2A}R$)	XRC with mini-G_s	(Carpenter *et al*, 2016)
	Cryo EM with mini-G_s + Gβγ	(García-Nafría *et al*, 2018a)
β_1-adrenergic (β_1AR)	XRC with nanobody	(Warne *et al*, 2019)
β_2-adrenergic (β_2AR)	XRC with G_s heterotrimer	(Rasmussen *et al*, 2011b)
	XRC with nanobody	(Rasmussen *et al*, 2011a; Ring *et al*, 2013)
	XRC with G_s peptide	(Liu *et al*, 2019)
Cannabinoid type 1 (CB1)	Cryo-EM with G_{i1} heterotrimer	(Krishna Kumar *et al*, 2019)
Kappa opioid (κOR)	XRC with nanobody	(Che *et al*, 2018)
M1 muscarinic (M_1R)	Cryo EM with G_{11} heterotrimer	(Maeda *et al*, 2019)
M2 muscarinic (M_2R)	XRC with nanobody	(Kruse *et al*, 2013)
	Cryo EM with G_{oA} heterotrimer	(Maeda *et al*, 2019)
μ-opioid (μOR)	XRC with nanobody	(Huang *et al*, 2015)
	Cryo EM with G_{i1} heterotrimer	(Koehl *et al*, 2018)
Neurotensin 1 (NTS1)	Cryo-EM with G_{i1} heterotrimer	(Kato *et al*, 2019)
Serotonin $5HT_{1B}$ ($5HT_{1B}R$)	Cryo-EM with mini-$G_{i/o}$ + Gβγ	(García-Nafría *et al*, 2018b)

Table 1.1: Class A receptors for which inactive & active structures are available. N.B. Only references to the active structures are given for simplicity. Rhodopsin also has several active-state structures and is discussed in the main text.

(Carpenter & Tate, 2016; Carpenter *et al*, 2017). Additionally, peptide mimetics of key regions of G proteins or arrestins have been successfully used for rhodopsin (Scheerer *et al*, 2008; Szczepek *et al*, 2014) and the β_2AR (Liu *et al*, 2019). Finally, perhaps the most desirable approach to obtaining active GPCR conformations is to complex the receptor with native signalling partners (see also section 1.2.5 & 1.2.6). This was first achieved for the β_2AR-Gs complex using crystallography - a considerable challenge given the size of the GPCR-Gαβγ complex coupled with the dynamicity and detergent-instability of its components (Rasmussen *et al*, 2011b). For GPCR-arrestin complexes, rhodopsin has been

solved in complex with visual arrestin using XFEL techniques (Kang *et al*, 2015; Zhou *et al*, 2017), requiring the use of receptor and arrestin mutants that were covalently linked.

It should be noted that rhodopsin is somewhat unique amongst class A GPCRs, and has been crystallised in an active state without an intracellular binding protein (Park *et al*, 2008). In addition, active state structures exist for rhodopsin in complex with G_{i1} (Kang *et al*, 2018; Tsai *et al*, 2019), mini-G_o (Tsai *et al*, 2018) and the native signalling partner, transducin (G_t) as well as a $G\alpha_t$ C-terminal peptide (Scheerer *et al*, 2008) and arrestin finger loop peptide (Szczepek *et al*, 2014).

1.2.4 Biophysical and computational studies of GPCR activation

Structural studies of GPCRs provide detailed snapshots of GPCR activation, and increasingly biophysical and computational studies are providing information that complements these snapshots.

Nuclear magnetic resonance (NMR) and double electron-electron resonance (DEER) studies of the β_2AR demonstrate that the unliganded receptor exhibits conformational heterogeneity which is increased when bound to an agonist (Nygaard *et al*, 2013; Manglik *et al*, 2015). A minority of the receptor population adopts an active state in the presence of an agonist, whilst addition of a nanobody leads to full occupation of such a state. This helps account for why active-state GPCR structures generally require the presence of stabilising intracellular binding partners – agonist binding alone appears insufficient for full population of the receptor active state. For the μOR, NMR studies demonstrate similar results, whereby the presence of a nanobody is required to observe the conformational changes associated with the receptor active state (Sounier *et al*, 2015). For the A_{2A}R, similar principles apply, but the receptor conformational landscape is rather different. For the unliganded receptor, at least two active and two inactive conformations are resolved (Ye *et al*, 2016), and there is significant population of receptor active states even in the absence of

an agonist. Accordingly, unlike the β_2AR, the agonist-bound A_{2A}R crystallises in a conformation that shows some features of the canonical active state (a so called 'intermediate-active' state) (Lebon *et al*, 2011; Carpenter *et al*, 2016). For rhodopsin, as previously noted, the receptor is capable of displaying a canonical active conformation in the absence of an intracellular binding partner, reflecting a rather different conformational landscape for this receptor. This leads to a more switch-like activation process in which near-full population of the active state can be achieved by light absorption (Manglik & Kobilka, 2014), consistent with its role as a low-noise photoreceptor.

Molecular dynamics simulations provide an additional dimension to the insights provided by structural and biophysical techniques. Simulations of the agonist-bound β_2AR in the active state reveal spontaneous de-activation of the receptor in the absence of a nanobody (Rosenbaum *et al*, 2011). Simulations of this receptor also provide detail of how the agonist-binding site, G-protein binding site and a region connecting them can undergo conformational changes that are weakly linked – so called "loose allosteric coupling" (Dror *et al*, 2011; Latorraca *et al*, 2017).

The general picture of GPCR activation when combining information from structural, biophysical and computational studies is therefore that agonist binding increases conformational sampling of the receptor and so increases the probability that a conformation appropriate for coupling to downstream signalling partners is adopted (figure 1.6). However, the precise energy landscape is likely to vary from receptor to receptor, and it is unclear whether receptors such as the β_2AR are representative of class A GPCRs as a whole.

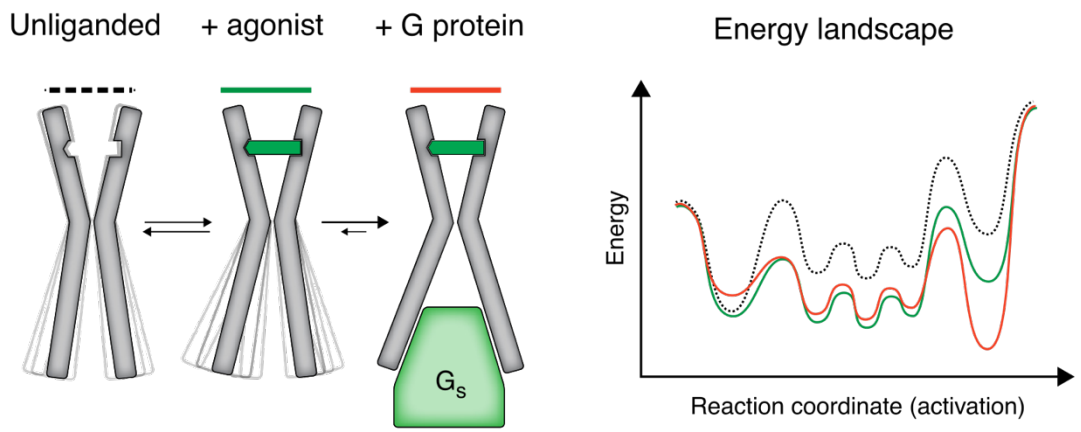


Figure 1.6: A model of GPCR activation based on studies of the β_2AR. The unliganded receptor shows conformational heterogeneity. Agonist binding leads to altered activation energies on the energy landscape, and so increased conformational sampling, including limited sampling of the active state. Addition of a G protein favours complete population of the active state. Figure reproduced from (Manglik & Kobilka, 2014).

1.2.5 Receptor-G protein interactions and selectivity

In the last year, an unprecedented number of structures of GPCR-G protein complexes have been solved, largely facilitated by the application of cryo-EM (García-Nafría & Tate, 2019). This formation of a stable complex generally requires the G protein to be in a nucleotide-free state (Rasmussen *et al*, 2011b). Analysis of the structures listed in section 1.2.3 reveals structures available for complexes containing G_s, G_i, G_o and G_{11}, covering 3 of the 4 G protein families. Despite diverse G protein identities, there is remarkable conservation of the GPCR-G protein interface. In every structure solved to date, the Gα α5 helix makes the majority of contacts (figure 1.7). Other regions of Gα may contribute to the interface, including the C-terminus of the HN helix (figure 1.7A) and various loop regions. Gβ also makes contacts to the receptor in some structures – for example, to ICL1 of the A_{2A}R (García-Nafría *et al*, 2018a) and to the C-terminus of the M_1R and rhodopsin (Maeda *et al*, 2019; Tsai *et al*, 2019).

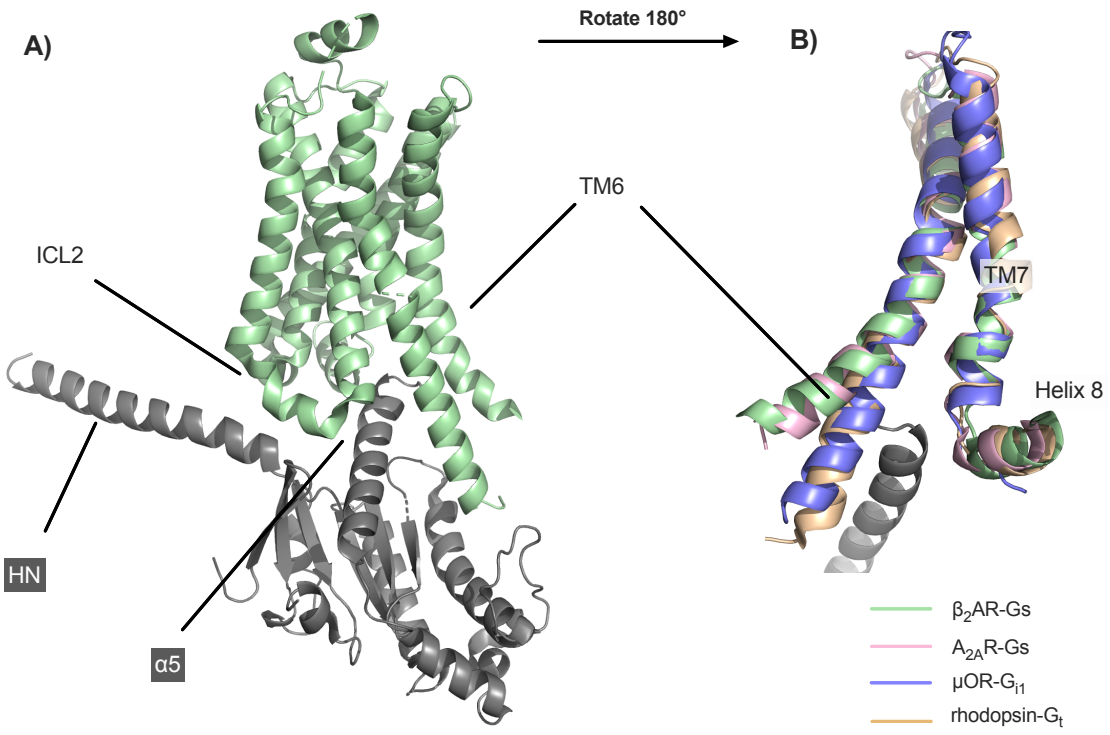


Figure 1.7: GPCR-G protein interactions. A) The interaction between β_2AR and G_s (PDB 3SN6 (Rasmussen et al, 2011b) is shown, with the alpha helical domain of $G\alpha_s$ and the $G\beta\gamma$ dimer omitted for simplicity. B) Alignments of TM6/TM7/helix 8 for representative GPCR-G_s and GPCR-G_i structures, demonstrating the greater TM6 tilt for the former class of structures. Shown are A_{2A}R-G_s (PDB 6GDG (García-Nafría et al, 2018a)), μOR-G_{i1} (PDB 6DDE, (Koehl et al, 2018)) and rhodopsin-G_t (PDB 60Y9 (Gao et al, 2019)).

Despite the growing abundance of structural information on GPCR-G protein interactions, molecular insights into receptor-G protein coupling selectivity are relatively sparse. Whilst there are subtle differences between complex structures with different G protein subtypes, it is difficult to know whether these differences are general for the coupling to a subtype of G protein, or reflect specific details of that particular GPCR-G protein coupling (García-Nafría & Tate, 2019). One of the few consistent trends that emerges is that $G_{i/o}$ coupled receptors show a smaller degree of TM6 tilt than the G_s-coupled receptors, which may in turn reflect the larger dimensions of the α5 helix of G_s vs G_i (Kato *et al*, 2019) (figure 1.7B).

Interestingly, a pair of recent biophysical studies using time-resolved mass spectrometry, molecular dynamics and XRC have suggested that the interactions observed in the nucleotide-free GPCR-G protein structures may not be relevant to determining selectivity. Instead, it is proposed that the GDP-bound G protein, which in a physiological context is most likely to make initial contact with the receptor, is responsible for mediating selective interactions with a GPCR (Du *et al*, 2019; Liu *et al*, 2019). Such studies demonstrate the difficulties that can arise in extrapolating insights from structural biology to the physiological context of GPCR signalling.

1.2.6 Receptor-arrestin interactions and functional selectivity

It has long been appreciated that arrestins can have multiple modes of interaction with a GPCR (Gurevich & Benovic, 1995). Different functional complexes of arrestin with rhodopsin have been demonstrated using fluorescence spectroscopy (Sommer *et al*, 2012), and different binding modes of arrestin have been directly visualised by negative stain electron microscopy (Shukla *et al*, 2014). Arrestin can dock to the receptor TM bundle ("core interaction"), or bind the receptor C-terminus ("tail interaction"), and these modes of engagement may mediate distinct functional outcomes (Kumari *et al*, 2016; Cahill *et al*, 2017): the core interaction is necessary for desensitisation of G protein signalling whilst the tail interaction is sufficient for arrestin signalling and receptor internalisation.

Structural insights into GPCR-arrestin interactions come from several complexes of rhodopsin. The first of these to be published shows binding of a peptide corresponding to the arrestin finger loop to a site on rhodopsin that overlaps with the site for the α5 peptide of $G\alpha_t$ (Szczepek *et al*, 2014). Subsequent structures of rhodopsin covalently linked to visual arrestin demonstrate that in addition to the receptor core-arrestin finger loop interface, several other receptor-arrestin interfaces exist, including interactions between the receptor

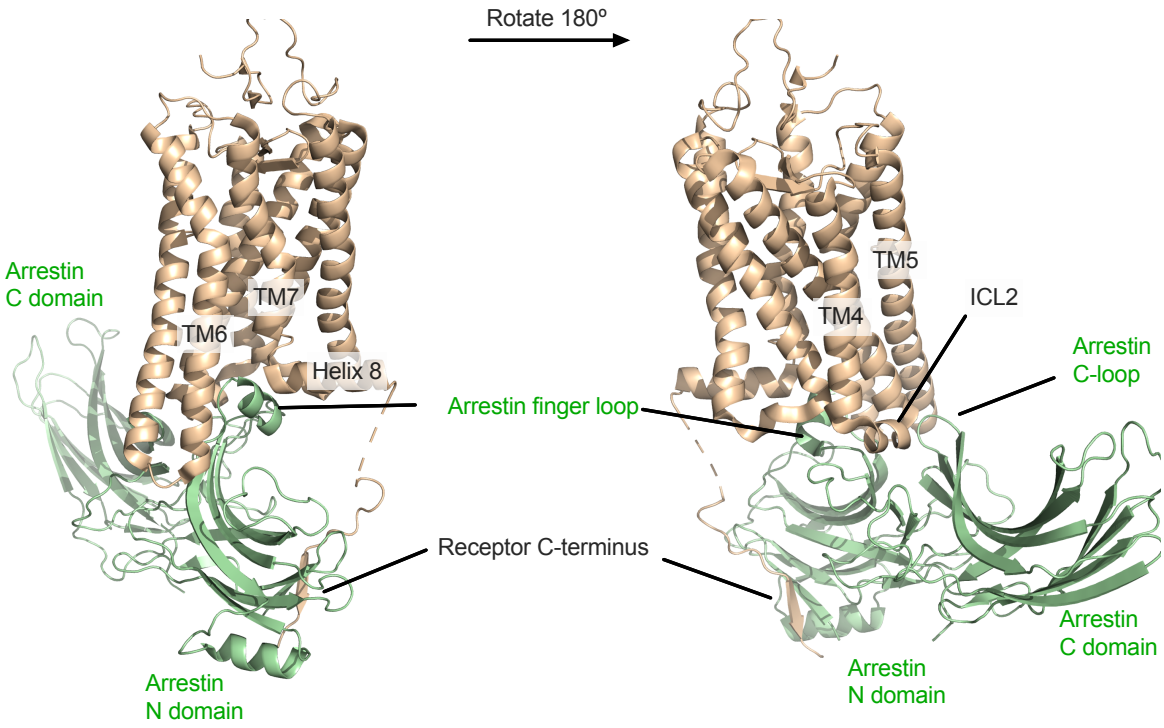


Figure 1.8: Rhodopsin-arrestin interactions. Two views of the rhodopsin-arrestin covalent complex are given (PDB ID 5WOP (Zhou et al, 2017)), highlighting elements of the receptor (labelled in black) and arrestin (labelled in green) involved in the binding interface.

ICL2 and the arrestin C-loop and middle loop (figure 1.8) (Kang *et al*, 2015; Zhou *et al*, 2017). In the most recent complex structure (Zhou *et al*, 2017), details are also resolved of the interface between phosphorylated residues on the rhodopsin C-terminus and a positively charged groove in the arrestin N-domain (figure 1.8), which was also previously observed in a structure of the C-terminal phosphopeptide of the vasopressin 2 receptor (V_2R) bound to β-arrestin$_1$ (Shukla *et al*, 2013). A recent landmark study using molecular dynamics and fluorescence spectroscopy has clarified the process by which a GPCR activates arrestin (Latorraca *et al*, 2018). This study reveals allosteric coupling between two distinct receptor-binding sites on arrestin, which allow for its activation by either receptor-tail engagement, core engagement, or both. Notably, whilst the arrestin finger loop is important in binding the receptor, this binding is poorly coupled to interdomain rotation of the arrestin (i.e. activation).

How does a receptor distinguish between arrestin and G protein binding? Whilst the binding sites for $G\alpha_t$ and the arrestin finger loop on rhodopsin overlap, the arrestin makes fewer contacts with receptor TM5/6 and thus TM7/helix 8 contacts are likely more important for arrestin binding (Szczepek *et al*, 2014). Several studies suggest that the receptor TM7 conformation plays a role in discriminating between binding of arrestin and G protein, including structures of the $5HT_{2B}$ serotonin receptor in complex with arrestin-biased ligands (Wacker *et al*, 2013; McCorvy *et al*, 2018), ^{19}F-NMR studies of the β_2AR with biased ligands (Liu *et al*, 2012a) and a recent DEER study of the AT_1R bound to ligands with arrestin-bias (Wingler *et al*, 2019a). However, it must be noted that bias observed at the cellular level is likely to result not just from aspects of receptor conformation, but also from the spatial organisation of the receptor and its signalling partners (Irannejad *et al*, 2017), the expression levels of these proteins, and temporal aspects of the signalling process (Grundmann & Kostenis, 2017).

1.2.7 Frontiers in understanding GPCR activation

There has been tremendous progress in understanding GPCR activation at the molecular level over the last decade. However, it should be noted that many structural and biophysical studies make use of highly-engineered receptors, and that most insights into class A GPCR activation come from a small number of receptors (especially the β_2AR). Whilst it is clear that aspects of GPCR activation are highly conserved, it is unclear to what extent the precise conformational changes and energy landscapes of these model receptors are representative of class A GPCRs as a whole.

1.2.8 Neurotensin Receptor 1

Neurotensin (NT) is a peptide consisting of 13 amino acids, first described in 1973, when it was extracted from the bovine hypothalamus and named for its hypotensive effects in rats (Leeman, 1973). NT has dual roles in the central nervous system and periphery (Vincent,

1995). In the brain it acts as a neurotransmitter and neuromodulator, with functions including modulation of dopaminergic signalling, pituitary hormone secretion and pain modulation (Vincent *et al*, 1999; Boules *et al*, 2013; Mustain *et al*, 2011). In peripheral tissues, most notably the gastrointestinal tract, it acts as a local hormone, with functions including control of gastric motility and both stimulation of growth and healing in intestinal mucosa (Vincent *et al*, 1999; Mustain *et al*, 2011). NT has also been implicated in various pathologies, including Parkinson's disease (Antonelli *et al*, 2007; Boules *et al*, 2013), obesity (Li *et al*, 2016), schizophrenia (Kinkead & Nemeroff, 2002) and multiple cancer types (Mustain *et al*, 2011; Ouyang *et al*, 2017).

The effects of neurotensin are mediated by its three receptors. Neurotensin receptor 2 (NTS2) is a class A GPCR that is sensitive to the drug levocabastine (Mazella *et al*, 1996), whilst neurotensin receptor 3 (NTS3) is a type I transmembrane protein also known as sortilin (Mazella *et al*, 1998). However, it is the neurotensin receptor 1 (NTS1, also NTSR1 and NTR1) which mediates most of the effects of NT (Dobner, 2005), and as such this receptor is of considerable biological interest given the diverse functions and pathologies that it is implicated in.

The rat NTS1 (rNTS1) sequence was first cloned in 1990 (Tanaka *et al*, 1990), with the human NTS1 (hNTS1) sequence later cloned and found to share 84% amino acid identity and 92% similarity to rNTS1 (Vita *et al*, 1993). The receptor is a class A GPCR that is expressed in the colon (Vita *et al*, 1993; Azriel & Burcher, 2001), pancreatic islets (Coppola *et al*, 2008) and central nervous system (Vita *et al*, 1993; Roussy *et al*, 2008). NTS1 binds two related endogenous ligands, NT and neuromedin N (NN), which are both agonists & produced from a shared precursor, pro-NT (Rostène & Alexander, 1997). The 8-13 fragment of neurotensin (NT_{8-13}) has the same biological activity as the full length peptide (St-Pierre *et al*, 1981; Kitabgi *et al*, 1977), and NT, NT_{8-13} and NN exhibit similar effects on

NTS1 expressed in CHO cells (Besserer-Offroy *et al*, 2017). The binding of NT to NTS1 is of nanomolar affinity in both membranes (Tanaka *et al*, 1990; Vita *et al*, 1993; Kitabgi *et al*, 1977) and detergent micelles (Harding *et al*, 2007; Seidel *et al*, 2013). This binding affinity is reduced by the presence of NaCl, due to the Na^+ binding pocket formed around $Asp^{2.50}$ that is highly conserved in class A GPCRs (Martin *et al*, 1999; Katritch *et al*, 2014).

NTS1 is notable for its promiscuity in G protein signalling (figure 1.9). Bioluminescence resonance energy transfer (BRET) studies in CHO-K1 cells reveals coupling of NTS1 to G_{oA}, G_{i1}, G_q & G_{13} in response to agonist stimulation, whilst measurement of secondary messengers demonstrates G_s coupling (Besserer-Offroy *et al*, 2017). Similarly, the NanoLuc® Binary Technology (NanoBiT) assay shows coupling of NTS1 to G_s, G_{i1}, G_o, G_q, G_{13} in HEK293 cells (Kato *et al*, 2019).

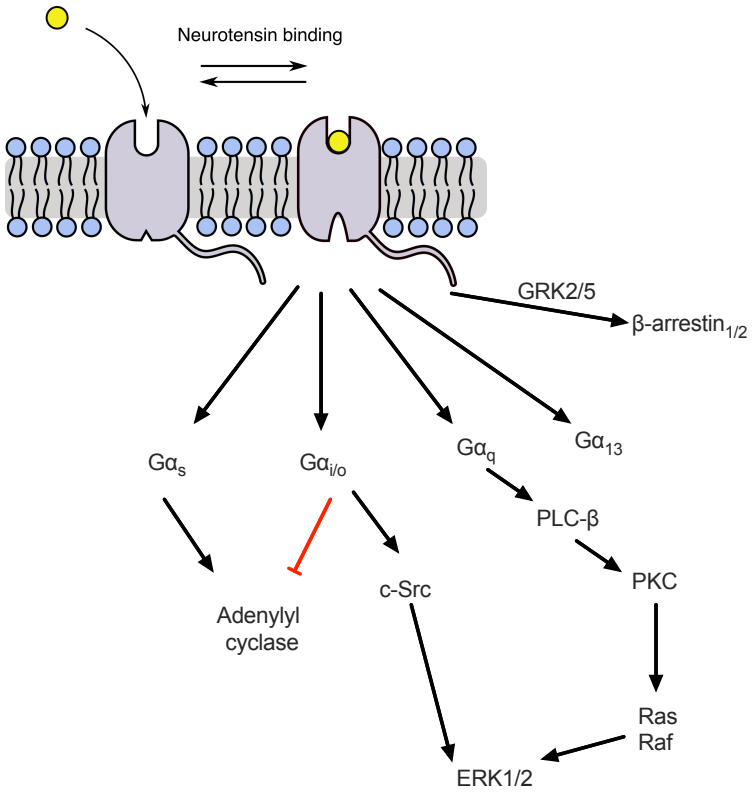


Figure 1.9: NTS1 interactome. Black arrows represent stimulation and red arrows represent inhibition. Based on diagrams in (Besserer-Offroy et al, 2017; Weis & Kobilka, 2018).

In vitro, nanodisc-reconstituted NTS1 interacts with the kinases GRK2 & GRK5, which phosphorylate NTS1 at sites on the C-terminus and ICL3 (Inagaki *et al*, 2015). In CHO-K1 cells, NT-stimulation recruits β-arrestin$_1$ and β-arrestin$_2$ to NTS1 in BRET experiments (Besserer-Offroy *et al*, 2017), and NTS1 is known to undergo significant internalisation upon agonist treatment, ultimately leading to movement of the receptor to the lysosome for degradation (Vandenbulcke *et al*, 2000; Anborgh *et al*, 2002).

1.2.8.1 NTS1 structural biology

To date, ten structures have been published for NTS1 in the PDB. The first eight structures published chronologically were all solved by X-ray crystallography; PDB IDs 4GRV (White *et al*, 2012), 4XEE & 4XES (Krumm *et al*, 2015), 5T04 (Krumm *et al*, 2016), 3ZEV, 4BUO, 4BV0 & 4BWB (Egloff *et al*, 2014) (table 1.2). All eight structures are based on the rNTS1 sequence with thermostabilising mutations introduced because of the poor stability of rNTS1 in detergent (Shibata *et al*, 2009). The constructs used and the approaches to crystallography are summarised in table 1.2.

All eight crystal structures are neurotensin-bound. 3ZEV, 4BUO, 4BVO and 4BWB display a typical inactive state conformation (figure 1.10A). Despite the inactive crystal conformation, the 3ZEV protein displays neurotensin-induced nucleotide exchange at the G_i heterotrimer in insect cell membranes, albeit at much lower levels than the wild type receptor as a result of thermostabilisation (Egloff *et al*, 2014). In 4XEE, 4XES, 4GRV and 5HT04, TM6 is rotated outwards and TM7 is moved inwards when compared to 4BUO (figure 1.10A and B). 4XEE and 4XES are considered to represent active or "active-like" states. 4GRV and 5T04 are both unusual in that TM7 adopts a conformation that occludes the canonical binding site of the Gα α5 helix and makes contacts with TM6. As such, their conformation has been described simply as "ambiguous" (Manglik & Kruse, 2017). When the constructs are expressed in insect cells without T4L insertions, the 4XEE

PDB ID	Sequence coverage	Mutations	Protein production & crystallography
4GRV	T43-K396 ICL3 deletion H269-R299 T4L insertion at ICL3	A86L, E166A, G215A, L310A, F358A, V360A	Sf9 expression Crystallisation in lipidic cubic phase
4XES	As 4GRV	A86L, E166A, G215A, V360A	As 4GRV
4XEE	As 4GRV	A86L, G215A, V360A	As 4GRV
5T04	As 4GRV	A86L, G215A, F358A, V360A	As 4GRV
3ZEV	G50-G390 ICL3 deletion V280-I295	A86L, H103D, H105Y, A161V, R167L, R213L, V234L, I253A, H305R, F358V, S362A	*E. coli* expression Crystallisation in short chain glucoside detergent
4BUO	G50-G390 ICL3 deletion E273-T290	As 3ZEV	As 3ZEV
4BV0	As 3ZEV	S83G, A86L, T101R, H103D, H105Y, L119F, M121L, E124D, L125V, R143K, D150E, A161V, R167L, C172R, A177H, M208V, R213L, V234L, V240L, I253A, N262R, K263R, H305R, V313M C332V, F342A, T354S, F358V, S362A	As 3ZEV
4BWB	As 3ZEV	S83G, A86L, T101R, H103D, H105Y, L119F, M121L, E124D, R143K, D150E, A161V, R167L, R213L, V234L, K235R, V240L, I253A, I260A, N262R, K263R, H305R, C332V, F342A, T354S, F358V, S362A	As 3ZEV

Table 1.2: Summary of constructs used to obtain crystal structures of rNTS1

construct shows near wild-type levels of G protein coupling in membranes, with 4XES showing lower levels and 4GRV and 5T04 showing no coupling (White *et al*, 2012; Krumm *et al*, 2015, 2016). In addition to these structures solved by crystallography, recently two structures were published of NTS1 in complex with the G_{i1} heterotrimer using cryo-EM (Kato *et al*, 2019) (figure 1.10C/D), using a near wild-type hNTS1 sequence with a 10 residue ICL3 truncation. The 6OS9 structure is similar to other GPCR-G_i complexes, and the receptor adopts a canonical active conformation much like the 4XEE structure but with a slightly greater TM6 tilt to accommodate the G protein. TM7 moves inwards, with $Y^{7.53}$ rotating to contact $R^{3.50}$. The interface with G_{i1} is made of up a series of polar and hydrophobic contacts, mediated predominantly by the α5 helix, but also by the N-terminal

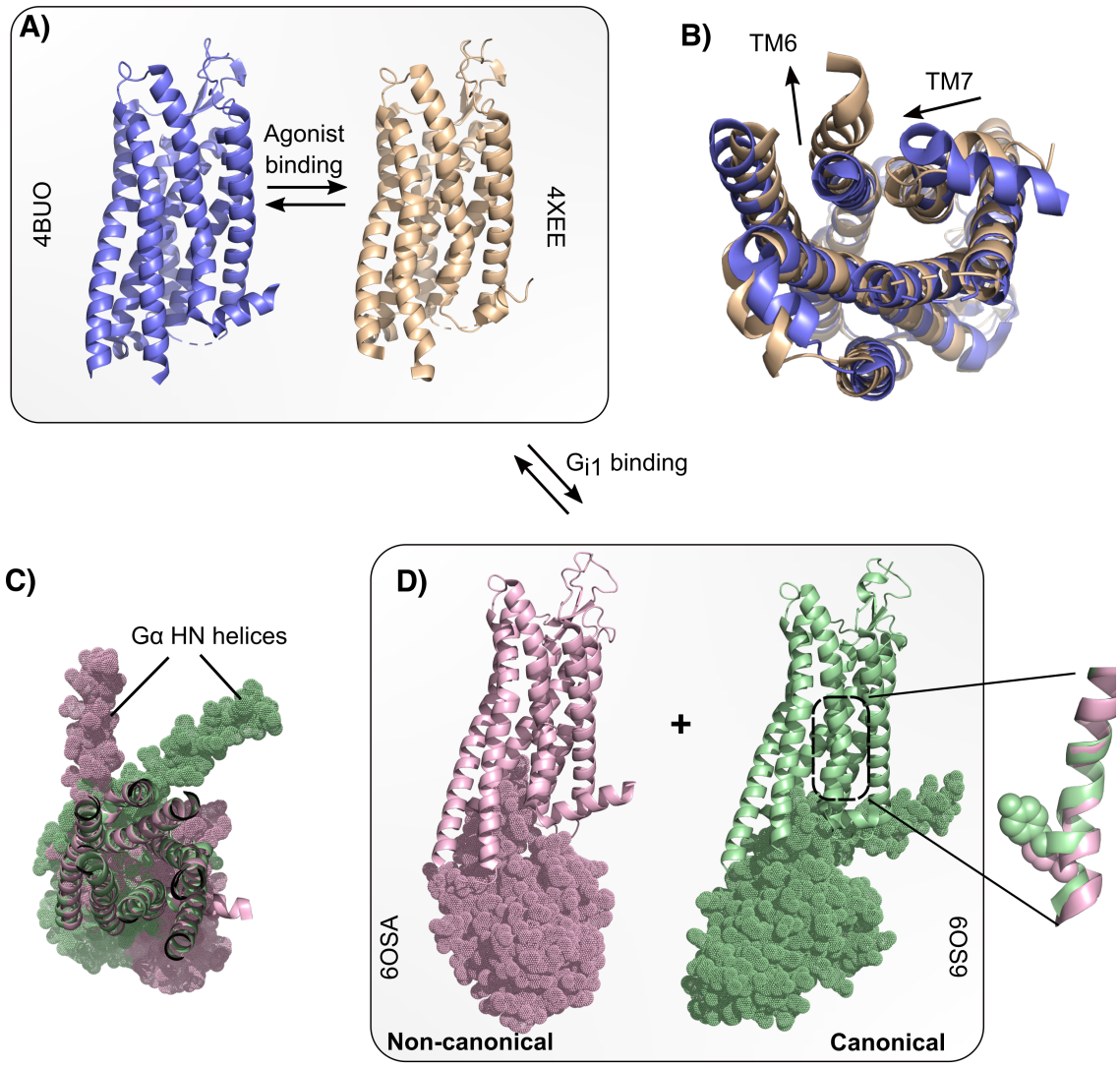


Figure 1.10: NTS1 structural biology. A) Side-on views of inactive (PDB 4BUO) and active states (PDB 4XEE) of NTS1; B) an intracellular view highlighting the movements of TM6 and TM7 upon ligand binding; C) an extracellular view of the two aligned NTS1-G_{i1} complexes (PDB 6OSA & 6OS9), highlighting the difference in G protein orientation. The Gβγ dimer is not shown for simplicity. D) Side-on views of the NTS1-G_{i1} complex conformations resolved by Cryo-EM, alongside a zoomed view of a TM7 alignment, with $Y^{7.53}$ shown using sphere representation.

HN helix and the αN-β1 loop of $G\alpha_{i1}$. Unexpectedly, a second, 'non-canonical' conformation of the hNTS1-G_{i1} complex could be resolved, where TM5 & 6 are active-like but TM7 is inactive-like – there is no inwards movement and the $Y^{7.53}$ residue does not contact $R^{3.50}$ (figure 1.10D). Notably, this receptor conformation is very similar to an intermediate state seen during simulations of β_2AR activation (Dror *et al*, 2011). The

disposition of the G protein with respect to the receptor is very different in the non-canonical conformation (figure 1.10C), and as such the precise receptor-G protein contacts change, whilst the G protein itself has a different conformation, including a less accessible nucleotide binding pocket. The fact that NTS1 shows active-like features upon crystallisation with an agonist and shows multiple G-protein bound conformations suggests that it has a different and potentially more complex conformational ensemble than the prototypical β_2AR. Such complexity may be related to the G protein coupling promiscuity of NTS1, with multiple conformations available to match multiple G protein partners.

1.3 Solubilisation and reconstitution of membrane proteins

Due to their hydrophobic nature, integral membrane proteins such as GPCRs are not soluble in aqueous solution in the absence of a lipid bilayer or a mimetic thereof. The following section outlines methods used to solubilise membrane proteins.

1.3.1 Detergents

Detergents are surfactants of an amphiphilic nature, with hydrophobic, non-polar "tail" and hydrophilic polar "head" moieties (figure 1.11, inset), which are capable of extracting and solubilising integral membrane proteins from lipid bilayers. In aqueous solution, detergents exist as monomers below the critical micellar concentration (CMC). Above the CMC, micellization occurs; detergents are driven by the hydrophobic effect to aggregate into structures called micelles, whereby the tail moieties pack together to reduce solvent exposure, whilst the headgroup moieties are presented to aqueous solution (figure 1.11, inset) (Anandan & Vrielink, 2016). Structures of some commonly used detergents are shown in figure 1.11.

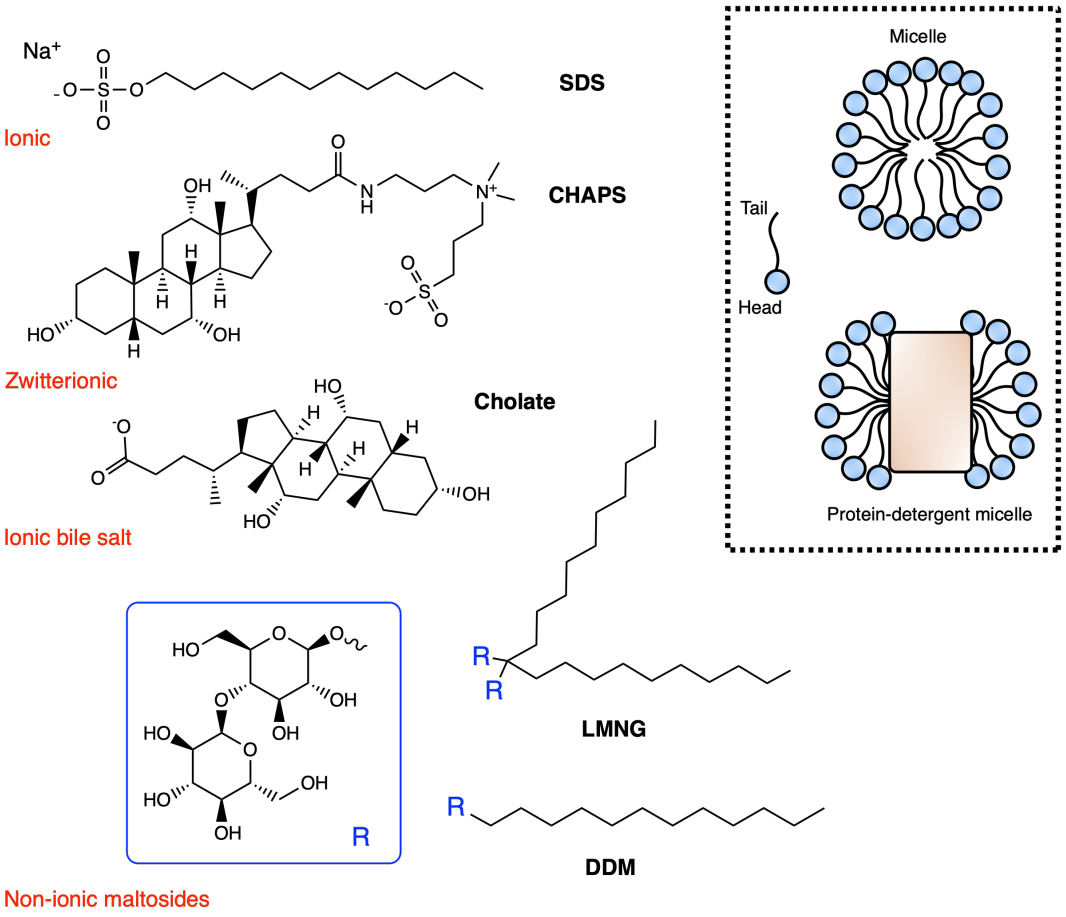


Figure 1.11: Structures of commonly used detergents. Examples of ionic, zwitterionic and non-ionic detergents are given. Inset: a detergent micelle and a protein-detergent micelle. See main text for abbreviations.

Detergents are typically classed as ionic (e.g. Sodium dodecyl sulfate (SDS), Sodium cholate), zwitterionic (e.g. 3-[(3-Cholamidopropyl)dimethylammonio]-1-propanesulfonate, CHAPS) or non-ionic (e.g. n-Dodecyl-β-D-Maltopyranoside, DDM) on the basis of the chemistry of the head moiety (Seddon *et al*, 2004). The non-ionic class are by far the most popular in membrane protein research (Stetsenko & Guskov, 2017), by virtue of the fact that their non-ionic headgroups are less competitive for protein-protein and protein-lipid interactions than ionic or zwitterionic detergents (Seddon *et al*, 2004). In addition to headgroup structure, it is generally found that shorter chain detergents are more denaturing (Tate, 2010). As such, non-ionic, longer-chained detergents are considered more "mild"/less "harsh" than ionic detergents based on their effects on protein activity.

Amongst the most popular detergents for solubilising poorly thermostable membrane proteins such as GPCRs are the maltoside detergents DDM and lauryl-maltose neopentyl glycol (LMNG) (Stetsenko & Guskov, 2017; Munk *et al*, 2019). However, even the mildest non-ionic detergents can potentially cause a loss of activity of membrane proteins during solubilisation, and so a variety of lipid-based systems have been developed to provide a more native-like environment for the study of membrane proteins.

1.3.2 Protein-based nanodiscs

Membrane scaffold proteins are amphipathic alpha helical proteins, derived from apoliprotein A-1, which will form nanoscale lipid bilayers upon mixing with a detergent-solubilised membrane protein and lipids when detergent is removed (Bayburt *et al*, 2002; Denisov *et al*, 2004). The particles are discoidal, with well-defined diameters which depend on the exact MSP construct used, but are in the 9-13 nm range (Denisov *et al*, 2004) and are generally referred to as "nanodiscs" (figure 1.12).

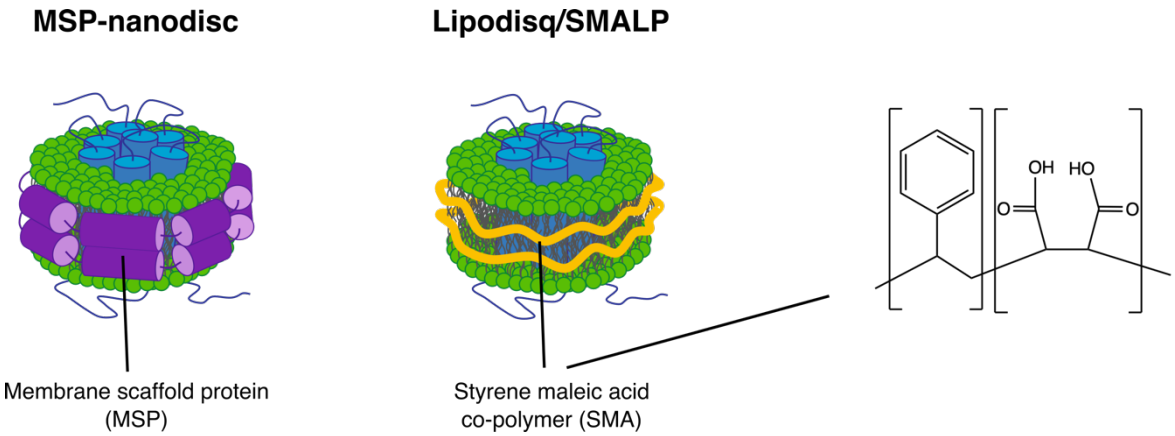


Figure 1.12: MSP-nanodiscs and SMALPs. In blue is a generic membrane protein consisting of transmembrane helices, with lipids in green. Amphipathic molecules act as "belts" which seal the edge of the bilayer; either membrane scaffold proteins or a styrene maleic acid co-polymer. Both approaches produce discoidal particles with diameters in the 10 nm range, but the Lipodisq approach does not require detergent. Nanodisc and SMALP cartoons reproduced from (Dörr et al, 2016).

They have been used to characterise membrane proteins, including GPCRs, by techniques including surface plasmon resonance (SPR) (Adamson & Watts, 2014), microscale

thermophoresis (MST) (Dijkman & Watts, 2015), double electron-electron resonance (DEER) (Van Eps *et al*, 2018), nuclear magnetic resonance (NMR) (Kofuku *et al*, 2014) and cryo-electron microscopy (Masiulis *et al*, 2019).

A similar technology, Salipro®, was first described in 2016 (Frauenfeld *et al*, 2016). Protein-lipid nanoparticles in this system are formed by reconstitution of detergent-solubilised lipid, membrane protein and an amphipathic protein called saposin A. Whereas a given MSP construct forms a nanodisc of a defined diameter, saposin A molecules oligomerise to form an appropriately proportioned nanodisc for the protein of interest. The system has seen use in the study of GPCRs by NMR (Chien *et al*, 2017) and was used to obtain a 3.8Å structure of the mitochondrial calcium uniporter by cryo-EM (Nguyen *et al*, 2018).

1.3.3 Polymer-based nanodiscs

An increasingly popular alternative to detergent based solubilisation is the use of styrene-maleic acid (SMA) co-polymers (Dörr *et al*, 2016; Bada Juarez *et al*, 2019). These polymers feature hydrophobic styrene and hydrophilic maleic acid monomers, with gross ratios of between 3:1 and 2:1 styrene:maleic acid being used (figure 1.12). SMA is capable of interacting with bilayers containing membrane proteins and solubilising them directly into lipid-protein nanoparticles known as Lipodisqs™ or SMALPs, in the complete absence of detergents (Knowles *et al*, 2009; Orwick *et al*, 2012) (figure 1.12). These discs are typically in the 10 nm range, similar to MSP-nanodiscs. As such, SMA is proposed to maintain functional protein-lipid interactions during purification, which may improve the activity and/or stability of the membrane protein compared to detergent-based methods (Overduin & Esmaili, 2019). Lipodisqs/SMALPs have also seen application in cryo-EM; the structure of the alternative complex III-cytochrome oxidase supercomplex solubilised with SMA was resolved to better than 4Å (Sun *et al*, 2018), with 11 lipid molecules resolved

in the EM density maps. Similarly, a 3.2Å structure of the AcrB multidrug exporter was solved in SMA, and again demonstrated well-ordered lipid densities (Qiu *et al*, 2018).

1.3.4 Liposomes

Liposomes are sealed bilayer vesicles containing aqueous lumens, which form spontaneously upon hydration of a dried lipid film and can possess a range of sizes and morphologies as summarised in figure 1.13 (Jesorka & Orwar, 2008).

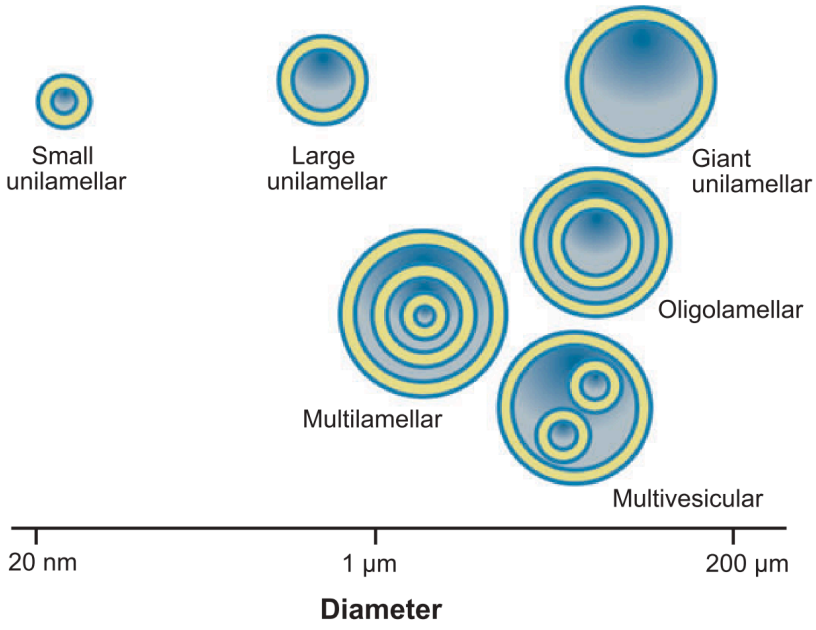


Figure 1.13: Size and morphology of different lipid vesicles. Vesicles are shown with a cross-sectional view. Reproduced from (Jesorka & Orwar, 2008)

Unilamellar vesicles generally have the most utility for membrane protein studies (Jesorka & Orwar, 2008). Of the unilamellar vesicles, large unilamellar vesicles (LUVs) are the most suitable for membrane protein reconstitution, since they are more easily handled than GUVs and have less curvature strain than SUVs (Warschawski *et al*, 2011). Reconstitution of membrane proteins into LUV liposomes involves the use of a purified detergent-solubilised protein, and a LUV preparation. LUVs are prepared from hydrated lipids by extrusion through polycarbonate filters, before the addition of a small amount of detergent

that saturates and destabilises the LUVs (Goddard *et al*, 2015). Reconstitution is then promoted by removal of detergent by rapid dilution below the CMC or use of adherent polystyrene beads.

LUVs are thus relatively easy to prepare and provide a native-like bilayer environment for membrane proteins (Serebryany *et al*, 2012; Warschawski *et al*, 2011). The bilayer formed is considerably larger than that in nanodisc systems, but the sealed nature of LUVs means it may be difficult to study processes which require access to both faces of a membrane protein.

1.4. Electron paramagnetic resonance

In electron paramagnetic resonance (EPR), also known as electron spin resonance (ESR), the signal arises from transitions between different energy states for an unpaired electron in a magnetic field. Continuous wave EPR (CW-EPR) refers to the application of continuous microwave radiation to the sample, to distinguish it from pulsed EPR techniques such as double electron-electron resonance (DEER).

1.4.1 Site-directed spin labelling (SDSL)

A majority of proteins and other biological macromolecules do not natively possess unpaired electrons, and so to study proteins by CW-EPR, a species containing an unpaired electron ("spin label") is covalently attached to the protein of interest at a specific site: site-directed spin labelling (SDSL). By far the most common spin labels are the nitroxide labels, and it is these species that will be considered in the description of EPR in this section. In particular, the most commonly used nitroxide label is the 2,2,5,5-tetramethyl-l-oxyl-3-methyl methanethiosulfonate compound, known commonly as MTSL (Hubbell *et al*, 1996; Berliner *et al*, 1982) (figure 1.14). This compound offers specific labelling of free thiols, and so can be used to introduce a stable free electron to proteins via cysteine residues. To gain

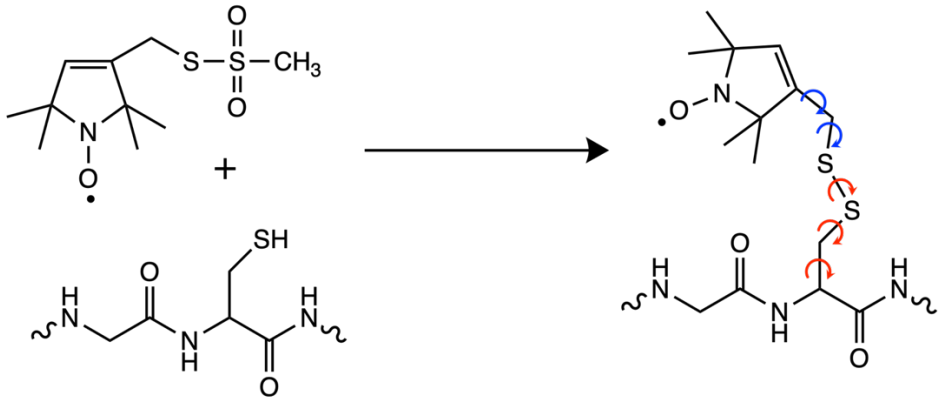


Figure 1.14. Site directed spin labelling of cysteine residues. Labelling of a protein cysteine by MTSL is shown. In the MTSL-protein product, 5 bonds connect the nitroxide ring to the alpha carbon of the cysteine. Only those shown with blue arrows show significant rotation (see section 1.4.4).

site-specific information, any native cysteine residues must be mutated (typically to alanine or serine) and then specific cysteine residues introduced. The MTSL label linked to a cysteine residue produces a relatively small label, especially when compared to most fluorophores. Spin labelling with MTSL is thus generally considered non-perturbing (Klug & Feix, 2008; Jeschke, 2013).

1.4.2 Basics of EPR

An electron possesses a spin, S, of ½. In the presence of an external magnetic field, B_0, two degenerate spin states or energy levels exist, described as m_s = + ½ or – ½ (figure 1.15). The lowest energy state (m_s = - ½) occurs when the electron spin is aligned with this field (the Zeeman effect). When considering the energy states for nitroxide labels such as MTSL, in addition to the Zeeman effect, the hyperfine interaction is also important. This arises from the interaction between the unpaired electron and the ^{14}N nucleus of the label. This nucleus has S = 1, giving states of m_I = +1, 0 or -1 that are available for each value of m_s. Consequently, there are six energy states for the unpaired electron in a nitroxide label (figure 1.15A), with three possible transitions that obey both the resonance condition and the quantum selection rules (figure 1.15B). Practically speaking, in CW-EPR, transitions between different electron energy states are achieved by sweeping the magnetic field for a

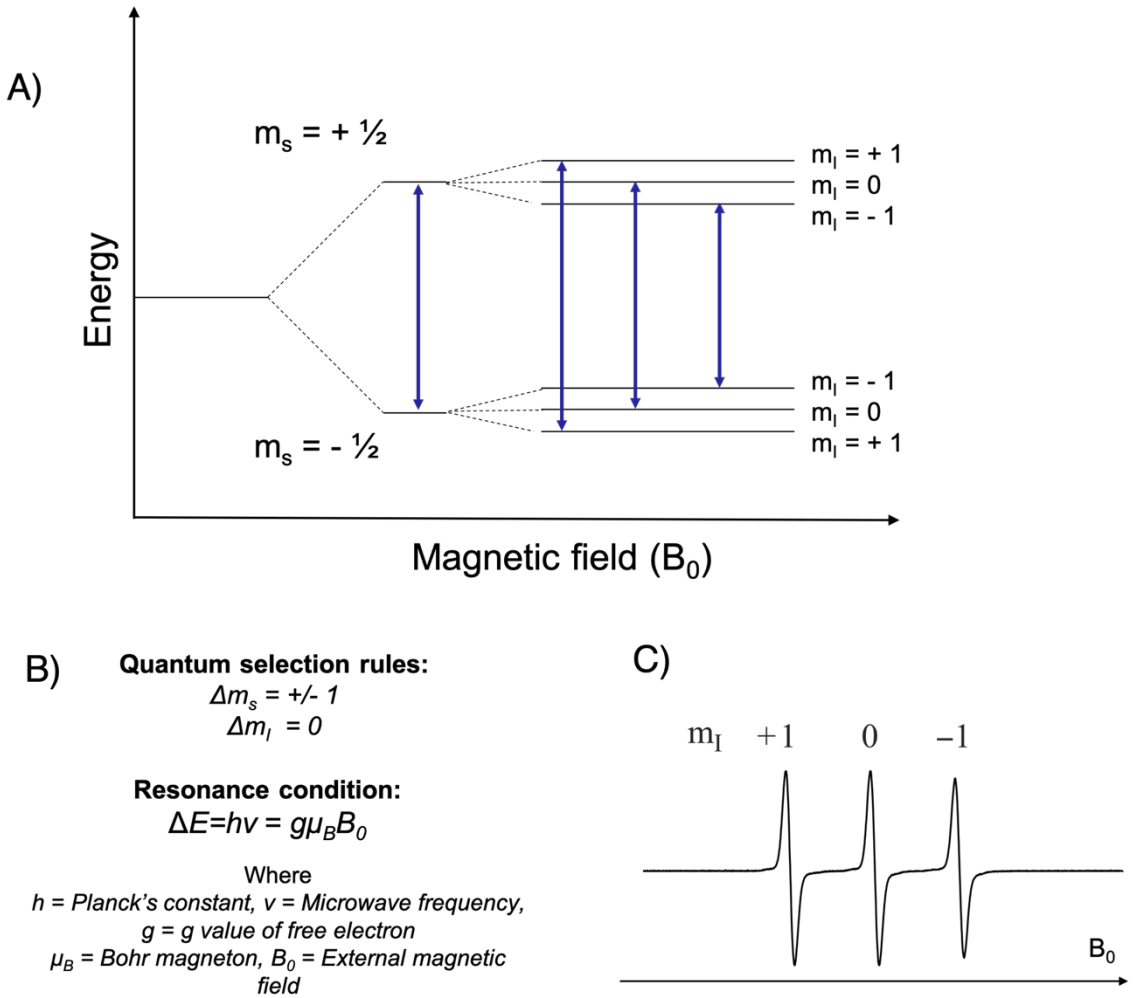


Figure 1.15: Basics of EPR. A) Energy levels for a nitroxide spin label in a magnetic field, with allowed transitions shown by blue arrows. B) Both the quantum selection rules and resonance condition must be satisfied for a transition to occur. C) solution-state first derivative spectrum for a nitroxide probe, reproduced from (Klug & Feix, 2008).

constant microwave energy. Sensitivity is also enhanced through frequency modulation – as B_0 is varied, it fluctuates at a frequency of ~100 kHz. The result is that the signal from the cavity is also modulated at the same frequency, which results in the signal being reported as a first derivative of absorption. For a free nitroxide label in solution, 3 spectral lines occur in the first derivative spectrum as a result of the 3 allowed transitions (figure 1.15C).

1.4.3 Anisotropy and motion in EPR

The distribution of unpaired electron density in the nitroxide makes the EPR spectral parameters anisotropic. Both the Zeeman splitting (described by the g-factor tensor) and the hyperfine splitting (described by the A-factor tensor) are anisotropic –that is, changes in the orientation of the spin label with respect to the resonant magnetic field will drastically alter spectral appearance. For a nitroxide probe in conventional CW-EPR, the hyperfine anisotropy dominates. In figure 1.16, spectra are shown for a crystalline nitroxide probe oriented along various axes to demonstrate this.

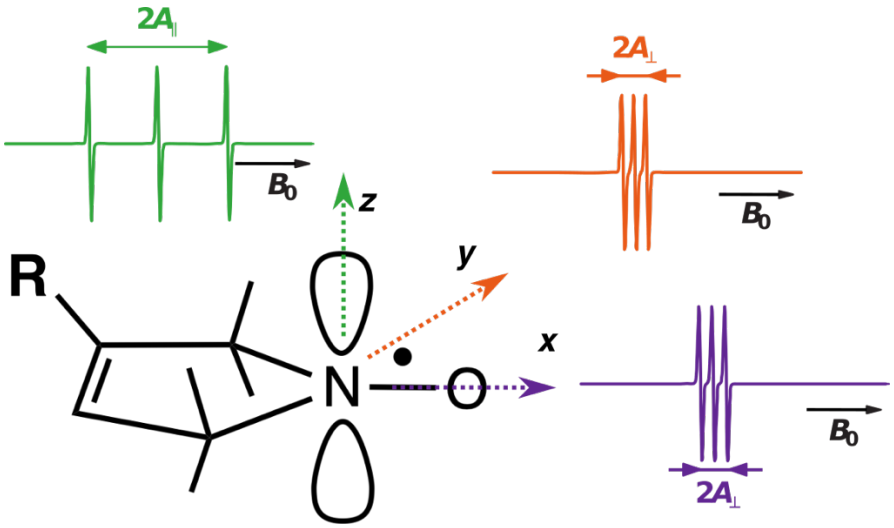


Figure 1.16: Orientation-dependence of nitroxide EPR spectra. Shown are spectra simulated for crystalline, oriented nitroxide spin label samples, adapted from (Jeschke, 2012). The '2A' parameters describe the splitting of the most extreme spectral features.

For a spin label in solution, rapid, isotropic tumbling of the molecule will average the anisotropy (figure 1.17). The rate of motion at which this occurs (the "fast limit") corresponds to a rotational correlation time, τ_c, of less than 100 ps, where τ_c is defined as:

$$\tau_c = \frac{4\pi\eta r^3}{3kT}$$

Where η is the solvent viscosity, r is the hydrodynamic radius, k is the Boltzmann constant and T the absolute temperature. Similarly, when τ_c > 100 ns, the spectral

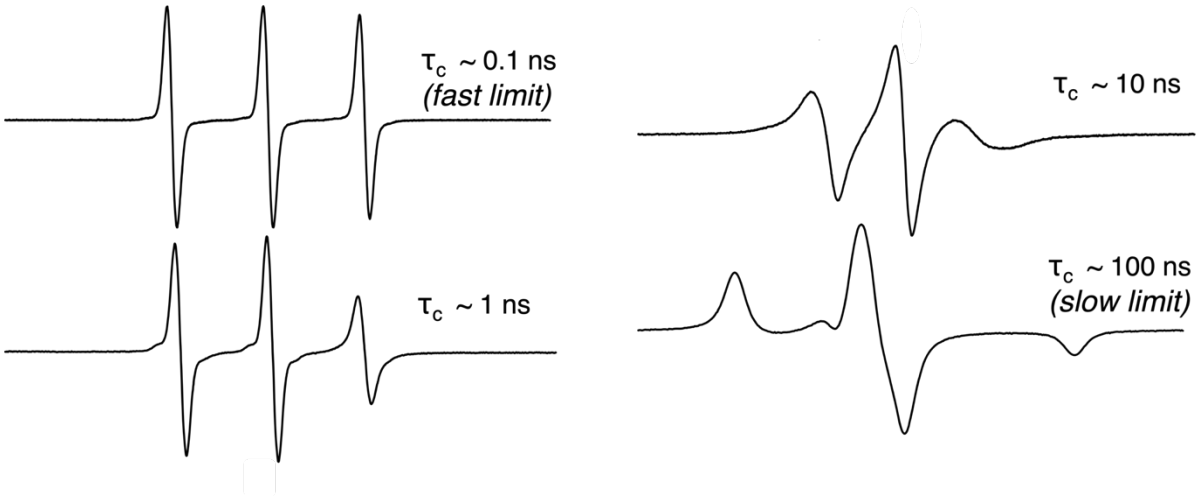


Figure 1.17: Sensitivity of nitroxide spectra to dynamics. Spectra reproduced from (Klug & Feix, 2008)

appearance corresponds to that of a "powder spectrum", whereby the spectrum is a sum of nitroxide signals over all orientations. Between these two limits, the appearance of the nitroxide EPR spectrum is highly sensitive to changes in dynamics of the spin label (figure 1.17).

1.4.4 CW-EPR and protein dynamics

For the MTSL label covalently linked to a cysteine side chain, there are multiple potential modes of motion, which together will average spectral anisotropy and contribute to the overall spectral shape (Klug & Feix, 2008; Wingler *et al*, 2019b).

Firstly, the internal motion of the tethered spin label should be considered. Of the 5 bonds that link the nitroxide ring to the Cysteine Cα (figure 1.14), spin label internal motion is dominated by oscillation about the final two bonds, giving this internal motion anisotropy (Columbus *et al*, 2001). Consequently, if the spin label is attached to a rigid, surface-exposed helix (where the backbone is relatively immobile and there are no spin label-protein interactions) these modes of motion will dominate the appearance of the spectrum (figure 1.18). The apparent mobility of the nitroxide (and consequently the spectral appearance) can then be modulated by other motions/interactions in the protein. Apparent mobility will be increased by fluctuations of the protein backbone, for example if

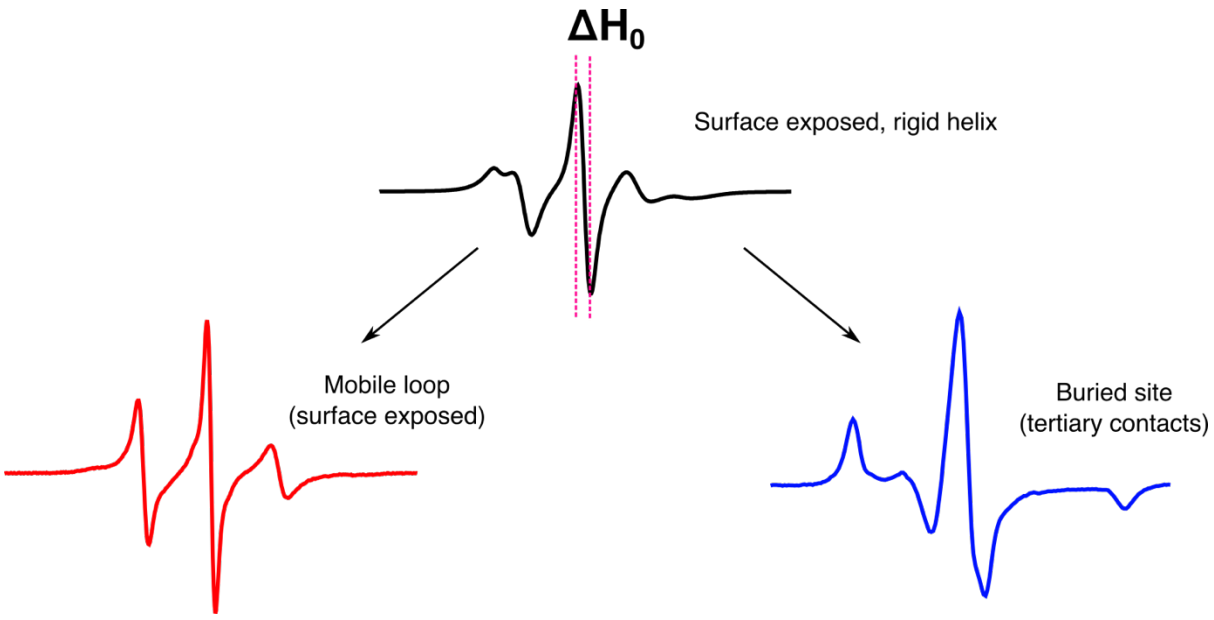


Figure 1.18: EPR and protein dynamics. Spectra are shown for a spin label in three different protein environments. Spectra reproduced from (Altenbach et al, 2015).

the spin label is placed in a more mobile surface-exposed helix or loop region. Mobility will be decreased by interaction with protein structure ('tertiary contacts') – for example, if the spin label is buried in the protein structure or involved in interaction with a binding partner. This is demonstrated in figure 1.18.

It should be noted that rotational diffusion of the entire protein can influence the spin label mobility, but under typical experimental conditions this is only true for small proteins of molecular weight <20 kDa (Bordignon, 2013). An important consequence of this phenomenon is that membrane proteins can be studied in native-like environments such as liposomes, without any spectral broadening.

Quantification of spin label mobility can be performed by simulation of spectral lineshapes (Columbus *et al*, 2001). However, simple visual inspection can be informative. As can be seen in figures 1.17 and 1.18, more mobile spin labels have narrower spectral features, especially the central linewidth, and less mobile spectra show line broadening and appearance of 'shoulders' at the extremes of the spectrum. The central linewidth, ΔH_0

(figure 1.18) can be used to give a simple, overall measure of spin label mobility. In particular, the inverse of the central linewidth, ΔH_0^{-1}, is frequently used, since this parameter increases with increasing spin label mobility.

Finally, it is not uncommon for EPR spectra of nitroxide-labelled proteins to contain contributions from several different spin label populations of different mobilities ('multi-component' spectra). This can result from multiple conformations of the protein in question, but it can also be a result of different rotameric states of MTSL (Altenbach *et al*, 2015). In the literature, contributions from less and more mobile components are often denoted by the labels "immobile" and "mobile".

1.4.5 CW-EPR and protein secondary structure

If a sequence is asymmetrically packed (for example, one surface faces the protein core and another solution), then as mobility measurements (typically ΔH_0^{-1}) are taken along the sequence, one can observe periodic oscillations in mobility that reflect the secondary structure of that sequence (Hubbell *et al*, 1996; Klug & Feix, 2008) (figure 1.19).

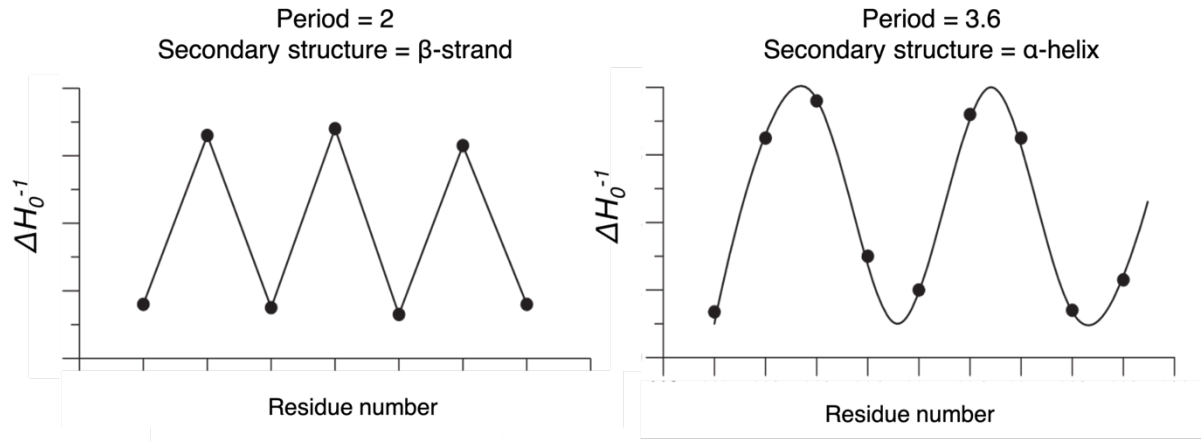


Figure 1.19: EPR and secondary structure. Theoretical mobility plots are shown for beta strands and alpha helices, adapted from (Klug & Feix, 2008).

This approach to determining protein topology has been demonstrated for a wide variety of proteins, including soluble proteins such as T4 lysozyme and cellular retinol binding

protein (CRBP) (Hubbell *et al*, 1996) as well as a host of membrane proteins. For the lactose permease, CW-EPR established the as-then unknown helical structure of its transmembrane segment (Voss *et al*, 1996), whilst for the MscL channel, mobility plots obtained in different functional states demonstrated considerable changes in conformation and dynamics (Perozo *et al*, 2002).

1.4.6 CW-EPR & GPCRs

The use of CW-EPR to define protein topology and conformational changes has been applied to a single GPCR to date, rhodopsin. A series of pioneering SDSL studies from Wayne Hubbell's lab in the 1990s used CW-EPR to define protein topology (Altenbach *et al*, 1996, 1999a, 1999b; Langen *et al*, 1999) and conformational changes (Farrens *et al*, 1996) that were validated by crystallographic approaches almost an entire decade later (Scheerer *et al*, 2008).

Whilst crystallography and cryo-EM are now well-established structural techniques and have solved a considerable number of GPCR structures, CW-EPR still has considerable utility. Structural techniques are typically conducted in detergents or lipidic cubic phases which poorly mimic bilayers, may require substantial receptor engineering and typically poorly resolve dynamic elements such as loops and termini. CW-EPR offers insights that can complement these techniques, since it can report on topology and dynamics in a native-like membrane environment such as a liposome and requires small amounts of material (nanomoles) that may facilitate the use of wild-type like receptor constructs.

1.5 Native mass spectrometry

Native mass spectrometry (native MS) refers to mass spectrometry techniques in which the sample to be studied is ionised from a solution in which it has a native like structure and/or activity, as opposed to methods that apply denatured samples to the mass spectrometer

(Leney & Heck, 2017). With this technique, it is possible to maintain non-covalent interactions and even native-like conformations of a macromolecule in the gas phase inside a mass spectrometer (Mehmood *et al*, 2015).

The development of native MS has relied on electrospray ionisation (ESI) techniques (figure 1.20). In particular, nano-ESI is fundamental to most native MS studies. In nano-ESI, a much smaller capillary is used, with a slower flow rate and smaller sample volume (microlitres) (Konijnenberg *et al*, 2015). An important consequence of this is that much smaller droplets are produced, and so organic solvents do not need to be added to the sample to ensure desolvation, and the process is more tolerant of salts (Mehmood *et al*, 2015; Leney & Heck, 2017). As such, this ionisation process is ideal for studying macromolecules since it allows the production of multiply charged gas phase ions directly from an aqueous solution that is compatible with biological activity of the macromolecule of interest.

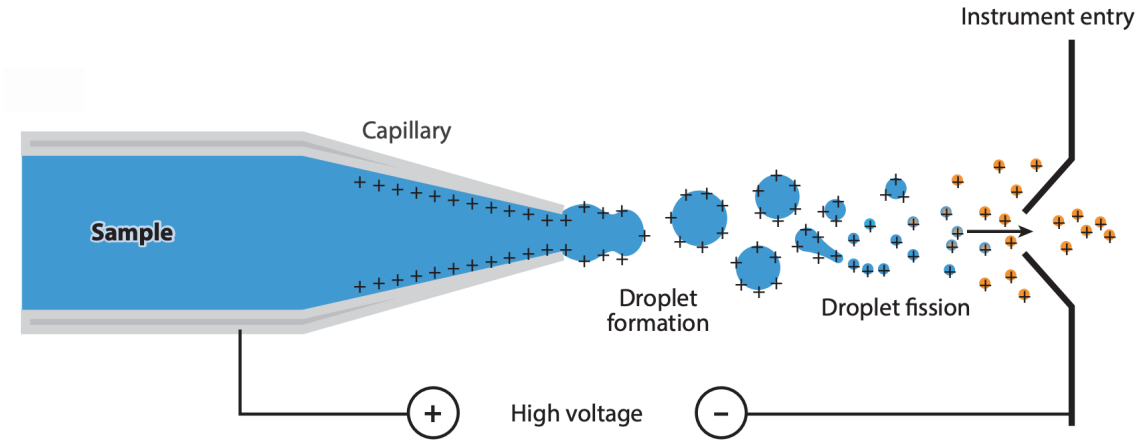


Figure 1.20: Electrospray ionisation. The sample of interest is passed through a capillary under voltage, which leads to production of charged droplets. These droplets then undergo fission events and ultimately form gas-phase ions that enter the mass spectrometer. Figure reproduced from (Mehmood et al, 2015).

In applying such a technique to membrane proteins, there are additional factors to consider. In order to gain interpretable mass information, ultimately the detergents that solubilise a membrane protein in solution must be removed (Mehmood *et al*, 2015).

Initially, detergents were anticipated to greatly suppress signals from membrane proteins (Konijnenberg *et al*, 2015). However, seminal work demonstrated that a membrane protein complex could remain intact inside the mass spectrometer when it was transferred into the gas phase whilst still protected by detergent (Barrera *et al*, 2008). The detergent could then be removed from the membrane protein by collisional-induced dissociation (CID), whereby ions are bombarded by neutral gas molecules.

Since this initial demonstration, the instrumentation and sample preparation for native MS have been optimised to the extent that the technique can now resolve bound lipids with subtly different acyl chain lengths (Gault *et al*, 2016). A typical modern experimental setup for high resolution native MS of membrane proteins involves nano-ESI to generate protein-detergent ions, which are then transferred under low voltage with a gentle gradient such that ions are not collisionally activated (Gault *et al*, 2016; Yen *et al*, 2017). The ions are then captured in an HCD cell, which is a CID cell with a higher voltage to allow for complete detergent removal, before the ions are transferred to an Orbitrap mass analyser for detection.

The application of native MS to GPCRs is still very much in its infancy, with just a handful of studies published to date. Spectra have been obtained for CCR5 (Gault *et al*, 2016), thermostabilised β_1AR (Gavriilidou *et al*, 2019; Yen *et al*, 2018), thermostabilised rNTS1 (Yen *et al*, 2018), A_{2A}R (Yen *et al*, 2018) & the purinergic P_2Y_1 receptor (P_2Y_1R) (Yen *et al*, 2017). Pioneering work by the Robinson group has identified detergent conditions under which the GPCR is active and can be transferred to the gas phase with the protein still protected by detergent (Yen *et al*, 2017). Using these conditions, it has been demonstrated that binding of both ligands, lipids and G proteins can be resolved by native MS (Yen *et al*, 2017, 2018). A such, there is considerable scope for native MS to inform on small molecule

binding and post-translational modifications of GPCRs, especially since the technique can reveal sample heterogeneities that are largely undetected by other techniques.

1.6 GTPase-Glo™ assay

The GTPase-Glo™ assay is a GTP turnover assay developed by Promega, to assay the GTPase activity of G proteins, including heterotrimeric G proteins (Mondal *et al*, 2015).

In this assay, the readout is a luminescent signal that reflects the amount of residual GTP in a sample (figure 1.21). As shown in figure 1.21, the *greater* the luminescence signal, the *less* active the G protein, since it reflects that less GTP hydrolysis has occurred.

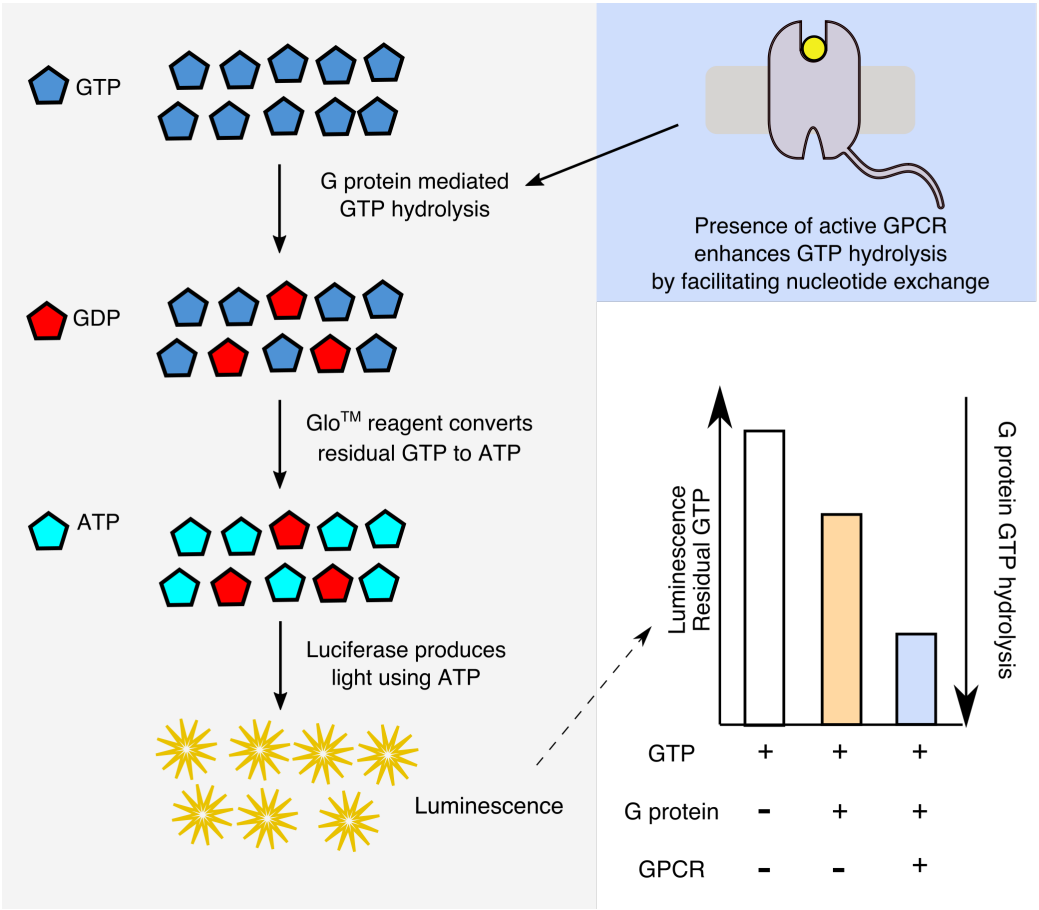


Figure 1.21: GTPase-Glo™ assay set-up. GTP and G protein are mixed to initiate the GTPase reaction. The GEF activity of a GPCR can stimulate further GTP hydrolysis (blue box). A series of enzymes then convert residual GTP to a luminescence signal, which is inversely related to G protein activity. Based on an image on Promega website. Receptor cartoon adapted from (Weis & Kobilka, 2018).

For heterotrimeric G proteins, the signal is also affected by the presence of $MgCl_2$ and GDP, since these compounds will modulate GDP release, which is the rate determining step for GTP hydrolysis by these proteins (Higashijima *et al*, 1987). The presence of an agonist-bound GPCR will stimulate GTP hydrolysis (figure 1.21, blue box), since the GPCR catalyses exchange of bound GDP for GTP. The assay therefore provides a functional readout of GPCR activity, since a more active GPCR will stimulate more GTP hydrolysis at the G protein. Consequently, this assay has been used to monitor the effects of ligands (Krishna Kumar *et al*, 2019), receptor ICL3 truncations (Kato *et al*, 2019) and lipids (Strohman *et al*, 2019) on GPCR activity at a G protein.

1.7 Aims

The primary aim of this thesis is to gain insights into GPCR function at the molecular level, using the neurotensin receptor 1 as a model.

- An *E.* coli expression system will be used to produce a series of specific cysteine mutants of a wild-type like rNTS1 construct, covering helix 8 and the proximal C-terminus of rNTS1. Published structures show conflicting conformations of this region, so SDSL and CW-EPR will be used to elucidate the conformational dynamics of the proximal C-terminus of NTS1 (chapter 2).
- Insect cell expression systems will be employed to express hNTS1 and two different heterotrimeric G protein signalling partners, G_{i1} and G_q, and a GTP turnover assay used to assay receptor-G protein coupling. In addition, native mass spectrometry will be used to explore the post-translational modifications and small molecule binding of hNTS1 (chapter 3).
- The GTP turnover assay will be used to elucidate how lipids modulate coupling of NTS1 to G_{i1} and G_q (chapter 4).

- A novel polymethacrylate polymer will be used to purify NTS1 in the total absence of detergent and compare the activity of the resulting material to detergent-solubilised material (chapter 5).

2. Conformational dynamics of NTS1 helix 8

2.1. Introduction

GPCR structures are characterised by a seven transmembrane helix topology, and in most cases, an additional non-transmembrane helix is located between TM7 and the C-terminus – the so-called "helix 8". Alignment of class A sequences using GPCRdb (Isberg *et al*, 2014; Pándy-Szekeres *et al*, 2018) identifies a semi-conserved sequence motif for helix 8 "xxxF(R/K)xx(F/L)xxxL" (figure 2.1A). The most conserved individual residue is $F^{8.50}$ (65%), but a pattern of polarity and hydrophobicity is also strongly conserved, which gives the helix amphipathicity. Indeed, in the canonical helix 8 conformation observed in class A GPCR structures (figure 2.1B), helix 8 sits almost perpendicular to the membrane plane, packed against TM1 and ICL1 of the receptor core. Membrane proximity and interaction may further be facilitated by the presence of S-palmitoylation on partially conserved cysteines at the C-terminus of helix 8 (reviewed in (Chini & Parenti, 2009; Escribá *et al*, 2007; Qanbar & Bouvier, 2003)).

2.1.1 Roles for helix 8 in GPCR function

The role of helix 8 in GPCR function remains ambiguous. In contrast to well-characterised structural elements such as TM6, helix 8 does not undergo consistent conformational changes when comparing receptor active and inactive states for class A receptors (Weis & Kobilka, 2018; García-Nafría & Tate, 2019) (see section 1.2.3 and figure 1.5).

A)

Residue position	8.47	8.48	8.49	8.50	8.51	8.52	8.53	8.54	8.55	8.56	8.57	8.58
Consensus	**N**	**K**	**N**	**F**	**R**	**R**	**A**	**F**	**R**	**R**	**L**	**L**
Conservation (%)	24	20	13	65	54	24	21	35	22	16	28	42
Hydrophobic (%)	13	18	14	93	9	17	42	92	39	22	76	85
Hydrogen bonding (%)	69	77	79	12	88	82	55	10	74	21	9	36
β_2AR	S	P	D	F	R	I	A	F	Q	E	L	L

B)

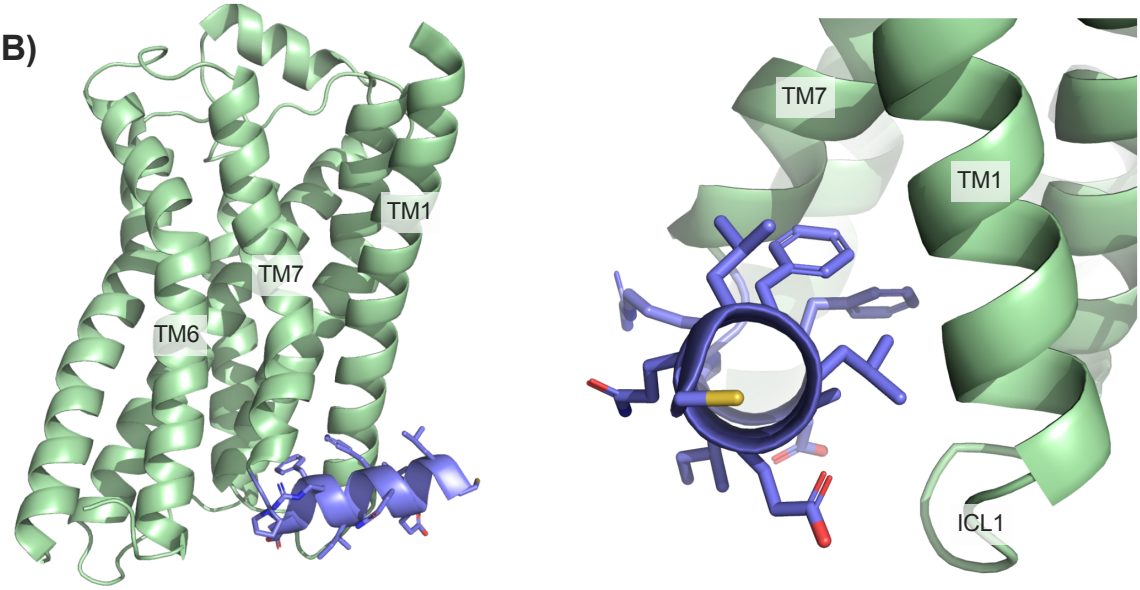


Figure 2.1: Helix 8 sequence & structural characteristics. A) Alignment of class A GPCR sequences reveals a consensus sequence for helix 8. Positions with >50% conservation are highlighted in red; only $F^{8.50}$ and $R^{8.51}$ show high conservation as specific residues, but the pattern of polarity across the sequence is highly conserved. The sequence corresponding to the prototypical β_2-adrenergic receptor is also shown. B) The canonical helix 8 conformation as viewed in the context of the whole receptor (left) and from the C-terminus of helix 8 (right), using the β_2AR in its inactive state (PDB 2RH1, (Cherezov et al, 2007)) as an example.

However, several studies point to a role for helix 8 in the interaction between receptor and G protein. From a structural perspective, some GPCR-G protein complex structures show contacts between the N-terminus of helix 8 and the Gα α5 helix, for example the G_s-coupled $A_{2A}R$ (García-Nafría *et al*, 2018a) and the G_i-coupled $5HT_{1B}$ (García-Nafría *et al*,

2018b). Moreover, synthetic peptides of rhodopsin helix 8 inhibit the receptor-G_t interaction (Marin *et al*, 2000), whilst for the AT_1R, helix 8 peptides are capable of binding and stimulating GTP turnover at the G_q heterotrimer (Sano *et al*, 1997). For the M_3R, crosslinking studies reveal that ligand binding induces contact between helix 8 residues and the α4-β6 loop of $G\alpha_q$ (Hu *et al*, 2010). In cellular signalling studies, truncation or deletion of the helix 8 sequence for AT_1R, protease-activated receptor 1 (PAR1) and rhodopsin leads to defective G protein signalling (Zhu *et al*, 2015; Swift *et al*, 2006; Marin *et al*, 2000; Sano *et al*, 1997). Similarly, point mutations in the melanocortin receptor 3 (MC_3R) helix 8 or a triple alanine mutation in the M_1R helix 8 cause defects in cAMP signalling (Yang *et al*, 2015; Kaye *et al*, 2011). Finally, a solution NMR study of the μOR showed significant changes in helix 8 dynamics upon agonist binding, suggesting helix 8 may be involved in initial binding of the G protein (Sounier *et al*, 2015).

There is also evidence that helix 8 plays a role in receptor-arrestin interactions. In both published rhodopsin–visual arrestin crystal structures (Kang *et al*, 2015; Zhou *et al*, 2017), the finger loop of visual arrestin sits close to the N-terminal portion of rhodopsin helix 8. Time-resolved fluorescence depolarisation studies of the same interaction reveal that the dynamics of helix 8 vary depending on the degree of rhodopsin-arrestin engagement (Kirchberg *et al*, 2011). Helix 8 is important for interaction of the bradykinin B2 receptor (B_2R) with GRK3 and β-$arrestin_1$ (Feierler *et al,* 2011), whilst for the thyrotropin releasing hormone receptor 1 (TRH_1R_1), helix 8 residues are required for receptor phosphorylation by GRKs and subsequent arrestin interaction (Gehret *et al*, 2010).

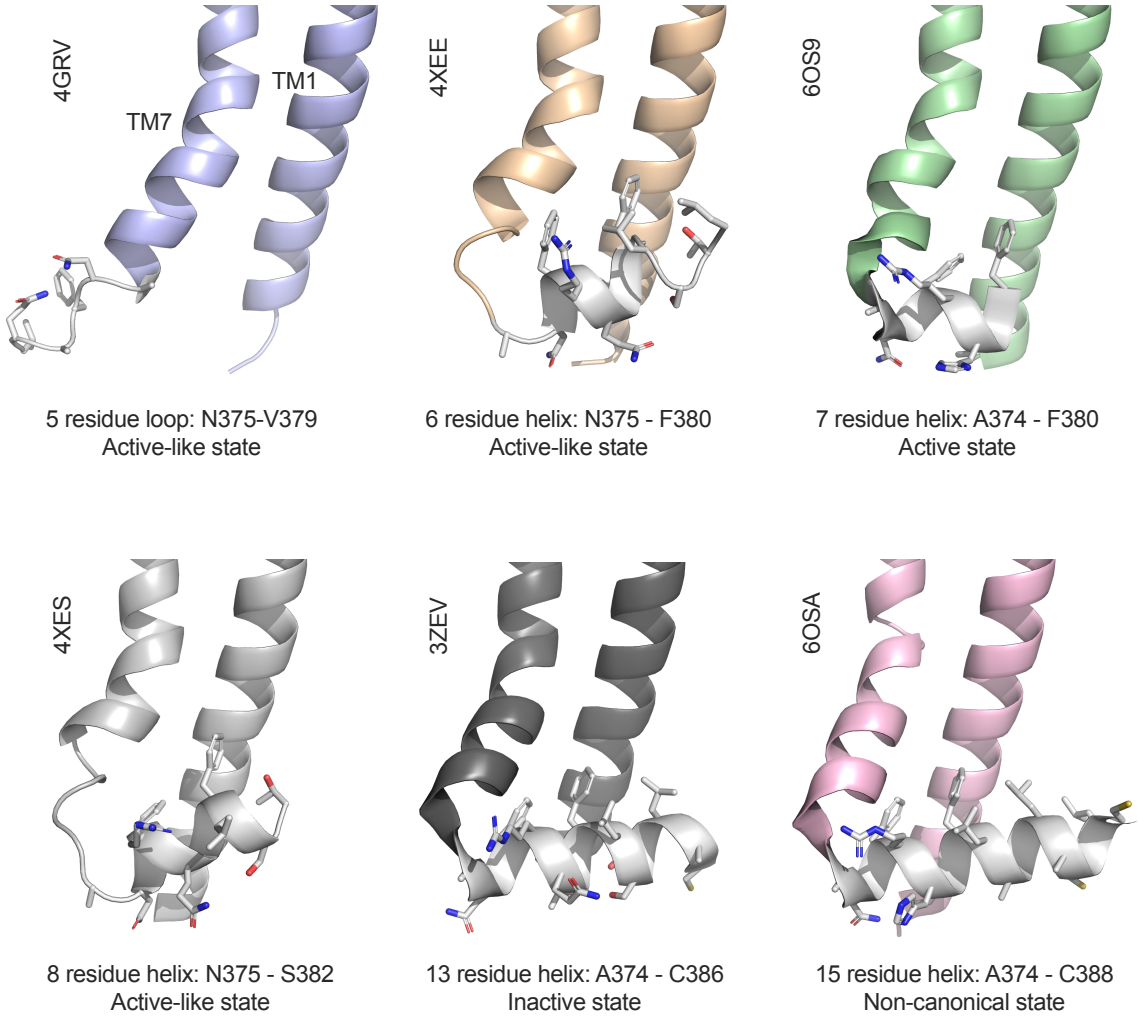
Helix 8 is also likely to have a role in lipid interactions. For rhodopsin, CB1 and β_2AR, studies on helix 8 peptides show that helix 8 structure depends on the presence of lipids or lipid mimetics (Krishna *et al*, 2002; Choi *et al*, 2005; Katragadda *et al*, 2004), whilst for the

AT_1R, the helix 8 sequence is proposed to interact with phosphatidylinositol phosphates (Hirst *et al*, 2015).

2.1.2 NTS1 helix 8

Truncation studies on rNTS1 define a role for its helix 8 in G protein activation. Truncation of the C-terminus beyond helix 8 does not affect $G_{i/o}$ and G_s signalling or receptor internalisation, but truncations of the C-terminus including helix 8 do (Najimi *et al*, 2002; Skrzydelski *et al*, 2003). More recently, a fusion construct containing a chimeric $G\alpha_{i1/q}$ protein fused N-terminally to the C-terminus of a thermostabilised rNTS1 construct was studied (Kumar & Plückthun, 2019). Various truncations of the receptor C-terminus were used, with truncations of helix 8 at A374, V379, L384 and P389 causing a significant loss of agonist-stimulated G protein coupling. Truncation after G390, leaving an intact helix 8, restores some of this coupling. This again defines a region of helix 8 and the C-terminus required for G protein stimulation.

Amongst the published NTS1 structures (see section 1.2.8.1), several different conformations of helix 8 are resolved (figure 2.2). The inactive-state structures published in (Egloff *et al*, 2014) all show a canonical-like helix 8 conformation, with the 13-residue helix of the 3ZEV structure shown as a representative example in figure 2.2. 4XEE and 4XES (Krumm *et al*, 2015) show shorter helices of 6 and 8 residues, respectively, with a different orientation of helix 8 compared to 3ZEV. The two recent cryo-EM structures of hNTS1 in complex with G_{i1} (Kato *et al*, 2019) show different helix 8 lengths. 6OSA has a 15 residue helix comparable to 3ZEV, whilst 6OS9 has a shorter helix. It should be noted that hNTS1 helix 8 sequence differs from rNTS1 by 3 residues (figure 2.2, bottom). Finally, the 4GRV (White *et al*, 2012) and 5T04 (Krumm *et al*, 2016) structures show no helix 8 at all. 4GRV is especially unusual in that helix 8 residues $N375^{8.49}$ – $V379^{8.53}$ form a loop structure at the end of TM7. In 5T04, TM7 terminates at V372. In all cases where helix 8



Residue position	8.47	8.48	8.49	8.50	8.51	8.52	8.53	8.54	8.55	8.56	8.57	8.58
Consensus	**N**	**K**	**N**	**F**	**R**	**R**	**A**	**F**	**R**	**R**	**L**	**L**
rNTS1	S	A	N	F	R	Q	V	F	L	S	T	L
hNTS1	S	A	N	F	R	H	I	F	L	A	T	L
rNTS1 numbering	373	374	375	376	377	378	379	380	381	382	383	384

Figure 2.2: NTS1 helix 8 conformations. Shown are views of TM1, TM7 and helix 8 for each structure, with side chain structures shown for helix 8. The length of helix 8 and the proposed receptor conformation is noted. 3ZEV is used as a representative of the four structures published in (Egloff et al, 2014). 5T04 is not shown, since there is no helix 8 and the core conformation is very similar to 4GRV. The 6OS9 and 6OSA structures are for an hNTS1 construct, but the numbering for the equivalent rat sequence is shown for simplicity. Bottom: NTS1 helix 8 sequences, with red residues denoting differences between the human and rat NTS1 sequences.

is resolved, it appears to be relatively poorly packed against TM1 compared to prototypical receptors such as rhodopsin, $A_{2A}R$ and β_2AR (Egloff *et al*, 2014).

The reasons for the structural plasticity of NTS1 helix 8 are currently unclear. Interpretation of the differing conformations is complicated by the use of different receptor sequences – as outlined in table 1.2 (section 1.2.8.1), the rNTS1 constructs used contain between 3 and 26 thermostabilising mutations, as well as different truncations, deletions and insertions of T4 lysozyme. Relatedly, the receptor constructs also have differing abilities to signal G proteins in *in vitro* assays, with 4XEE and the 6OS9/6OSA constructs showing wild-type like signalling, 4XES and 3ZEV showing reduced signalling and 4GRV and 5T04 showing no signalling. Whilst there is no clear correlation between the length & orientation of NTS1 helix 8 and the proposed overall inactive/active state conformation of the receptor, molecular dynamics simulations have suggested that agonist activation of NTS1 leads to changes in helix 8 dynamics (Lee *et al*, 2015; Nagarajan *et al*, 2019), and it is clear that helix 8 can play a role in G protein coupling for both NTS1 and many other GPCRs. It is tempting to speculate, therefore, that the different conformations of NTS1 helix 8 may have functional significance.

NTS1 is not the only GPCR to have a structure solved without helix 8, but such receptors are in the minority (22 out of >320 GPCR structures, representing 12 receptors; see appendix A1 for discussion). Even then, NTS1 is very unusual amongst such receptors in that it possesses the sequence determinants of helix 8 (figure 2.2, bottom) and is capable of displaying a canonical-like helix 8 orientation in addition to the more unusual conformations.

2.2 Aims

Given the potential role of helix 8 in GPCR function, the presence of different helix 8 conformations in NTS1 structures is suggestive of a role for helix 8 conformation and dynamics in receptor function. The aims of this chapter were therefore to:

- Establish the conformation of rNTS1 helix 8 in the absence of thermostabilising mutations or T4L insertions, and in a native-like lipid environment.
- Understand how helix 8 structure and dynamics are affected by activation of the receptor, by studying the receptor in the presence of agonist and the downstream signalling partners $G\alpha_{i1}$ and β-arrestin$_1$

To achieve these aims, 20 receptor mutants, each with a single accessible cysteine, were expressed, purified and spin labelled, to give a library of receptors each labelled at a specific position on helix 8. CW-EPR was then used to obtain site-specific dynamics and structural information on helix 8.

2.3 Materials and methods

2.3.1 Constructs used

In this chapter, the rNTS1 construct used is derived from the NTS1BH$_6$ construct described in (Dijkman & Watts, 2015), which in turn is based on the NTS1B construct described in (White *et al*, 2004). In order to ensure spin labelling of specific cysteines, a "ΔCys" construct was obtained, in which native surface accessible cysteines were mutated to serine or alanine. On this background, specific cysteines were introduced for labelling. The production and characterisation of the ΔCys construct was conducted by Dr Patricia Dijkman and is described in (Dijkman *et al*, 2018). Dr Dijkman also produced DNA for the 20 single cysteine mutants, which was used in expression & purification of rNTS1 here.

Figure 2.3 shows a schematic and snake plot of the rNTS1 sequence used, along with the native cysteine residues that were mutated, and the helix 8 sequence for which cysteine mutants were generated.

Tobacco etch virus (TEV) protease protein was a kind donation of Dr Roslin Adamson, who used a TEV-his$_6$ construct for expression, which was a kind donation to the Watts lab from Dr Huanting Liu and Dr Jim Naismith.

Gα_{i1} and β-arrestin$_1^{R169E}$ proteins were kind donations of Dr Patricia Dijkman and Dr Rosana Thevenot, respectively.

2.3.2 Expression & purification of NTS1 from *E. coli*

Expression & purification of the 20 NTS1BH$_6$ ΔCys mutants was carried out as described in (Dijkman & Watts, 2015). Full detail is given in appendix A2.

For spin labelling, NTS1 that had eluted from a ligand-affinity column was first concentrated by loading onto a 1 mL HisTrap equilibrated in 50 mM Tris pH 7.4, 15% glycerol, 200 mM NaCl, 0.1% DDM, 0.01% CHS. Resin was washed with this buffer and material eluted in 500 µL fractions by supplementation of the buffer with 500 mM Imidazole. The spin label MTSL (Toronto Research Chemicals) was prepared as a 50 mM solution in DMSO, diluted to 5 mM in MQ H_2O and added in 10-fold molar excess of NTS1 (22°C, 20 minutes), followed by a further 10-fold molar excess (22°C, 20 minutes). Material was then passed over two tandem 5 mL HiTrap HP desalting columns (GE healthcare) to remove free spin label and exchange into a final buffer of 50 mM Tris pH 7.4, 15% glycerol, 150 mM NaCl, 0.1% DDM, 0.01% CHS, 1 mM EDTA.

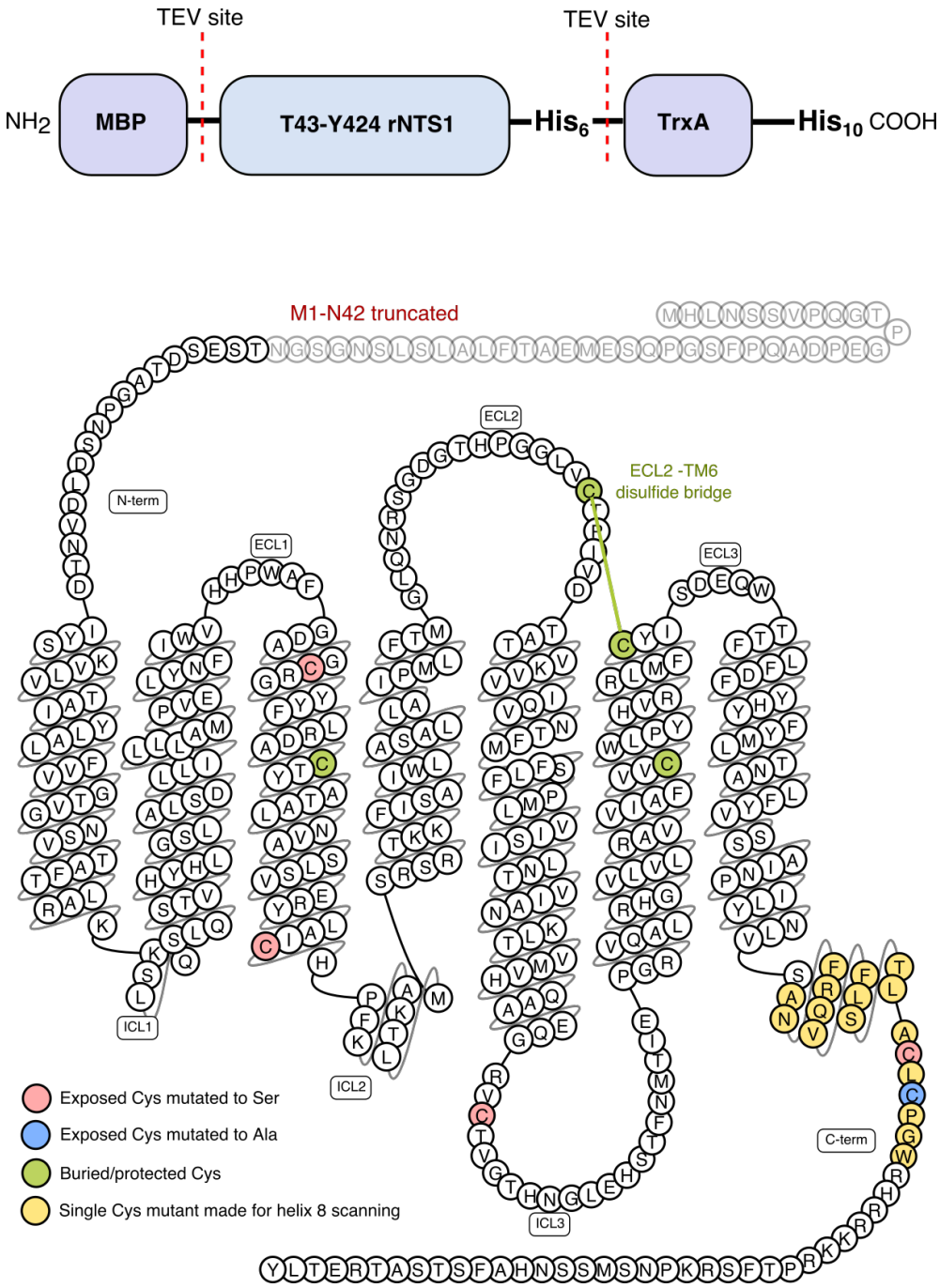


Figure 2.3: Features of the NTS1 constructs used in chapter 2. The features of NTS1BH$_6$ construct (top) and the rNTS1 sequence used (bottom) are shown. NTS1BH$_6$ features MBP and TrxA fusion partners for improved expression & stability. These are linked to the rNTS1 sequence by Tobacco etch virus (TEV) protease cleavage sites. The rNTS1 sequence features an N-terminal truncation. Red & blue highlighted cysteines were considered accessible and mutated. Yellow residues were individually mutated to cysteines for spin labelling. The snake plot diagram was generated using GPCRdb (Isberg et al, 2014; Pándy-Szekeres et al, 2018).

2.3.3 Preparation of NTS1 proteoliposomes

Lipids were purchased from Avanti Polar lipids as chloroform stocks. For this chapter, the Porcine "Brain Polar Lipid" (BPL) mix was used (table 2.3), which has been show to maximise ligand binding to NTS1 (Oates *et al*, 2012) and support high affinity $G\alpha_{i1}$ binding (Dijkman & Watts, 2015) versus simpler lipid compositions. On this basis the BPL mix is proposed to provide a functionally supportive lipid environment, which may mimic a native-like plasma membrane composition for the receptor. It should be noted that the mixture may be enriched or depleted in certain components versus a native membrane, and that the acyl chain composition of BPL lipids is not known. Given the presence of polyunsaturated fatty acyl chains in neuronal membranes (Sastry, 1985), it is anticipated these chains will be present in the mix and may have beneficial effects on receptor activity by analogy to rhodopsin, whereby polyunsaturated chains enhance receptor activation (Soubias *et al*, 2006) (see also section 4.1.1 of this thesis).

Lipid species	Percentage (wt/total wt)
PC	12.6
PE	33.1
PI	4.1
PS	18.5
PA	0.8
Unknown	30.9

Table 2.3: Lipid composition of Brain Polar Lipid Extract (Porcine). Reproduced from https://avantilipids.com/product/141101.

Hamilton syringes were used to decant an appropriate amount of lipid into a clean glass vessel, which was dried under a stream of nitrogen gas or using a rotatory evaporator depending on volume. This film was desiccated overnight under vacuum ($<10^{-5}$ torr). Lipid film was resuspended to 5 mg/mL in a buffer of 50 mM Tris pH 7.4, 50 mM NaCl, 1 mM

EDTA and 10% (w/v) glycerol ("liposome buffer"). A bath sonicator was used to ensure all lipid was dispersed from the glass surface. Lipids were then freeze-thawed 10 times using liquid nitrogen and a water bath (37°C) to facilitate formation of unilamellar vesicles. These vesicles were then sized with a mini extruder (Avanti Polar Lipids) by passing the material through 100 nm polycarbonate filters (Whatman) at least 11 times. Lipids were destabilised by addition of a saturating concentration of DDM (0.025% w/v, 1hr, 22°C).

For reconstitution of NTS1, lipids prepared freshly as above were mixed with NTS1 at a protein: lipid molar ratio of 1:1500 P:L (1hr with rotation, 4°C). For neurotensin-bound samples, the neurotensin 8-13 peptide (NT_{8-13}, Sigma Aldrich) was also included in the reconstitution mixture in molar excess to a final concentration of >5 μM. Biobeads (BioRad) were prepared by washing extensively in MeOH, H_2O and liposome buffer successively before addition of 300 mg wet Biobeads per 1 mL sample. The lipid-protein-Biobead mix was left rotating overnight at 4°C. The next day, Biobeads were removed by centrifugation and the supernatant ultracentrifuged (>120,000g, 4°C, 3 hrs). Pelleted liposomes were resuspended in liposome buffer and loaded into 0.5 mm glass capillaries, which were sealed by a flame at one end. Typically, each capillary contained approximately 10-20 μL of sample with 1-2 nmol of NTS1. For neurotensin-bound samples of NTS1 liposomes, NT_{8-13} was also included in the resuspension buffer to 20 μM, to ensure that the peptide was present on both sides of the liposomal membranes, since a random distribution of receptor insertion topologies is assumed.

For experiments involving $G\alpha_{i1}$, a 15-fold molar excess of the protein versus the receptor was introduced both during reconstitution and in the resuspension buffer. Where GTPγS was used, it was added to the reconstitution and resuspension buffers to 100 μM final. For experiments with β-$arrestin_1$, a 2-fold molar excess with respect to receptor was used. The β-$arrestin_1$ R169E mutant was used, since this protein has a disrupted polar core that

renders it constitutively active and so able to bind unphosphorylated receptors (Gray *et al*, 2003). Unless otherwise stated, for all cysteine mutants, two replicate samples from the same purification were prepared for EPR data collection.

2.3.4. CW-EPR experiments and analysis

Data were collected on an X-band EMXmicro CW spectrometer (Bruker) at the CAESR facility in the Department of Chemistry, Oxford. A temperature of 295K was maintained by a stream of N_2 gas applied to the sample holder, and the temperature was regularly monitored by a probe thermometer between sample measurements.

Data were collected with a sweep width of 200 G centered at 3300 G, with a sweep time of 45s and a time constant set to 1/10 of the conversion time. Modulation amplitude was set to 1.5 G, microwave power was set to 10 mW and receiver gain to 60 dB. 10-30 scans were recorded per sample.

EPR spectra were plotted in Microsoft Excel and normalised by integration of the absorption spectrum to calculate the relative number of spins in each sample.

The ΔH_0^{-1} parameter was derived using the "area under curve" function in Graphpad Prism to find the width of the central line and thus its inverse (ΔH_0^{-1}). A plot of ΔH_0^{-1} vs residue number then fit to a sine wave with a period of 3.6 using Graphpad Prism. In fitting the sine wave, a minimal number of helices (i.e. discontinuous sine waves) were used to avoid overfitting and the start and end of the helix was constrained to fall on a residue. The residuals produced by the fit were inspected for random distribution.

2.3.5 Acknowledgement

Protein expression, purification and spin labelling and EPR data collection were all performed in collaboration with Dr Patricia Dijkman, with the work split equally.

2.4. Results

2.4.1 Purification of NTS1 cysteine mutants

In order to assess the dynamics of the putative helix 8 region, 20 cysteine mutants were chosen which cover from the end of TM7 (A374) into the distal C-terminus (H393C) (figure 2.4A). This sequence covers well beyond the length of any of the helix 8 lengths resolved by structural biology techniques to date (figure 2.2).

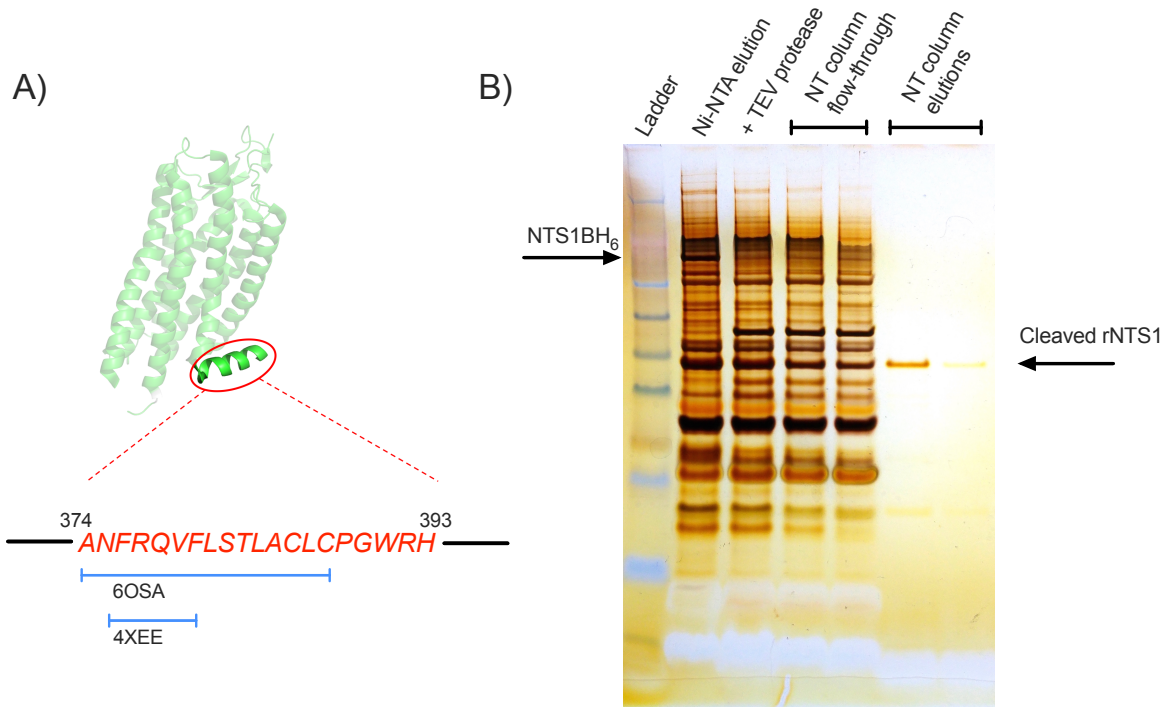


Figure 2.4: Purification of 20 cysteine mutants of rNTS1 A) Schematic showing the sequence for which individual cysteine mutants were made, with the lengths of the longest and shortest helices resolved by structural methods indicated, and the 3ZEV structure as a reference. B) Silver-stained SDS-PAGE gel demonstrating TEV cleavage of the F376C receptor and its salt-sensitive elution during ligand-affinity chromatography.

Purification of the receptor involves an initial purification using the affinity of the his-tagged receptor for Ni-NTA resin, followed by TEV cleavage of fusion tags and final purification using a column containing an immobilised form of the NTS1 agonist, NT_{8-13}.

The SDS-PAGE gel in figure 2.4B outlines this purification process, using cysteine mutant F376C as a representative example.

The gel shows the crude material that elutes from Ni-NTA resin, followed by TEV cleavage of fusion tags and purification of the receptor by ligand affinity chromatography. The gel lanes show that a majority of receptor material is found in the flow through of this column, which is a known limitation of the *E. coli* expression system (White & Grisshammer, 2010). Nonetheless, a clean NTS1 band can be seen upon elution with 1M NaCl, demonstrating that the receptor is functional with respect to ligand binding (White *et al*, 2004). This was found to be the case for each of the 20 cysteine mutants, demonstrating that no helix 8 mutation perturbed the ability of the receptor to bind its ligand.

2.4.2 CW-EPR spectra

All mutants were spin labelled with MTSL and reconstituted into a native-like lipid mixture. The CW-EPR spectra obtained for the receptor constructs demonstrate the success of the spin labelling and reconstitution procedure, since a strong signal is obtained for each mutant with no detectable contribution from free spin label (figure 2.5). The latter is easily detected since its mobility differs considerably from that of spin labels covalently linked to proteins (Klug & Feix, 2008).

The CW-EPR spectra for the apo receptor at all 20 positions are shown in figure 2.5. These spectra represent the average of two repeats. The lineshapes for all 20 mutants are generally similar, and all are qualitatively consistent with MTSL linked to a structured protein sequence (Hubbell *et al*, 1996). The spectra are multi-component, with the apparent lineshape originating from at least two populations of different mobility.

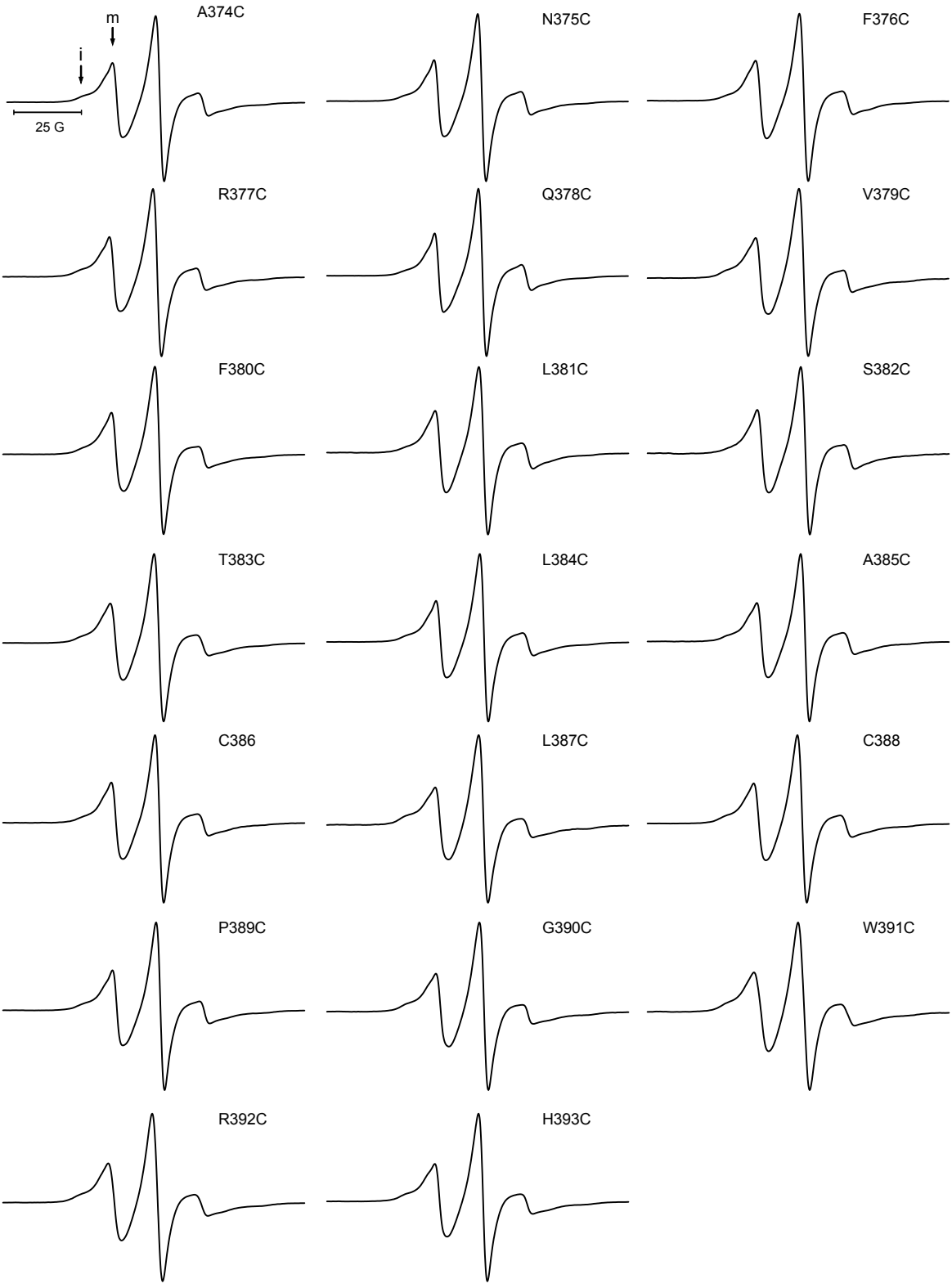


Figure 2.5: CW-EPR spectra of apo-rNTS1. All spectra represent the average of two biological repeats and show no obvious signal from free spin label. Spectral features corresponding to contributions from relatively mobile (m) and relatively immobile (i) populations are noted on one spectrum but apply to all 20 positions.

2.4.3 Secondary structure of the apo-receptor C terminus

In order to assess the secondary structure of the rNTS1 putative helix 8 sequence, CW-EPR spectra were analysed to derive the ΔH_0^{-1} parameter, as a general metric of mobility (see also section 1.4.5). Figure 2.6 reveals the pattern of mobility that occurs when ΔH_0^{-1} is plotted against rNTS1 residue number; it is apparent on visual inspection that the mobility of the C-terminal residues oscillates moving along the sequence. The mobility pattern fits a sine wave with a period of 3.6 between residues A374C and F380C, consistent with an α-helix. A second sine wave can be fit further down the C-terminus, between residues A385 and W391, but the intervening region does not fit well to an α-helix.

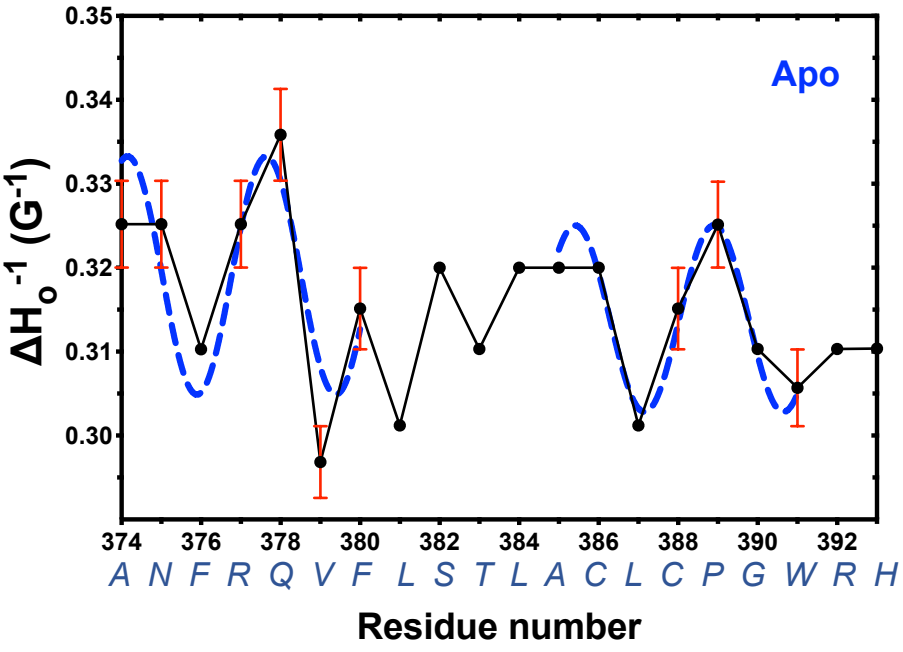


Figure 2.6: Helicity of apo-rNTS1 C-terminus. The ΔH_0^{-1} parameter for each position is plotted, with error bars representing standard error of the mean (SEM) (n=2).

2.4.4 Effects of agonist binding

The same analysis was repeated for samples bound to the NT_{8-13} agonist. As shown in figure 2.7, a similar mobility plot is obtained. The fit for the first helix is less good at the N-terminus when compared to the apo receptor (figure 2.6), extending by one residue to give a helix from A374C–L381C. The helicity further down the C-terminus (A385C-W391C) is

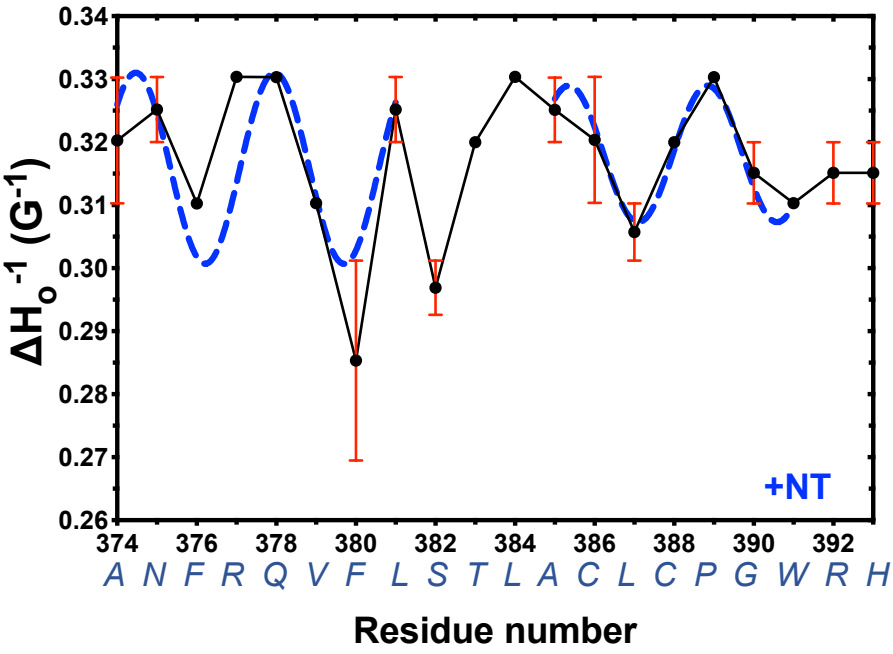


Figure 2.7: Helicity of the agonist-bound rNTS1 C-terminus The ΔH_0^{-1} parameter for each position is plotted, with error bars representing standard error of the mean (n=2).

unchanged. The main differences in mobility are localised to the region between V379C and S382C, as emphasised in figure 2.8.

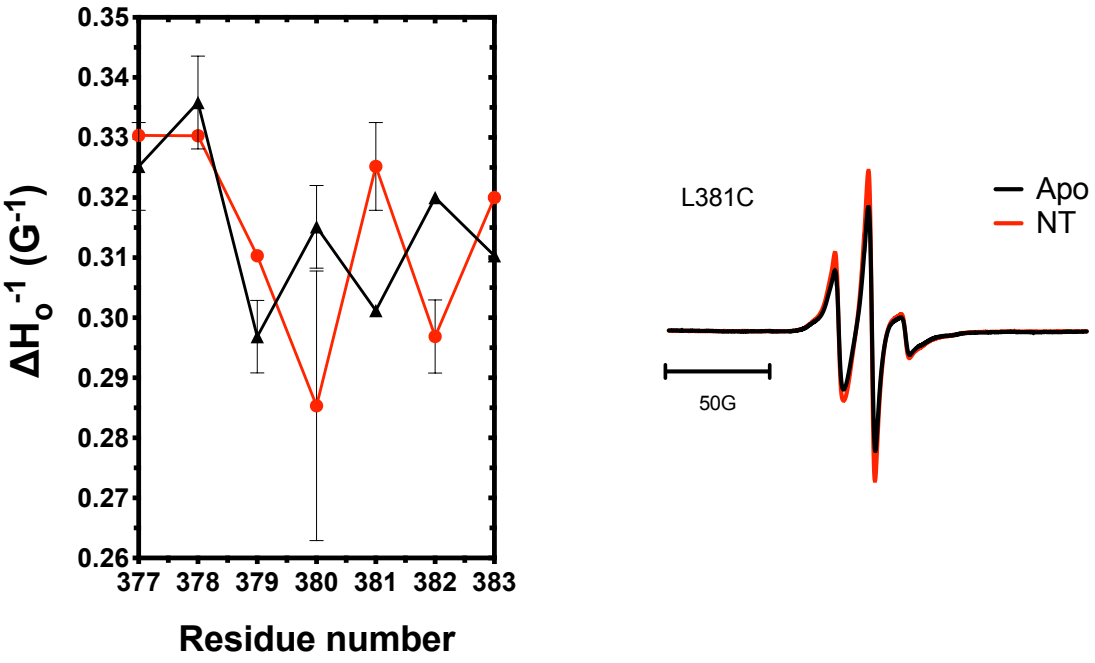


Figure 2.8: Agonist induced changes in helix 8 dynamics. Left: a comparison of mobility in the R377C-T383C region of the rNTS1 C terminus. Right: overlaid apo & NT-receptor spectra for the L381C position.

None of the differences in ΔH_0^{-1} are particularly large, but both these values and the overall spectral appearance show some difference in probe mobility in response to agonist binding. L381C is shown as an example in figure 2.8: addition of agonist increases the spectral intensity in regions relating to the more mobile spin label population.

2.4.5 Effects of $G\alpha_{i1}$ and β-arrestin$_1$ on rNTS1 helix 8

Given the modest effects on the EPR spectra of rNTS1 induced by agonist binding (figure 2.8), EPR samples were assembled in the presence of a 15-fold molar excess of $G\alpha_{i1}$ protein on both sides of the liposomal membrane. Receptor mutant S382C was chosen since it is one of the positions that changes mobility upon agonist binding, and expresses relatively highly. Figure 2.9A shows the EPR spectrum for S382C that results from the addition of $G\alpha_{i1}$ to the EPR sample, compared to the apo spectrum. The resulting spectrum shows sharp central lines, consistent with a very mobile (m) spin label population. In addition, features corresponding to an immobile population (i) also appear. To determine the cause of these effects, the non-hydrolysable GTP analogue GTPγS was added to EPR samples, in order to uncouple $G\alpha_{i1}$ from rNTS1 (figure 2.9B). Unexpectedly, addition of GTPγS did not cause the disappearance of the sharp spectral lines corresponding to the more mobile spin label population. Instead, the features corresponding to the less mobile population disappeared, and the resulting spectrum is very similar to that of the free MTSL spin label.

Next, the effects of β-arrestin$_1$ (R169E) on the EPR spectrum of the rNTS1 S382C position were investigated. As was the case for the addition of $G\alpha_{i1}$, addition of β-arrestin$_1$ leads to spectral features corresponding to a more mobile spin label population (figure 2.10), but here this population is less significant. More notable is the appearance of significant spectral features corresponding to immobilisation of the spin label. These are similar to those which appear in the $G\alpha_{i1}$ spectrum (figure 2.9) but are made more obvious by the lack of sharp central lines (figure 2.10).

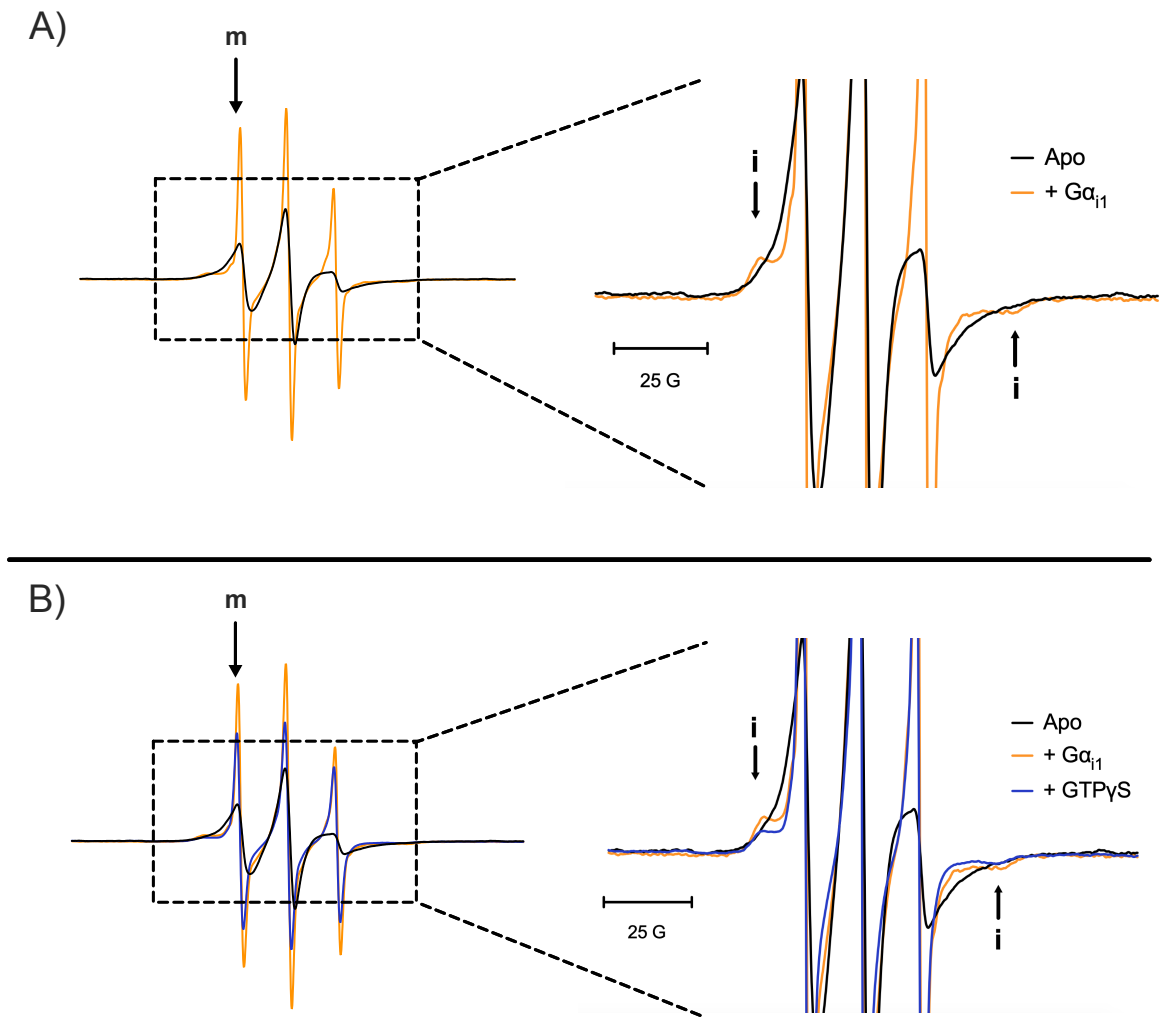


Figure 2.9: Effects of Ga_{i1} on S382C spectral appearance. A) Addition of Ga_{i1} leads to appearance of additional mobile (m) and immobile (i) features compared to the apo spectrum. A magnified view of the central spectral features makes the immobile features more apparent. B) Addition of GTPγS to a sample containing S382C and Ga_{i1} leads to the loss of (i) but not (m) features. NB the spectrum for GTPγS represents data from a single sample, in contrast to the average of data from two samples for all other conditions.

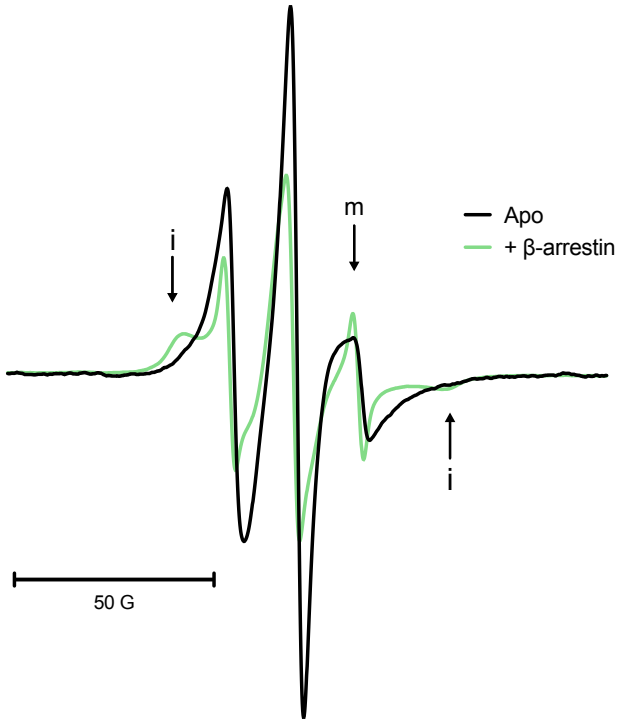


Figure 2.10: Effects of β-arrestin on S382C spectral appearance. Addition of β-arrestin leads to appearance of immobile (i) and mobile (m) features in the EPR spectrum.

2.5 Discussion

2.5.1 The presence and extent of rNTS1 helix 8

The results presented in figures 2.6 & 2.7 demonstrate a short, asymmetrically packed helix after TM7 in rNTS1, in the absence of thermostabilising mutations and with the receptor reconstituted into a lipid composition that supports ligand binding activity (Oates *et al*, 2012). The data fit an α-helical periodicity well for positions A374C through to F380C, and such a helix would be in close agreement with the 4XEE rNTS1 structure (helix 8 from N375 to F380) and the 6OS9 hNTS1 structure (helix 8 from A374 to F380). Reassuringly, the constructs used for these structures are native-like both in terms of sequence and in terms of the ability of the receptor to signal to G proteins.

The 4GRV and 5T04 structures do not show an ordered helix 8, and 4GRV instead shows a membrane distal loop-like structure (figure 2.2). The CW-EPR data do not exclude that

the helix 8 sequence is not membrane-associated, provided that the sequence is asymmetrically packed. However, the data do not support the largely disordered sequences seen in 4GRV and given the amphipathicity of the NTS1 helix 8 sequence and presence of lipids in these CW-EPR experiments, a membrane-associated conformation seems most likely.

A second helix, from A385C-W391C, is also resolved by CW-EPR. This helix is not observed in NTS1 structures, but the lack of a native-like membrane environment may preclude observation of this helix. It also should be noted that this second helix overlaps partially with the longer, continuous helix 8 seen in 3ZEV (A374-C386) and 6OSA (A374-C388). Whilst the CW-EPR mobility plot does not fit well to a helix in the F380C-L384C region, it is possible that under the conditions used for XRC or cryo-EM, a continuous helix forms, or that thermostabilising mutations in 3ZEV or the presence of G_{i1} in 6OS9 stabilise a longer helix 8.

As noted in section 2.1.4, truncations of rNTS1 at L384 and P389 cause reduced coupling to a $G\alpha_{i1/q}$ chimera, so it is noteworthy that the CW-EPR experiments detect regular secondary structure in this region. This A385C-W391C helix occurs just before a polybasic motif in the NTS1 C-terminus (P_{389}GWRHRRKKR$_{398}$), which is proposed to have a role in coupling to $G_{q/11}$, since it is conserved in receptors coupling to this class of G protein (Qin *et al*, 2011). Indeed, a recent cryo-EM structure of the M_1R receptor in complex with G_{11} (Maeda *et al*, 2019) demonstrates that this region is involved in interaction with G protein. The rNTS1 A385C-W391C helix could therefore plausibly play a role in display of this polybasic motif for $G_{q/11}$ binding.

2.5.2 Comparison of rNTS1 and rhodopsin helix 8

A similar CW-EPR study of helix 8 mobility, and the inspiration for these experiments, was conducted for rhodopsin in decyl-maltoside (DM) micelles (Altenbach *et al*, 1999a).

This data correctly predicted the presence of helix 8 later seen in crystal structures (Palczewski *et al*, 2000). Given that this data was collected at the same temperature used here for rNTS1, we can directly compare the two data sets. In figure 2.11, the relevant region of figure 2.6 is compared to the data available for rhodopsin.

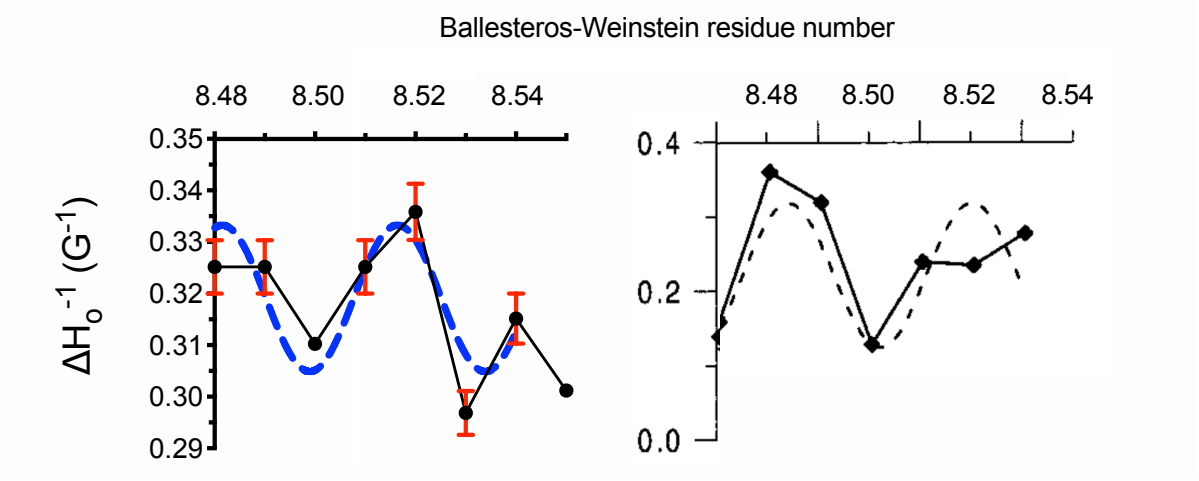


Figure 2.11: Comparison of rNTS1 and rhodopsin helix 8 EPR data. The data from figure 2.6 are reproduced here (left panel) in a form more comparable with the published data for rhodopsin (right panel) (Altenbach et al, 1999a).

Whilst the pattern of oscillation is quite similar, the *range* of ΔH_0^{-1} values observed is much greater for rhodopsin (approximately 0.18 – 0.39 G) than for rNTS1 (0.28 – 0.34 G). In other words, the difference in the mobility of the two faces of helix 8 is less for rNTS1 in a lipid bilayer than rhodopsin in DM micelles. Most of this difference appears to stem from the less mobile face of the helix, since the ΔH_0^{-1} values for the more mobile face fall within a similar range for both receptors. This in turn suggests that the differences in the two data sets arise from differences in the interactions of the less mobile face with the transmembrane portion of the receptor and/or lipids – i.e. that the rNTS1 helix is less constrained than the rhodopsin helix.

Indeed, several rhodopsin spectra for residues on the less mobile face show features consistent with immobilising tertiary contacts back on the receptor, whilst these features

are minor or absent in the rNTS1 spectra. Thus, comparing the rNTS1 and rhodopsin data is consistent with the analysis presented in (Egloff *et al*, 2014), that "the canonical helix 8 arrangement in NTR1 is significantly less stable than in A2AR" (and similarly, rhodopsin) due to a poorer packing of helix 8 with the transmembrane portion of the receptor.

2.5.3 Interpreting effects of agonist binding

Saturation of the receptor with the $NT_{8\text{-}13}$ agonist led to modest changes in these experiments. As demonstrated by the mobility plots & EPR spectra in figures 2.7 & 2.8, the overall structure and dynamics of helix 8 are similar in the presence or absence of neurotensin, with changes localised to the V379C-S382C region. For rhodopsin, some spectral changes were observed for two positions upon photoactivation ($F313C^{8.50}$ and $C316C^{8.53}$) but the spectra for the rest of the sequence were essentially unchanged (Altenbach *et al*, 1999a).

The CW-EPR data presented here therefore do not support a large change in helix 8 dynamics upon agonist binding, excluding the possibility that there is a switch in conformation from a 4XEE-like ordered, short helix 8 to a 4GRV-like disordered sequence upon agonist binding under the experimental conditions used. The data also suggest that the receptor does not switch between a shorter 4XEE-like helix and a longer 3ZEV-like helix upon agonist binding, but it is possible that binding of effector proteins may induce such changes.

Whilst the CW-EPR technique is sensitive to changes in spin label mobility, conformational changes may occur in a way that does not strongly alter this parameter. In particular, rigid body motions may occur, in which the mobility of the probe is unaltered. For example, in a study of the β_2AR, a spin label placed at the end of TM6 showed very similar CW-EPR spectra before and after receptor activation, whilst distances obtained

between this label and a TM4 spin label by DEER spectroscopy clearly increase, reflecting the movement of TM6 (Manglik *et al*, 2015).

As was discussed in section 1.2.4, the emerging paradigm of GPCR activation is that agonist binding alone is insufficient to fully stabilise the active state of the receptor. As such, it is possible that in comparing apo and agonist-bound CW-EPR spectra of rNTS1 helix 8, we are not actually comparing a fully inactive population to a fully active population of the receptor. However, some NTS1 structures show active-state features in the presence of agonist and without G protein, suggesting agonist binding is sufficient to cause at least some population of an active or active-like receptor conformation. Moreover, the helix 8 length resolved in both the presence and absence of agonist is very similar to the helix 8 resolved in the 4XEE and 6OS9 structures, both of which represent active states of the receptor. Consequently, it is possible that under the experimental conditions used, the receptor displays an active-like conformation even in the absence of an agonist (i.e. has a high basal activity).

2.5.4 Interpreting effects of $G\alpha_{i1}$ and β-arrestin$_1$

Based on the failure of agonist binding to cause large changes at helix 8 by CW-EPR, the downstream signalling partners $G\alpha_{i1}$ and β-arrestin$_1$ were included in EPR samples in an attempt to stabilise an active receptor conformation. In both cases, the presence of these proteins caused complex changes in spectral appearance for the receptor S382C position when compared to the apo state for the same position.

Focussing first on the more mobile population seen upon addition of $G\alpha_{i1}$ (figure 2.9A), it is tempting to speculate that these changes in mobility correspond to a disordering of helix 8 into a 4GRV-like, membrane-associated structure. However, these changes cannot be reversed by GTPγS, and so cannot result from a conformational change induced by $G\alpha_{i1}$. Instead, the effects are proposed to be artefactual, and the origin of the highly mobile spin

label population seems likely to be free spin label in the sample. This putative free spin label signal cannot originate from excess spin label during labelling, since the labelled receptor sample used to collect the data in figure 2.9 comes from the same sample preparation as that used to generate the apo and NT spectra, where there is no detectable contribution of free spin label (figure 2.5). It seems possible that the presence of $G\alpha_{i1}$ somehow causes liberation of the spin label from the receptor. MTSL is known to be labile (Jeschke, 2013; Bordignon & Bleicken, 2018) and indeed others have reported that formation of protein-protein complexes can lead to spin label liberation from one of the complex components (D Hilger, personal communication, 2018). The α5 helix of $G\alpha_{i1}$ contains a cysteine which could plausibly approach the spin label on NTS1 helix 8 close enough to cleave away the MTSL.

However, in addition to the putative free spin label population, an immobile population appears upon $G\alpha_{i1}$ addition (figure 2.9), which does not persist in the presence of GTPγS. This spectral change, whilst minor, is consistent with spin label immobilisation due to (reversible) NTS1- $G\alpha_{i1}$ tertiary contact. This spectral change in turn is consistent with data suggesting a role for helix 8 residues in G protein signalling, and with polar interactions between hNTS1 and $G\alpha_{i1}$ observed in the the non-canonical hNTS1-G_{i1} structure (figure 2.12A) (Kato *et al*, 2019).

For β-arrestin$_1^{R169E}$, the appearance of a more mobile spin label population compared to apo- or NT-bound receptor (figure 2.10) is again assumed to result from spin label liberation. The appearance of a more immobile population for β-arrestin$_1^{R169E}$ (figure 2.10) may reflect tertiary contact between receptor and arrestin. In rhodopsin-visual arrestin complex structures, rhodopsin helix 8 contacts the arrestin finger loop (figure 2.12B) (Kang *et al*, 2015; Zhou *et al*, 2017). Given the proposed dynamicity of the arrestin-receptor interaction, and the roles of arrestin and receptor loop regions (Latorraca *et al*, 2018), it

seems plausible that arrestin makes tertiary contacts sufficiently near to the S382C$^{8.56}$ position of rNTS1 to cause the immobilisation seen in figure 2.10.

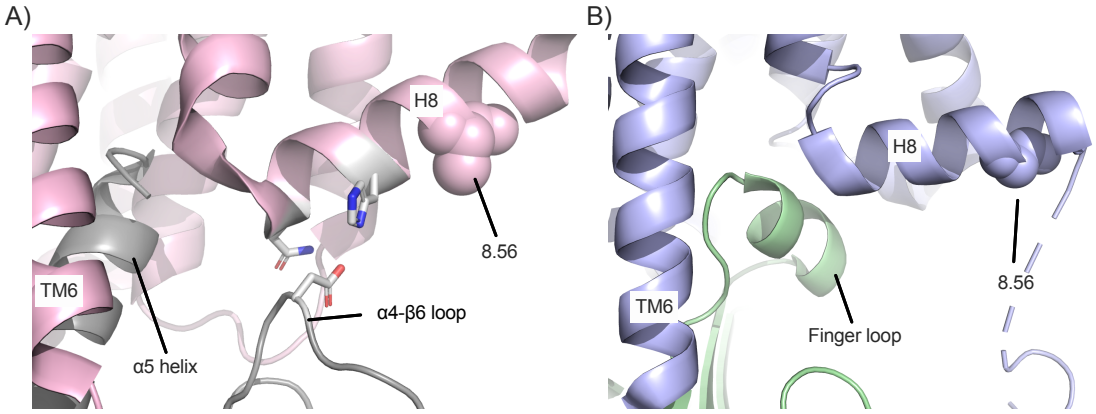


Figure 2.12: Helix 8 contacts to Ga_{i1} and arrestin. In all cases, the comparable residue to rNTS1 S382$^{8.56}$ is shown with sphere representation. A) The non-canonical hNTS1-G_{i1} complex structure shows a polar interaction network between hNTS1 and the a4-β6 loop of Ga_{i1}. B) The visual arrestin finger loop contacts the N-terminus of rhodopsin helix 8.

As such, the EPR data generated in the presence of downstream signalling proteins are suggestive of direct contact between NTS1 helix 8 and both $G\alpha_{i1}$ and β-$arrestin_1$. These CW-EPR experiments thus appear to corroborate structural data conducted in detergent or lipidic cubic phase environments. The sealed nature of liposomal samples used in this chapter prevent direct functional assays of the spin-labelled receptor samples, but it should be noted that similar receptor constructs in detergent or BPL nanodiscs have previously been shown to bind $G\alpha_{i1}$ with high affinity using microscale thermophoresis (Dijkman & Watts, 2015; Dijkman *et al*, 2018). Alternative spin labels, with different labelling chemistries, will be explored in future to try to navigate the issues seen with spin label liberation during sample preparation. Similarly, the use of receptor nanodiscs will be explored, to allow functional assays to be performed on the same sample as that used for CW-EPR experiments. In particular it is anticipated that GTP turnover assays could be used to ascertain G protein coupling (Mondal *et al*, 2015) and fluorescently-labelled arrestins used to demonstrate arrestin activation by the receptor (Sommer *et al*, 2012).

2.5.5 Roles for lipids in helix 8 stability

In the CW-EPR experiments presented, the lipid environment was not varied. However, complementary molecular dynamics (MD) experiments were performed by Dr Juan Muñoz-Garcia (formerly Department of Biochemistry, Oxford, now School of Pharmacy, University of East Anglia) (figure 2.13).

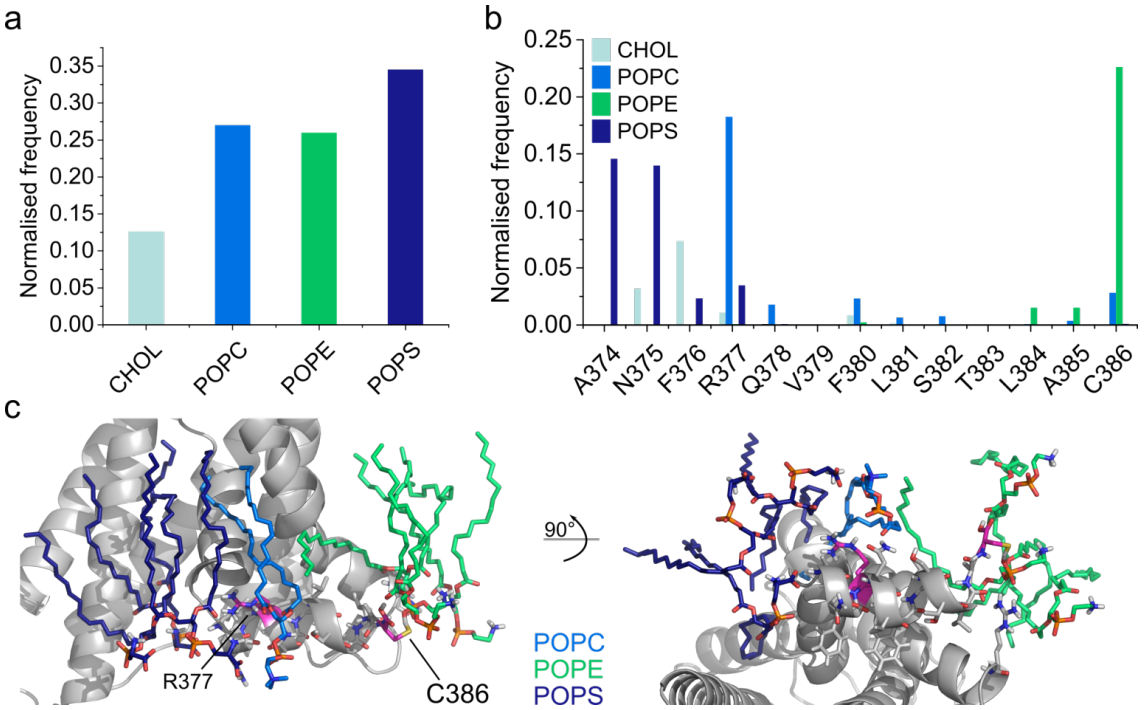


Figure 2.13: MD simulation of NTS1 in lipid bilayers. A) Normalised frequency of helix 8 contacts to specific lipid types over the course of the simulation. B) Normalised frequency of helix 8 contacts by residue. C) Views of helix 8 interacting with POPC (light blue), POPE (green) and POPS (navy) lipids. Data & figure courtesy of Dr Juan Muñoz Garcia.

200 ns simulations were performed on the agonist-bound 4BUO structure, with thermostabilising mutations reverted to wild type sequences, in either a simple POPC bilayer or in a bilayer mimicking the BPL lipid composition (15% POPC, 22% POPS, 39% POPE & 24% cholesterol). A helix was observed from A374-L381 in POPC, and stabilising R377-POPC interactions were observed. In the BPL-like bilayer simulations, the helix was slightly longer (A374-L384), with lower RMSD values (3.5±0.3 Å vs 4.2±0.9 Å for POPC). This additional stability can be attributed to interactions of helix 8 with the

POPE and POPS components of the BPL-like bilayer.

The helix seen in the POPC bilayer is in good agreement with the CW-EPR data conducted in BPL liposomes (A374C-L381C in the presence of NT). Helix 8 for the receptor simulated in a BPL-like bilayer is slightly longer than the helix experimentally observed by CW-EPR (A374-L384 vs A374-L381).These discrepancies could reflect that the simulations may be biased by the longer helix or lack of resolved C-terminus beyond C386 in the starting 4BUO conformation. It should also be noted that whilst the BPL headgroup composition was well-mimicked in the molecular dynamics simulations, the acyl chains of the BPL lipids used experimentally are likely to contain many components other than the simple 1-palmitoyl, 2-oleoyl chains used in the simulations. Specific acyl chains present in the experimental BPL liposomes may therefore stabilise a different conformation of helix 8 when compared the acyl chains used in simulations. In any case, several specific lipid headgroup interactions were detected in the simulations that may stabilise the otherwise dynamic rNTS1 helix 8. Indeed, these lipid contacts may help compensate for the relatively weak contact between helix 8 and the TM bundle and may explain why helix 8 is sometimes absent in crystal structures, which lack a native-like membrane environment.

It should also be noted that the rNTS1 constructs produced in *E. coli* lack palmitoylation modifications proposed to occur on C386 and C388 ((Heakal *et al*, 2011), see also chapter 3). CW-EPR studies on rhodopsin suggest that the palmitoylation has a limited and highly localised effect on the dynamics and structure of the sequence in detergent (Langen *et al*, 1999). It should also be noted that the 5HT04 & 4GRV have no helix 8 but are expressed in a eukaryotic system in which helix 8 is presumably palmitoylated, and thus palmitoylation alone is unlikely to be sufficient for helicity. However, this interpretation is complicated by the lack of a native-like membrane in a crystallographic or detergent

environment, which may be required for anchorage of palmitoyl groups. It therefore should be noted that limited effects of palmitoylation on the structure of helix 8 in crystallographic and detergent environments do not exclude a role for palmitoylation in modulating helix 8 structure and dynamics in the native, highly heterogeneous membrane environment that NTS1 signals from. It is clear that the helix 8 palmitoylation state can affect G protein signalling for rhodopsin (Heck *et al*, 2003), and NTS1 (Heakal *et al*, 2011).

2.5.6 Conclusions

The data presented in this chapter demonstrate that for rNTS1 in the absence of thermostabilising mutations and in the presence of a lipid environment, the receptor possesses a short, dynamic helix 8. This work thus resolves a literature dispute and demonstrates the utility of studies on GPCRs without thermostabilisation and in lipid environments.

The dynamics of the helix are consistent with weak contact with the receptor transmembrane region, and lipids may play a role in stabilising the helical structure. The structure and dynamics of the helix are similar in the absence and presence of agonist, whilst tertiary contacts are made to both $G\alpha_{i1}$ and $\beta\text{-arrestin}_1^{R169E}$. The data do not support a model whereby helix 8 is disordered into a 4GRV-like conformation upon agonist binding. Limitations of the experiment mean such a conformational state may exist but is not accessible to the receptor under the conditions tested, or different conformational changes may occur to which the technique is insensitive. Indeed, given the observed dynamics of helix 8, and the reported sensitivity of its conformation to lipids, it is not implausible that a relatively disordered, membrane-distal conformation could exist under certain conditions. Indeed, several membrane-distal helix 8 conformations have been recently observed for other receptors (Zhang *et al*, 2017a; Toyoda *et al*, 2019; Morimoto *et al*, 2019) and highlight that helix 8 is a worthy target of further study in the GPCR field.

3. Expression, purification & characterisation of hNTS1 & heterotrimeric G proteins

3.1 Introduction

3.1.1 Limitations of *E. coli* as an expression host for NTS1

The *E. coli* system for rNTS1 expression can yield approximately 20 nmol (~1mg) of cleaved, functional protein per 8-12 L culture. The system has been used to study rNTS1 ligand binding (Oates *et al*, 2012), dimerisation (Harding *et al*, 2009; Dijkman *et al*, 2018) and interactions with Gα proteins (Adamson & Watts, 2014; Dijkman & Watts, 2015). As demonstrated in the previous chapter, the bacterial expression system allows for production of many receptor mutants in relatively little time, which makes EPR studies of the receptor particularly feasible.

However, several limitations of the system exist. Yields of rNTS1 are rather inconsistent, with large amounts of material sometimes lost during ligand affinity chromatography (White & Grisshammer, 2010). In addition, the receptor construct tends to aggregate during purification in detergent, especially when centrifugal concentrators are used. Indeed, these limitations of the system provided the motivation for the development of thermostabilised *E. coli*-expressed rNTS1 constructs by the Plückthun lab (Schlinkmann *et al*, 2012).

In addition to issues with yield and stability, the *E. coli*-expressed receptor lacks post-translational modifications that may have functional importance, most notably the palmitoylation of two cysteines in the proximal C-terminus. For hNTS1, palmitoylation is

proposed to occur on C381 & C383 (which are conserved as C386/C388 in rNTS1, respectively) (Heakal *et al*, 2011) and mutations of these residues suggest that palmitoylation plays a role in hNTS1-G_q coupling and receptor localisation in the membrane.

As such, whilst various attempts at optimisation of the *E. coli* system were made during this thesis, expression of NTS1 in a eukaryotic system was also explored as an option.

3.1.2 Limitations of *E. coli* as an expression host for G proteins

E. coli can be used to produce $G\alpha_s$ & $G\alpha_i$ subunits in a form capable of nucleotide binding, at high expression levels (Greentree & Linder, 2004). Indeed, previous work in the Watts laboratory has demonstrated that these proteins can bind to rNTS1 in nanodiscs (Adamson & Watts, 2014; Dijkman & Watts, 2015).

However, to study receptor-G protein interactions in a more physiological context, eukaryotic expression hosts for G proteins are required. G protein heterotrimers are lipidated (table 3.1) by enzymes that *E. coli* do not possess, and these lipid modifications have important structural and functional roles. Additionally, neither Gβγ nor some specific Gα subtypes (e.g. $G\alpha_q$) express in a functional form in *E. coli* (Higgins & Caseys, 1994; Greentree & Linder, 2004). Whilst the interface with Gα dominates GPCR-G protein interactions (see section 1.2.5), some structures show interactions between the receptor core and Gβ (reviewed in (García-Nafría & Tate, 2019)) and more recently the receptor C-terminus and Gβγ (Maeda *et al*, 2019; Gao *et al*, 2019). Indeed, it is generally the case that the presence of Gβγ improves the coupling of the receptor to Gα, and may provide selectivity determinants in this process (Florio & Sternweis, 1985; Woodfork *et al*, 2002; Jian *et al*, 2001).

There are two common approaches used to obtain lipidated heterotrimers from heterologous expression systems. One route is to co-infect insect cells with baculoviruses

Lipid modification	Location	Functional role
Myristoylation *(NB only Gi/o are myristoylated)*	Gα N-terminal glycine	Membrane association of Gα (Mumby & Linder, 1994) Regulation of N-terminal structure (Preininger *et al*, 2003) Interaction of Gα with Gβγ (Mumby & Linder, 1994)
Palmitoylation	Gα N-terminal cysteine	A membrane localisation signal (Wedegaertner *et al*, 1993; Takida & Wedegaertner, 2003)
Farnesylation or geranylgeranylation	Gγ C-terminal cysteine	Coupling of heterotrimer to receptors (Myung *et al*, 2006; Woodfork *et al*, 2002) Binding of Gβγ to effectors (Myung *et al*, 2006)

Table 3.1: Post-translational lipid modifications of G protein heterotrimers. The location and function of these modifications are indicated.

that encode all three G protein subunits (typically one virus for Gα and one for Gβγ) and where necessary the Ric8A chaperone (Chan *et al*, 2013). The second route is to reconstitute bacterially expressed Gα with Gβγ either purified from native sources or from heterologous overexpression in insect cells. This system can be made more native-like by co-expressing the Gα subunit in *E. coli* with N-myristoyltransferase 1 (NMT-1); when myristic acid is supplied in the growth medium, NMT-1 can post translationally myristoylate the Gα subunit in the *E. coli* cytoplasm with high efficiency (Greentree & Linder, 2004; Preininger *et al*, 2003).

3.2 Aims

A discussion with members of Brian Kobilka's Laboratory (Stanford University) at a conference led to a visit to Stanford, in order to obtain training in expression of the human NTS1 receptor (hNTS1) in *Spodoptera frugiperda* (Sf9) cells, as well as production of heterotrimeric G proteins. In particular, two G proteins previously studied in the context of NTS1-G protein coupling where chosen, G_q & G_{i1}.

The primary aim of this chapter was therefore to express & purify:

- A wild-type like hNTS1 construct from Sf9 insect cells;
- The G_q heterotrimer using *Trichoplusia ni* High Five™ insect cells;
- The G_{i1} heterotrimer using Sf9 insect cells for $G\beta\gamma$ and *E. coli* for myristoylated-$G\alpha_{i1}$.

Purified material was then used to:

- Establish a GTP turnover assay to demonstrate the activity of the expressed proteins and provide an opportunity to assay e.g. lipids for their effect on receptor activity
- Explore the potential of native mass spectrometry for analysis of receptor post-translational modifications and co-purified small molecules.

3.3 Materials & methods

3.3.1 Insect cell culture

Cells grown in Stanford were expanded from frozen, low-passage aliquots by Betsy White. For virus production and expression, cells were expanded and maintained in glass Erlenmeyer flasks using ESF921™ (Expression systems) medium.

Cells grown in Oxford were expanded from frozen, low-passage aliquots gifted by Gabriel Kuteyi, Newstead Lab. Cells were expanded and maintained in disposable Erlenmeyer flasks (Corning and Thermo Scientific brands) and Optimum Growth™ flasks (Thomson), using Sf-900 II (Gibco) media.

In all cases, cells were regularly counted using a haemocytometer with Trypan blue staining to assess cell viability. Cells were maintained with a density of 0.5-6 million/mL and a viability of >95%.

3.3.2 Expression and purification of hNTS1 from Sf9

3.3.2.1 hNTS1-eGFP construct

The hNTS1-eGFP construct used in this chapter and the remainder of this thesis was originally developed by Dr Hideaki Kato, Stanford University as described in (Kato *et al*, 2019). Figure 3.1 summarises the features of this construct, showing the wild type-like nature of the sequence.

3.3.2.2 Large scale expression of hNTS1

For large scale expression, typically 4-8 L of Sf9 at 2.5-4 million cells/mL were prepared and infected with an appropriate volume of P2 virus for 48-54 hours, after which cells were harvested by centrifugation and snap frozen in liquid N_2 for storage at -80°C.

3.3.2.3 Purification of hNTS1 protein from Sf9

Purification of the receptor was achieved broadly as outlined in (Kato *et al*, 2019). Some minor modifications were made when establishing this protocol in Oxford.

To minimise the mass of detergent required, membranes were prepared from Sf9 cells by resuspension in six pellet volumes of hypotonic buffer (10-20 mM HEPES pH 7.4, 150 mg/L Benzamidine,10 µM Leupeptin & 1 mM EDTA) using a dounce homogeniser. The cell suspension was stirred for 20 minutes at 4°C, before ultracentrifugation (125,000g, 45 mins, 4°C). Pellets were then resuspended in high salt buffer (20 mM HEPES pH 7.4, 500 mM NaCl, inhibitors) with extensive dounce homogenisation on ice. The homogenised membranes were re-pelleted by ultracentrifugation, followed by a further resuspension-ultracentrifugation cycle in low salt buffer (20 mM HEPES pH 7.4, 100 mM NaCl). Further cycles of resuspension and ultracentrifugation were performed as necessary, and the membranes were weighed, resuspended to 250 mg/mL in low salt buffer and snap frozen in liquid N_2 for storage at -80°C. Throughout purifications, the NTS1 ligand NT_{8-13} was included at >100 nM final concentration. Membranes were typically solubilised for

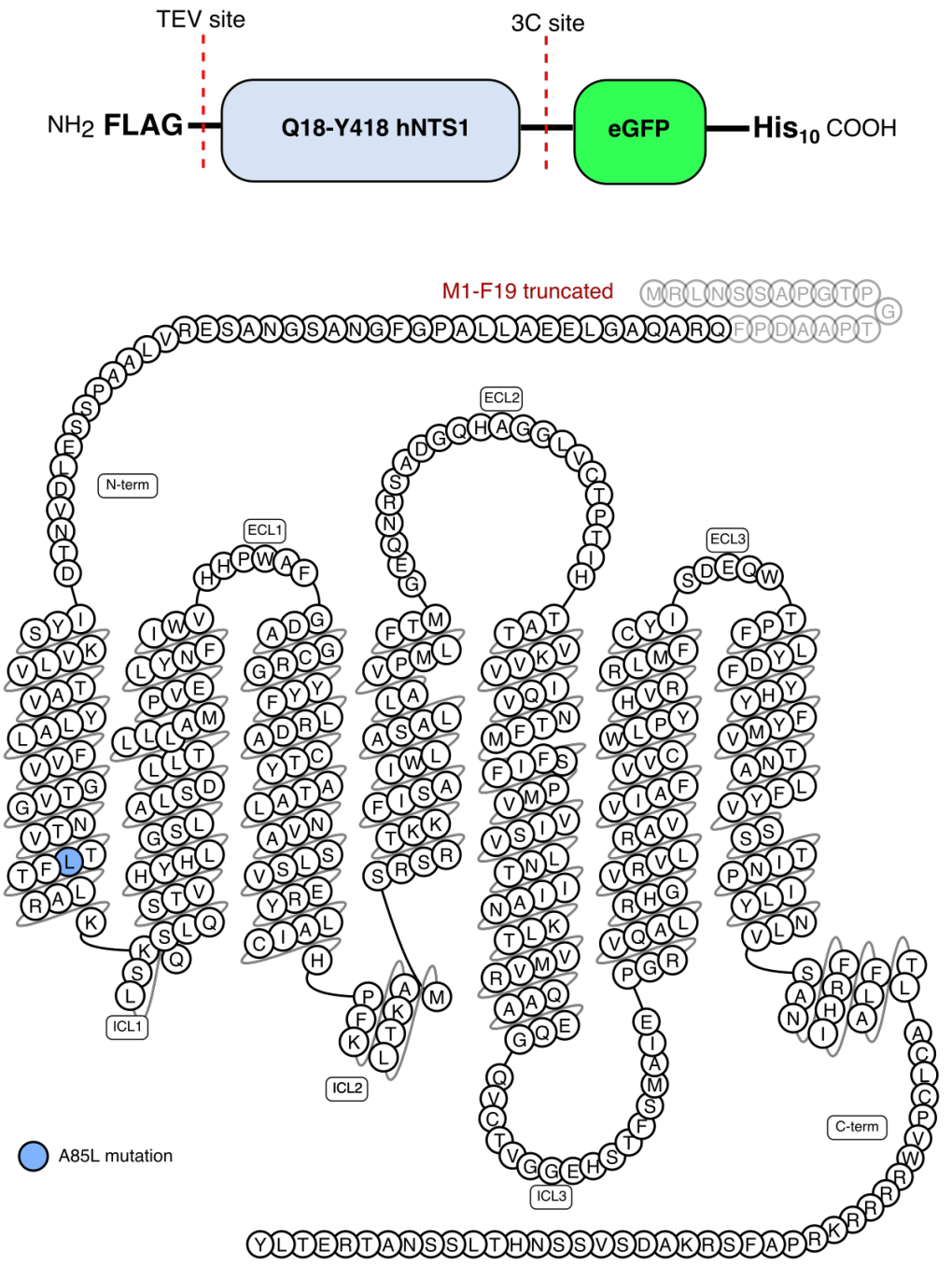


Figure 3.1: Features of the hNTS1-GFP construct used in chapter 3. The features of the hNTS1 fusion construct (top) and the hNTS1 sequence used (bottom) are shown. An N-terminal FLAG tag is linked to the hNTS1 sequence by a Tobacco etch virus (TEV) protease cleavage site, whilst a C-terminal eGFP-his$_{10}$ tag is linked by a human rhinovirus 3C protease cleavage site. The snake plot diagram was generated using GPCRdb (Isberg et al, 2014; Pándy-Szekeres et al, 2018).

2 hr using a buffer with final concentrations of 1% MNG, 0.1% CHS (w/v), 20 mM HEPES pH 7.4, 500 mM NaCl, 100 µM TCEP & 20% glycerol (w/v). Material was then

centrifuged (>38,000g, 50 mins, 4°C), topped up to 5-10 mM imidazole final and applied to Ni-NTA resin (Thermo Scientific) that had been prepared in equilibration buffer (0.01% MNG / 0.001% CHS, 20 mM HEPES pH 7.4, 500 mM NaCl, 5-10 mM imidazole, 10% glycerol) for 2 hr at 4°C. The resin was washed in equilibration buffer supplemented with 20 mM imidazole and material eluted at 300 mM imidazole. This was then dialysed overnight against dialysis buffer (equivalent to equilibration buffer without imidazole and 200 mM NaCl). 3C protease was included to cleave eGFP (either as a his-3C protease (donation from Betsy White, Stanford University) or as GST-3C protease (donation from Dr Sebastian Zoll, Oxford University)).

Protein was further purified using M1 anti-FLAG immunoaffinity agarose resin (donation of Prof Brian K Kobilka, Stanford University) before size-exclusion chromatography. M1 anti-FLAG affinity chromatography was performed by incubating cleaved receptor material from with 5 mL resin in the presence of 2 mM $CaCl_2$. Resin was washed in dialysis buffer supplemented with 2 mM $CaCl_2$ followed by the same buffer at 500 mM NaCl. Elution was achieved using 200 μg/mL FLAG peptide (Apex Biotech). In some cases, reverse Ni-NTA was also used before M1 anti-FLAG affinity chromatography, whereby cleaved material was passed over 5mL Ni-NTA and the flow-through collected.

Material eluting from M1 anti-FLAG resin was subjected to size-exclusion chromatography on a Superdex S200 increase column (GE healthcare) at 0.5-0.7 mL/min, 4°C in a buffer of 0.01% MNG, 0.001% CHS, 20 mM HEPES pH 7.4, 100 mM NaCl, 5% glycerol. 0.5 mL fractions were collected and analysed by SDS-PAGE. Appropriate fractions were pooled, concentrated and snap frozen with 10% glycerol.

Some purifications were made using DDM in place of MNG (1% w/v during solubilisation and 0.1% w/v thereafter), and sometimes uncleaved receptor was prepared by omitting 3C-protease during overnight dialysis. Occasionally receptor was purified

directly from Sf9 cells rather than membranes, in which case cells were initially resuspended in hypotonic lysis buffer, pelleted and resuspended in solubilisation buffer with protease inhibitors.

3.3.3 Expression & purification of G proteins

3.3.3.1 Expression & purification of G_q heterotrimer

G_q heterotrimer was produced in High Five™ cell cultures at 4L scale. Cells at 3-3.5 million/mL were co-infected with P2 viruses for a) $G\alpha_q$ and b) $G\beta_1\gamma_1$ and the Ric8A chaperone at ratios previously determined. Cells were harvested at 48 hours post infection and snap frozen in liquid N_2 for storage at -80°C.

The lipidated G_q heterotrimer was purified as described previously for other G protein heterotrimers (Dror *et al*, 2015; Kato *et al*, 2019). Full detail is given in appendix A3.1.

Viruses for the G_q heterotrimer were kindly provided by Dr Hideaki Kato, Stanford University. Additional material in the form of cell pellets was kindly donated by Dr Kaavya Krishna Kumar, Stanford University.

3.3.3.2 Expression & purification of G_{i1} heterotrimer

The G_{i1} heterotrimer was produced by reconstituting $G\beta\gamma$ produced in Sf9 cells with myristoylated $G\alpha_{i1}$ produced in *E. coli*.

A frozen P1 virus for $G\beta_1\gamma_1$ containing a cleavable his_6 tag on the β_1 N-terminus was kindly provided by Dr Hideaki Kato, Stanford University. The P1 stock was thawed and expanded to a P2 by infection of Sf9 at 1.5-2 million cells/mL for 4 days until 30-50% cell death had occurred. Small scale purifications from 30 mL cultures were used to established appropriate expression conditions, and large scale purification was conducted using an analogous protocol to that for the G_q heterotrimer (appendix A3.1), except GDP and $MgCl_2$ were omitted from purification buffers.

A pETduet NMT-1/$G\alpha_{i1}$ plasmid was kindly provided by Dr Daniel Hilger, Stanford University. Competent *E. coli* BL21(DE3) cells (Novagen) were transformed according to standard heat shock protocols and plated on LB Agar with 100 µg/mL ampicillin. Overnight culture in terrific broth (TB) with ampicillin was inoculated with a single colony, and then used to inoculate 2-4L of TB with ampicillin the following day. Cells were grown to an OD of 0.6 at 37°C, then induced with 0.5 mM IPTG and supplemented with myristic acid (30 µM from a stock of 30 mM in EtOH). Cells were grown for a further 16-20 hours at 24°C before they were harvested by centrifugation (8,000g,15 minutes, 4°C) and snap frozen in liquid N_2 for storage at -80°C. Protein was purified according to (Greentree & Linder, 2004), except that 100 µM TCEP was used in place of β-mercaptoethanol and the Ni-NTA and phenyl sepharose steps were each followed by overnight dialysis to remove imidazole and ammonium sulphate, respectively. Full detail is given in appendix A3.2.

E. coli -produced myristoylated $G\alpha_{i1}$ protein was reconstituted with Sf9-produced Gβγ by incubation at a 1:1.2 molar ratio Gα:Gβγ (4°C, 1hr, with rotation). Material was then loaded onto a S200 increase size exclusion column (GE healthcare) and fractions collected. SDS-PAGE was used to check for the presence of heterotrimeric G_{i1}, and appropriate fractions were pooled, concentrated and snap frozen in liquid N_2 for storage at -80°C.

3.3.4 GTPase-Glo™ assays

The GTPase-Glo™ assay (Promega) was performed according to the manufacturer's instructions, with minor modifications.

G proteins were prepared to twice the desired final concentration in assay buffer (20 mM HEPES pH 7.4, 100 mM NaCl, 10mM $MgCl_2$, 100 µM TCEP, 0.1% DDM/0.01% CHS). GTP, and where appropriate, receptor-GTP mixes, were prepared in the same buffer but with 10 µM GTP. G protein (2.5 µL) was added to a 384 well plate and mixed

with the GTP/receptor-GTP stock (2.5 µL, 30 mins, RT) to give 5 µM GTP final. In addition, GTP-only, or receptor-GTP-only controls were included by mixing 10 µM GTP (+/- receptor) solution (2.5 µL) with assay buffer without G protein (2.5 µL). Where receptor was used, it was pre-incubated with a saturating concentration of the NT_{8-13} ligand (>1 µM) for 30 minutes on ice before use in the assay.

Following the incubation of buffer or G protein with GTP or GTP + receptor, 5 µL ADP-Glo reagent prepared in assay buffer was added to the plate for 30 minutes at room temperature. Detection reagent (10 µL) was then added for 5-10 minutes and luminescence read on a SpectraMax M3 plate reader. Unless specified otherwise, all experiments were performed in triplicate. Data were analysed in GraphPad Prism and normalised so that the GTP-only or GTP + G-protein condition represents 100% of the signal, as appropriate.

3.3.5 Native mass spectrometry

Native mass spectrometry experiments were performed in collaboration with Dr Hsin-Yung Yen (laboratory of Carol Robinson, University of Oxford). Protein was prepared for native mass spectrometry as outlined in section 3.3.2, except that the protein was treated with 10 µL PNGaseF (New England Biolabs) prior to Ni-NTA chromatography.

Purified receptor was exchanged into a buffer of 200 mM ammonium acetate (pH 8) supplemented with an optimised detergent mixture (0.001% LMNG/Foscholine) and immediately introduced into a modified Q-Exactive mass spectrometer (Thermo), as described previously (Gault *et al*, 2016; Yen *et al*, 2017, 2018). Protein was subjected to nanoESI with a capillary voltage of 1.1 kV, and a gentle voltage gradient used to transfer ions into the HCD cell (injection flatapole, inter-flatapole lens, bent flatapole, transfer multipole: 7.9, 6.94, 5.9, 4 V respectively). A constant backing pressure of ~1.00×10^{-9} mbar was maintained. To remove detergents, an acceleration voltage of 120 V was applied

at the HCD cell. Acquisition of spectra was performed using a noise level of 3 for averaging and Xcalibur 2.2 SP1.48 was used for data analysis.

For depalmitoylation of the receptor, purified NTS1 was incubated with a recombinant human Palmitoyl-Protein Thioesterase 1 (PPT-1, SinoBiological) at a 4:1 molar ratio (RT, 1hr). The depalmitoylated receptor was then analysed in the same manner as the palmitoylated receptor.

3.4 Results

3.4.1 Purification of G protein heterotrimers

The G_q heterotrimer was purified from High Five™ cells, using a simple purification scheme as outlined in figure 3.2A. After Ni-NTA chromatography, 3C cleavage and reverse Ni-NTA chromatography, most contaminants have been removed (figure 3.2B). Size exclusion chromatography (SEC) then separates the heterotrimer from aggregates and free Gβγ dimers to yield approximately 2-3 mg of $G\alpha_q\beta\gamma$ /L culture (figure 3.2C).

For the G_{i1} heterotrimer, the Gβγ subunits were expressed in Sf9 cells at > 2 mg /L culture and purified similarly to the G_q heterotrimer. The myristoylated-$G\alpha_{i1}$ subunit was expressed in *E. coli* alongside its cognate myristoyltransferase, NMT-1 and purified as outlined in figure 3.3A. After initial Ni-NTA purification, ammonium sulphate is added, and hydrophobic interaction chromatography performed using a phenyl sepharose column (figure 3.3B). After loading, the ammonium sulphate concentration is slowly lowered, with contaminants and any unlipidated $G\alpha_{i1}$ eluting before a final peak containing the lipidated $G\alpha_{i1}$ subunit is seen (figure 3.3B). Approximately 2 mg purified protein/L culture is obtained by this method, and is then mixed with Gβγ subunits and the mixture further purified by SEC (figure 3.3C).

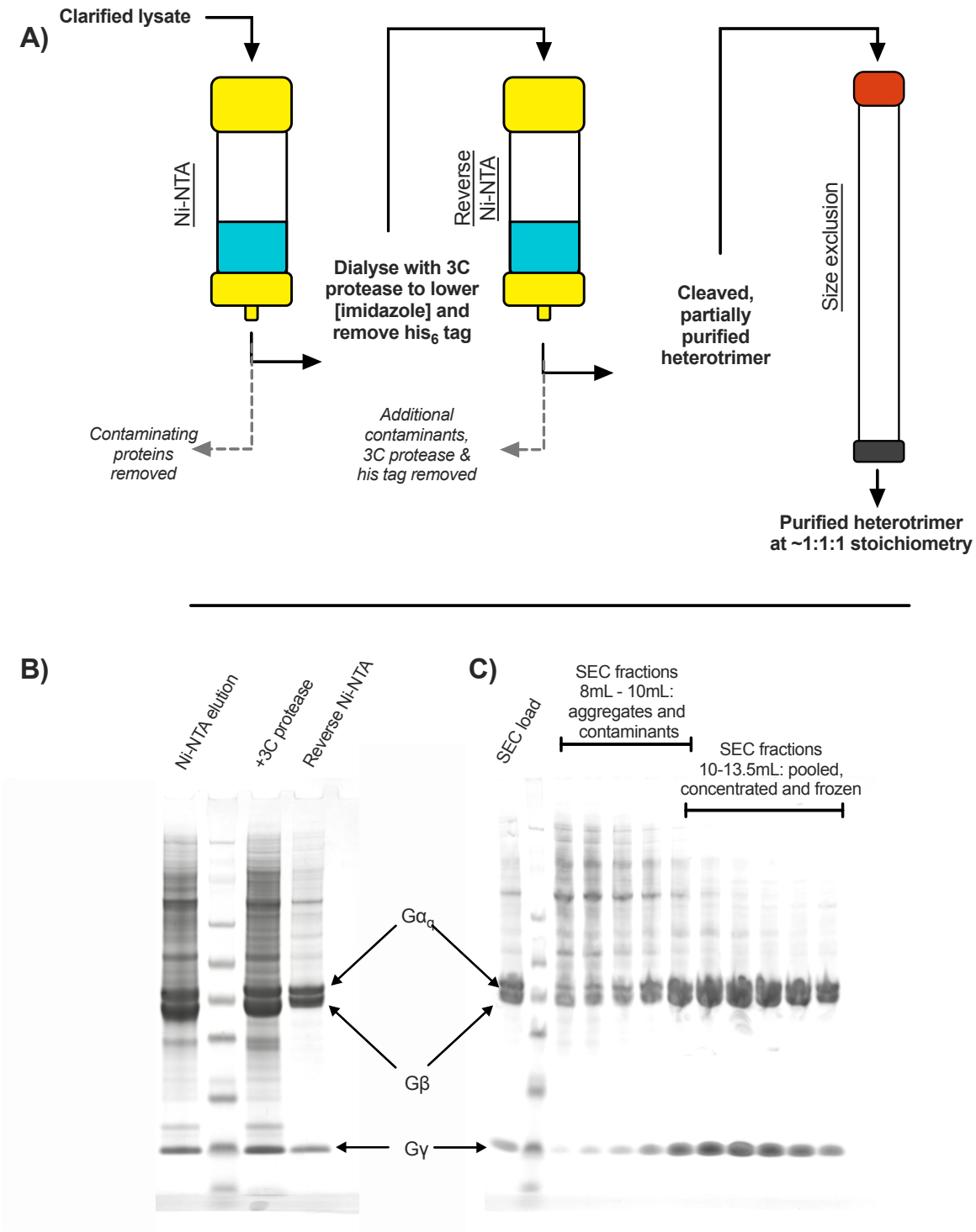


Figure 3.2: Purification of G_q heterotrimer. A) Schematic outlining purification of G_q. Bottom: SDS-PAGE of a representative purification, demonstrating the purity and stoichiometry of G_q after B) Ni-NTA, 3C cleavage and reverse Ni-NTA and C) SEC purification stages. FT = flow-through, SEC = size exclusion chromatography.

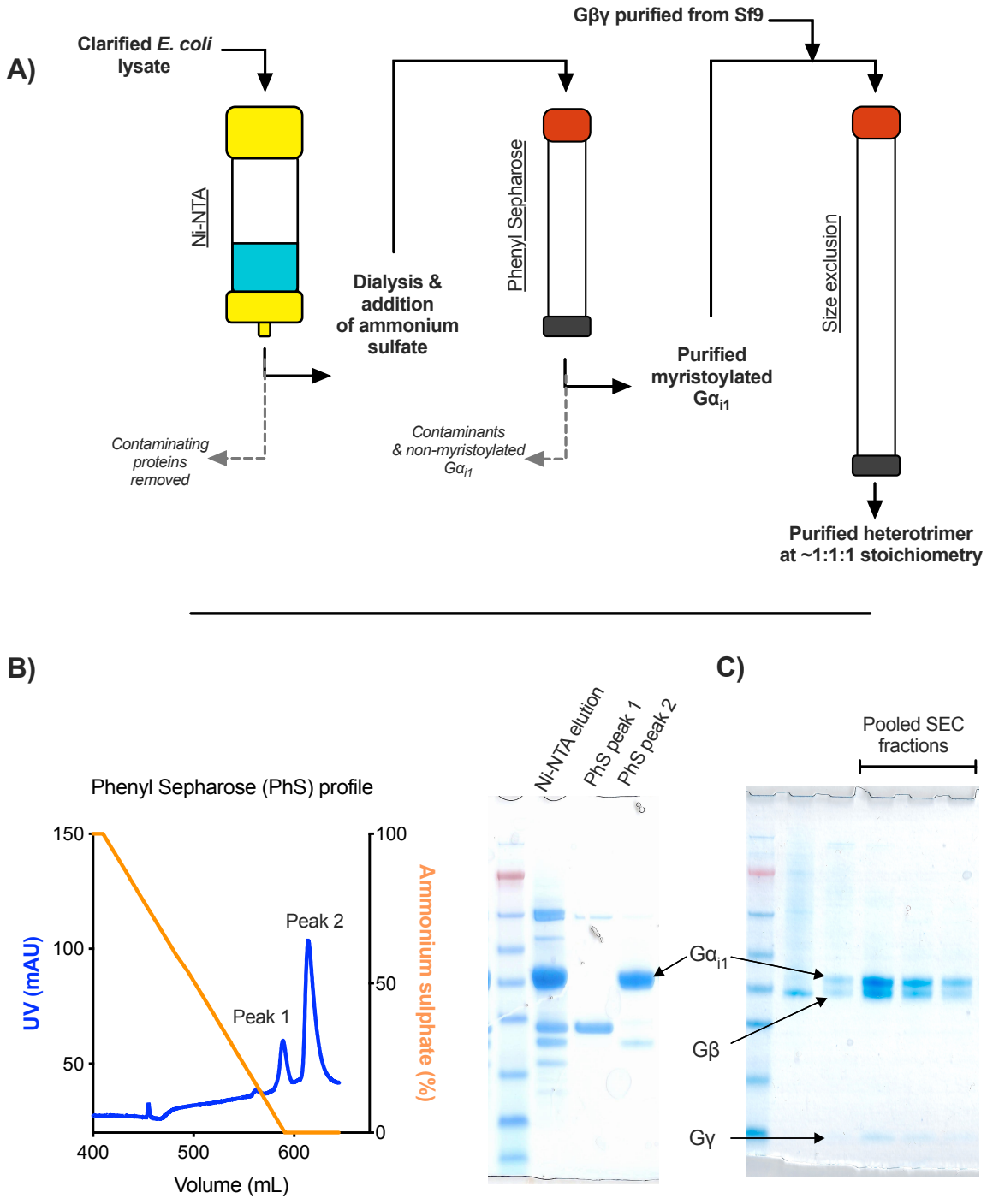


Figure 3.3: Purification and reconstitution of G_{i1} heterotrimer. A) Schematic outlining purification of myristoylated $G\alpha_{i1}$ and its reconstitution with Gβγ. B) Chromatogram and corresponding SDS-PAGE for the phenyl sepharose column. 100% ammonium sulphate corresponds to an absolute concentration of 1.2 M. PhS = phenyl sepharose. C) SDS-PAGE of SEC purification of the reconstituted heterotrimer.

3.4.2 Purification of hNTS1

Following protocols established by Dr Hideaki Kato in the Kobilka lab, the hNTS1-eGFP construct was successfully expressed and purified using the scheme outlined in figure 3.4.

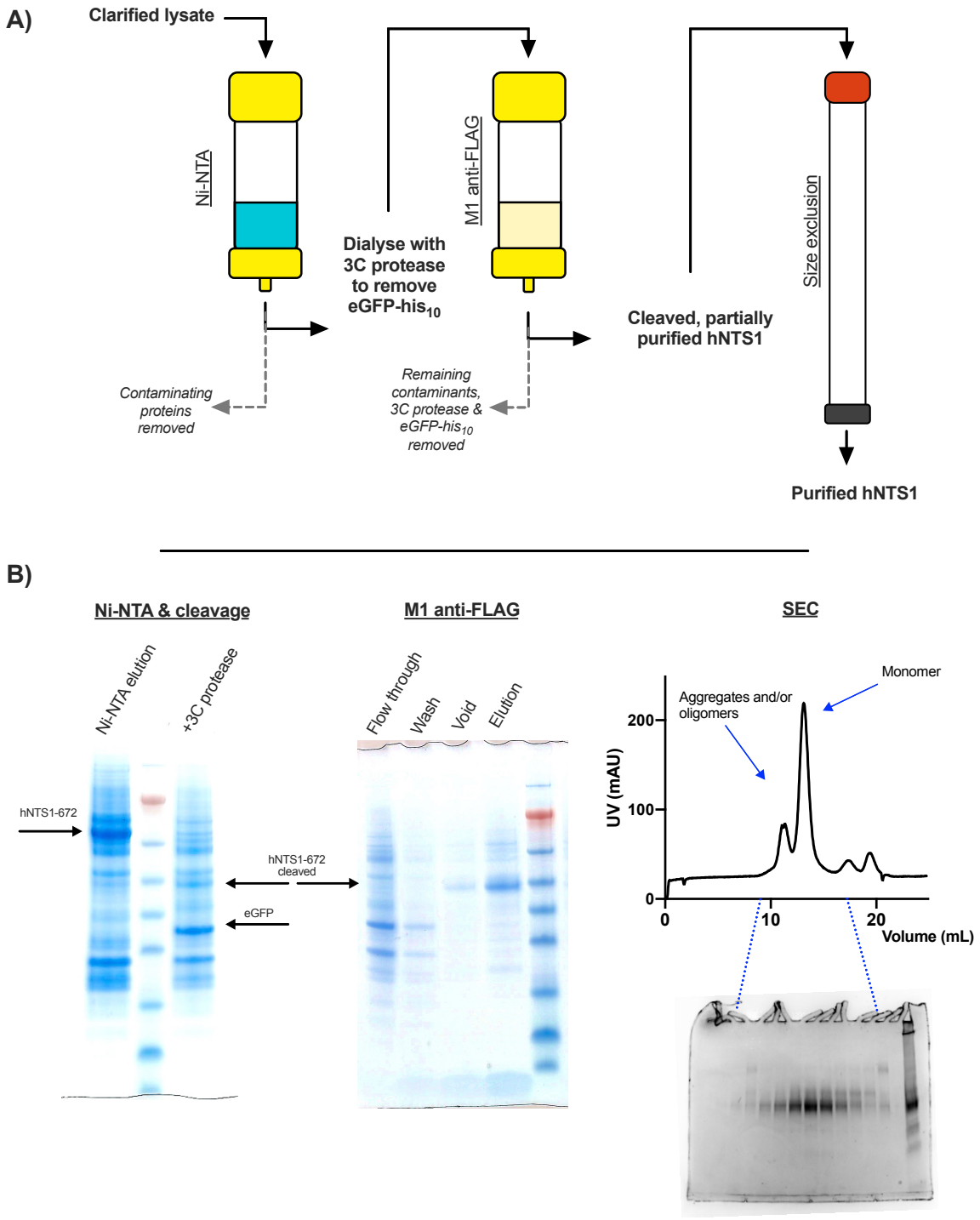


Figure 3.4: Purification of hNTS1. A) Schematic outlining purification and cleavage of hNTS1. B) SDS-PAGE gels and size exclusion chromatogram representative of the various purification steps.

Ni-NTA chromatography enriches the eGFP tagged receptor (figure 3.5B), which is then cleaved by 3C protease before removal of remaining contaminants and eGFP by M1 anti-FLAG chromatography. Size exclusion chromatography then removes aggregates to leave monodisperse, pure, monomeric NTS1.

3.4.3 Activity of hNTS1 and G proteins

In order to assess the activity of the receptor and G proteins, the GTPase-Glo™ GTP turnover assay (section 1.6) was used. Both heterotrimers were assayed for their intrinsic GTPase activity by serial dilution in an assay buffer containing 0.1% DDM, 0.01% CHS (w/v), followed by addition of GTP to a final concentration of 5 μM (figure 3.5A and B).

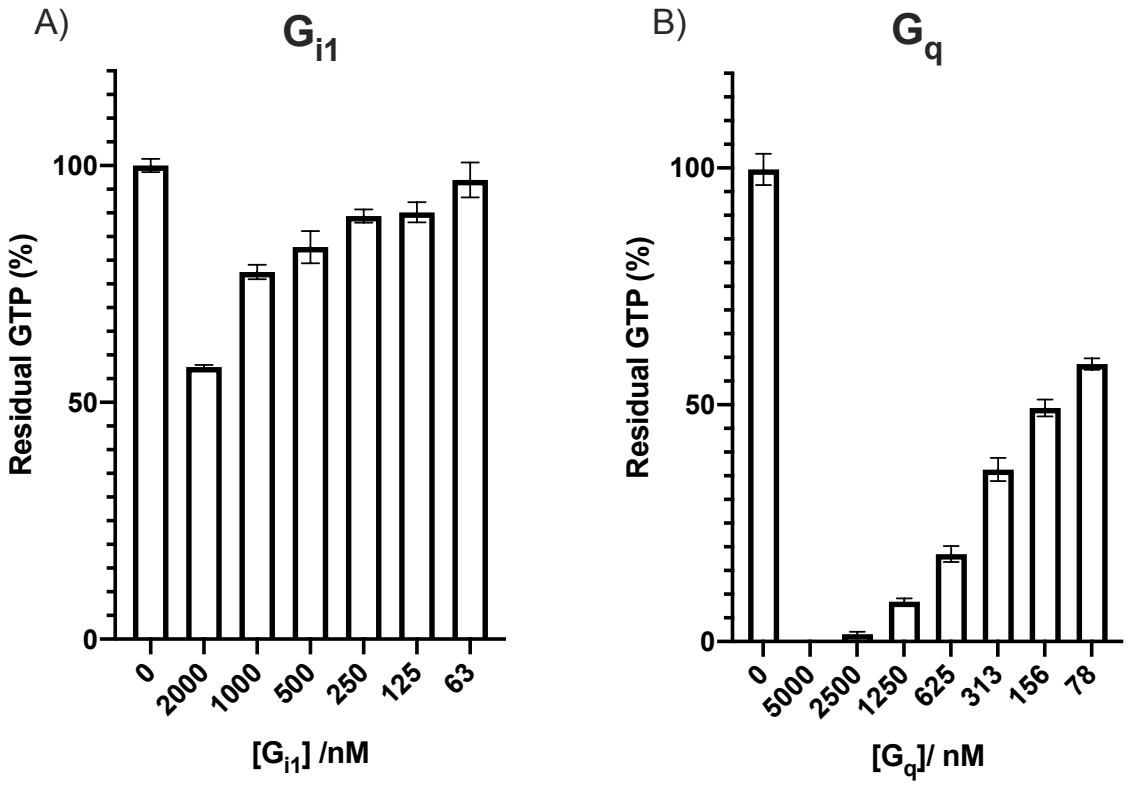


Figure 3.5: Intrinsic GTPase activity of A) G_{i1} and B) G_q. Error bars correspond to +/- standard error of the mean (SEM), with n=3 for G_{i1} and n=4 for G_q. Values are normalised to the GTP-only control.

Both G_{i1} (figure 3.5A) and G_q (figure 3.5B) are capable of hydrolysing GTP in the absence of receptor, as indicated by the decrease in residual GTP. G_q shows considerably more

GTPase activity than G_{i1} under these conditions. From these experiments, a G protein concentration was selected, and the receptor titrated against the G protein, in order to ascertain the activity of the receptor on the given G protein.

For G_{i1}, a final G protein concentration of 0.5 μM was chosen, since at this concentration the intrinsic GTPase activity of the protein can be reliably detected. Receptor was serially diluted into a buffer containing 0.1% DDM, 0.01% CHS & 10 μM GTP, and mixed with G_{i1} to give a final concentration of 5 μM GTP. As demonstrated in figure 3.6A, even at very low concentrations, the receptor causes a significant stimulation of G_{i1} GTP hydrolysis, demonstrating the activity of both receptor and G protein.

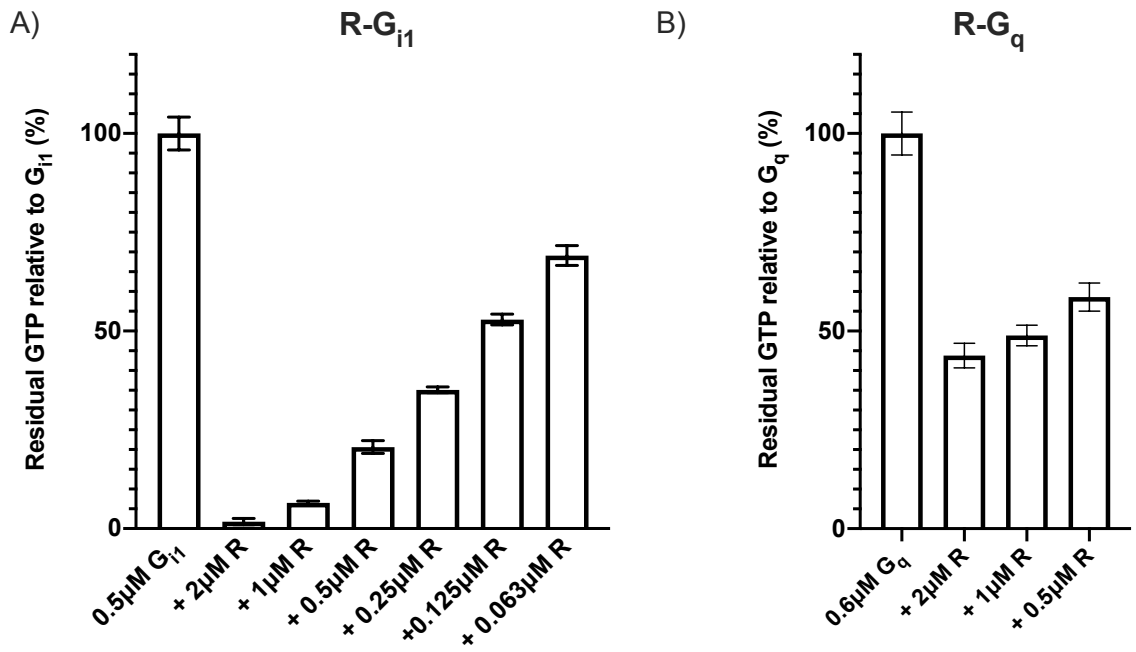


Figure 3.6: Activity of hNTS1 on A) G_{i1} and B) G_q. Error bars correspond to +/- SEM, with n=3 for both proteins. Values are normalised to the residual GTP in the presence of the G protein. "R" = hNTS1.

For G_q, the final concentration of G protein used was 0.6 μM, since initial attempts using less G protein failed to detect significant receptor activity. Receptor stimulated GTP hydrolysis can also be detected for this G protein (figure 3.6B), albeit at higher receptor concentrations than for G_{i1}, again demonstrating the activity of receptor and G protein.

3.4.4 Native mass spectrometry of hNTS1

Purified, PNGaseF-treated hNTS1 material was studied by native mass spectrometry. Using an optimised detergent mixture and acceleration voltage, a native mass spectrum with low noise could be obtained for the receptor (figure 3.7).

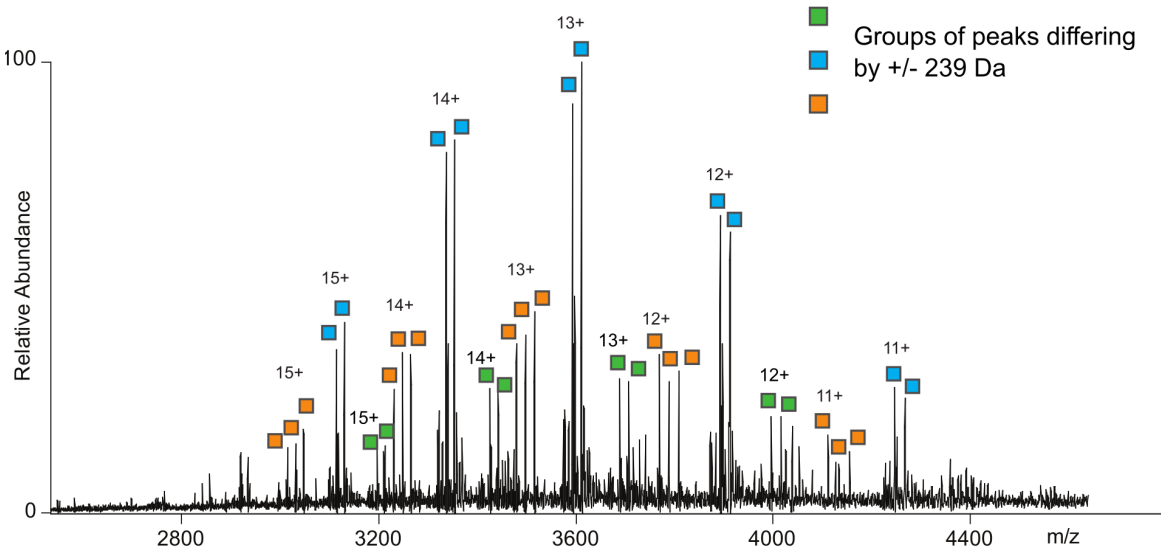


Figure 3.7: Native mass spectrum for hNTS1 treated with PNGaseF. Charge states from 11+ to 15+ are observed. Three groups of masses are identified that differ by the mass of a palmitate group, 239 Da.

It is clear from figure 3.7 that there are many mass states for the receptor. Each charge state (11+ to 15+) possesses three groups of masses, labelled as green, yellow and blue for simplicity. Each of these groups contains masses that differ by the mass of a palmitate group, 239Da, suggesting multiple palmitoylation states of the receptor. In order to determine how these states are related to the unpalmitoylated receptor, the receptor was treated with the enzyme palmitoyl-protein thioesterase (PPT-1) to leave the receptor in its unpalmitoylated state (0P).

As anticipated, the PPT-1 sample has a greatly simplified mass spectrum (figure 3.8, top). Aligning the spectra for the treated and untreated samples reveals the masses of the unpalmitoylated state for each of the three groups, and thus discerns the palmitoylation states seen in the untreated spectrum (figure 3.8, bottom).

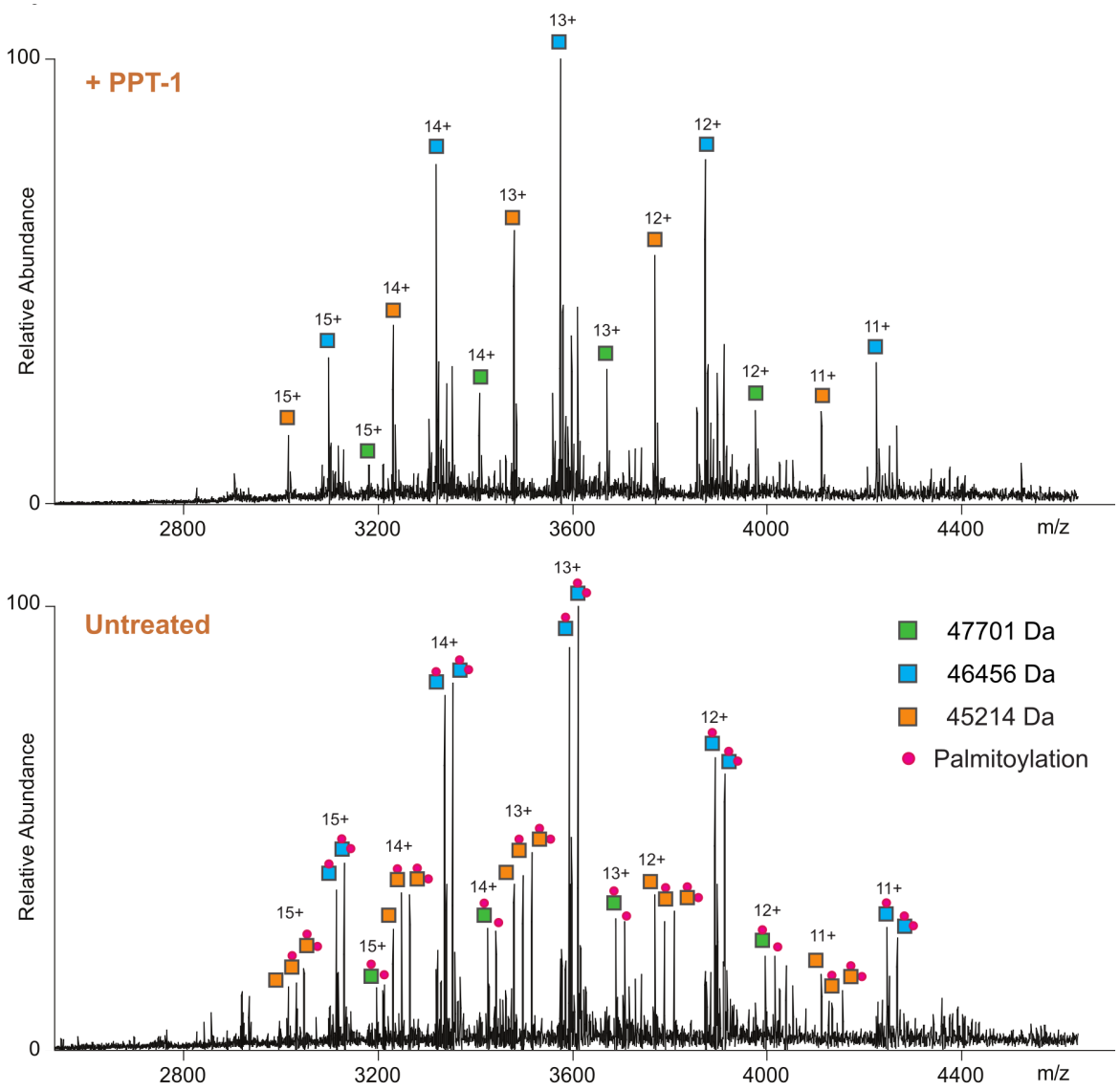


Figure 3.8: Effects of PPT-1 treatement on the hNTS1 native mass spectrum. Depalmitoylation of the sample with PPT-1 reveals the unpalmitoylated masses of the receptor (top), which in turn allows assignment of the palmitoylation states observed in the untreated sample (bottom, same as figure 3.7).

For the most abundant "blue" mass, the 0P state has a mass of 46,456 Da, and this state is of very low abundance in the untreated sample. Instead, once-palmitoylated (1P) and twice-palmitoylated (2P) states are present with roughly equal populations in the untreated sample (figure 3.8, bottom). A similar situation is found for the "green" mass group, where the 0P state has a mass of 47,701 Da and the 1P and 2P states dominate without PPT-1 treatment. The "orange" mass group has a 0P mass of 45,214 Da. This 0P state exists in roughly equal populations alongside the 1P and 2P states in the untreated sample. It

should be noted that all three mass states are smaller than the theoretical mass of the hNTS1 construct after 3C cleavage and without post-translational modifications, 49,424 Da.

In addition to revealing the presence of several receptor masses with different palmitoylation states, a number of mass adducts persist in the presence of PPT-1. These are revealed by a magnified view of the 13+ state for the blue, 46,456 Da mass (figure 3.9). Notably, a 62-63 Da species is found bound to all of the different adducts of the 46,456 Da species (black arrow, figure 3.9).

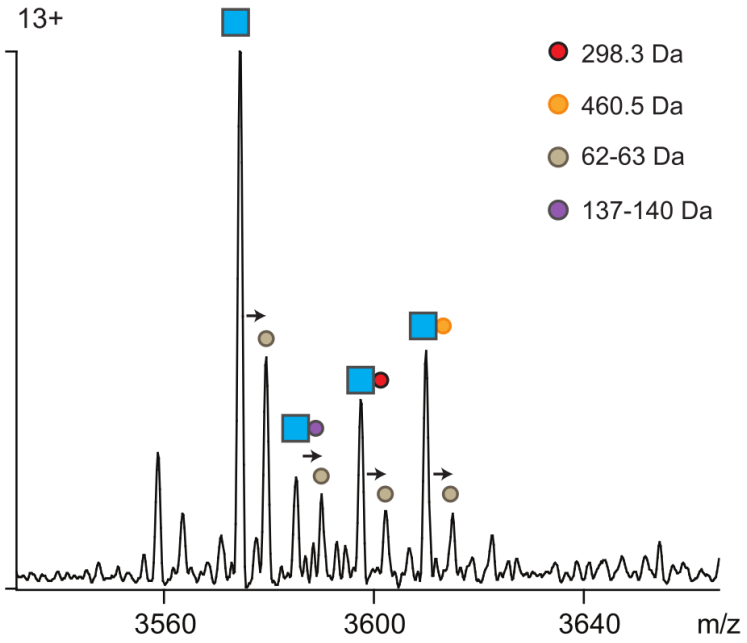


Figure 3.9: Adducts of hNTS1 observed in native mass spectrum of the PPT-1 treated sample. The receptor exhibits several modifications in addition to palmitoylation. The black arrow shows the modification of each receptor mass state by an additional adduct of 62-63 Da.

3.5 Discussion

3.5.1 Production and characterisation of G_{i1}, G_q and hNTS1

The primary aim of this chapter was to obtain purified G_{i1}, G_q and hNTS1 for further studies, and all three proteins were indeed purified in sufficient quantity and at sufficient purity for the work performed in the remainder of this thesis.

The GTPase activity assays conducted in this chapter demonstrate that both the receptor and the two G proteins are functionally active: both G proteins display intrinsic GTPase activity (figure 3.5), and addition of purified receptor stimulates further GTP hydrolysis (figure 3.6), consistent with the GEF activity of hNTS1. The Glo-GTPase™ assay is an end-point assay, and not a kinetic assay, so does not provide time-resolved detail of G activation. However, it does provide a convenient readout of GPCR activity on G proteins, which can be compared across different conditions provided incubation times are kept constant. The sample requirements are relatively low and the system is tolerant of detergents and phospholipids (Strohman *et al*, 2019). Since a reasonable activation "window" could be observed for the effect of the receptor on each G protein, this assay should allow for screening of variables that affect receptor activity on these G proteins – most notably, the presence of specific phospholipids.

Whilst G_{i1} could clearly cause GTP hydrolysis, its intrinsic GTPase activity was lower than that reported elsewhere using the same assay (figure 3.5A) (Kato *et al*, 2019), where a G_{i1} heterotrimer produced in High Five™ cells was used at a lower detergent concentration. It is possible this discrepancy reflects that G_{i1} used in this chapter was myristoylated but not palmitoylated, or reflects the sensitivity of G_{i1} activity to detergents, which has been demonstrated elsewhere (Kubota *et al*, 2009; Sarvazyan *et al*, 1998). It must be noted the incubation time used in a previous report (Kato *et al*, 2019) is longer than used here, and

since an end-point assay is used, comparison of protein activity in experiments conducted with different incubation times is not straightforward. Nonetheless, the G_q heterotrimer produced in this chapter displayed a strong intrinsic GTPase activity (figure 3.5B), similar to results published elsewhere using the same High Five™ expression system and purification scheme (Kato *et al*, 2019).

GTP hydrolysis by G_{i1} was robustly stimulated by agonist bound hNTS1, even at receptor concentrations below 100 nM (figure 3.6A), which is consistent with results elsewhere (Kato *et al*, 2019). Compared to G_{i1}, higher concentrations of receptor were required to detect receptor stimulation of G_q GTP hydrolysis (figure 3.6B), suggesting that under the conditions used, coupling of hNTS1 to G_{i1} is more efficient. This suggests a greater sensitivity of the hNTS1-G_q interaction to the presence of detergents and/or absence of lipids– indeed, published results using lower detergent concentrations than those used here demonstrate stronger hNTS1-G_q coupling (Kato *et al*, 2019).

3.5.2 Native mass spectrometry

To date, a very limited number of GPCRs have been studied by native mass spectrometry. A very high quality set of spectra were obtained for a near wild-type GPCR sequence. They allow clear quantification of palmitoylation and identification of adducts, even in the presence of at least three different mass states of the receptor. Several points of interest are raised by these spectra.

3.5.2.1 Proteolysis of hNTS1

The masses resolved for the receptor in the 0P/unpalmitoylated states are lower than the predicted mass of the 3C-cleaved hNTS1 construct, suggesting proteolysis (table 3.2). Proteolysis in baculovirus-based insect cell systems has been previously documented (Hom & Volkman, 1998; Gómez-Sebastián *et al*, 2014), and may persist even in the presence of commonly used protease inhibitors (Gotoh *et al*, 2001). The protein used for these native

mass spectrometry experiments was produced in the same way to that for a recent cryo-EM structure in which continuous protein density for the receptor core is observed (Kato *et al*, 2019). C-terminal cleavage of the protein is possible and could readily account for the observed differences as outlined in table 3.2. Such cleavage would have to occur after the initial Ni-NTA purification step, since the his_{10} tag used in the initial Ni-NTA purification is located on the extreme C-terminus of the construct – i.e. this purification step requires an intact C-terminus. One possibility is that during the 3C protease mediated cleavage after Ni-NTA, the removal of eGFP from the receptor construct reveals a cryptic protease site and/or makes the receptor a better substrate for contaminating proteases. The presence of even a very small amount of protease could have a significant effect since the sample is left to dialyse for 16 hours at 4°C. N-terminal cleavage events are less plausible, since the intact N-terminus is needed for M1 anti-FLAG purification to work, and this step occurs later in the purification process, when contaminating proteases are much less likely to be present.

Mass from spectrum (Da)	**Difference from theoretical mass (Da)**	**Proposed explanation**
45214	4210	Cleavage of the C-terminus could account for the mass difference, with the constraint that the palmitoylation sites at C381/C383 must be intact. The following C-terminal peptides have a mass of ~4.2kDa: W386-E420, R387-L422, R388-F423
46456	2968	Smaller cleavages, or cleavage as above plus residual glycosylation
47701	1723	Smaller cleavages, or cleavage as above plus residual glycosylation

Table 3.2: Accounting for the difference between theoretical hNTS1 mass and those observed by native mass spectrometry

The remaining receptor masses would then represent either different cleavages, or differently glycosylated states of the proteolysed receptor. Whilst the receptor was treated with PNGaseF before native mass spectrometry, it is possible this enzymatic deglycosylation was incomplete or glycans are present that cannot be cleaved by this enzyme. In particular, insect species tend to produce glycans with α(1-3) fucosylation, which is inhibitory to PNGaseF (Tretter *et al*, 1991; Walski *et al*, 2017).

3.5.2.2 Palmitoylation of hNTS1

Palmitoylation at C-terminal cysteines has been demonstrated for many GPCRs (reviewed in (Qanbar & Bouvier, 2003)), and inferred for others based on sequence homology. Typically, techniques such as metabolic labelling with tritiated palmitate are used to demonstrate palmitoylation, with site directed mutagenesis identifying the residues that are targeted by this modification. However, with these techniques it can be difficult to pinpoint the extent of palmitoylation, and one must distinguish between the effects of abolishing palmitoylation and mutation of the receptor sequence. Using hNTS1 as an example, metabolic labelling and a fatty acyl exchange assay were used to demonstrate receptor palmitoylation in human cells (Heakal *et al*, 2011), and a double C381S-C383S mutant demonstrates that one or both of these cysteines are sites of palmitoylation. The Western blots presented in this paper suggest that some receptor exists in an unpalmitoylated state, but this is very difficult to quantify from the data presented. By contrast, native mass spectrometry allows direct detection of the different mass states of a receptor, and indeed the native mass spectra in this chapter (figure 3.7 and figure 3.8) clearly demonstrate receptor palmitoylation. To the best of our knowledge, this is the first time that palmitoylation states of a GPCR have been directly observed by native mass spectrometry.

When considering the receptor population as a whole, almost all receptor masses identified in the native mass spectra (figure 3.8) possess at least one palmitoyl group. The

unpalmitoylated state is of a low abundance, whilst the doubly-palmitoylated (2P) state is of similar abundance to the singly palmitoylated (1P) state. The 2P state is interpreted to represent a receptor with C381-palmitoyl and C383-palmitoyl modifications. The 1P state could represent a mix of C381-palmitoyl and C383-palmitoyl states, such that neither cysteine is fully palmitoylated in this population. Alternatively, the 1P state could represent fully palmitoylated C381 or C383. Given that many GPCRs only have one cysteine that is targeted by palmitoylation (Qanbar & Bouvier, 2003), it is suggested that full palmitoylation at one cysteine is more likely. In any case, the heterogeneity of palmitoylation states is of interest, since it is typically assumed that receptors purified from Sf9 or HEK293 cells are fully palmitoylated.

The origin of the heterogeneity in palmitoylation is unclear. One possibility is that the results obtained are a faithful reproduction of the overall palmitoylation state of the receptor in a human cell. However, it should be noted that the receptor was expressed in Sf9. Whilst this eukaryotic system has been documented to perform a wide variety of post-translational modifications (Klenk, 1996), the patterns of glycosylation are different to those seen in mammalian systems and it cannot be excluded that the mixture of palmitoylation states seen for hNTS1 is a result of some lower efficiency of the Sf9 palmitoylation machinery. Another possibility is that some of the palmitoylation modification is lost during the purification process.

Nonetheless, the data presented in figures 3.7, 3.8 & 3.9 clearly show the potential for native mass spectrometry to resolve the post-translational modifications of even difficult to study membrane proteins such as GPCRs, and to provide unique insights into the relative abundance of such modifications.

3.5.2.3 Small molecule adducts of hNTS1

In addition to palmitoylation, several small molecule adducts were identified in the PPT-treated mass spectrum (figure 3.9). The relatively small masses preclude obvious candidates such as NTS1 ligands (namely NT_{8-13}) or phospholipids. It is not yet possible to make firm conclusions on the identity of these adducts, and work is ongoing to identify them by tandem MS. However, the data presented clearly demonstrate the potential of native mass spectrometry to identify ligands and lipids that co-purify with the receptor, even in relatively complex cases such as that seen for hNTS1.

3.5.3 Conclusions

hNTS1, G_q and G_{i1} were expressed and purified in a functional form. The GTPase-Glo™ assay was established and should allow for screening of compounds that modulate receptor activity, most notably lipids.

Native mass spectrometry of hNTS1 represents the state of the art in this field, with very high quality spectra allowing for identification and relative quantification of receptor palmitoylation. As such, the data presented pave the way for further native mass spectrometric studies of wild-type like GPCRs. In particular, work is ongoing to identify small molecule adducts by tandem mass spectrometry, and to analyse the relative G protein coupling abilities of the 0P, 1P and 2P states.

4. Lipid determinants of NTS1-G protein coupling

4.1 Introduction

4.1.1 Roles for lipids in GPCR function

GPCRs conduct their physiological roles embedded in a membrane, and there exist a plethora of ways in which this membrane, and the lipids of which it consists, can modulate GPCR function.

Modes of lipid action on GPCR function can be broadly classified into three groups (Oates & Watts, 2011) (figure 4.1). Firstly, specific receptor-lipid contacts may occur, which can be thought of as "ligand-like effects" (Salas-Estrada *et al*, 2018) (figure 4.1A). Secondly, the lateral organisation of biological membranes into microdomains may regulate receptor activity by trafficking the receptor to parts of the membrane that are enriched in certain downstream signalling partners (figure 4.1B). Finally, lipids modulate physical properties of the bilayer, which may in turn favour one conformation of the receptor over another - "solvent-like effects" (Salas-Estrada *et al*, 2018) (figure 4.1C). These properties could include membrane fluidity and thickness, whereby the membrane may stretch or compress to accommodate the hydrophobic portion of the receptor (which may differ in different conformations). In a related way, the membrane may be under curvature stress due to the presence of lipids which prefer to adopt curved monolayers (e.g. phosphatidylethanolamine), which may in turn favour one receptor conformation over another.

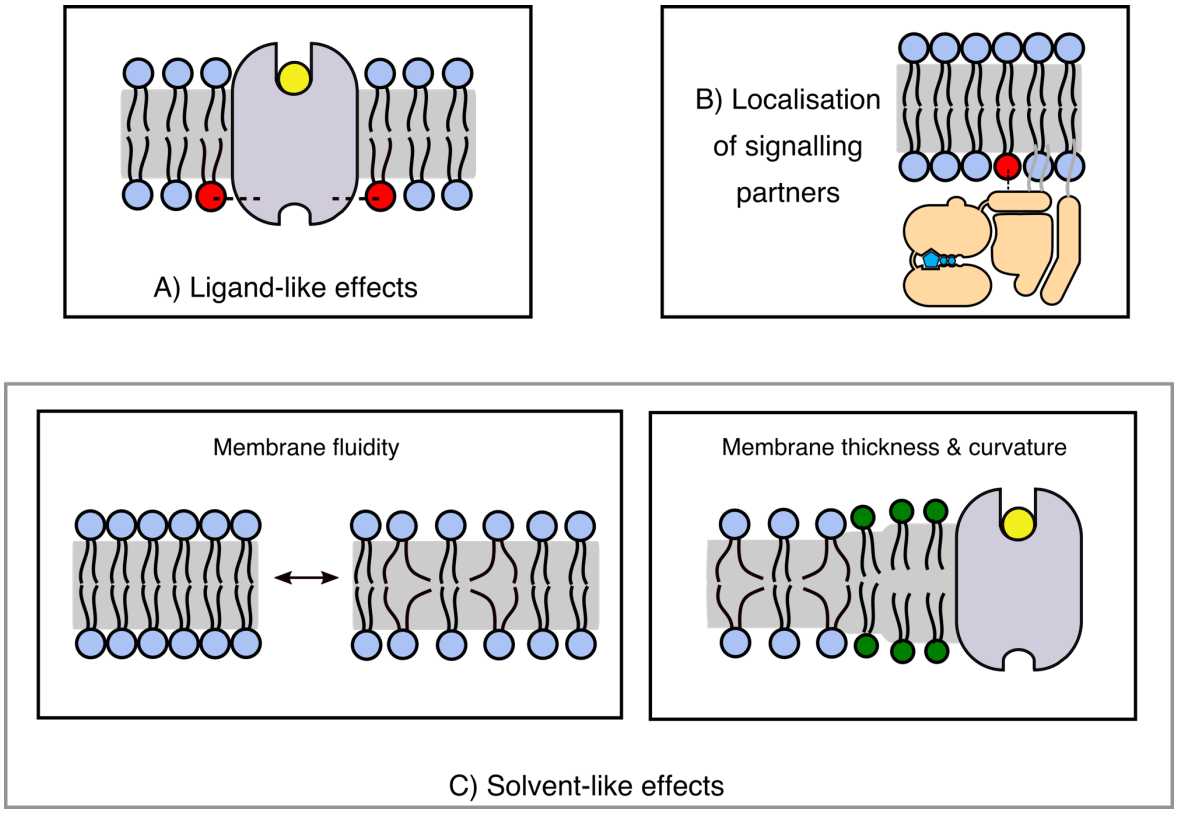


Figure 4.1: Modes of action by which lipids modulate GPCR activity. A) Ligand-like effects of lipids resulting from specific lipid-receptor contacts (dashed line). B) Membrane composition may also affect localisation of signalling partners such as the G protein shown here. C) Solvent like-effects include changes in membrane fluidity and hydrophobic mismatch/curvature stress. A green headgroup is used to indicate a lipid with a preference for curved monolayers. Based on figures in (Oates & Watts, 2011; Weis & Kobilka, 2018) .

The roles of lipids on receptor activity are best-studied for the photoreceptor rhodopsin. Early studies demonstrated the sensitivity of rhodopsin-G_t coupling to removal of lipids by detergents (Bubis, 1998). Zwitterionic phosphatidylethanolamine (PE) lipids enhance rhodopsin activation and recruitment of G_t (Botelho *et al*, 2002; Alves *et al*, 2005), lipids containing polyunsaturated docoshexanoic acid (DHA) acyl chains (Feller *et al*, 2003) favour an active state of rhodopsin and the presence of cholesterol inhibits activation (Mitchell *et al*, 2001; Niu *et al*, 2001). These effects were initially proposed as being solvent-like, modulating the receptor through changes in membrane curvature stress (Botelho *et al*, 2002). Indeed, pioneering CW-EPR studies (Watts *et al*, 1979) reveal that rhodopsin does

not specifically bind spin labelled analogues of stearic acid, phosphatidylcholine (PC) or cardiolipin. However, evidence has also accumulated for ligand-like effects of PE headgroups and DHA chains on rhodopsin. Saturation-transfer NMR studies show direct, preferential binding of DHA chains and PE headgroups to the receptor (Soubias *et al*, 2006), and a follow up study (Soubias *et al*, 2010) demonstrates that PE headgroups activate rhodopsin both through inducing curvature stress, and through direct hydrogen bonding to the receptor. Direct binding events of PE and DHA have also been visualised by molecular dynamics simulations (Salas-Estrada *et al*, 2018). Work by Hessel and colleagues suggests that rhodopsin may organise its local lipid environment through a flippase activity that distributes lipids such as PS to the inner leaflet, which may facilitate G_t coupling (Hessel *et al*, 2000, 2001, 2003).

Like rhodopsin, the activities of other class A GPCRs show sensitivity to cholesterol. The literature on GPCR modulation by cholesterol is considerable and has been the subject of numerous reviews (Oates & Watts, 2011; Goddard & Watts, 2012; Jafurulla *et al*, 2019), but no consistent trends for cholesterol modulation of GPCRs emerge. As examples, cholesterol has been observed to modulate ligand binding both positively (Harikumar *et al*, 2005) and negatively (Guixà-González *et al*, 2017), to modulate the dimerisation of receptors (Gahbauer *et al*, 2018) and has been observed bound to receptors in crystal structures (Hanson *et al*, 2008; Liu *et al*, 2012b).

In addition to cholesterol, a series of recent studies point towards roles for ligand-like effects of phospholipids on the function of a prototypical class A GPCR, the β_2AR. Anionic phosphatidylinositol (PI), phosphatidylserine (PS) and especially phosphatidylglycerol (PG) phospholipids favour agonist binding to the β_2AR, whilst the zwitterionic PE favours antagonist binding (Dawaliby *et al*, 2016a). Moreover, the kinetics of receptor activation by a nanobody are faster in anionic lipids than zwitterionic lipids, although in all cases an

active conformation is achieved by addition of a nanobody. Unlike G proteins, the nanobody does not bind lipids, and so these results likely reflect how lipids alter the conformational transitions of the receptor itself. Molecular dynamics simulations of the β_2AR corroborate these experiments; phospholipids are observed to penetrate between TM helices 6 and 7 in order to form an ionic contact with the conserved $R^{3.50}$ residue of the ionic lock, in turn leading to acyl chains occupying the orthosteric binding site of the receptor (Neale *et al*, 2015). This interaction is more favourable with an active-like conformation of the receptor, with the anionic PG making stronger contacts than the zwitterionic PC.

A follow-up paper has suggested a role for lipids in the G protein selectivity of the β_2AR (Strohman *et al*, 2019). Negative phospholipids facilitate the interaction of the β_2AR and G_s, consistent with previous results using a nanobody. By contrast, zwitterionic PE facilitates coupling between β_2AR and G_{i3}. Interestingly, anionic phospholipids also stimulate this pairing, provided that Mg^{2+} or Ca^{2+} cations are present. Without these cations, deleterious repulsions occur between anionic phospholipids and an anionic "EDGE" motif in the N-terminal HN helix of $G\alpha_{i3}$, which in turn inhibit β_2AR-G_{i3} coupling. As such, this study highlights that in the context of receptor-G protein interactions, lipid-G protein interactions can also affect receptor coupling. Notably, the soluble, anionic cholesterol analogue cholesteryl hemisuccinate (CHS) is inhibitory to the β_2AR- G_{i3} interaction in much the same manner as anionic phospholipids in these studies. The notion that receptor and downstream signalling partner may have differing lipid preferences has also been demonstrated for rhodopsin, whereby negatively charged PS, phosphatidic acid (PA) and PI do not affect receptor activation, but do facilitate recruitment of arrestin to the activated, phosphorylated, detergent-solubilised receptor (Sommer *et al*, 2006), with the C-edge loops of arrestin acting as a membrane contact

region (Lally *et al*, 2017).

In both studies of the lipid dependence of β_2AR activation, nanodiscs of varying lipid composition were used (Dawaliby *et al*, 2016a; Strohman *et al*, 2019). However, the same effects were also seen when the detergent-solubilised receptor was supplemented with detergent-solubilised lipids, suggesting that the lipid effects on the receptor and/or G protein are ligand-like.

4.1.2 Roles for lipids in NTS1 function

Two separate approaches have identified lipid binding preferences for NTS1.

A CW-EPR study by (Bolivar *et al*, 2016) using rNTS1 reconstituted into PC liposomes alongside specific spin-labelled lipids demonstrates that, relative to PC, stearic acid and PS lipids show stronger binding, whilst cholesterol and PE are similar to PC. Accordingly, atomistic simulations of the 4BUO rNTS1 structure in a mixed bilayer reveal roughly twice the contacts of the receptor to PS compared to PC, PE or cholesterol, with PS binding at the intracellular ends of TM4 and TM6.

Native mass spectrometry has also been used to study NTS1-lipid binding, in detergent micelles and using a similar thermostabilised rNTS1 construct as that used to obtain the 4BWB structure (see table 1.2, section 1.2.8.1) (Yen *et al*, 2018). The *E. coli* expressed receptor is observed to co-purify with phosphatidic acid (PA) lipids, and bind to exogeneous, detergent-solubilised anionic PA, PS & PI lipids, whilst PC, PG and diacylglycerol (DAG) show no binding. Of the PI lipid species tested, specificity for phosphatidylinositol 4,5 bisphosphate ($PI(4,5)P_2$) is observed, and this lipid shows a higher degree of binding than any other lipid tested. Course grained molecular dynamics simulations of the 4BUO rNTS1 structure in POPC bilayers supplemented with PIP_2, PS or both reveal strong headgroup-mediated contacts between receptor residues and the PIP_2 headgroup (Yen *et al*, 2018; Hedger, 2017). Fewer interactions with PS are seen, and these

are largely lost in the presence of PIP_2. PIP_2 interacts with positively charged groups on the intracellular face of the receptor, and mutations of these sites accordingly reduce the lipid binding observed by native mass spectrometry. These lipid binding sites again map to the intracellular end of TM4.

Two studies have addressed the dependence of NTS1-ligand binding on lipid composition. Ligand binding of NTS1 is reported to be the same in PC or 1:1 PC-PG nanodiscs (Inagaki *et al*, 2012), whilst brain polar lipid (BPL) liposomes support higher ligand binding activity than mixtures of PE/PC and PE/PC/cholesterol (Oates *et al*, 2012). As such, NTS1 seems to differ from the β_2AR, where PG enhances agonist binding.

There is also evidence that lipids modulate NTS1-G protein coupling. NTS1 in PC-PG nanodiscs shows a higher apparent affinity for $G\alpha_q$ than in PC nanodiscs (Inagaki *et al*, 2012), suggesting that the anionic PG lipid favours an active receptor conformation, enhances the receptor-G protein interaction, or both. The affinity of NTS1 for $G\alpha_{i1}$ has also been explored, using microscale thermophoresis (MST) and nanodiscs of different compositions (Dijkman & Watts, 2015). The receptor in BPL nanodiscs shows a higher affinity for $G\alpha_{i1}$ than receptor-nanodiscs consisting of PC-PG (1:1) or PC-PG-BPL (1.5:1:1.07). As such, the interaction is sensitive to the presence of some component of the BPL mix, and the authors argue that PE plays a role in the interaction by analogy with rhodopsin. Roles for the other known BPL components (namely PS and PI) cannot be excluded and it should also be noted that the $G\alpha_{i1}$ protein shows a similar pattern of affinity for empty nanodiscs as rNTS1-loaded nanodiscs, suggesting that the intrinsic lipid binding of the G protein accounts at least partially for the observed trends. Finally, for the HTGH4-ΔIC3B rNTS1 construct, the GTPase-Glo™ assay shows that $PI(4,5)P_2$ potentiates the effect of the receptor on G_i activity(Yen *et al*, 2018).

These data taken together demonstrate that NTS1-G protein coupling is sensitive to modulation by lipids, and that different lipids may be involved in potentiating NTS1-G_i vs NTS1-G_q coupling, especially in the context of similar findings for β_2AR- G_{i3} vs β_2AR-G_s coupling. This is yet to be directly demonstrated, and it is difficult to compare the existing data, since they have been produced using different experimental approaches and receptor constructs.

4.2 Aims

Given the wealth of data on lipid modulation of GPCRs, including NTS1, and given that NTS1 shows a promiscuous G-protein coupling profile, the primary aim of this chapter was to identify lipids that modulate the interaction of NTS1 with G_{i1} and G_q proteins.

To this end, the GTPase-Glo™ assay described in section 1.6 and chapter 3 was employed to screen lipids for their effects both on the G proteins alone, and on the ability of the receptor to simulate the G proteins. Detergent-solubilised lipids were chosen so as to isolate ligand-like effects of the lipids.

4.3 Materials & methods

4.3.1 Protein expression & purification

All protein material used in this chapter was expressed and purified as outlined in section 3.3 and appendix section A3.

4.3.2 Lipid preparation

The lipids used in the work to be described in this chapter are illustrated in figure 4.2: 1-palmitoyl-2-oleoyl-*sn*-phosphatidylglycerol, 1-palmitoyl-2-oleoyl-*sn*-phosphatidylserine, dioctanoyl-*sn*-phosphatidylinositol(4,5) bisphosphate, and the brain polar lipid mix. For simplicity, these lipids are referred to as PG, PS, PIP_2 and BPL, respectively, from hereon-

in. All lipids were purchased from Avanti Polar Lipids. PS, PG and BPL were supplied dissolved in chloroform. These lipids were aliquoted into glass tubes and dried to a film with a stream of N_2 gas followed by 2-4 hours in a vacuum desiccator. Films were resuspended in 20 mM HEPES pH 7.4, 100 mM NaCl and sonicated in a bath sonicator, before addition of DDM to give a final solution of 1% DDM, 20 mM HEPES pH 7.4, 100 mM NaCl and 15-20 mM lipid. Solutions were incubated (4°C, 18 hour), with bursts of sonication (30-90 s) employed 3-4 times during this incubation. These lipid stock solutions were diluted to appropriate concentrations in the appropriate assay buffer.

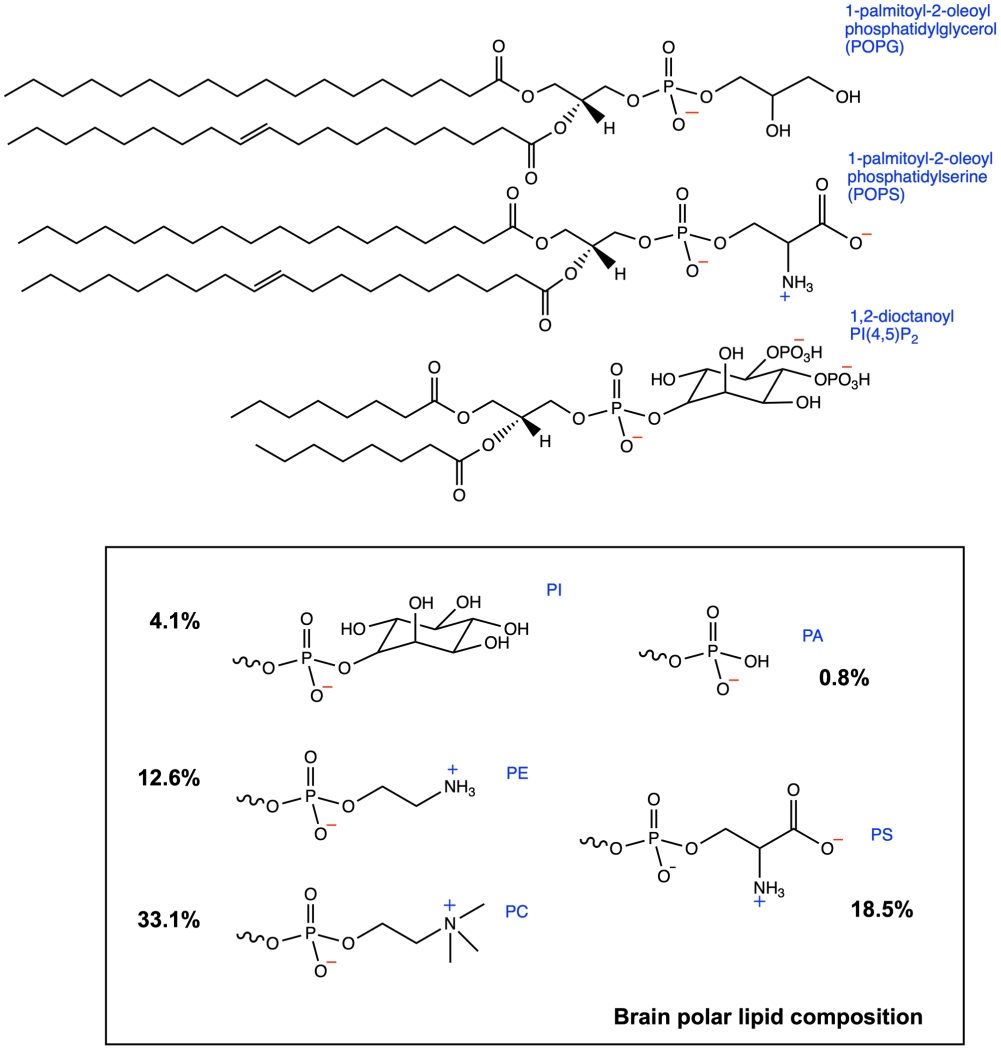


Figure 4.2: Chemical structures of lipids used chapter 4. The headgroup composition of the brain polar lipid mix is indicated in the black box. Diacylglycerols are not shown for BPL, as the acyl chain composition of the BPL extract is heterogeneous.

PIP_2 was purchased from Avanti Polar Lipids as a powder and resuspended directly into the appropriate assay buffer to a stock concentration of 800 μM with bath sonication (~90 s).

4.3.3 GTPase-Glo™ assays

GTPase-Glo™ assays were performed as outlined in section 3.3.4 with some modifications. Unless specified otherwise, the assay buffer used was 20 mM HEPES, 100 mM NaCl, 0.1% DDM (w/v), 100 μM TCEP & 10 mM $MgCl_2$. Unlike in chapter 3, CHS was not included in the buffer, since it was anticipated that this anionic compound may mask the effects of anionic lipids. A high $MgCl_2$ concentration was chosen so as to screen potentially deleterious anionic-anionic repulsions between G protein and lipid, based on previous observations elsewhere (Strohman *et al*, 2019).

To study the effects of lipids alongside a lipid-free control, a mix of receptor and GTP at 4x final concentrations was prepared (i.e. 4 μM receptor for G_q conditions, 500 nM receptor for G_{i1} conditions & 20 μM GTP in all cases). This was then diluted to a 2x stock in either assay buffer or a lipid stock. Receptor was incubated with buffer/lipids on ice for 30 minutes, before mixing with assay buffer or G protein on a 384 well microplate. Similarly, for controls assaying the effect of lipids on G proteins, essentially the same preparation was made but minus the receptor: 20 μM GTP was diluted to 10 μM by addition of buffer/lipid for 30 minutes on ice, before being added to G proteins on the microplate to a final concentration of 5 μM GTP. Unless otherwise specified, the final concentration used for all lipids was 200 μM.

4.3.4 Data processing

In analysing the effects of lipids on G proteins (without receptor), data were normalised such that the counts given by a control containing receptor and 5 μM GTP (i.e. no G protein) are taken as representing 100% residual GTP.

Where necessary, to facilitate comparison of the effects of different lipids on a given receptor-G protein pairing, the following processing was performed. The residual GTP counts for each receptor & G protein (+/- lipid) condition were divided by the counts given by the respective G protein condition (+/- lipid) without receptor. In processing these data, the errors on the relevant data sets were also combined according to equation 4.1. For ease of comparison, the resulting quotients were then normalised such that 100% residual GTP is given by the lipid free condition (i.e. receptor-G protein divided by G protein). For transparency, complete normalised data sets are also given in appendix A4.

$$\frac{\sigma_{RG/G}}{RG/G} = \sqrt[2]{(\frac{\sigma_{RG}}{RG})^2 + (\frac{\sigma_G}{G})^2}$$

Equation 4.1. Combination of standard deviations for two data sets in a quotient. RG/G is the quotient for the receptor + G protein condition divided by the respective G protein only condition, and $\sigma_{RG/G}$ is the standard deviation of this quotient.

For statistical analysis, unpaired, two-tailed Student's t-tests were performed in GraphPad Prism.

4.4 Results

4.4.1 Effects of BPL, PG & PS on hNTS1-G_{i1} coupling

Firstly, the effects of BPL, PG & PS lipids on the intrinsic GTPase activity of G_{i1} were analysed. Figure 4.3A demonstrates that none of these lipids caused a statistically significant decrease in GTP counts versus G protein alone. None of the lipids therefore stimulate the intrinsic GTPase activity of the G protein.

As anticipated from previous results (section 3.4.3), addition of the receptor to the G protein caused a considerable decrease in the GTP counts (figure 4.3A, 39% of counts given by G protein alone), reflecting receptor GEF activity on G_{i1}. When the receptor was incubated with lipids, a clear effect of the BPL lipid mix could be seen on receptor-

stimulated G_{i1} activity. With the receptor without lipid giving relative counts of 100%, the addition of BPL reduced the counts to 74%, which is significantly different to the lipid-free control to $p<0.05$. In contrast, in the presence of PG or PS, the readout was not significantly different to the lipid-free control. As such, BPL lipids, but not PG or PS, potentiate the effects of hNTS1 on G_{i1} activity under these conditions.

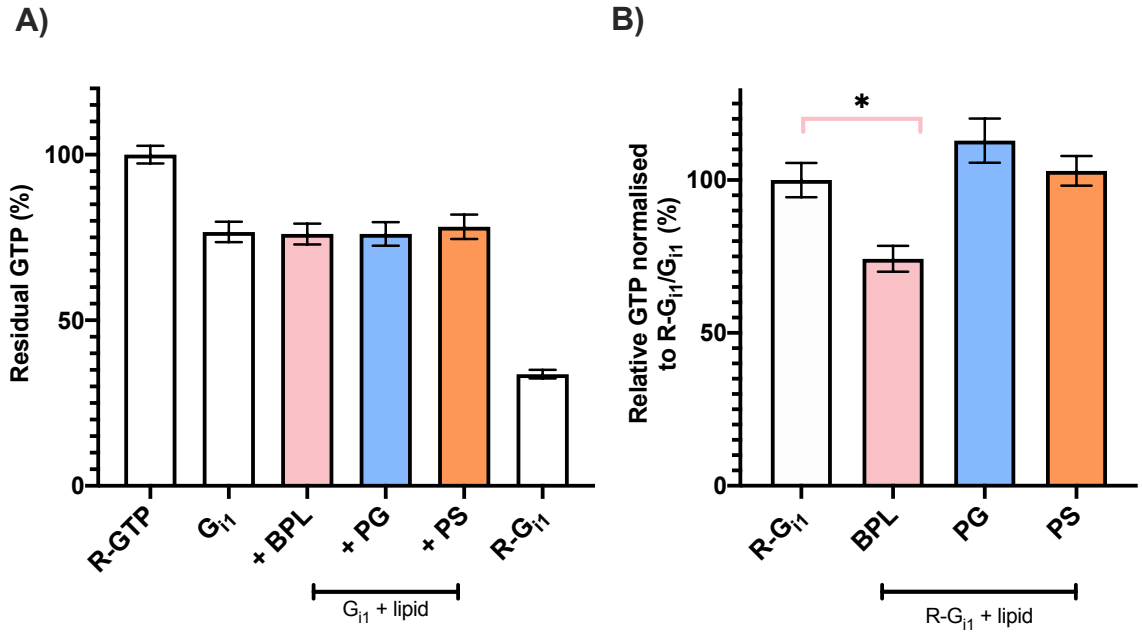


*Figure 4.3: Effects of BPL, PG & PS on A) intrinsic G_{i1}-GTPase and B) hNTS1-stimulated G_{i1} activity. R = hNTS1. In all cases, the final concentrations of G protein, receptor and lipid were 500 nM, 125 nM & 200 µM respectively. [$MgCl_2$] was 10 mM. Error bars are +/- SEM, n=3. Statistical significance was determined by two-tailed Student's t-tests, with * indicating data sets that are significantly different to $p<0.05$.*

4.4.2 Effects of BPL, PG & PS on hNTS1-G_q coupling

For the hNTS1-G_q pairing, higher concentrations of receptor and G_q were employed (both 1 µM final) such that the degree of receptor stimulation compared to the G protein control was comparable to G_{i1} in the absence of lipids. To ensure that this high concentration of G protein did not deplete GTP to a level that was difficult to reliably detect, GDP was included to a final concentration of 5 µM to suppress the intrinsic GTPase activity of G_q. Otherwise, buffer conditions were the same as for assays on G_{i1} (figure 4.3).

Neither BPL nor PG caused a statistically significant change in the intrinsic GTPase activity of G_q (figure 4.4A). PS did show a very slight, but statistically significant decrease (91%, $p<0.05$) in the residual GTP counts versus G_q without lipid, suggesting that this lipid has a very modest activating effect on the G protein in the absence of the receptor.

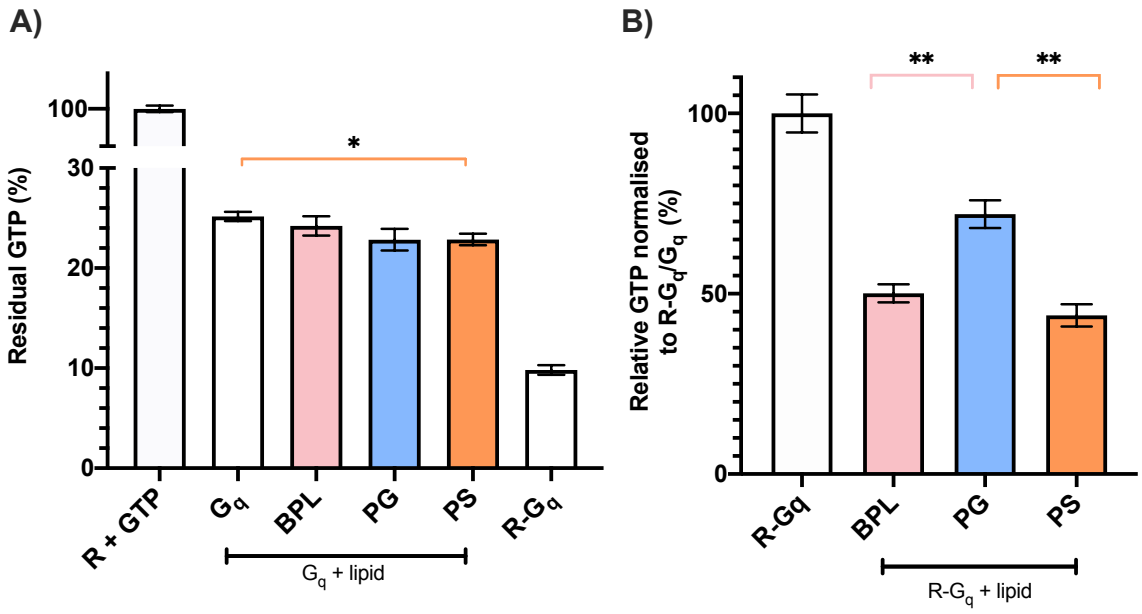


*Figure 4.4: Effects of the lipids BPL, PG & PS on A) intrinsic G_q-GTPase activity and B) hNTS1-stimulated G_q activity. Final concentrations of G protein, receptor and lipid were 1 µM, 1 µM and 200 µM respectively. [$MgCl_2$] was 10 mM. Error bars are +/- SEM, n=3. Statistical significance was determined by two-tailed Student's t-tests, with * and ** indicating $p<0.05$ and $p<0.01$, respectively.*

Addition of the receptor to G_q caused a large decrease in the residual GTP counts under all conditions tested (figure 4.4.A), with a similar decrease to that seen for R-G_{i1} (~40% of the GTP counts given by G protein alone). Incubation of the receptor with BPL, PG or PS potentiated the effects of the receptor on G_q activity (figure 4.4B). In all three cases, when normalised to their respective controls, the incubations with lipid are significantly different ($p<0.05$) from the lipid-free control (NB these significant differences are not indicated on figure 4.4 for simplicity). Furthermore, the relative counts for the PS and BPL conditions were significantly less ($p<0.01$) than those for the PG condition. Where the PG condition gives 72% of the counts compared to the lipid-free control, the BPL condition gives 50%

and the PS condition gives 44%, respectively. The difference between the PS and BPL conditions is not statistically significant (p=0.2).

4.4.3 Effects of $MgCl_2$ & PIP_2 on hNTS1-G_{i1} protein coupling

The GTP turnover assay was also conducted on G_{i1} under low Mg^{2+} conditions (50 µM $MgCl_2$ final) to explore potential screening effects of the cation on the receptor-G protein interaction and to facilitate the inclusion of the polyanionic PIP_2 lipid in the assay, since this lipid is poorly soluble in the presence of divalent cations (Szatmári *et al*, 2018).

Under these conditions, G_{i1} in the presence of PIP_2 at 200 µM produces a statistically significant (p<0.001) decrease in residual GTP compared to G_{i1} alone, demonstrating that the lipid stimulates the GTPase activity of G_{i1} in the absence of the receptor (figure 4.5).

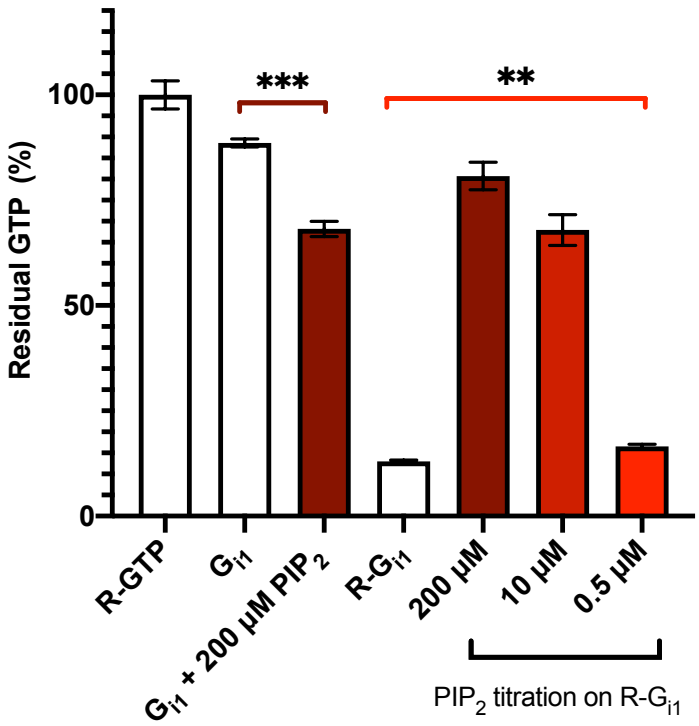


*Figure 4.5: Effects of PIP_2 on the intrinsic and hNTS1-stimulated activities of G_{i1}. Final concentrations of G protein and receptor were 500 nM and 125 nM, respectively. $MgCl_2$ was present at 50 µM. Error bars are +/- SEM, n=3. Statistical significance was determined by two-tailed Student's t-tests, with ** and *** indicating p<0.01 and p<0.001, respectively.*

When receptor was added to G_{i1} without lipids, the increase in GTP hydrolysis was considerable (15% of counts given by G protein alone), and much higher than the stimulation seen at 10 mM $MgCl_2$ (39%, figure 4.3A). When the receptor was incubated with 200 µM PIP_2 and added to G_{i1}, the residual GTP was higher than in the absence of receptor. As such, the lipid appears to inhibit the effects of the receptor on the G protein. This was further explored by including PIP_2 at lower concentrations of 10 and 0.5 µM. As PIP_2 concentration decreases, so too do the inhibitory effects. However, even when PIP_2 concentration is lowered to 0.5 µM (1:4 receptor to lipid molar ratio) the residual GTP levels were still significantly higher ($p<0.01$) than for the receptor + G_{i1} without lipid, even without accounting for differences in the G protein controls.

To explore the effects of low $MgCl_2$ further, BPL was included in the assay (figure 4.6).

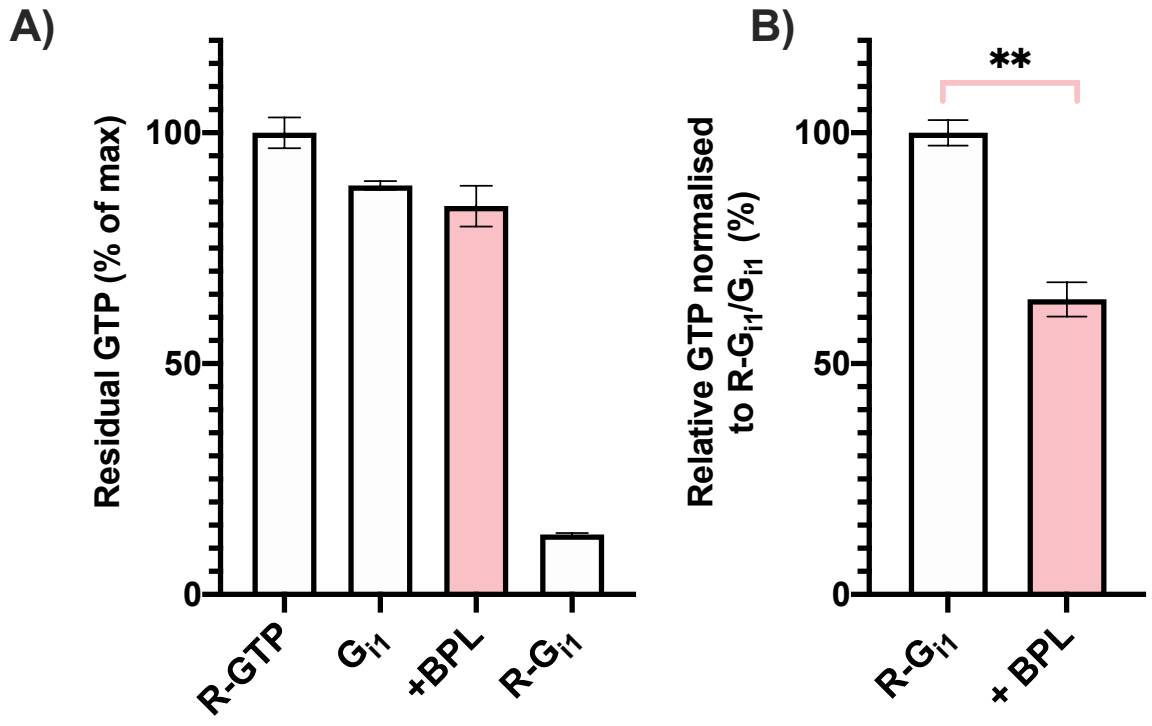


*Figure 4.6: Effects of BPL on the A) intrinsic GTPase activity of G_{i1} and B) hNTS1-stimulated activity of G_{i1} at low $MgCl_2$. Final concentrations of G protein, receptor and lipid were 500 nM, 125 nM & 200 µM respectively. Error bars are +/- SEM, n=3. Statistical significance was determined by a two-tailed Student's t-test, with ** indicating $p<0.01$.*

As was the case under high $MgCl_2$ conditions (figure 4.3A), BPL did not stimulate the GTPase activity of the G protein in the absence of the receptor (figure 4.6A). Even though the lipid-free receptor is much more active at G_{i1} under low $MgCl_2$ conditions, the presence of BPL still caused a statistically significant ($p<0.01$) decrease in residual GTP relative to the lipid-free control (figure 4.6B). The magnitude of this effect is similar to that under high $MgCl_2$ conditions, with the receptor in the presence of BPL giving ~ 65% of the relative GTP counts compared to the lipid-free control.

4.5 Discussion

4.5.1 Effects of lipids on hNTS1-G_{i1} coupling

For the receptor-G_{i1} pairing, the BPL mix, but not PS or PG, was capable of enhancing the effects of the receptor on G_{i1} GTP hydrolysis (figure 4.3B). Notably, none of these lipids had an effect on GTP hydrolysis in the absence of the receptor (figure 4.3A). This is consistent with previous studies showing that increasing the BPL content of nanodiscs increases the affinity of rNTS1 for $G\alpha_{i1}$, whilst PG content appears to have no effect (Dijkman & Watts, 2015). It is possible that PS and PG have subtle effects that were not detectable here, but both were present to a final concentration of 200 μM, which is well above what was required to observe effects of these lipids on the β_2AR in detergent (Dawaliby *et al*, 2016a).

In trying to elucidate which component (or components) of BPL (see figure 4.2) are responsible for the observed effects on hNTS1-G_{i1} coupling, PS can be excluded. Of the known components of BPL, this leaves the anionic PA (0.8% of BPL by weight) and PI (4.1%) and the zwitterionic PE (33.1%) and PC (12.6%). Given that both PS and PG are anionic and had no effect on hNTS1-G_{i1} coupling, it is tempting to speculate that the BPL component responsible for the observed effects is not anionic, especially since the anionic

PA and PI lipids are very minor components of BPL relative to the zwitterionic lipids. Importantly, the effects of BPL persisted when the GTPase-Glo™ assay was conducted at lower $MgCl_2$ concentrations (figure 4.6). By analogy with studies on the β_2AR (Strohman *et al*, 2019), one would expect the effects of an anionic lipid to diminish at lower $MgCl_2$ concentrations, since G_{i1}, like G_{i3}, has the anionic EDGE motif in its N-terminal helix (see also section 4.5.3 and figure 4.8). However, the effects of BPL are at least as potent at low $MgCl_2$, suggesting that Mg^{2+} does not bridge/shield repulsive interactions between BPL and the G protein. Whilst roles for other lipids cannot be conclusively excluded, it therefore seems likely that the effects of BPL on NTS1-G_{i1} coupling are mediated by a zwitterionic lipid, namely PE or PC. Of these two lipids, PE is a more attractive candidate, since its headgroup is able to form direct (non-water mediated) hydrogen bonds with protein residues (Sixl & Watts, 1983). This is also consistent with the effects of PE on rhodopsin, whereby the presence of PE both activates the receptor and increases the affinity of the G protein for the receptor (Alves *et al*, 2005), with specific headgroup contacts proposed to play a role in this phenomenon (Soubias *et al*, 2010). Notably, the transducin Gα protein to which rhodopsin couples belongs to the $G_{i/o}$ subtype, as does the G_{i1} protein studied with hNTS1 here (Flock *et al*, 2017).

Finally, PIP_2 also influenced NTS1-G_{i1} coupling. Contrary to a recent report (Yen *et al*, 2018), PIP_2 appears to A) stimulate the G protein in the absence of receptor and B) inhibit the effects of the receptor on the G protein. Figure 4.7 presents the data from (Yen *et al*, 2018) alongside the equivalent experimental data from this chapter extracted from figure 4.5.

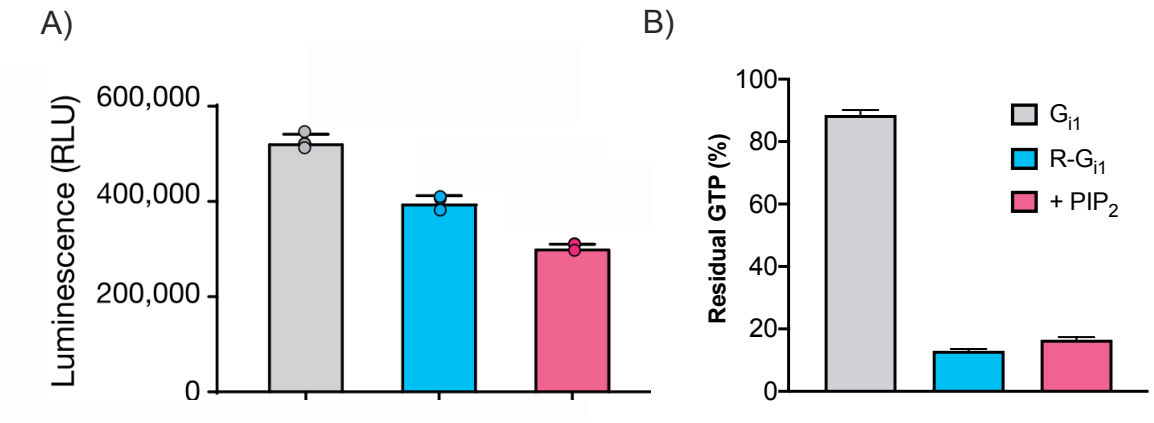


Figure 4.7: Effects of PIP_2 on NTS1-G_{i1} coupling. A) Data reproduced from (Yen et al, 2018), with 2.5 µM G protein, an unspecified receptor concentration and PIP_2 present in 3 fold molar excess over receptor B) Equivalent data from the work in this chapter (see also figure 4.5), presented in a comparable fashion, with 0.5 µM G protein, 0.125 µM receptor and 0.5 µM PIP_2. Error bars are +/- standard deviation in all cases.

In comparing these results, there are several considerations. It was difficult to replicate the experimental conditions used previously (Yen *et al*, 2018), since no receptor concentration is specified. It is known is that PIP_2 was present in 3 fold molar excess over the receptor, and G protein was present at 2.5 µM final concentration. With that in mind, it is notable that the increase in GTP hydrolysis seen upon receptor addition is very small, especially with such a high amount of G protein in the assay, suggesting that either a very low receptor concentration is used in the previous study, and/or that the receptor in the previous study is of a much lower activity than the one studied in this chapter. The receptor used in this chapter is almost an wild-type hNTS1 construct, whilst the protein used in (Yen *et al*, 2018) is a thermostabilised rNTS1 construct containing 26 mutations and ICL3 and C-terminal truncations, with altered signalling properties compared to the wild type receptor (White *et al*, 2012). It should also be noted that the final detergent conditions in (Yen *et al*, 2018) are also different (0.12% DM, 0.005% MNG final) to those used here (0.1% DDM). It is therefore possible that the conflict between the two data sets is some reflection of differences in receptor activity. However, it cannot be excluded that the

conflicting data sets result from differing assay conditions, which may modulate the availability of PIP_2 to the receptor, for example. It also cannot be excluded that some of the observed effects of PIP_2 come from its stimulation of the intrinsic GTPase activity of the G protein, which was demonstrated here (figure 4.5) but not shown previously (Yen *et al*, 2018). The native mass spectrometry data presented previously (Yen *et al*, 2018) clearly show that PIP_2 selectively binds the thermostabilised receptor over other lipids, and such *binding* events and are not inconsistent with the data presented here.

4.5.2 Effects of lipids on hNTS1-G_q coupling

For the receptor-G_q pairing, all three lipid conditions tested were observed to enhance the effects of hNTS1 on G_q activity (figure 4.4). The activity of PG on hNTS1-G_q coupling is consistent with previous literature in which the presence of PG in nanodiscs enhanced the interaction of G_q and hNTS1 (Inagaki *et al*, 2012). Both PS and the BPL mix had more significant effects on the hNTS1-G_q coupling than PG (figure 4.4B) which is an entirely novel finding since these lipids have not been previously tested in this context.

PS did cause a very small decrease in residual GTP content for the G protein versus the lipid-free G protein control (figure 4.4A), suggesting the lipid can modestly stimulate GTP hydrolysis by G_q even in the absence of receptor. However, when the activity of PS on G_q in the presence of receptor is normalised against this G protein control, the effect of PS is still greater than PG normalised to its respective control (figure 4.4B). Both EPR and nMS have detected an affinity of NTS1 for PS (Bolivar *et al*, 2016; Yen *et al*, 2018), even though the experiments were conducted under very different conditions (liposomes compared to detergent) with very different constructs (almost wild-type versus heavily thermostabilised rNTS1 sequences). Likewise, two separate molecular dynamics simulations suggest PS binding sites exist on the intracellular face of the receptor (Bolivar *et al*, 2016; Yen *et al*, 2018).

The BPL mix also potentiated hNTS1-G_q coupling, without any significant effect on G_q alone. The same mix also stimulates hNTS1-G_{i1} coupling, but it is tempting to speculate that the lipid component of the mix that is responsible for these effects is different in each case, since both anionic PS and PG had an effect on hNTS1-G_q coupling (figure 4.4B) but no detectable effect on hNTS1-G_{i1} coupling (figure 4.3B). As such it is plausible that an anionic component of BPL (e.g. PS) stimulates hNTS1-G_q coupling, whilst a zwitterionic component of BPL (e.g. PE) stimulates hNTS1-G_{i1} coupling.

4.5.3 Lipid determinants of hNTS1-G protein selectivity

The results presented in this chapter demonstrate that PS and PG can both potentiate hNTS1 stimulation of G_q but not G_{i1}.The BPL mix potentiated hNTS1 stimulation of both G proteins, but it is proposed that a zwitterionic component (especially PE) potentiates G_{i1} coupling, whilst an anionic component potentiates G_q coupling. Consequently, it appears that specific lipids can favour signalling of hNTS1 to one G protein over another.

How might such effects operate? Because the effects are observed in detergent solution, it seems likely there is a considerable ligand-like component of the effects of these lipids – i.e. they operate by direct contact to the receptor. Lipid contacts may modulate NTS1-G protein coupling by a number of different mechanisms.

One possible mechanism is that the lipid contact with the receptor modulates the receptor conformation directly. If so, given that PS and PG potentiate hNTS1-G_q but not hNTS1-G_{i1} signalling, it seems unlikely that these lipids favour a generic active conformation of the receptor. Instead, it is possible that the lipids favour a G_q-biased conformation. This is in contrast to the situation observed for the β_2AR coupling to G_s and G_{i3} (Strohman *et al*, 2019), where anionic phospholipids were stimulatory to both pairings provided $MgCl_2$ was present (which it was for hNTS1-G_q and G_{i1} assays in this chapter).

A second plausible mechanism is that lipids bound to the receptor help to recruit the G

protein to the receptor and/or stabilise it in an appropriate conformation at the receptor, through lipid headgroup-G protein interactions. Previous mutagenesis studies have highlighted that a polybasic region at the C-terminal end of the HN helix of $G\alpha_q$ is important in membrane interaction (Crouthamel *et al*, 2008) (figure 4.8). It is therefore plausible that PS/PG potentiate hNTS1-G_q coupling by favourable electrostatic interactions with this region (or other regions) of the G protein. As has been previously mentioned, the anionic EDGE sequence in the HN helix of $G\alpha_{i1}$ (figure 4.8) might make favourable interactions with the positively charged $-NH_3^+$ group of the zwitterionic PE lipid and so potentially account for potentiation of hNTS1-G_{i1} coupling by BPL. A previous study demonstrated affinity of the non-myristoylated $G\alpha_{i1}$ subunit for BPL nanodiscs (Dijkman & Watts, 2015), so irrespective of the precise components of the lipid-G protein interaction, it seems likely that BPL-G_{i1} interactions account at least partly for the observed effects of BPL on hNTS1-G_{i1} coupling.

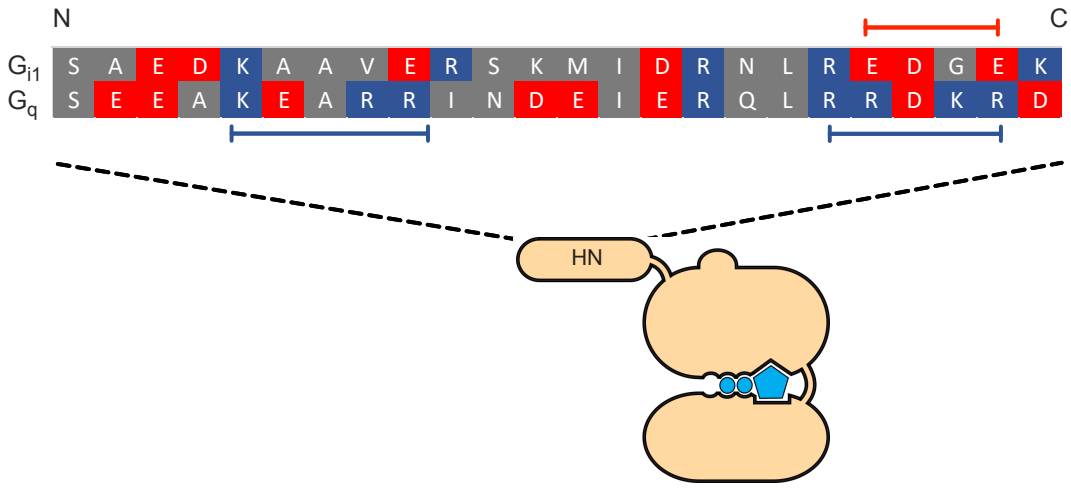


Figure 4.8: Charge motifs in the HN helix of Gα. Shown are the aligned sequences of G_{i1} and G_q, with basic residues in blue and acidic residues in red. The red bar highlights the $G\alpha_{i1}$ EDGE motif discussed in (Strohman et al, 2019), whilst the blue bars highlight basic residues of $G\alpha_q$ that were found to be important in (Crouthamel et al, 2008). G protein cartoon based on image in (Weis & Kobilka, 2018).

Lipids may therefore exert effects at the level of both receptor conformation and G protein recruitment, consistent with previous observations for PE and rhodopsin (Alves *et al*, 2005).

Are the findings presented here biologically plausible? Although PG modulates hNTS1 activity *in vitro*, it is perhaps less plausible as a modulator *in vivo*, since it is not observed to bind thermostabilised rNTS1 by native mass spectrometry (Yen *et al*, 2018) and is present at very low concentrations in mammalian membranes (Dawaliby *et al*, 2016b). PS, by contrast, represents approximately 12% of plasma membrane lipids, and is almost exclusively found in the inner leaflet (Leventis & Grinstein, 2010; Ingólfsson *et al*, 2014). Moreover, PS may be enriched in certain nanodomains of the membrane (Raghupathy *et al*, 2015), suggesting that receptor localisation in the membrane may potentiate G_q signalling versus G_{i1} signalling. Indeed, this suggestion is consistent with two previous studies showing that NTS1 signals to G_q from membrane nanodomains (Heakal & Kester, 2009; Heakal *et al*, 2011). PE does not show a particularly high affinity for NTS1 by EPR, but is highly abundant in the inner leaflet of the plasma membrane (Leventis & Grinstein, 2010; Ingólfsson *et al*, 2014) and so low-affinity interactions may be sufficient for receptor modulation.

Finally, it should be noted that experiments in this chapter were conducted at Mg^{2+} concentrations of 10 mM and 0.05 mM, neither of which are physiological since free intracellular Mg^{2+} is ~1 mM (Romani, 2011). In the case of the BPL potentiation of hNTS1-G_{i1} coupling, the lipid effect persisted at both Mg^{2+} concentrations, which suggests that it would also do so at physiological Mg^{2+} concentrations. For hNTS1-G_q coupling, potentiating effects of PS, PG and BPL were tested only at 10 mM Mg^{2+}, so it is possible that at physiological Mg^{2+} concentrations the effects of these lipids do not persist. If this lipid potentiation is based on charge complementarity between anionic headgroups and receptor residues and/or functionally important cationic motifs in the G_q N terminal helix (figure 4.8), it is unlikely that lowering the Mg^{2+} concentration to physiological levels would inhibit the effects of these lipids. However, it cannot be excluded that 10 mM Mg^{2+} screens

interactions that would be deleterious at ~1mM.

4.5.4 Conclusions and future directions

The data here demonstrate, for the first time, the existence of lipid determinants of hNTS1 G protein selectivity, which may operate both at the level of receptor conformation and receptor-G protein binding, and may reflect differential signalling of NTS1 from different domains of the membrane (figure 4.9). Aspects of this modulation are shared with both rhodopsin and β_2AR, but the precise pattern of modulation observed for hNTS1 seems to be specific to this receptor. This data should be of use in trying to elucidate how GPCRs select between different G proteins.

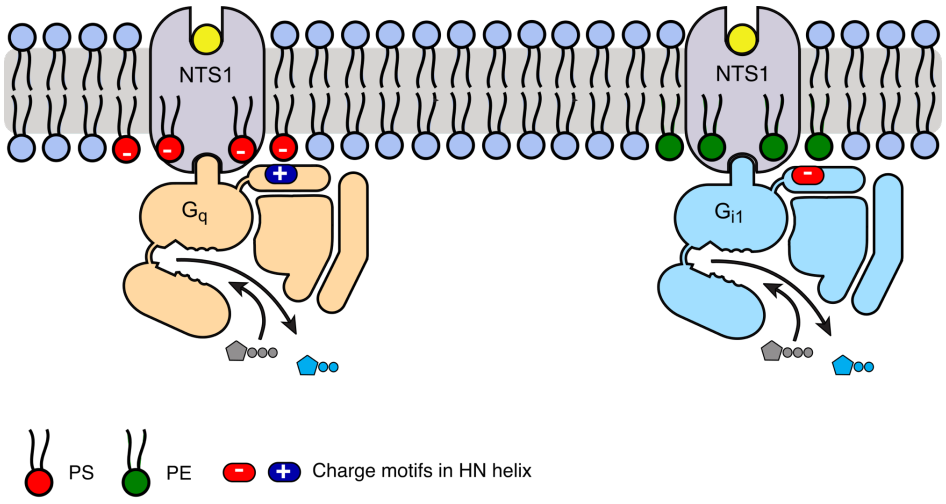


Figure 4.9: Cartoon summary of the roles of lipids in hNTS1-G protein selectivity. Receptor and G protein cartoons adapted from (Weis & Kobilka, 2018).

Work is ongoing to identify the components of BPL (including PE and PC lipids) that stimulate G_{i1} and G_q, to screen G_q coupling under low $MgCl_2$ conditions and to further understand the effects of PIP_2 on hNTS1-G protein coupling. Moreover, these studies will be extended to the G_s heterotrimer and to detergent-free systems such as nanodiscs or SMALPs. Finally, efforts are ongoing to develop a conformation-sensitive assay for NTS1 that will distinguish lipid effects at the level of receptor conformation from those at the level of G protein recruitment to the receptor.

5. Detergent-free purification of hNTS1 using a polymethacrylate polymer

5.1 Introduction

5.1.1 Limitations of detergent-based studies of GPCRs

Detergent solubilisation of GPCRs necessitates the disruption of the bilayer environment in which these receptors have evolved to be functional. A practically important consequence of this is that many GPCRs show very poor thermostability in detergent micelles (Grisshammer, 2009), which is generally assumed to result from the conformational flexibility of GPCRs (Jaakola *et al*, 2008). Indeed, molecular dynamics simulations have suggested that thermostabilising mutations act by reducing the conformational flexibility of GPCRs (Vaidehi *et al*, 2015), and that short-chain detergents facilitate greater receptor flexibility that ultimately allows for ingress of the detergent into the transmembrane helix bundle (Lee *et al*, 2016a). Functional yields of wild-type or wild-type like GPCR constructs are consequently generally poor, since low receptor thermostability leads to losses via receptor denaturation and aggregation.

Successful approaches to the obstacles of GPCR detergent-sensitivity include thermostabilisation of receptor sequences (e.g. for the β_1AR (Serrano-Vega *et al*, 2008) or parathyroid hormone 1 receptor (Ehrenmann *et al*, 2018)), or formation of receptor MSP-nanodiscs directly after membrane solubilisation to minimise detergent exposure (Mitra *et al*, 2013). For the glucagon-like peptide 1 receptor, the receptor alone was so poorly stable in detergent that a complex with G_s had to be formed in membranes first to stabilise the receptor before detergent extraction (Zhang *et al*, 2017c).

Studies on rhodopsin stability in various detergents helped establish the popularity of the detergent DDM in GPCR studies, since rhodopsin shows higher thermal stability in DDM than detergents such as CHAPS, Triton X-100 and cholate (De Grip, 1982; Cha *et al*, 2000). There has since been progress in generating detergents that better preserve receptor activity (Chae *et al*, 2010; Bae *et al*, 2016, 2019; Das *et al*, 2019), with LMNG amongst the most widely used of these. Such detergents are believed to reduce receptor conformational flexibility (Chung *et al*, 2012), and in many cases allow wild-type or near-wild type receptors to be purified, including the hNTS1 construct used in this thesis. Nonetheless, even in cases where a GPCR is reasonably thermostable in detergent, the micelle environment is still a poor mimetic of the bilayer environment. Even if a micelle is supplemented with specific lipids that exert ligand-like effects (as demonstrated in chapter 4), a bilayer environment can modulate the activity of a membrane protein through solvent-like effects (see section 4.1) that detergents and detergent-solubilised lipids cannot replicate.

Ultimately, it is desirable to study any biological molecule in as native an environment as possible. As such, the development of detergent-free systems for membrane protein solubilisation, such as the use of the styrene-maleic acid (SMA) co-polymer, hold considerable interest for studies of GPCRs. Such systems in theory allow for the co-purification of a receptor and relevant lipids as a functional unit (Overduin & Esmaili, 2019). In addition to facilitating purification of especially detergent-sensitive receptors, detergent-free approaches may provide a general method for studying receptors in an appropriate lipid context, in a form that is soluble and amenable to biophysical analysis.

5.1.2 Detergent-free studies of GPCRs with SMA

The use of SMA to purify membrane proteins into "SMALP" or "Lipodisq®" nanoparticles has become increasingly popular in recent years (Dörr *et al*, 2016; Bada Juarez *et al*, 2019) (see also section 1.3.3).

The first detergent-free purification of a GPCR using SMA was performed for the $A_{2A}R$ expressed in *Pichia pastoris* (Jamshad *et al*, 2015). This material was purified by Ni-NTA affinity chromatography to a reasonable purity and yield. In addition, $A_{2A}R$ was solubilised from HEK293 membranes, although no purification was demonstrated. In both cases, the $A_{2A}R$ -SMALPs showed a slight increase (~5°C) in thermostability versus the detergent solubilised receptor. Notably, specific binding of ligands to the receptor was lost by multiple freeze-thaw cycles when in detergent, but not in SMALPs.

The melatonin-1 receptor (MT_1R) has also been purified from *Pichia pastoris* using SMA (Logez *et al*, 2016). This material was purified by Ni-NTA affinity chromatography and size-exclusion chromatography and the identity of the receptor confirmed by Western blotting. However, no SDS-PAGE gel was presented to demonstrate the final purity of the material. A large amount of aggregated material was seen by size-exclusion chromatography, but the material eluting at a volume of 11.5 mL showed robust ligand binding, activation of the G_i heterotrimer and recruitment of β-$arrestin_2$.

The SMA polymer and similar technologies therefore show promise for detergent-free preparation of GPCRs from native membranes. It is clear that in the presented cases, the activity of the GPCR is not hindered by the polymer, and that the protein-lipid nanoparticle may have higher thermostability and resistance to freeze-thawing than the receptor in detergent micelles. There are however, very few applications to draw conclusions from and generally it is unclear how the SMA-based purification compares to

conventional detergents in terms of yield and purity. Hence there is considerable scope for further exploration of the use of amphipathic co-polymers to study GPCRs.

5.1.3 Other amphipathic co-polymers

Whilst SMA is the best established and characterised amphipathic co-polymer for membrane solubilisation, several other polymers have been developed to address the limitations of SMA. These limitations include the interfering optical absorption properties of styrene, the poor solubility of the polymer in the presence of divalent cations at millimolar concentrations, and the limited operating pH range of ~6-9 (dependent on the styrene-maleic acid ratio) (Dörr *et al*, 2016; Bada Juarez *et al*, 2019). There are also reports that SMA can interact non-specifically with affinity resins and size exclusion resins used for protein purification (Dörr *et al*, 2016; Qiu *et al*, 2018; Autzen *et al*, 2019). Finally, the relatively small reported diameter of 10 nm for SMA discs may limit the extent to which the nanoparticle can mimic a bilayer environment (Autzen *et al*, 2019).

There is therefore considerable interest in developing new amphipathic polymers to address these concerns. A wide range of alternative polymers are now available, namely SMA-EA (Ravula *et al*, 2017), SMI (Hall *et al*, 2018), SMA-QA (Ravula *et al*, 2018), DIBMA (Oluwole *et al*, 2017) & PMA (Yasuhara *et al*, 2017). Their structures and solubilisation characteristics are outlined in table 5.1. Other than SMA, only DIBMA and SMI have been used for explicit solubilisation of membrane proteins from biological membranes to date (Barniol-Xicota & Verhelst, 2018; Hall *et al*, 2018). In particular, SMI has been used to solubilise two GPCRs ($A_{2A}R$ and Vasopressin 1A Receptor ($V_{1A}R$)) from HEK293T cells (Hall *et al*, 2018). No purification was performed, with radioligand binding being used on the crude solubilised material to demonstrate that specific binding existed for both receptors. In both cases, a considerable amount of non-specific binding was also observed.

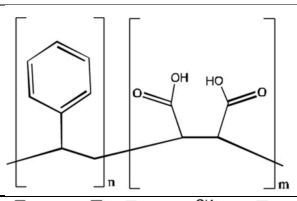
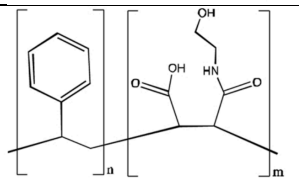
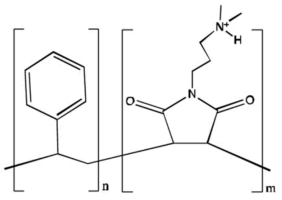
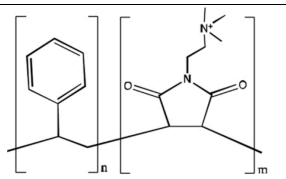
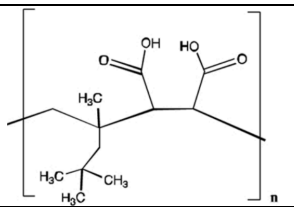
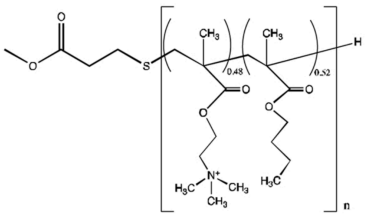
Polymer	Structure	Comments
SMA		
SMA-EA		Tolerant to divalent cation concentrations of > 9 mM. Large – up to 60 nm diameter.
SMI		Tolerant to divalent cations concentrations >100 mM. Solubilises over pH 5-7.8 range.
SMA-QA		Tolerant to divalent cation concentrations > 200 mM. Discs stable over pH 2-10 range. Large, up to 30 nm diameter.
DIBMA		Tolerant to divalent cation concentrations > 20 mM. Styrene-free.
PMA		Large – 20 nm diameter. Styrene and maleic acid free.

Table 5.1: Summary of amphipathic polymers available for membrane solubilisation. Structures are given alongside comments on nanoparticle size and stability with respect to pH and divalent cation concentration (where this data is available). Images reproduced from (Bada Juarez et al, 2019).

Notably, only the polymethacrylate (PMA) co-polymers are entirely styrene and maleic-acid free. The use of PMA polymers in forming nanodiscs was first described in (Yasuhara *et al*, 2017). Here, a free radical polymerisation mechanism was used to synthesise random amphipathic co-polymers from hydrophobic butylmethacrylate and cationic methacroylcholine chloride monomers (figure 5.1), with control over the degree of hydrophobicity and molecular weight of the co-polymer. The resulting polymers were

analysed for their ability to solubilise DMPC-LUVs, and it was found that a larger molecular weight and intermediate hydrophobicity (i.e. balance of the two monomers) gave the most effective solubilisation. The "N-C4-60-4.7" co-polymer is one such species, and when mixed with DMPC-LUVs was found to form discoidal particles of ~20 nm by negative stain EM and DLS. Addition of this polymer to live *E. coli* cells also resulted in production of nanoparticles, suggesting utility of the polymer in membrane protein studies.

PMA polymers therefore offer an interesting alternative to SMA. The two polymers are similar only in the sense that they are both amphipathic, with the nature of both the hydrophilic and hydrophobic moieties being entirely different. Indeed, initial data generated in the Watts Laboratory has suggested that PMA mediated solubilisation of DMPC LUVs can occur over a wide pH range and in the presence of millimolar concentrations of divalent cations (Henry Sawczyc, personal communication, 2019). Furthermore, the PMA polymer can form larger discs which could potentially accommodate a greater number of lipids around the target protein of interest.

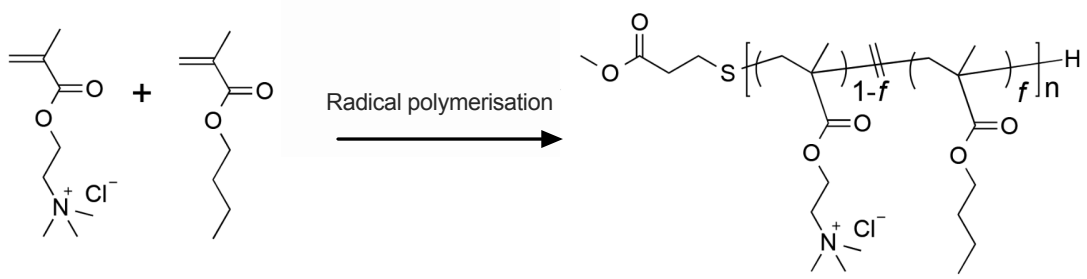


Figure 5.1: Synthesis of polymethacrylate co-polymers. Neutral butyl-methacrylate and cationic methacroylcholine monomers undergo radical polymerisation to produce a polymethacrylate polymer defined by its hydrophobic (f) and cationic fractions (1-f). Diagram adapted from (Yasuhara et al, 2017).

5.1.4 Mechanism of polymer-nanodisc formation & practical considerations

The mechanisms by which amphipathic co-polymers solubilise membranes are best studied

for SMA, but similar principles are anticipated to apply to most polymers. Membrane solubilisation by SMA involves initial deposition of polymer on the membrane, which is modulated by charged interactions between polymer and lipid headgroups, and screened by salts (Scheidelaar *et al*, 2015). The second step involves intercalation of the polymer into the hydrophobic core of the membrane, which is modulated by membrane fluidity, which in turn depends on the chemistry of lipid acyl chains and experimental temperature.

As such, practical considerations for membrane solubilisation by polymers will include the temperature and NaCl concentration, as well as the pH and relative amounts of lipid and polymer. For SMA, a weight excess of polymer relative to the membrane is generally recommended (Lee *et al*, 2016b).

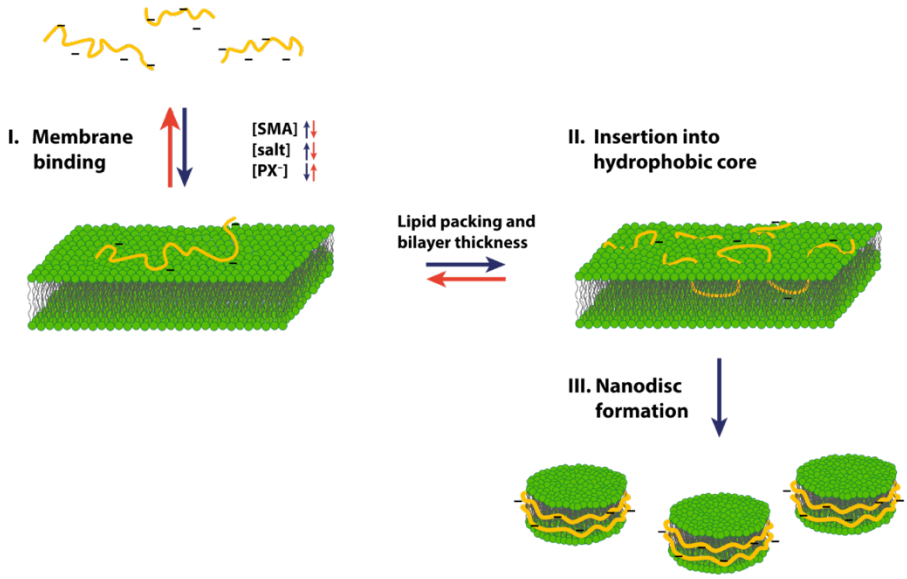


Figure 5.2: Mechanism of nanodisc formation by SMA. Nanodiscs are formed after an initial membrane deposition step, followed by intercalation of the polymer with the membrane hydrophobic core. PX^- = negatively charged phospholipids, which repel SMA. Figure adapted from (Dörr et al, 2016).

It should be noted that most studies of polymer-membrane interactions are based on simplified LUV systems (Orwick *et al*, 2012; Orwick-Rydmark *et al*, 2012; Scheidelaar *et al*, 2015, 2016). Relatively few studies have addressed variables affecting solubilisation of biological membranes. One exception is a study of SMA solubilisation of *E. coli*

membranes (Dörr, 2017), where it was found that optimal solubilisation occurred at pH 8-9, 300 mM NaCl, in contrast to reports using LUVs that found increased pH to inhibit the rate of SMA-mediated solubilisation (Scheidelaar *et al*, 2016).

5.2 Aims

Amphipathic polymers offer the potential for detergent-free purification of membrane proteins in protein-lipid nanoparticles. To date, they have seen limited application to the often detergent-sensitive GPCR family, and only SMA and SMI have been demonstrated to solubilise GPCRs. A novel polymer, PMA, offers several potential advantages over the best characterised polymer, SMA.

The aims of this chapter were therefore to:

- Establish if the novel PMA polymer could be used to solubilise hNTS1 from Sf9 membranes and to optimise conditions for this process;
- Purify hNTS1 in the absence of detergent using the PMA polymer;
- Compare the activity of hNTS1 material purified using the PMA polymer with that purified using conventional detergents.

5.3 Materials & methods

5.3.1 Receptor expression and membrane preparation

Membranes were produced from Sf9 cells expressing hNTS1-eGFP as outlined in section 3.3.2. After membrane preparation, the wet mass of the membrane was recorded before resuspension and aliquoting. In this chapter, references to membrane mass (e.g. "1mg membrane") correspond to the wet membrane mass in suspension and do not reflect protein content. All experiments in this chapter were performed on aliquots from a single membrane preparation.

5.3.2 Polymer preparation

PMA N-C4-60-4.7 polymer was kindly supplied by Avanti Polar Lipids™. The polymer was prepared to 100 mg/mL (10 % w/v) in 200 mM HEPES of an appropriate pH.

5.3.3 Solubilisation screens

For screening experiments, 1 mg of membrane containing hNTS1 was used unless otherwise stated. Samples were assembled at appropriate final pH (buffered by 40 mM HEPES-NaOH final), temperature and NaCl concentration before addition of solubilising agent and incubation with agitation for the specified time. The solubilising agents were either 10% w/v PMA or SMA, 10%/1% DDM/CHS or 5%/0.5% MNG/CHS. These were all added to 1% final, except CHS (0.1% final). The membranes were thoroughly resuspended by dounce homogenisation to a concentration of 50 mg/mL before sample assembly, and once solubilising agent was added rapid pipetting (without aeration of the sample) was used to ensure homogeneity. Where pH was a variable, final pH was confirmed with a pH electrode. Where temperature was a variable, incubation was controlled using a Stewart B3 rotator located in a cold room (4°C) set to 8 rpm or an Innova® 44 shaking incubator set to 16°C, 26°C or 37°C and 90 rpm. Unsolubilised material was removed by ultracentrifugation (120,000g, 45 mins, 4°C). Supernatant (75 µL) was then applied to a black 384 well plate and GFP counts were read on a SpectraMax M3 plate reader (Molecular Devices) set to an excitation wavelength of 488 nm and emission of 512 nm. Unless otherwise noted, 3 samples were prepared for each condition.

5.3.4 Purification of receptor in PMA-nanoparticles

For Ni-NTA and M1 anti-FLAG purifications, a similar protocol to that described for the detergent-solubilised receptor in section 3.3.2 was performed, except that detergents were excluded from the buffers for PMA containing samples. For 3C protease cleavage,

commercial his-tagged 3C protease (Sigma Aldrich or Genscript) or GST-3C protease was used.

5.3.5 GTPase-Glo™ assays

GTPase-Glo™ assays were carried out similarly to the protocols described in sections 3.3.4 and 4.3.3, with modifications. To avoid detergent disruption of the PMA solubilised material during the GPCR-G protein incubation step of the assay, the G protein stocks for the assay (at 2x final concentration) were prepared to 0.01% DDM (w/v), such that upon addition of an equal volume of PMA material, DDM is diluted below its CMC (~0.0087% (w/v) (VanAken *et al*, 1986)). For comparability, the same G protein stocks were used to assay detergent-solubilised receptor in this chapter. Detergent solubilised receptor 2x stocks were prepared to 0.1% DDM /0.01% CHS and as such, the final detergent concentrations for the detergent-solubilised receptor samples were 0.055% DDM / 0.0055% CHS.

Data were normalised so that the GTP-only or GTP + G-protein condition represents 100% of the signal, as appropriate. Additionally, corrections were made for differences in the GTP-only condition for DDM-solubilised and PMA-solubilised samples, with errors combined as outlined in section 4.3.4 as appropriate. Unprocessed data are also supplied in appendix A4.

5.3 Results

5.3.1 Solubilising hNTS1 from Sf9 membranes with the PMA co-polymer

To date, PMA has been demonstrated merely to fragment live *E. coli* cells. Here, conditions for solubilisation of hNTS1 from Sf9 membranes by PMA have been screened. This was achieved by addition of PMA under defined incubation conditions, followed by removal of unsolubilised material by ultracentrifugation and then analysis of GFP

fluorescence in the supernatant as a reporter for the presence of solubilised hNTS1. As a starting condition, analogous parameters were chosen to those used successfully for detergent purification of the receptor. Membranes were thus incubated under final conditions of 40 mM HEPES, pH 7.4, 500 mM NaCl, 1% (w/v) final PMA and 10 mg/mL final membrane, giving a 1:1 weight-weight ratio of membrane and polymer. Various incubation temperatures and lengths were used alongside a control containing 1%DDM/0.1% CHS, incubated at 4ºC for 1hr (figure 5.3).

The detection of GFP fluorescence in the sample supernatant after ultracentrifugation indicates that PMA is able to solubilise hNTS1 from Sf9 membranes (figure 5.3). Incubation at 26°C for 1 hr gave 80% of the GFP counts given by DDM/CHS solubilisation. Increasing the incubation temperature to 37°C gave no further improvement in solubilisation, whilst lowering the temperature to 16°C or 4°C gave lower yields which could be improved by extending the incubation to 18 hrs (overnight).

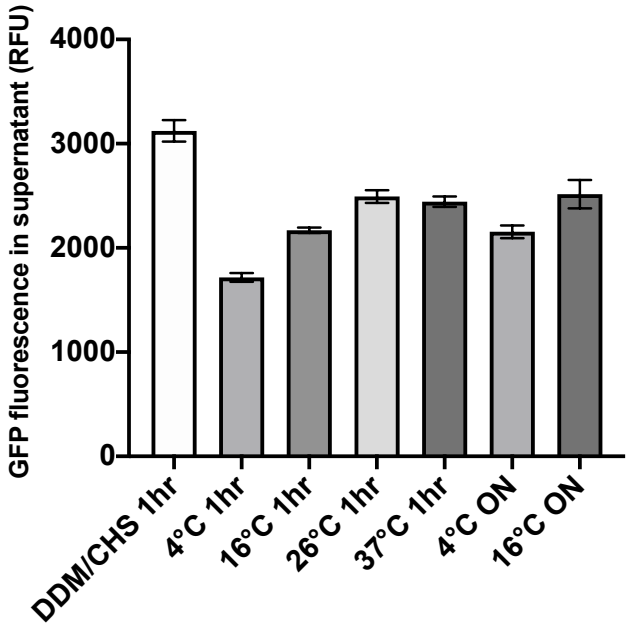


Figure 5.3: Effects of temperature and incubation length on PMA solubilisation efficiency. The graph displays the GFP counts in the supernatant after ultracentrifugation as a proxy for the amount of hNTS1. n=3, except for DDM/CHS, where n=8. Errors bars show +/- SEM. ON = overnight.

The 26°C 1hr condition was chosen to screen the effects of pH (figure 5.4A). A relatively narrow range of pH 6.8 to 7.9 was chosen, since a single buffer compound, HEPES, is a good buffer over this entire range and since a majority of proteins will show optimal activity in this pH range. The data demonstrate comparable yields of GFP counts at pH 7.4 and 7.9, whilst pH 6.8 gave slightly poorer yields. pH 7.4 was thus chosen for all subsequent screening conditions.

The concentration of NaCl was then varied, with final concentrations of 100, 250 or 500 mM (figure 5.4B). Here, 100 mM NaCl gave just 36% of the counts observed for the 500 mM NaCl solubilisation.

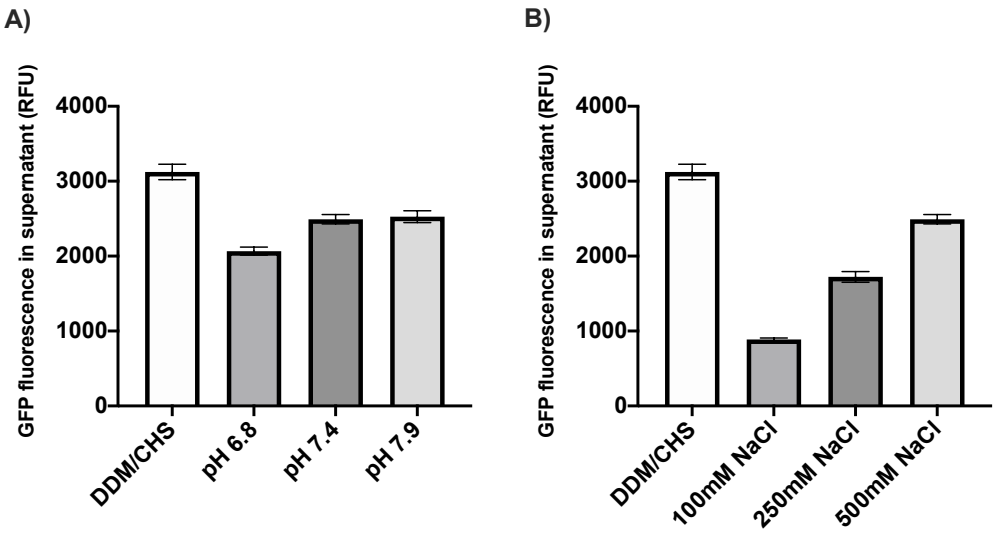


Figure 5.4: Effect of A) pH and B) NaCl concentration on PMA solubilisation efficiency. n=3, except for DDM/CHS, where n=8. Errors bars show +/- SEM.

Finally, attempts were made to ascertain the importance of the ratio of PMA to membrane (P:M) on the solubilisation yield. The mass of either PMA or membrane was fixed at 1 mg, and the mass of the other component was varied at 0.5 mg, 1 mg or 2 mg for a fixed sample volume (figure 5.5A & B). When the mass of PMA was fixed at 1 mg (a concentration of 1% w/v), 0.5 mg of membrane yielded 53% of the GFP counts given using 1 mg of membrane, whilst 2 mg of membrane yielded 160% of the counts for 1 mg of membrane (figure 5.5A). When the mass of membrane was held constant (figure 5.5B),

halving the amount of polymer to 0.5 mg PMA gave >73% of the GFP counts observed for 1 mg PMA, whilst doubling the amount of polymer gave similar GFP counts to those for 1mg PMA. The trends in these experiments become more obvious when the data are normalised to the mass of membrane present in each sample (figure 5.5C). As can be seen, 2mg polymer to 1mg membrane and 1mg polymer to 0.5mg membrane (both coloured green in respective panels) give very similar results when normalised. In both cases, the ratio is 2:1 P:M, and the amount of NTS1-GFP solubilised per mg membrane is similar to the results obtained at 1:1 P:M. This suggests that a large polymer excess over the membrane yields little improvement in solubilisation. 2mg membrane to 1mg polymer and 1mg membrane to 0.5mg polymer (both coloured blue in respective panels) also give similar results when normalised. At this ratio of 0.5:1 P:M, the amount of NTS1-GFP solubilised per mg of membrane is less than that at 1:1 P:M, but it is still much more than 50% of the counts at 1:1 P:M. As such, maximal solubilisation appears to occur at a P:M ratio of 0.5-1:1.

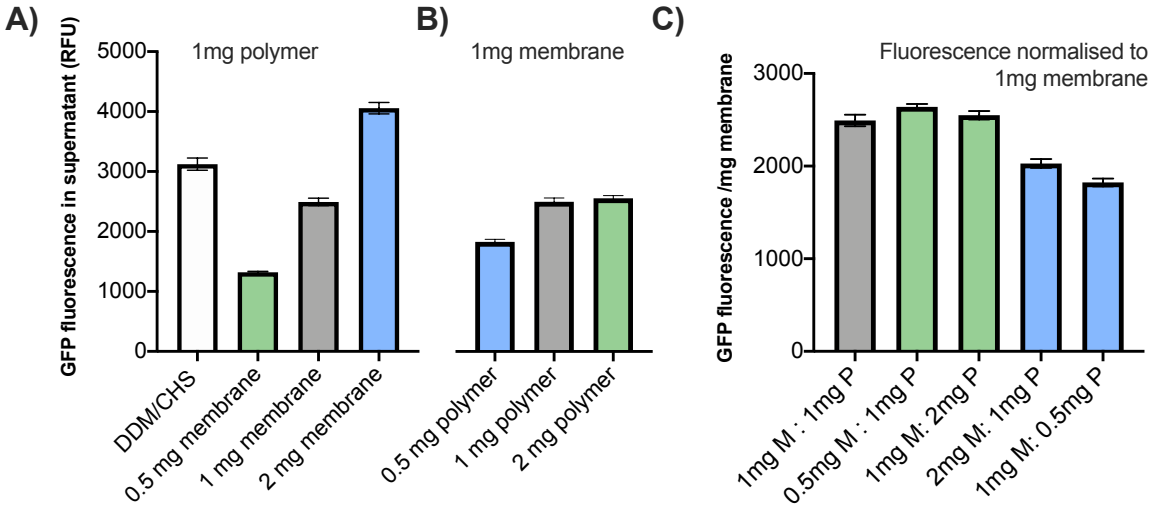


Figure 5.5: Effect of varying polymer to membrane ratio on PMA solubilisation efficiency. A) Solubilisation with a fixed amount of polymer and variable amount of membrane. B) Solubilisation with a fixed amount of membrane and variable amount of polymer. C) GFP counts from panels A and B divided by mgs of membrane to give GFP counts/mg of membrane. n=3, except for DDM/CHS, where n=8. Errors bars show +/- SEM. For DDM/CHS, 1mg of membrane was used.

5.3.2 Detergent-free purification of hNTS1 from Sf9 membranes

Once it was established that PMA could solubilise hNTS1 from Sf9 membranes, attempts were made to purify hNTS1-containing PMA nanoparticles (termed PMA-NPs from hereon in). As an initial test, membrane samples (40 mg) were solubilised with either 1% PMA or 1% MNG/0.1% CHS and after centrifugation were incubated with Ni-NTA beads. After collecting and washing the beads, material was eluted with 300 mM imidazole and subjected to SDS-PAGE and fluorimetry to assess GFP counts. Figure 5.6 demonstrates the relative purity and amount of hNTS1 in the Ni-NTA elutions for either solubilising agent.

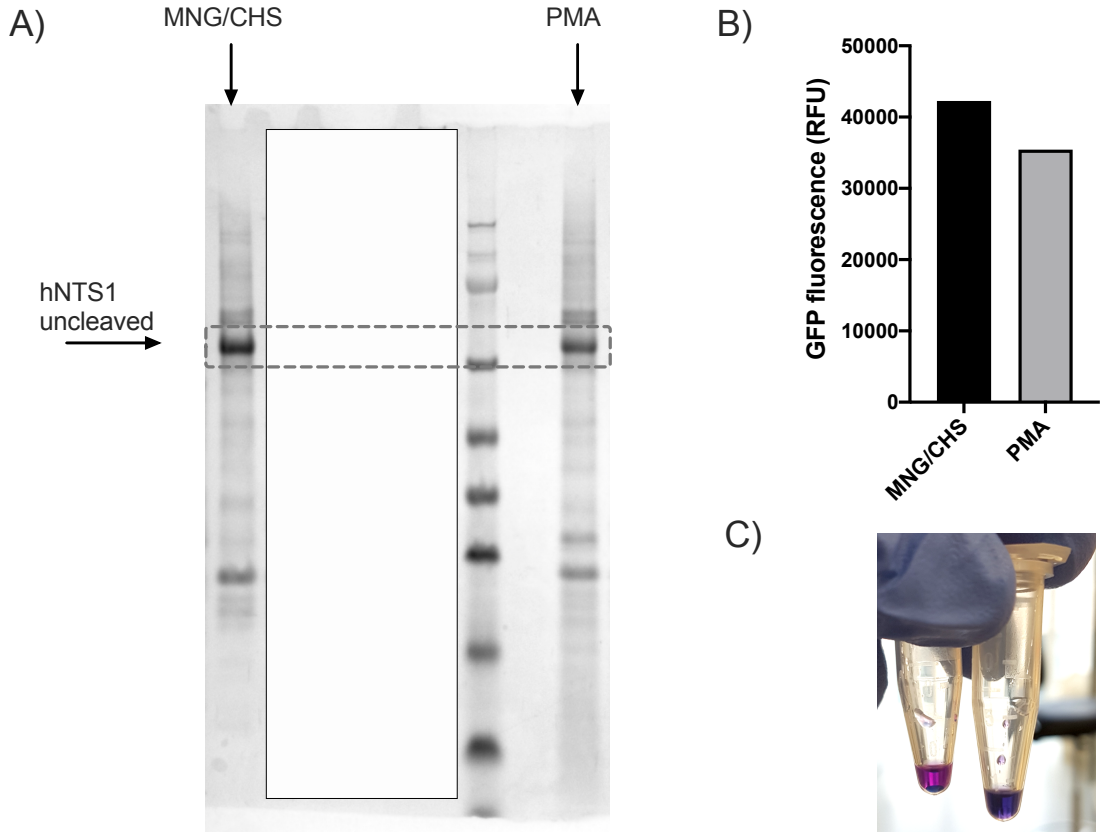


Figure 5.6: Purification of hNTS1 in PMA-NPs or MNG/CHS detergent using Ni-NTA resin. A Coomassie-stained SDS-PAGE gel demonstrating purity of elution from Ni-NTA. The white box is present to obscure irrelevant lanes of the gel; B) GFP fluorescence counts from Ni-NTA elutions; C) Photograph demonstrating the precipitation occurring when crude PMA-solubilised membranes are added to LDS sample buffer (left), compared with the normal appearance of LDS sample buffer (right).

It should be noted that it was not possible to assess fractions containing a high amount of free PMA polymer by SDS-PAGE, since addition of this material to the Lithium dodecyl sulfate (LDS) sample buffer lead to precipitation (figure 5.6C). The SDS-PAGE (figure 5.6A) and GFP counts (figure 5.6B) demonstrate that hNTS1-containing material of a similar amount and purity elutes from Ni-NTA for both PMA and MNG/CHS.

The compatibility of PMA-NPs with M1 anti-FLAG immunoaffinity resin was also tested. PMA solubilised samples were incubated with the resin in the presence 2 mM $CaCl_2$, alongside a sample prepared in DDM/CHS for comparison. After washing the resin, samples were eluted with 200 µg/mL FLAG peptide. The elutions were then analysed by SDS-PAGE and fluorimetry (figure 5.7).

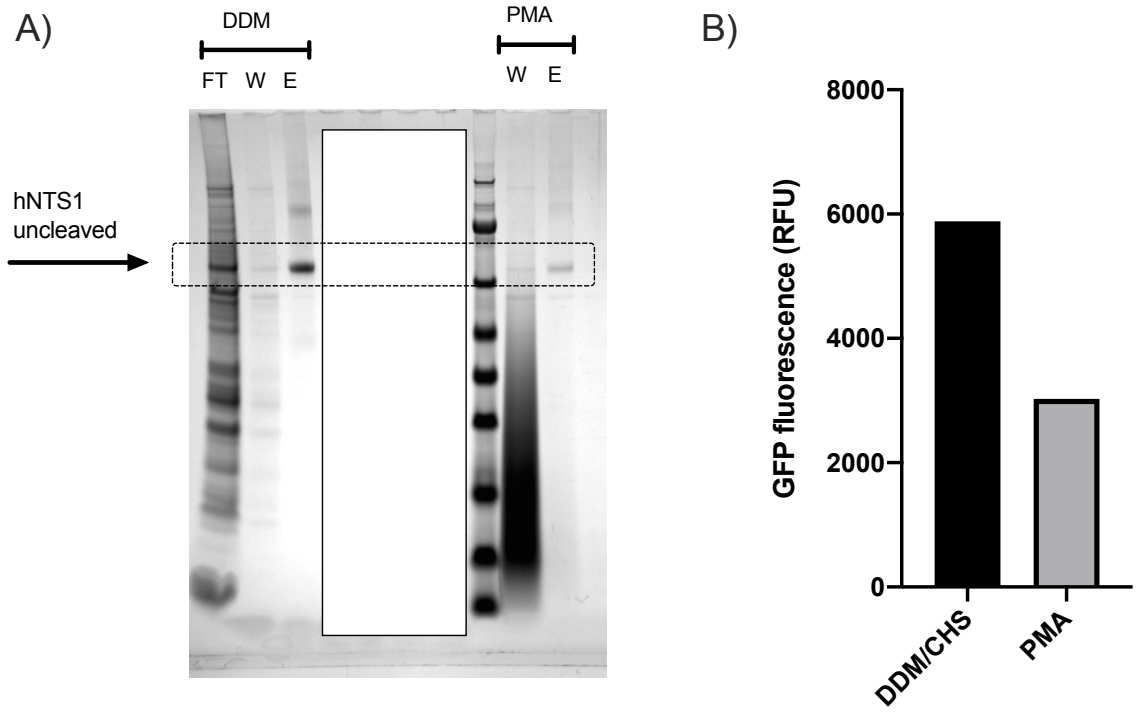


Figure 5.7: Purification of hNTS1 in PMA-NPs or DDM/CHS detergent using M1 anti-FLAG resin. A) Coomassie-stained SDS-PAGE gel demonstrating purity of elution from M1 anti-FLAG resin. The white box is present to obscure irrelevant lanes of the gel. FT=flow through, W=wash, E=elution. B) GFP fluorescence counts from resin elutions.

hNTS1 material is clearly present in the elution for the PMA solubilised membranes (figure 5.7A). However, the yield of the material is approximately 50% of that obtained using a conventional detergent-based approach based on GFP fluorescence counts (figure 5.7B). Nonetheless, this result suggests that the PMA-NPs are soluble in the presence of 2 mM $CaCl_2$. It is possible that the limited yield of PMA material stems from the inhibition of resin-hNTS1 interaction by the high free PMA concentration.

Since the PMA-NPs were found to be compatible with the purification resins normally used for DDM/CHS or MNG/CHS purification of hNTS1, a multiple step purification was employed analogous to that used in large scale purification in an attempt to obtain purified, cleaved receptor. Here, an initial Ni-NTA step was employed to capture receptor material and provide an opportunity to wash away the free PMA polymer whilst hNTS1 material is immobilised via the his_{10} tag. This step was followed by overnight dialysis with GST-3C protease to cleave off eGFP and then incubation with M1 anti-FLAG resin to improve purity and to remove the protease and eGFP. SDS-PAGE for an attempted purification using 600 mg of membrane is given in figure 5.8.

The SDS-PAGE result and related observations establish the following points. The receptor can be cleaved by 3C protease in the PMA-NP, which in turn requires that the cleavage site located between the hNTS1 C-terminus and the eGFP fusion tag is accessible to the protease active site. Whilst some uncleaved material remains after 16 hour incubation with the enzyme at 4°C, incomplete cleavage is also sometimes observed in detergent (see figure 5.9). The polymer material appears to be compatible with dialysis and is further purified by M1 anti-FLAG resin in the presence of > 2 mM $CaCl_2$, demonstrating the solubility of PMA solubilised material in the presence of Ca^{2+}. Lastly, the material eluting from the M1 anti-FLAG resin can be concentrated with a centrifugal concentrator using a 10K MWCO polyethersulfonate membrane without noticeable

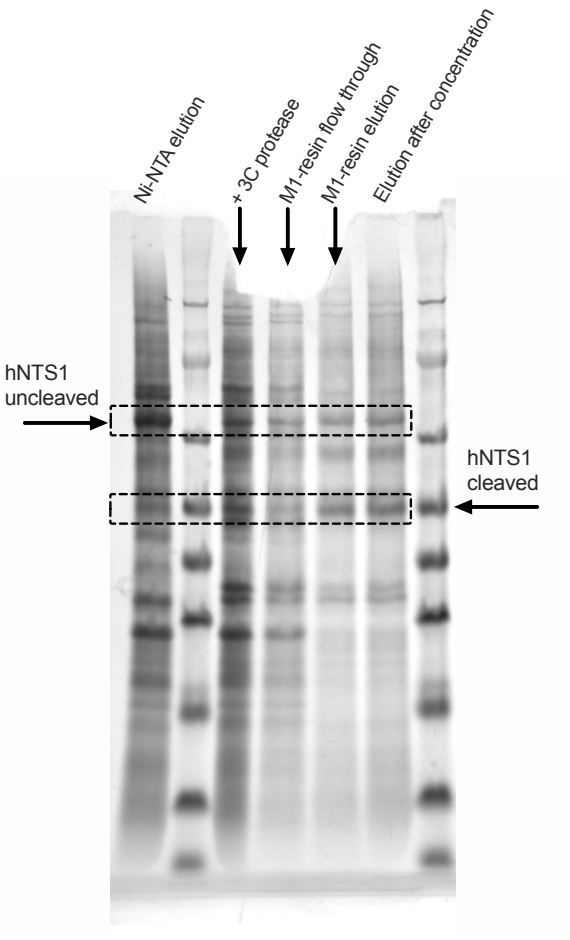


Figure 5.8: Purification of cleaved hNTS1 in PMA-NPs. Coomassie-stained SDS-PAGE gel of various purification fractions is shown.

precipitation, or loss of material as observed by measurements at A_{280}. By contrast, material was lost when using cellulose-based membranes. The material is of lower final purity than the M1-resin purified material seen using detergents (chapter 3, figure 3.4 & figure 5.9, this chapter).

5.3.4 Characterisation of hNTS1-PMA-NPs.

Since the amount of hNTS1-containing material obtained from direct solubilisation of Sf9 membranes is small and unlikely to be amenable to further purification without considerable losses, the material was used without further purification in the GTPase-Glo™ assay. To estimate the concentration of the material, it was run on SDS-PAGE against detergent-purified hNTS1 samples of known concentration (figure 5.9). Attempts to

quantify the amount of PMA-hNTS1 material by densitometry were complicated by the higher background of the PMA sample lane on SDS-PAGE and the smearing given by the detergent-solubilised sample. Nonetheless, it is apparent from the gel that the amount of hNTS1 in the PMA sample is less than that of the lowest standard, 4.7 pmol. Accounting for dilution and the volume of PMA material, the stock concentration of PMA was therefore estimated to be no more than 600 nM.

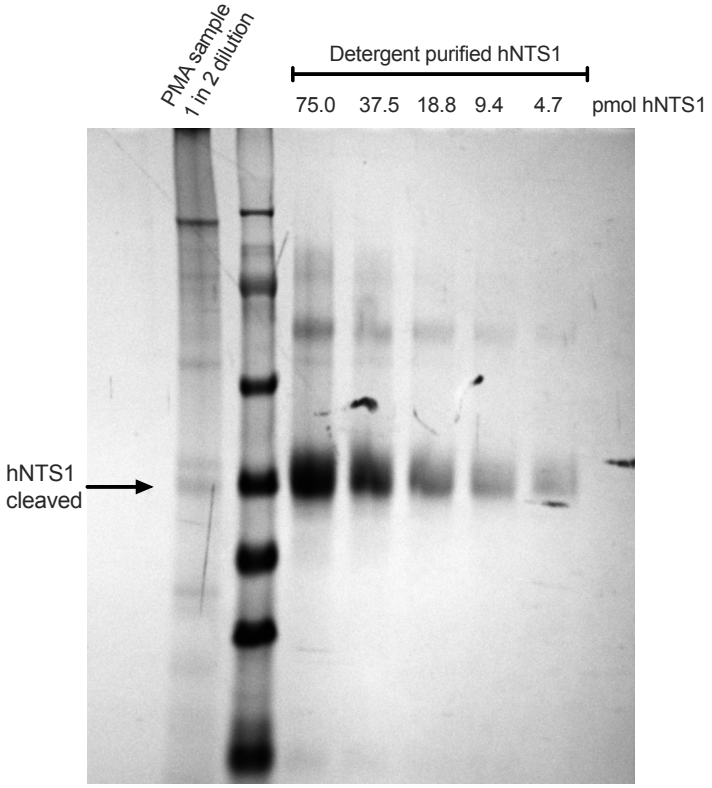


Figure 5.9: Estimation of PMA-hNTS1 amount relative to detergent-solubilised standards. Coomassie-stained SDS-PAGE was run for diluted PMA-NPs against detergent-solubilised hNTS1 of known concentration.

For the GTPase-Glo™ assay, PMA solubilised material was diluted 6-fold in detergent-free assay buffer. Material was incubated with 10 μM NT_{8-13} before dilution with an equal volume of G protein to give a total 12-fold receptor dilution. The final concentration of hNTS1-PMA-NPs (R_{PMA}) assayed was therefore $\leq$ 50 nM, with G_{i1} and G_q at final concentrations of 500 nM. Receptor in DDM (R_{DDM}) was also included in the experiments

to provide a reference of receptor activity. 100 nM R_{DDM} was used in experiments with G_{i1}, whilst for experiments with G_q a higher concentration of 500 nM was used. These concentrations were chosen based on results in chapters 3 & 4, whereby G_q required higher receptor concentrations for stimulation.

Firstly, control experiments (figure 5.10) were performed in 5 μM GTP for each of R_{DDM} (at 500 nM and 100 nM), R_{PMA} (at 50 nM) and G_q and G_{i1} (at 500 nM each), to test the activity of the G proteins and to ascertain if the partially-purified R_{PMA} sample has any GTP hydrolysis versus the pure R_{DDM} sample. Both G proteins behaved as expected, demonstrating intrinsic GTPase activity. Whilst the luminescence counts for the R_{PMA} control are slightly less than for the R_{DDM} controls, these differences were not statistically significant using a 2-tailed, unpaired Student's t-test (not shown).

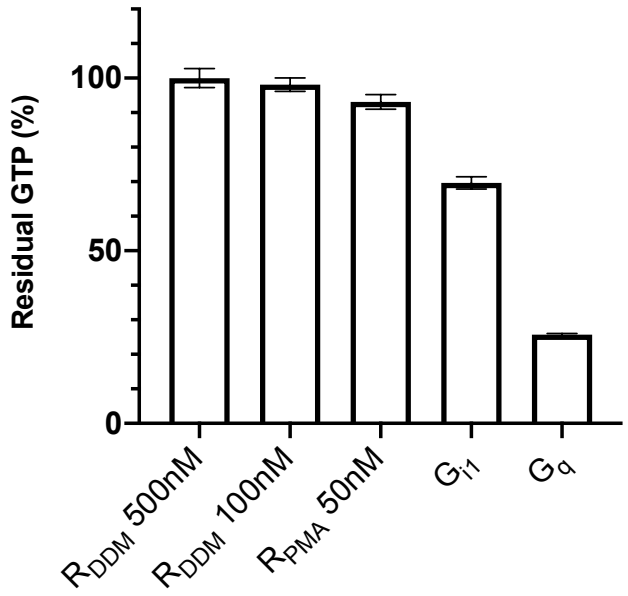


Figure 5.10: Control GTP turnover experiments with receptor in DDM or PMA. Here the GTP hydrolysing activities of the receptor and G protein conditions were tested individually. Error bars = +/- SEM, n=3, except for R_{PMA} where n=6.

Next, R_{DDM} and R_{PMA} were mixed with G proteins (figure 5.11). In each case, 100% residual GTP is given by GTP counts for the G protein alone, and data for R_{DDM} with G protein and R_{PMA} with G protein were normalised for the differences in the controls shown

in figure 5.10. For the G_{i1} heterotrimer (figure 5.11A), R_{PMA} at $\leq$ 50 nM stimulated GTP hydrolysis at G_{i1} to a similar extent compared to R_{DDM} at 100 nM. For G_q (figure 5.11B), the effect appears even greater, with R_{PMA} at $\leq$50 nM having a similar stimulation of G_q activity as R_{DDM} at 500 nM.

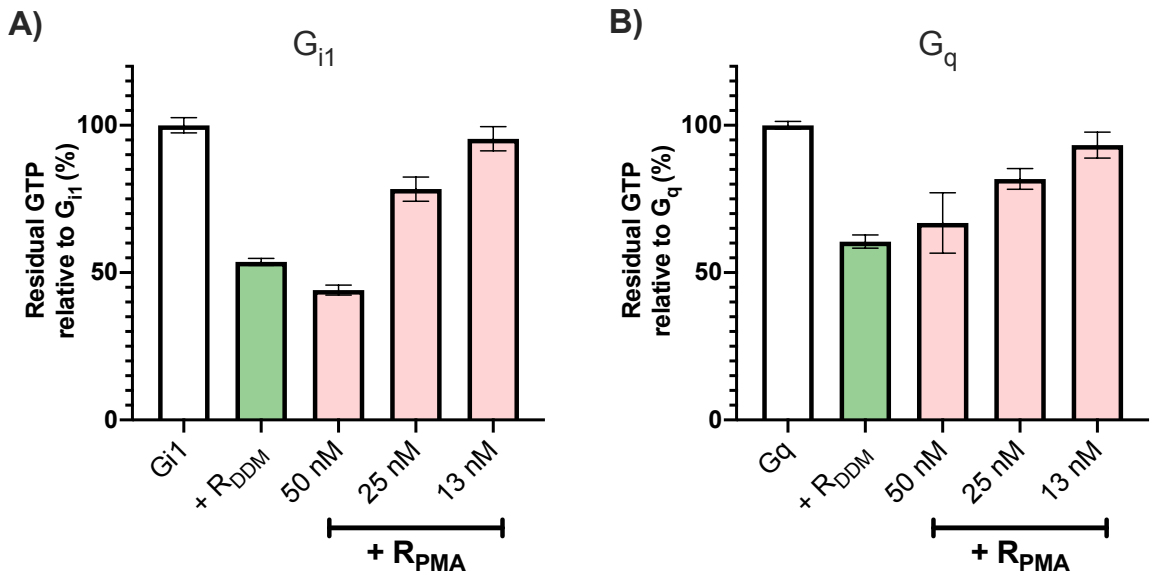


Figure 5.11: Stimulation of A) G_{i1} and B) G_q by hNTS1 in DDM or PMA. Error bars = +/- SEM, n=3. R_{PMA} values were corrected for the slightly lower luminescence given by the R_{PMA} control in figure 5.10 versus the R_{DDM} controls.

5.5 Discussion

5.5.1 Solubilisation of Sf9 membranes with PMA

The results presented in this chapter represent the first solubilisation of a specific membrane protein using PMA. The degree of solubilisation by PMA under optimal conditions compared favourably with that given by the conventional detergents, with PMA giving approximately 80% of the GFP counts when using DDM/CHS (figure 5.3). Using Sf9 membranes, several clear trends affecting PMA-mediated solubilisation emerge.

Firstly, the best incubation temperature for a 1 hr solubilisation amongst those tested is 26°C (figure 5.3). It is interesting to note that this temperature is similar to the temperature

at which Sf9 cells are typically cultured (27°C), possibly reflecting that at this temperature, the lipids in the membrane are suitably fluid for efficient solubilisation by PMA. Elevating the temperature to 37°C did not improve the solubilisation yield. Moreover, if the target protein is suspected to be particularly sensitive to temperature, incubation at 4°C and 16°C overnight both provided good solubilisation yields.

With respect to pH, the polymer gave similar solubilisation at pH 7.4 and pH 7.9 (figure 5.4A). Unpublished results from the Watts Lab suggest solubilisation of DMPC LUVs by PMA is invariant over a wide pH range (Henry Sawczyc, personal communication, 2019). It is speculated that the reduction in solubilisation efficiency below pH 7 does not reflect a change in polymer behaviour, but rather some effect of the Sf9 membranes or the membrane proteins contained within, that is not observed for the much simpler DMPC vesicle membranes.

Varying NaCl concentration had some of the most significant effects on hNTS1 solubilisation by PMA (figure 5.4B), with the 500 mM NaCl condition giving 240% of the GFP counts of the 100 mM NaCl condition. Indeed, it is possible that increasing the concentration of NaCl to above 500 mM (not tested here) may improve solubilisation even further. This is somewhat different to the situation with SMA, where it is reported that an intermediate concentration of 300mM NaCl is optimal (Dörr, 2017). In turn, this probably reflects different charges carried by the anionic SMA and cationic PMA. Whilst SMA needs to be screened from anionic lipids such as PG, it is anticipated that PMA deposition on the membrane requires salt-mediated screening from zwitterionic lipids such as PE and PC. Notably, the combined abundance of PE and PC in Sf9 membranes (>50% of total lipid) is higher than that of anionic lipids (PS + PI + PG <35% of total lipid), (Dawaliby *et al*, 2016b), which could explain why a higher concentration of NaCl is optimal for PMA compared to SMA.

Finally, solubilisation screens in which the amount and concentration of polymer and membrane were varied demonstrate that optimal solubilisation of Sf9 membranes by PMA occurs at a P:M ratio of between 0.5:1 and 1:1. When the amount of PMA is halved from 1mg to 0.5mg, PMA solubilises more than half the material solubilised at 1mg (figure 5.5A). Likewise, when 2mg of membrane is added to 1mg of polymer, increased solubilisation is seen, albeit not twice as great – even with PMA at the same concentration (figure 5.5B). When normalising for the amount of membrane in the samples (figure 5.5C), it is clear that at a 0.5:1 P:M ratio, more than half the material per mg membrane is solubilised than at a 1:1 ratio. Practically, this means adding PMA at greater than a 1:1 weight ratio with the membrane will lead to little additional solubilisation. It should be noted that previous studies for some other polymers suggests that altering the lipid to polymer ratio can affect the final size of the resulting nanoparticles (e.g. for SMA-QA (Ravula *et al*, 2018)), which was not studied here.

The relative roles of PMA concentration compared to PMA amount on its solubilisation efficiency were not precisely delineated here. 0.5mg polymer gives a concentration of 0.5% (w/v) under the tested conditions, and it is clear that 0.5% (w/v) polymer on 1mg membrane works more than 50% as well as 1% polymer on 1mg membrane (figure 5.5A), suggesting that polymer amount is the more important variable here and that concentrations above 0.5% are not required provided a sufficient amount of polymer is present. This is in agreement with recent reports on SMA, in which above 0.5% w/v SMA, no additional solubilisation of *E. coli* membranes was observed (Dörr, 2017).

Whilst only one target protein was tested here, it is anticipated that similar conclusions would apply to most proteins contained in Sf9 membranes; given proposed mechanisms for polymer-mediated solubilisation, the process is anticipated to be affected mostly by

interaction of the polymer with the membrane than the membrane protein itself (Dörr *et al*, 2016).

5.5.2 Purification of PMA-NPs

PMA solubilised material was compatible with Ni-NTA (figure 5.6) and M1 anti-FLAG affinity resins (figure 5.7). The latter resin is used in the presence of 2 mM $CaCl_2$, with which the PMA-NPs appeared to be compatible, in contrast to SMA which is reported to precipitate under such conditions (Oluwole *et al*, 2017).

In addition, PMA-NPs were compatible with dialysis and centrifugal concentration using polyethersulfonate membranes (figure 5.8). Promisingly, hNTS1 solubilised by PMA could be cleaved by 3C protease, which requires that the specific 3C cleavage site present on the hNTS1 C-terminus is solvent accessible.

The yield and purity of PMA material after the Ni-NTA step was comparable with that solubilised by detergent (figure 5.6). No modifications were required to the standard detergent-based protocol other than the removal of detergents from buffers. Using M1 anti-FLAG chromatography as the first purification step also worked for PMA solubilised material, but the yield was approximately half of that for an equivalent detergent sample (figure 5.7B). It is suggested that the poorer purification of PMA reflects some inhibitory effect of the high concentration of free cationic polymer on binding to the anti-FLAG resin. The M1 antibody which is used on this resin requires Ca^{2+} for epitope binding (Einhauer & Jungbauer, 2001), and it is possible that the cationic polymer competes for Ca^{2+} binding and so inhibits epitope binding.

Combining Ni-NTA, 3C cleavage and M1 anti-FLAG chromatography allowed for partial purification of cleaved hNTS1, with a final purity that was lower than normally observed in detergent (figure 5.8). These purifications were performed at a scale of less than 1g of membrane material and with small resin volumes, and at such a scale the potential for loss

of material is generally much greater. In addition, detergent-solubilised hNTS1 samples are typically further purified by size-exclusion chromatography, which was not employed here for PMA-NPs because of the small amount of material, the unknown compatibility of the polymer with the superdex 200 resin and because the proposed size of the PMA-NPs may cause them to run very close to the void volume of an S200 10/300 GL column. Efforts are ongoing to optimise the purification in order to yield material of a higher purity.

The results presented here demonstrate the partial purification of a GPCR using an amphipathic polymer, which to date has only been demonstrated explicitly for two other receptors ($A_{2A}R$ and MT_1R), both expressed in *Pichia pastoris* (Jamshad *et al*, 2015; Logez *et al*, 2016). Hence this chapter presents the first detergent-free extraction from the widely used Sf9 expression host. More generally, the results demonstrate a potentially broad utility of PMA, given its compatibility with centrifugal concentrators and different affinity resins.

5.5.3 hNTS1 activity in PMA vs detergent

Importantly, the hNTS1-PMA-NPs prepared from Sf9 membranes display significant stimulation of both G_{i1} and G_q proteins when using very low receptor concentrations (figure 5.11).

The ability of the receptor to bind its agonist and stimulate a G protein demonstrates that both the intracellular and extracellular faces of the receptor must be solvent accessible. These functional studies therefore suggest a nanoparticle morphology that is discoidal or at least disc-like, consistent with previous negative stain electron micrographs of PMA-solubilised LUVs showing coin-shaped discs (Yasuhara *et al*, 2017).

For both G proteins studied here, the PMA-NPs stimulate a level of GTP hydrolysis that is comparable to the results obtained with detergent-solubilised receptor at much higher concentration. This may be a result of the presence of specific lipids in the PMA-NP, the existence of a bilayer-like structure, the absence of detergent, or a combination of these

factors. As was seen in chapter 4, specific lipids stimulate coupling of NTS1 to both G_{i1} and G_q. In addition, the absence of detergent and/or presence of a bilayer structure could assist in recruitment of the lipidated G proteins to the receptor. A very recent paper, published during the writing of this thesis, demonstrated a similar phenomenon for the β_2AR interaction with the G_s protein: receptor in MSP-nanodiscs at 1 nM stimulate G_s GTP hydrolysis to a similar extent as the receptor in detergent at 25 nM (Staus *et al*, 2019). Notably, these results were obtained by specifically including the activating PG lipid, whereas the results using PMA in this chapter (figure 5.11) do not involve any exogeneous lipids, presumably reflecting the co-purification of functionally relevant lipids with the receptor in the PMA-NP.

The difference between PMA-NP stimulated GTP hydrolysis and detergent-solubilised receptor stimulated GTP hydrolysis appeared greater for G_q than G_{i1} (figure 5.11), when considering that 500 nM R_{DDM} is required to give similar stimulation of G_q to R_{PMA} at $\leq$50 nM (versus 100 nM R_{DDM} for G_{i1}). It is speculated that this reflects that G_q signalling is more sensitive to lipids than G_{i1}. Whilst specific detergent-solubilised lipids can increase hNTS1 stimulation of G_{i1} in detergent (chapter 4), the effect of hNTS1 on this G protein is nevertheless strong even in the absence of exogenous lipids. A stable nucleotide free hNTS1-G_{i1} complex can be formed in detergent (Kato *et al*, 2019), whilst efforts to form a similar complex for hNTS1-G_q have to date failed (H Kato, personal communication, 2018). Comparatively, in a cellular context hNTS1 signals strongly to both G_{i1} and G_q.

5.6 Conclusions

For the first time, the amphipathic polymethacrylate co-polymer (PMA) has been used to solubilise and purify a membrane protein in the absence of detergent, and the results suggest a broad utility of this polymer in membrane protein studies.

More specifically, this chapter demonstrates the first detergent-free extraction of a GPCR from Sf9 insect cells, and only the third detergent-free extraction of a GPCR from biological membranes alongside two extractions using SMA (Jamshad *et al*, 2015; Logez *et al*, 2016) The GPCR, hNTS1, was partially purified and demonstrated higher activity on G_{i1} and G_q in PMA nanoparticles than in detergent. The extent of PMA-solubilised receptor activity on the G_q heterotrimer is suggestive of some effect of the bilayer or specific lipids on the hNTS1-G_q interaction.

Efforts are ongoing to explore the morphology of the hNTS1-PMA discs, and their potential for use in structural biology. In addition, native mass spectrometry will be used to identify lipids that co-purify with hNTS1 in the PMA discs.

6. Conclusions and future work

The number of GPCR structures solved continues to grow, recently augmented by the application of cryo-EM to complexes of GPCRs with G protein heterotrimers (García-Nafría & Tate, 2019; Munk *et al*, 2019). As more static snapshots are obtained by crystallographic and cryo-EM approaches, so grows the need to explore GPCR structure and dynamics by complementary means. In particular, sequence modifications necessary for structure determination may have deleterious consequences on receptor function that complicate interpretation of the structure, and structural determination is typically conducted in environments that poorly mimic biological membranes.

The CW-EPR study of rNTS1 helix 8 (chapter 2) provides a clear example of the utility of biophysical studies in complementing structural studies of GPCRs. The CW-EPR technique allows for the use of small amounts of receptor material with a near wild-type sequence, reconstituted into a native-like lipid environment. Scanning of the NTS1 proximal C-terminus using SDSL CW-EPR reveals a short, dynamic helix 8 that is similar in length to the two structures solved using the most native-like receptor sequences. The helix does not appear to undergo large changes in dynamics upon agonist binding and provides a site of contact for both $G\alpha_{i1}$ and β-arrestin$_1$. Future directions in this area include using alternative labelling strategies to circumvent issues with studying complexes between NTS1 and downstream signalling partners. At present, the CW-EPR spectra obtained for such complexes were sufficient to demonstrate tertiary contacts between the components, but if a different, less labile spin label can be employed alongside heterotrimeric G proteins, a more precise CW-EPR study of the effects of G proteins and β-arrestins on helix 8 dynamics can be performed. Whilst the CW-EPR data presented in this thesis demonstrate a dynamic, short helix, they do not exclude the possibility of

additional helix 8 conformations. Efforts will be made to apply the double electron-electron resonance technique to obtain distances that can define the helix 8 conformation under different conditions more precisely. Given that the polybasic motif that follows NTS1 helix 8 has been implicated in G_q-specific signalling for other receptors (Qin *et al*, 2011; Maeda *et al*, 2019), it is speculated that in NTS1, such a motif acts as a selectivity determinant. As such, the conformation of NTS1 helix 8 and/or the second C-terminal helix resolved by CW-EPR may be important in establishing initial interaction with G_q in a "fishing line" mechanism similar to that proposed for receptor C tail – arrestin interactions (Shukla *et al*, 2014).

Post-translational modification of the GPCR C-terminus with palmitate groups is well-established, and a plethora of phenotypes for palmitoylation-deficient receptors are known (Qanbar & Bouvier, 2003). The maturation of the native mass spectrometry technique has allowed its application to low-expressing, detergent-sensitive proteins such as GPCRs (Gault *et al*, 2016), and this technique provides new opportunities for studying modifications such as palmitoylation. The native mass spectrometry study of hNTS1 (chapter 3) demonstrates that it is possible to identify the palmitoylation states of the receptor, even with a near wild-type receptor construct and in the presence of mass heterogeneity of the receptor. The results obtained suggest that the receptor exists in a variety of palmitoylation states. In order to isolate the origin of this heterogeneity, the use of mammalian expression hosts will be explored. It has been recently demonstrated that intact GPCR-G protein complexes can be observed in a mass spectrometer (Yen *et al*, 2018). It will therefore be very interesting to try to complex the heterogeneously palmitoylated hNTS1 with different G proteins, since it should be possible to resolve if a specific palmitoylation state of the receptor preferentially binds specific G proteins. Indeed, there is some precedent for this, since the palmitoylation deficient C381S-C383S hNTS1

mutant is reported to be deficient in G_q signalling (Heakal *et al*, 2011). Similarly, it is anticipated that the native mass spectrometry technique will be highly useful in exploring receptor phosphorylation modifications important for arrestin interaction.

Whilst most structural studies of GPCRs are conducted in the absence of lipids, there is a growing appreciation of the roles of phospholipids in GPCR function. Understanding of such phenomena is advanced by the study of lipid-modulated NTS1-G_q/G_{i1} coupling in chapter 4. It is demonstrated using a GTP turnover assay that the coupling of the receptor to both G proteins is lipid-sensitive, and most significantly, that the anionic PS and PG lipids selectively promote NTS1-G_q coupling over G_{i1} coupling. The importance of lipids on NTS1 function (and GPCR function in general) is further supported by the activity of NTS1 purified in the absence of detergent, using a novel polymethacrylate (PMA) polymer (chapter 5). The receptor in PMA-NPs displays similar activity to the detergent-solubilised receptor towards G_{i1} when at $\leq$50% of the detergent-solubilised receptor concentration and towards G_q when at $\leq$10% of the detergent-solubilised receptor concentration. Based on the combined results of chapters 4 and 5, it is speculated that hNTS1-G_q signalling is more lipid-sensitive than hNTS1-G_{i1} signalling. Since hNTS1-G_q signalling is proposed to be sensitive to receptor palmitoylation state, and a palmitoylation-deficient receptor shows reduced localisation to membrane microdomains (Heakal *et al*, 2011), it seems plausible that membrane lipid composition and receptor palmitoylation state co-operate to modulate receptor-G protein selectivity. Information regarding lipid modulation of hNTS1-G_q coupling will be leveraged towards structural determination of a stable nucleotide-free hNTS1-G_q complex using PMA-NPs and/or mixed lipid-detergent micelles. A structure of hNTS1 with G_q would make hNTS1 the first GPCR for which structures bound to multiple subtypes of G protein are available, which could advance understanding of GPCR-G protein selectivity considerably. More generally, future directions in this area will

involve merging bottom-up lipid screening in the GTP turnover assay with top-down lipid identification by native mass spectrometry using PMA-NPs derived from Sf9 or mammalian expression hosts. It will be of considerable interest to observe if the lipids co-purifying with NTS1 in PMA-NPs change under certain conditions – for example, incubation of membranes with different signalling partners.

Novel insights into NTS1 structure, dynamics, post-translational modifications and lipid modulation are thus demonstrated in this thesis. These insights also advance the GPCR field in general. Most studies of GPCRs have focussed on a small number of model receptors, most notably the β_2AR and rhodopsin. These model receptors have well-defined G protein specificity; β_2AR signals primarily to G_s and to G_i under certain conditions (Strohman *et al*, 2019), whilst rhodopsin couples to G_t of the G_i family (Stryer, 1991). NTS1 is by comparison very promiscuous in its G protein coupling profile (Besserer-Offroy *et al*, 2017; Kato *et al*, 2019), but a recent study suggests that promiscuity in G protein coupling may in fact be quite common across class A GPCRs (Inoue *et al*, 2019). As such, NTS1 may be an appropriate model for a wide range of class A GPCRs.

In addition to advancing understanding of GPCRs, the work in this thesis also presents a technological advance that is pertinent to the study of a wide range of biologically and pharmaceutically relevant membrane proteins – the application of the novel polymethacrylate polymer (PMA) to detergent-free membrane protein purification (chapter 5). The optimisation of solubilisation parameters presented here should be useful in screening PMA for solubilisation of other membrane proteins expressed in Sf9 and other expression hosts, and may help determine aspects of the polymer mechanism of action. The purification of NTS1 using PMA represents the first extraction of a membrane protein with this polymer, and in general is one of the very few examples of detergent-free purification of a GPCR. The detergent-sensitivity of GPCRs and indeed many other

membrane proteins is often a limiting factor in obtaining material for structural and biophysical study, and so the results in chapter 5 may pave the way for studying GPCRs and other membrane proteins that have proved too unstable to study in conventional detergents. Indeed, detergent-free purification using PMA or related polymers could potentially provide a much more native-like alternative to thermostabilisation of membrane proteins; rather than modifying the protein sequence to be more stable in the absence of lipids, the lipid environment is simply maintained around the protein.

Appendix

A1 Receptors without helix 8

Given the potential significance of helix 8 in GPCR function (section 2.1.1), it is interesting to note that several structures exist of GPCRs without a helix 8 resolved (table A1). The receptor structures concerned are for NTS1 (White *et al*, 2012; Egloff *et al*, 2014; Krumm *et al*, 2016; Kato *et al*, 2019), A_1R (Draper-Joyce *et al*, 2018; Glukhova *et al*, 2017; Cheng *et al*, 2017), AT_IR (Zhang *et al*, 2015b, 2015c; Wingler *et al*, 2019c), $AT_{II}R$ (Zhang *et al*, 2017a; Asada *et al*, 2018), platelet-activating factor receptor (PAFR) (Cao *et al*, 2018), P_2Y_1R (Zhang *et al*, 2015a), $P_2Y_{12}R$ (Zhang *et al*, 2014a, 2014b), chemokine receptor 4 (CXCR4) (Wu *et al*, 2010; Zhao *et al*, 2014), lysophosphatidic acid receptor 6 (LPA_6R) (Taniguchi *et al*, 2017), leukotriene B4 receptor 1 (BLT_1R) (Hori *et al*, 2018), protease-activated receptor 1 (PAR1) (Zhang *et al*, 2012) and free-fatty acid receptor 1 (FFAR1) (Srivastava *et al*, 2014; Lu *et al*, 2017; Ho *et al*, 2018).

In some cases (CXCR4, LPA_6R, BLT_1R, PAR1 & FFAR1), the lack of helix 8 appears to be due to divergence from the semi-conserved motif, most notably the lack of phenylalanine or a bulky hydrophobic residue at positions 8.5/8.54, and/or lack of a cationic residue at 8.51 (table A1). In the case of the angiotensin receptors and PAFR, the lack of helix 8 may be related to the ability of these receptors to display membrane-distal helix 8 conformations (see section A1.1 below). The A_1R, P_2Y_{12} and NTS1 receptors are all interesting cases since they possess a consensus-like sequence, show a canonical helix 8 conformation in some structures and no helix in others. NTS1 is especially interesting in that it has the greatest total number of structures for the receptors discussed in this section, there are multiple different helix 8 conformations, and there is supporting functional data suggesting a role for helix 8 in G protein activation (see section 2.1.2).

Residue position	*8.47*	*8.48*	*8.49*	*8.50*	*8.51*	*8.52*	*8.53*	*8.54*	*8.55*	*8.56*	*8.57*	*8.58*	*8.59*	Structures without helix 8
Consensus	**N**	**K**	**N**	**F**	**R**	**R**	**A**	**F**	**R**	**R**	**L**	**L**	**-**	
NTS1	S	A	N	F	R	Q	V	F	L	S	T	L	C	2/10
A_1R	I	Q	K	F	R	V	T	F	L	K	I	W	N	1/3
AT_1R	G	K	K	F	K	R	Y	F	L	Q	L	L	K	1/3
$AT_{II}R$	G	N	R	F	Q	Q	K	L	R	S	V	F	R	1/4
PAFR	-	-	-	F	R	K	H	L	T	E	K	F	Y	1/2
P_2Y_1R	G	D	T	F	R	R	R	L	S	R	A	T	R	2/2
$P_2Y_{12}R$	C	K	S	F	R	N	S	L	I	S	M	-	-	2/3
CXCR4	G	A	K	F	K	T	S	A	Q	H	A	L	T	6/6
LPA_6R	S	E	T	I	Q	N	S	I	K	R	K	T	Q	1/1
BLT_1R	G	G	G	L	L	R	S	A	G	V	G	F	V	1/1
PAR1	S	S	E	C	Q	R	Y	V	Y	S	I	L	C	1/1
FFA1R	G	R	G	P	G	L	K	T	V	C	A	A	R	3/3

Table A1: Receptors without helix 8.

A1.1 Receptors with unusual helix 8 conformations

In addition to receptors without helix 8 and receptors with canonical helix 8 conformations, a number of recent structures have displayed unusual conformations for helix 8. A membrane distal conformation was observed for angiotensin II type 1 & type 2 receptors (Zhang *et al*, 2015c, 2017a) and the prostaglandin E receptors EP_3R & EP_4R (Morimoto *et al*, 2019; Toyoda *et al*, 2019). For C5aR, a reversed, looped orientation was observed (Liu *et al*, 2018), whilst for PAFR, helix 8 makes extensive interactions back on the TM helix bundle (Cao *et al*, 2018).

A2 Expression & purification of rNTS1BH$_6$ and mutants thereof

Competent BL21(DE3) *E. coli* (Novagen) cells were transformed with NTS1 constructs and selected by plating on LB-Agar with 100 µg/mL Ampicillin. A 200mL overnight culture of T2Y medium was prepared with a single colony and 100 µg/mL Ampicillin, then the next day was used to inoculate large scale cultures. 4-10 L *E. coli* were was grown to an OD of 0.6 at 37°C and induced by addition of 0.25 mM IPTG, with growth continued for 16 hours post induction at 26°C. Cells were harvested by centrifugation (8,000g, 15 minutes, 4°C) and pellets were snap frozen in liquid N_2.

For purification, cells were thawed and resuspended in 2x sol buffer (100mM Tris pH 7.4, 100 mM Tris pH 7.4, 30% glycerol, 400 mM NaCl) and homogenised with a hand blender. Lysozyme and DNase I were added to final concentrations of ~200 µg/mL and 20 µg/mL, respectively, and stirred for 30 minutes at 4°C. The detergents DDM, CHAPS and CHS were added dropwise to final concentrations of 1%, 0.5% & 0.01% (w/v), respectively, and left stirring at 4°C for a minimum of 3 hrs. The lysate was clarified by centrifugation at 75,000g for 45 minutes, passed through a 0.22 µm filter and topped up to 50 mM imidazole.

The clarified lysate was loaded onto a 5 mL HisTrap HP column (GE Healthcare) equilibrated in NiA buffer (50 mM Tris pH 7.4, 15% glycerol, 200 mM NaCl, 0.5% CHAPS, 0.1% DDM, 0.1% CHS, 50 mM imidazole) at 0.5mL/min overnight, using a refrigerated Akta™ Pure system (GE healthcare). The column was washed extensively with NiA buffer, before elution with NiA + 500mM imidazole. Eluted material was diluted to <100mM imidazole and <70mM NaCl with NT0 (50mM Tris, pH 7.4, 15% glycerol,

1mM EDTA, 0.1% DDM, 0.01% CHS). TEV protease was added at an approximately 1:1 molar ratio with NTS1 and incubated overnight at 4°C with rotation.

Cleaved NTS1 was purified further by ligand affinity chromatography. A ligand affinity column was produced by coupling Cys-NT (Alta Biotech) to Ultralink™ Iodoacetyl resin (Thermo Fisher) according to the manufacturer's protocol. Briefly, Cys-NT in a buffer containing 25mM TCEP at pH 8.5 was added to the resin for 3 hours at room temperature. Resin was left to settle and OD_{280} of load and flow through compared to assess coupling efficiency, before blocking with L-Cysteine and washing in a buffer containing 1M NaCl. Resin was stored in B3 buffer (50mM Tris pH 7.4, 150mM NaCl, 0.05% Azide w/v).

For purification, resin was drained of B3 buffer, washed in MQ H_2O and equilibrated in NT0 buffer. Sample was added to ~2mL of resin with >100 nmol/mL of NT coupled and incubated at 4°C for 2-4 hours. Flow through was collected and re-applied to a 2nd equilibrated column. Drained resin was washed with NT0, followed by NT70 (NT0 with 70mM NaCl and without EDTA) and NT150 (NT70 but with 150mM NaCl), before elution in NT1K (NT150 but with 1M NaCl). Eluted fractions were checked by SDS-PAGE and where necessary, snap frozen.

For spin labelling, NTS1 was first concentrated by loading onto a 1mL HisTrap equilibrated in 50 mM Tris pH 7.4, 15% glycerol, 200 mM NaCl, 0.1% DDM, 0.01% CHS. Resin was washed with this buffer and material eluted in 500 µL fractions by supplementation of the buffer with 500 mM imidazole. The spin label MTSL (Toronto Research Chemicals) was prepared as a 50mM solution in DMSO, diluted to 5 mM in MQ H_2O and added in 10 fold molar excess of NTS1 at room temperature for 20 minutes, followed by a further 10 fold molar excess for 20 minutes. Material was then passed over two tandem 5 mL HiTrap HP desalting columns (GE healthcare) to remove

free spin label and exchange into a final buffer of 50 mM Tris pH 7.4, 15% glycerol, 150 mM NaCl, 0.1% DDM, 0.01% CHS, 1 mM EDTA.

A3 Expression & purification of proteins for Chapters 3-5

A3.1 Expression & purification of G_q heterotrimer

For purification, cell pellets were thawed and resuspended in a buffer of 10mM HEPES 7.4, 100 µM $MgCl_2$, 5mM BME, 10-20 µM GDP, 150 mg/L Benzamidine and 10 µM leupeptin with stirring at 4°C. Crude membranes were pelleted (38,000g, 50 mins, 4°C) and solubilised by dounce homogenisation in solubilisation buffer (20mM HEPES 7.4, 100mM NaCl, 1% sodium cholate, 0.05% DDM, 20 µM GDP, 1mM $MgCl_2$ and protease inhibitors, 100 µM TCEP and 5 µL Benzonase® or 10 mg/mL DNase I), followed by stirring for 60 minutes. Material was clarified by centrifugation (38,000g, 50 mins, 4°C) and 10 mM imidazole was added before batch loading onto Ni-NTA resin (Thermo Scientific) equilibrated in solubilisation buffer (+ 10 mM imidazole) for 90 minutes at 4°C. Resin was harvested and the resin was washed (solubilisation buffer without cholate or inhibitors, and with 20 mM imidazole) to gradually remove cholate and contaminants. Material was eluted at 250 mM imidazole, 300 µg of his-3C protease was added and the mixture was dialysed (overnight, 4°C) in a 3.5 K MWCO cassette (Thermo Fisher) against a buffer of 20 mM HEPES pH 7.4, 100 mM NaCl, 0.05% DDM, 1 mM $MgCl_2$, 20 µM GDP and 100 µM TCEP.

The next morning, dialysed material was passed over Ni-NTA resin for removal of his tag and 3C protease. The flow through was concentrated and applied to an S200 increase column (0.6mL/min, 4°C) to purify intact heterotrimer from excess Gβγ, as judged by SDS PAGE of fractions. Homogeneous heterotrimer was concentrated and snap frozen in liquid N_2.

A3.2 Expression & purification of myristoylated $G\alpha_{i1}$

Cell pellets were resuspended in lysis buffer (50 mM HEPES pH 7.5. 100 mM NaCl, 1 mM MgCl2, 100 µM TCEP, 5 mM Imidazole, 50 µM GDP & 150 mg/L Benzamidine and 10 µM Leupeptin). 50 mL aliquots of lysate were sonicated at 70% amplitude in six bursts of 45 seconds. Lysate was clarified by centrifugation (30,000g, 30 minutes, 4°C) and incubated (60 mins, 4°C, with rotation) with Ni-NTA resin (1.5 mL resin/L culture) equilibrated in lysis buffer. Resin was harvested by centrifugation (700g, 10 minutes, 4°C) and washed in a gravity flow column using 10 CV high salt buffer (20 mM HEPES pH 7.4, 500 mM NaCl, 20 mM imidazole, 10 µM GDP, 1 mM MgCl2, 100 µM TCEP, inhibitors) then with 10 CV low salt buffer (same as above but with 100 mM NaCl). Protein was eluted in low salt buffer supplemented with 200 mM imidazole and dialysed (overnight, 4°C) against a buffer of 50 mM Tris pH 7.5, 1 mM EDTA, 2 mM DTT, 10 µM GDP, 100 mM NaCl using a 10K MWCO dialysis cassette. Ammonium sulphate was added to the dialysed material to final 1.2 M ammonium sulfate at a volume of 30 mL. Precipitated material was removed by centrifugation (4,000g, 20 mins, 4°C) and syringe filtration. Filtered material was applied to a HiPrep® Phenyl Sepharose column at 4 mL/min. The column was washed with 5 CV of 50 mM Tris pH 7.5, 100 mM NaCl, 1 mM EDTA, 2 mM DTT, 10 µM GDP, 1.2 M ammonium sulfate. Elution was achieved with a linear gradient of elution buffer (50 mM Tris pH 7.5, 100 mM NaCl, 1 mM EDTA, 2 mM DTT, 10 µM GDP). The gradient was set to reach 100% over 180 mL. Eluted protein was analysed by SDS-PAGE, appropriate fractions were pooled and dialysed (overnight, 4°C) in 20 mM HEPES pH 7.5, 100 mM NaCl, 1 mM MgCl2, 100 µM TCEP, 10 µM GDP before concentration to >10mg/mL and snap freezing in liquid N_2.

A4 Data sets for GTPase-Glo™ assay

Presented below are data sets used in chapter 4 & 5. The data are unprocessed other than normalization such that 100% corresponds to the counts given by a sample containing receptor + 5 μM GTP.

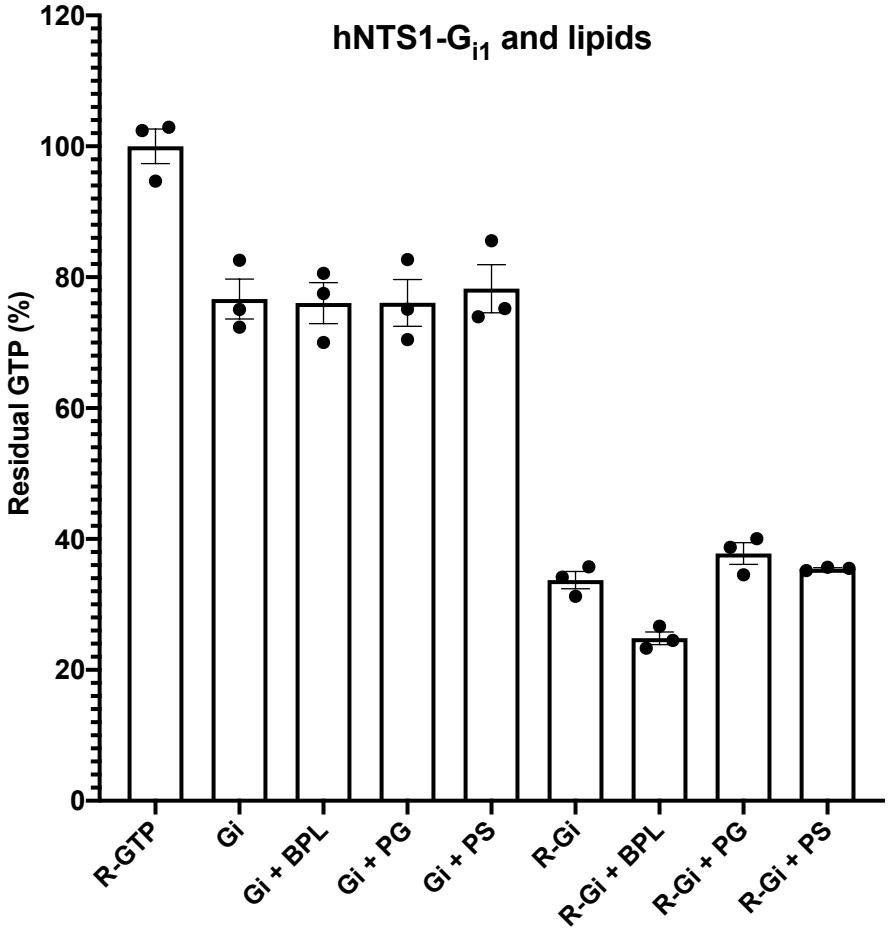


Figure A1. Data used to produce figure 4.3A and 4.3B. All values are normalised to the GTP control. Error bars represent +/- SEM and individual data points are also shown. In all cases, the final concentrations of G protein, receptor and lipid were 500 nM, 125 nM & 200 μM respectively. See section 4.3.3 for full experimental detail.

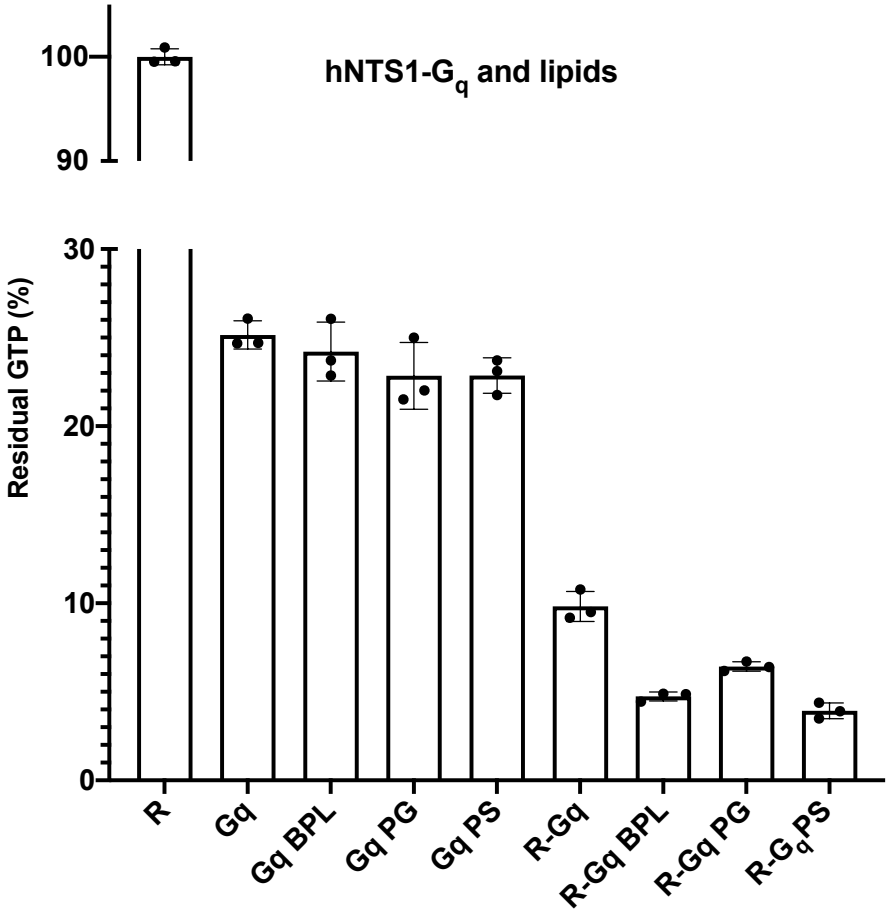


Figure A2: Data used to produce figure 4.4. All values are normalised to the GTP control. Error bars represent +/- SEM and individual data points are also shown. Final concentrations of G protein, receptor and lipid were 1 μM, 1 μM and 200 μM respectively. GDP is present at 5μM. See section 4.3.3 for full experimental detail.

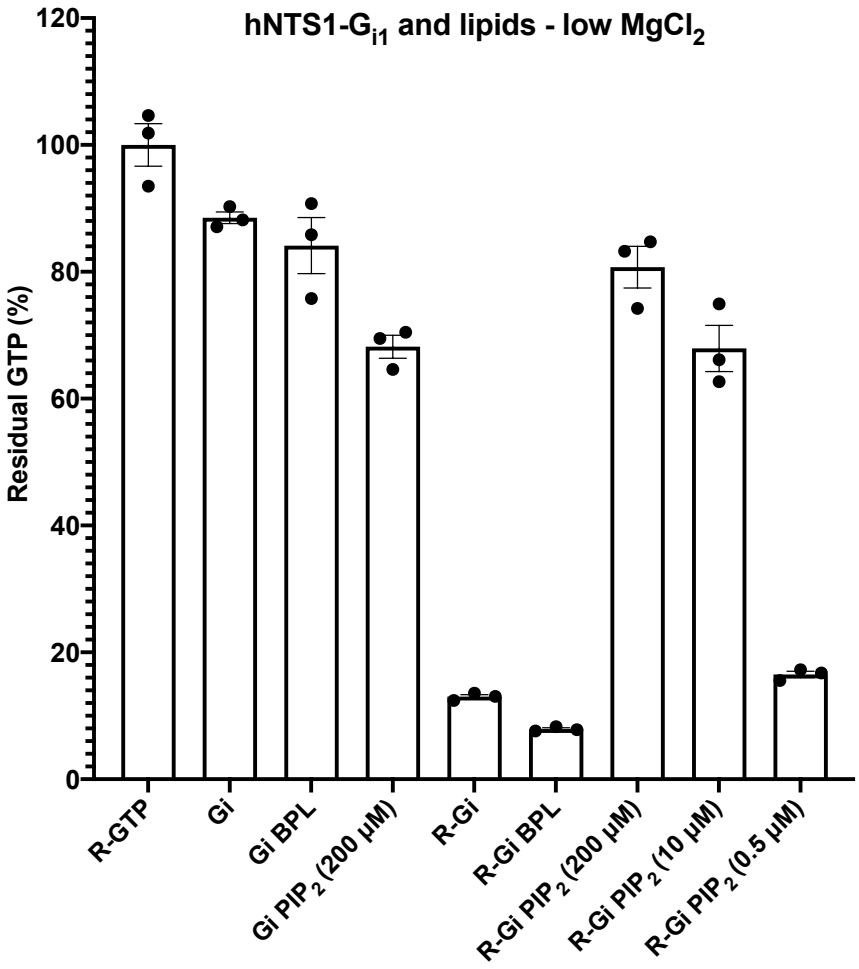


Figure A3: Data used to produce figures 4.5 & 4.6. All values are normalised to the GTP control. Error bars represent +/- SEM and individual data points are also shown. Final concentrations of G protein and receptor were 500 nM and 125 nM, respectively. $MgCl_2$ was present at 50 µM, BPL at 200 µM and PIP_2 at 0.5 - 200 µM as noted. See section 4.3.3 for full experimental detail.

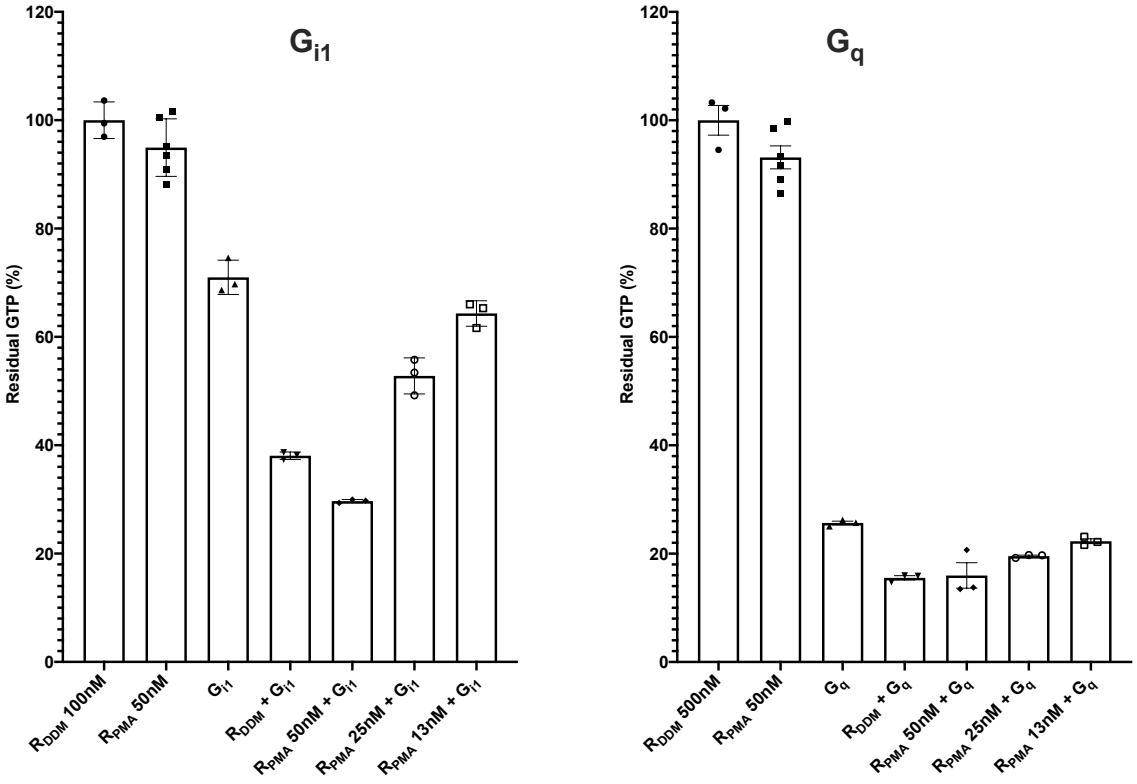


Figure A4: Data used to produce figure 5.10 & 5.11. All values are normalised to the GTP + R_{DDM} control. Error bars represent +/- SEM and individual data points are also shown. R_{DDM} = detergent-solubilised receptor (100 nM for G_{i1} conditions, 500 nM for G_q conditions), R_{PMA} = receptor in PMA-NPs. Both G proteins were present at 500 nM. See section 5.3.5 for full experimental detail.

Bibliography

Adamson RJ & Watts A (2014) Kinetics of the early events of GPCR signalling. *FEBS Lett.* **588:** 4701–4707

Almén M, Nordström KJV, Fredriksson R & Schiöth HB (2009) Mapping the human membrane proteome: a majority of the human membrane proteins can be classified according to function and evolutionary origin. *BMC Biol.* **7:** 50

Altenbach C, Cai K, Khorana HG & Hubbell WL (1999a) Structural Features and Light-Dependent Changes in the Sequence 306 - 322 Extending from Helix VII to the Palmitoylation Sites in Rhodopsin : A Site-Directed Spin-Labeling Study. *Biochemistry* **38:** 7931–7937

Altenbach C, Klein-Seetharaman J, Hwa J, Gobind Khorana H & Hubbell WL (1999b) Structural Features and Light-Dependent Changes in the Sequence 59-75 Connecting Helices I and II in Rhodopsin: A Site-Directed Spin-Labeling Study. *Biochemistry* **38:** 7945–7949

Altenbach C, López CJ, Hideg K & Hubbell WL (2015) Exploring Structure, Dynamics, and Topology of Nitroxide Spin-Labeled Proteins Using Continuous-Wave Electron Paramagnetic Resonance Spectroscopy. *Methods Enzymol.* **564:** 59–100

Altenbach C, Yang K, Farrens DL, Farahbakhsh ZT, Gobind Khorana H & Hubbell WL (1996) Structural Features and Light-Dependent Changes in the Cytoplasmic Interhelical E-F Loop Region of Rhodopsin: A Site-Directed Spin-Labeling Study. *Biochemistry* **35:** 12470–12478

Alves ID, Salgado GFJ, Salamon Z, Brown MF, Tollin G & Hruby VJ (2005) Phosphatidylethanolamine enhances rhodopsin photoactivation and transducin binding in a solid supported lipid bilayer as determined using plasmon-waveguide resonance spectroscopy. *Biophys. J.* **88:** 198–210

Anandan A & Vrielink A (2016) Detergents in Membrane Protein Purification and Crystallisation. In *The Next Generation in Membrane Protein Structure Determination*, Moraes I (ed) pp 13–28. Springer

Anborgh PH, Caron MG, Barak LS, Laporte SA, Zhang J & Ferguson SSG (2002) Cellular Trafficking of G Protein-coupled Receptor/β-Arrestin Endocytic Complexes.

J. Biol. Chem. **274:** 10999–11006

Antonelli T, Fuxe K, Tomasini MC, Mazzoni E, Agnati LF, Tanganelli S & Ferraro L (2007) Neurotensin receptor mechanisms and its modulation of glutamate transmission in the brain. Relevance for neurodegenerative diseases and their treatment. *Prog. Neurobiol.* **83:** 92–109

Asada H, Horita S, Hirata K, Shiroishi M, Shiimura Y, Iwanari H, Hamakubo T, Shimamura T, Nomura N, Kusano-Arai O, Uemura T, Suno C, Kobayashi T & Iwata S (2018) Crystal structure of the human angiotensin II type 2 receptor bound to an angiotensin II analog. *Nat. Struct. Mol. Biol.* **25:** 570–576

Attramadal H, Arriza JL, Aoki C, Dawson TM, Codina J, Kwatra MM, Snyder SH, Caron MG & Lefkowitz RJ (1992) β-Arrestin2, a novel member of the arrestin/β-arrestin gene family. *J. Biol. Chem.* **267:** 17882–17890

Autzen HE, Julius D & Cheng Y (2019) Membrane mimetic systems in CryoEM: keeping membrane proteins in their native environment. *Curr. Opin. Struct. Biol.* **52:** 1–10

Azriel Y & Burcher E (2001) Characterization and Autoradiographic Localization of Neurotensin Binding Sites in Human Sigmoid Colon. *J. Pharmacol. Exp. Ther.* **297:** 1074–1081

Bada Juarez JF, Harper AJ, Judge PJ, Tonge SR & Watts A (2019) From polymer chemistry to structural biology: The development of SMA and related amphipathic polymers for membrane protein extraction and solubilisation. *Chem. Phys. Lipids* **221:** 167–175

Bae HE, Du Y, Hariharan P, Mortensen JS, Kumar KK, Ha B, Das M, Lee HS, Loland CJ, Guan L, Kobilka BK & Chae PS (2019) Asymmetric maltose neopentyl glycol amphiphiles for a membrane protein study: effect of detergent asymmetricity on protein stability. *Chem. Sci.* **10:** 1107–1116

Bae HE, Mortensen JS, Ribeiro O, Du Y, Ehsan M, Kobilka BK, Loland CJ, Byrne B & Chae PS (2016) Tandem neopentyl glycol maltosides (TNMs) for membrane protein stabilisation. *Chem. Commun.* **52:** 12104–12107

Bai X chen, McMullan G & Scheres SHW (2015) How cryo-EM is revolutionizing structural biology. *Trends Biochem. Sci.* **40:** 49–57

Ballesteros JA & Weinstein H (1995) Integrated methods for the construction of three-

dimensional models and computational probing of structure-function relations in G protein-coupled receptors. *Methods Neurosci.* **25:** 366–428

Barniol-Xicota M & Verhelst SHL (2018) Stable and Functional Rhomboid Proteases in Lipid Nanodiscs by Using Diisobutylene/Maleic Acid Copolymers. *J. Am. Chem. Soc.* **140:** 14557–14561

Barrera NP, Di Bartolo N, Booth PJ & Robinson C V (2008) Micelles Protect Membrane Complexes from Solution to Vacuum. *Science* **321:** 243–246

Bayburt TH, Grinkova Y V. & Sligar SG (2002) Self-Assembly of Discoidal Phospholipid Bilayer Nanoparticles with Membrane Scaffold Proteins. *Nano Lett.* **2:** 853–856

Berliner LJ, Grunwald J, Hankovszky HO & Hideg K (1982) A novel reversible thiol-specific spin label: Papain active site labeling and inhibition. *Anal. Biochem.* **119:** 450–455

Besserer-Offroy É, Brouillette RL, Lavenus S, Froehlich U, Brumwell A, Murza A, Longpré JM, Marsault É, Grandbois M, Sarret P & Leduc R (2017) The signaling signature of the neurotensin type 1 receptor with endogenous ligands. *Eur. J. Pharmacol.* **805:** 1–13

Bill RM, Henderson PJF, Iwata S, Kunji ERS, Michel H, Neutze R, Newstead S, Poolman B, Tate CG & Vogel H (2011) Overcoming barriers to membrane protein structure determination. *Nat. Biotechnol.* **29:** 335–340

Bolivar JH, Muñoz-garcía JC, Castro-dopico T, Dijkman PM, Stansfeld PJ & Watts A (2016) Interaction of lipids with the neurotensin receptor 1. *Biochim. Biophys. Acta - Biomembr.* **1858:** 1278–1287

Bordignon E (2013) Spin-Labeling EPR of Proteins: Dynamics and Water Accessibility of Spin-Label Side Chains. In *Encyclopedia of Biophysics* pp 2439–2447. Springer Berlin Heidelberg

Bordignon E & Bleicken S (2018) New limits of sensitivity of site-directed spin labeling electron paramagnetic resonance for membrane proteins. *Biochim. Biophys. Acta - Biomembr.* **1860:** 841–853

Botelho AV, Gibson NJ, Thurmond RL, Wang Y & Brown MF (2002) Conformational energetics of rhodopsin modulated by nonlamellar-forming lipids. *Biochemistry* **41:** 6354–6368

Boules M, Li Z, Smith K, Fredrickson P & Richelson E (2013) Diverse roles of neurotensin agonists in the central nervous system. *Front. Endocrinol. (Lausanne).* **4:** 1–16

Bubis J (1998) Effect of detergents and lipids on transducin photoactivation by rhodopsin. *Biol. Res.* **31:** 59–71

Cahill TJ, Thomsen ARB, Tarrasch JT, Plouffe B, Nguyen AH, Yang F, Huang L-Y, Kahsai AW, Bassoni DL, Gavino BJ, Lamerdin JE, Triest S, Shukla AK, Berger B, Little J, Antar A, Blanc A, Qu C-X, Chen X, Kawakami K, et al (2017) Distinct conformations of GPCR–β-arrestin complexes mediate desensitization, signaling, and endocytosis. *Proc. Natl. Acad. Sci. U. S. A.* **114:** 2562–2567

Cao C, Tan Q, Xu C, He L, Yang L, Zhou Y, Zhou Y, Qiao A, Lu M, Yi C, Han GW, Wang X, Li X, Yang H, Rao Z, Jiang H, Zhao Y, Liu J, Stevens RC, Zhao Q, et al (2018) Structural basis for signal recognition and transduction by platelet-activating-factor receptor. *Nat. Struct. Mol. Biol.* **25:** 488–495

Carpenter B, Nehmé R, Warne T, Andrew GW, Tate CG, Leslie AGW & Tate CG (2016) Structure of the adenosine A2A receptor bound to an engineered G protein. *Nature* **536:** 104–107

Carpenter B, Singhal A, Strege A, Edwards PC, White CF, Du H, Grisshammer R & Tate CG (2017) Mini-G proteins : Novel tools for studying GPCRs in their active conformation. *PLoS One* **12:** e0175642

Carpenter B & Tate CG (2016) Engineering a minimal G protein to facilitate crystallisation of G protein-coupled receptors in their active conformation. *Protein Eng. Des. Sel.* **29:** 583–593

Cha K, Reeves PJ & Khorana HG (2000) Structure and function in rhodopsin: Destabilization of rhodopsin by the binding of an antibody at the N-terminal segment provides support for involvement of the latter in an intradiscal tertiary structure. *Proc. Natl. Acad. Sci. U. S. A.* **97:** 3016–3021

Chae PS, Rasmussen SGF, Rana RR, Gotfryd K, Chandra R, Goren MA, Kruse AC, Nurva S, Loland CJ, Pierre Y, Drew D, Popot JL, Picot D, Fox BG, Guan L, Gether U, Byrne B, Kobilka B & Gellman SH (2010) Maltose-neopentyl glycol (MNG) amphiphiles for solubilization, stabilization and crystallization of membrane proteins. *Nat. Methods* **7:** 1003–1008

Chan P, Thomas CJ, Sprang SR & Tall GG (2013) Molecular chaperoning function of Ric-8 is to fold nascent heterotrimeric G protein alpha subunits. *Proc. Natl. Acad. Sci.* **110:** 3794–3799

Che T, Majumdar S, Zaidi SA, Ondachi P, McCorvy JD, Wang S, Mosier PD, Uprety R, Vardy E, Krumm BE, Han GW, Lee MY, Pardon E, Steyaert J, Huang XP, Strachan RT, Tribo AR, Pasternak GW, Carroll FI, Stevens RC, et al (2018) Structure of the Nanobody-Stabilized Active State of the Kappa Opioid Receptor. *Cell* **172:** 55–67

Cheng RKY, Segala E, Robertson N, Deflorian F, Doré AS, Errey JC, Fiez-Vandal C, Marshall FH & Cooke RM (2017) Structures of Human A1 and A2A Adenosine Receptors with Xanthines Reveal Determinants of Selectivity. *Structure* **25:** 1275–1285

Cherezov V (2009) Crystallizing membrane proteins using lipidic mesophases. *Nat. Protoc.* **4:** 706–731

Cherezov V, Rosenbaum DM, Hanson MA, Rasmussen SGF, Thian FS, Kobilka TS, Choi HJ, Kuhn P, Weis WI, Kobilka BK & Stevens RC (2007) High-resolution crystal structure of an engineered human beta(2)-adrenergic G protein-coupled receptor. *Science* **318:** 1258–1265

Chien CTH, Helfinger LR, Bostock MJ, Solt A, Tan YL & Nietlispach D (2017) An Adaptable Phospholipid Membrane Mimetic System for Solution NMR Studies of Membrane Proteins. *J. Am. Chem. Soc.* **139:** 14829–14832

Chini B & Parenti M (2009) G-protein-coupled receptors, cholesterol and palmitoylation: facts about fats. *J. Mol. Endocrinol.* **42:** 371–379

Choi G, Guo J & Makriyannis A (2005) The conformation of the cytoplasmic helix 8 of the CB1 cannabinoid receptor using NMR and circular dichroism. *Biochim. Biophys. Acta - Biomembr.* **1668:** 1–9

Chun E, Thompson AA, Liu W, Roth CB, Griffith MT, Katritch V, Kunken J, Xu F, Cherezov V, Hanson MA & Stevens RC (2012) Fusion partner toolchest for the stabilization and crystallization of G protein-coupled receptors. *Structure* **20:** 967–976

Chung KY, Kim TH, Manglik A, Alvares R, Kobilka BK & Prosser RS (2012) Role of detergents in conformational exchange of a G protein-coupled receptor. *J. Biol. Chem.* **287:** 36305–36311

Columbus L, Kálai T, Jekö J, Hideg K & Hubbell WL (2001) Molecular motion of spin labeled side chains in α-helices: Analysis by variation of side chain structure. *Biochemistry* **40:** 3828–3846

Connor M & Christie MJ (2006) Opioid Receptor Signalling Mechanisms. *Clin. Exp. Pharmacol. Physiol.* **26:** 493–499

Coppola T, Béraud-Dufour S, Antoine A, Vincent JP & Mazella J (2008) Neurotensin protects pancreatic beta cells from apoptosis. *Int. J. Biochem. Cell Biol.* **40:** 2296–2302

Crouthamel M, Thiyagarajan MM, Evanko DS & Wedegaertner PB (2008) N-terminal polybasic motifs are required for plasma membrane localization of Gαs and Gαq. *Cell. Signal.* **20:** 1900–1910

Das M, Du Y, Mortensen JS, Ramos M, Ghani L, Lee HJ, Bae HE, Byrne B, Guan L, Loland CJ, Kobilka BK & Chae PS (2019) Trehalose-cored amphiphiles for membrane protein stabilization: Importance of the detergent micelle size in GPCR stability. *Org. Biomol. Chem.* **17:** 3249–3257

Dawaliby R, Trubbia C, Delporte C, Masureel M, Van Antwerpen P, Kobilka BK & Govaerts C (2016a) Allosteric regulation of G protein–coupled receptor activity by phospholipids. *Nat. Chem. Biol.* **12:** 35–39

Dawaliby R, Trubbia C, Delporte C, Noyon C, Ruysschaert JM, Van Antwerpen P & Govaerts C (2016b) Phosphatidylethanolamine is a key regulator of membrane fluidity in eukaryotic cells. *J. Biol. Chem.* **291:** 3658–3667

Denisov IG, Grinkova Y V, Lazarides AA, Sligar SG, Science M, V DU & Carolina N (2004) Directed Self-Assembly of Monodisperse Phospholipid Bilayer Nanodiscs with Controlled Size. *J. Am. Chem. Soc.* **126:** 3477–3487

DeWire SM, Ahn S, Lefkowitz RJ & Shenoy SK (2007) β-Arrestins and Cell Signaling. *Annu. Rev. Physiol.* **69:** 483–510

Dijkman PM, Castell OK, Goddard AD, Munoz-Garcia JC, de Graaf C, Wallace MI & Watts A (2018) Dynamic tuneable G protein-coupled receptor monomer-dimer populations. *Nat. Commun.* **9:** 1710

Dijkman PM & Watts A (2015) Lipid modulation of early G protein-coupled receptor signalling events. *Biochim. Biophys. Acta - Biomembr.* **1848:** 2889–2897

Dobner PR (2005) Multitasking with neurotensin in the central nervous system. *Cell. Mol. Life Sci.* **62:** 1946–1963

Dodevski I & Plückthun A (2011) Evolution of three human GPCRs for higher expression and stability. *J. Mol. Biol.* **408:** 599–615

Dörr JM (2017) Membrane Solubilization by Styrene – Maleic Acid Copolymers: towards new applications in membrane protein research. PhD thesis, Utretch University

Dörr JM, Scheidelaar S, Koorengevel MC, Dominguez JJ, Schäfer M, van Walree CA & Killian JA (2016) The styrene–maleic acid copolymer: a versatile tool in membrane research. *Eur. Biophys. J.* **45:** 3–21

Dorsam RT & Gutkind JS (2007) G-protein-coupled receptors and cancer. *Nat. Rev. Cancer* **7:** 79–94

Downes GB & Gautam N (1999) The G protein subunit gene families. *Genomics* **62:** 544–552

Draper-Joyce CJ, Khoshouei M, Thal DM, Liang Y, Nguyen ATN, Furness SGB, Venugopal H, Baltos J, Plitzko JM, Danev R, Baumeister W, May LT, Wootten D, Sexton PM, Glukhova A & Christopoulos A (2018) Structure of the adenosine-bound human adenosine A1 receptor-Gi complex. *Nature* **558:** 559–563

Dror RO, Arlow DH, Maragakis P, Mildorf TJ, Pan AC, Xu H, Borhani DW & Shaw DE (2011) Activation mechanism of the β2-adrenergic receptor. *Proc. Natl. Acad. Sci. U. S. A.* **108:** 18684–18689

Dror RO, Mildorf TJ, Hilger D, Manglik A, Borhani DW, Arlow DH, Philippsen A, Villanueva N, Yang Z, Lerch MT, Hubbell WL, Kobilka BK, Sunahara RK & Shaw DE (2015) Structural basis for nucleotide exchange in heterotrimeric G proteins. *Science* **348:** 1361–1365

Du Y, Duc NM, Rasmussen SGF, Hilger D, Kubiak X, Wang L, Bohon J, Kim HR, Wegrecki M, Asuru A, Jeong KM, Lee J, Chance MR, Lodowski DT, Kobilka BK & Chung KY (2019) Assembly of a GPCR-G Protein Complex. *Cell* **177:** 1–11

Egloff P, Hillenbrand M, Klenk C, Batyuk A, Heine P, Balada S, Schlinkmann KM, Scott DJ, Schütz M & Plückthun A (2014) Structure of signaling-competent neurotensin receptor 1 obtained by directed evolution in Escherichia coli. *Proc. Natl. Acad. Sci.* **111:** E655–E662

Ehrenmann J, Schöppe J, Klenk C, Rappas M, Kummer L, Doré AS & Plückthun A (2018) High-resolution crystal structure of parathyroid hormone 1 receptor in complex with a peptide agonist. *Nat. Struct. Mol. Biol.* **25:** 1086–1092

Einhauer A & Jungbauer A (2001) Affinity of the monoclonal antibody M1 directed against the FLAG peptide. *J. Chromatogr. A* **921:** 25–30

Van Eps N, Altenbach C, Caro LN, Latorraca NR, Hollingsworth SA, Dror RO, Ernst OP & Hubbell WL (2018) Gi- and Gs-coupled GPCRs show different modes of G-protein binding. *Proc. Natl. Acad. Sci. U. S. A.* **115:** 2383–2388

Escribá P V., Wedegaertner PB, Goñi FM & Vögler O (2007) Lipid-protein interactions in GPCR-associated signaling. *Biochim. Biophys. Acta - Biomembr.* **1768:** 836–852

Fairman JW, Noinaj N & Buchanan SK (2011) The structural biology of β-barrel membrane proteins: A summary of recent reports. *Curr. Opin. Struct. Biol.* **21:** 523–531

Fang Y, Kenakin T & Liu C (2015) Editorial: Orphan GPCRs As Emerging Drug Targets. *Front. Pharmacol.* **6:** 295

Farrens DL, Altenbach C, Yang K, Hubbell WL & Khorana HG (1996) Requirement of rigid-body motion of transmembrane helices for light activation of rhodopsin. *Science* **274:** 768–770

Feierler J, Wirth M, Welte B, Schüssler S, Jochum M & Faussner A (2011) Helix 8 plays a crucial role in bradykinin B 2 receptor trafficking and signaling. *J. Biol. Chem.* **286:** 43282–43293

Feller SE, Gawrisch K & Woolf TB (2003) Rhodopsin exhibits a preference for solvation by polyunsaturated docosohexaenoic acid. *J. Am. Chem. Soc.* **125:** 4434–4435

Fernandez-Leiro R & Scheres SHW (2016) Unravelling biological macromolecules with cryo-electron microscopy. *Nature* **537:** 339–346

Flock T, Hauser AS, Lund N, Gloriam DE, Balaji S, Babu MM, Hauser SA, Lund N, Gloriam ED, Balaji S & Babu MM (2017) Selectivity determinants of GPCR-G-protein binding. *Nature* **545:** 317–322

Flock T, Ravarani CNJ, Sun D, Venkatakrishnan a J, Kayikci M, Tate CG, Veprintsev DB & Babu MM (2015) Universal allosteric mechanism for Gα activation by GPCRs. *Nature* **524:** 173–179

Florio VA & Sternweis PC (1985) Reconstitution of resolved muscarinic cholinergic receptors with purified GTP-binding proteins. *J. Biol. Chem.* **260:** 3477–3483

Frauenfeld J, Löving R, Armache J, Sonnen AF, Guettou F, Moberg P, Zhu L, Jegerschöld C, Flayhan A, Briggs JAG, Garoff H & Löw C (2016) A saposin-lipoprotein nanoparticle system for membrane proteins. *Nat. Methods* **13:** 345–351

Fredriksson R, Lagerström MC, Lundin L-G & Schiöth HB (2003) The G-protein-coupled receptors in the human genome form five main families. Phylogenetic analysis, paralogon groups, and fingerprints. *Mol. Pharmacol.* **63:** 1256–1272

Gahbauer S, Pluhackova K & Böckmann RA (2018) Closely related, yet unique: Distinct homo- and heterodimerization patterns of G protein coupled chemokine receptors and their fine-tuning by cholesterol. *PLoS Comput. Biol.* **14:** 3

Gao Y, Hu H, Ramachandran S, Erickson JW, Cerione RA & Skiniotis G (2019) Structures of the Rhodopsin-Transducin Complex: Insights into G-Protein Activation. *Mol. Cell* **75:** 1–10

García-Nafría J, Lee Y, Bai X, Carpenter B & Tate CG (2018a) Cryo-EM structure of the adenosine A2A receptor coupled to an engineered heterotrimeric G protein. *Elife* **7:** e35946

García-Nafría J, Nehmé R, Edwards PC & Tate CG (2018b) Cryo-EM structure of the serotonin 5-HT1B receptor coupled to heterotrimeric Go. *Nature* **558:** 620–623

García-Nafría J & Tate CG (2019) Cryo-EM structures of GPCRs coupled to Gs , Gi and Go. *Mol. Cell. Endocrinol.* **488:** 1–13

Gault J, Donlan JAC, Liko I, Hopper JTS, Gupta K, Housden NG, Struwe WB, Marty MT, Mize T, Bechara C, Zhu Y, Wu B, Kleanthous C, Belov M, Damoc E, Makarov A & Robinson C V. (2016) High-resolution mass spectrometry of small molecules bound to membrane proteins. *Nat. Methods* **13:** 333–336

Gavriilidou AFM, Hunziker H, Mayer D, Vuckovic Z, Veprintsev DB & Zenobi R (2019) Insights into the Basal Activity and Activation Mechanism of the β1 Adrenergic Receptor Using Native Mass Spectrometry. *J. Am. Soc. Mass Spectrom.* **30:** 529–537

Gehret AU, Jones BBW, Tran PNP, Cook LB, Greuber EK & Hinkle PM (2010) Role of helix 8 of the thyrotropin-releasing hormone receptor in phosphorylation by G protein-coupled receptor kinase. *Mol. Pharmacol.* **77:** 288–297

Ghosh E, Kumari P, Jaiman D & Shukla AK (2015) Methodological advances: The unsung heroes of the GPCR structural revolution. *Nat. Rev. Mol. Cell Biol.* **16:** 69–81

Glukhova A, Thal DM, Nguyen AT, Vecchio EA, Jörg M, Scammells PJ, May LT, Sexton PM & Christopoulos A (2017) Structure of the Adenosine A1 Receptor Reveals the Basis for Subtype Selectivity. *Cell* **168:** 867–877

Goddard AD, Dijkman PM, Adamson RJ, Dos Reis RI & Watts A (2015) Reconstitution of Membrane Proteins: A GPCR as an Example. In *Methods in Enzymology* pp 405–424.

Goddard AD & Watts A (2012) Regulation of G protein-coupled receptors by palmitoylation and cholesterol. *BMC Biol.* **10:** 27

Gómez-Sebastián S, López-Vidal J & Escribano JM (2014) Significant Productivity Improvement of the Baculovirus Expression Vector System by Engineering a Novel Expression Cassette. *PLoS One* **9:** e96562

Gotoh T, Miyazaki Y, Sato W, Kikuchi K-I & Bentley WE (2001) Proteolytic Activity and Recombinant Protein Production in Virus-Infected Sf-9 Insect Cell Cultures Supplemented with Carboxyl and Cysteine Protease Inhibitors. *J. Biosci. Bioeng.* **92:** 248–255

Gray JA, Bhatnagar A, Gurevich V V. & Roth BL (2003) The interaction of a constitutively active arrestin with the arrestin-insensitive 5-HT2A receptor induces agonist-independent internalization. *Mol. Pharmacol.* **63:** 961–972

Greentree WK & Linder ME (2004) Purification of recombinant G protein alpha subunits from Escherichia coli. *Methods Mol. Biol.* **237:** 3–20

De Grip WJ (1982) Thermal Stability of Rhodopsin and Opsin in Some Novel Detergents. *Methods Enzymol.* **81:** 256–265

Grisshammer R (2009) Purification of Recombinant G-Protein-Coupled Receptors. *Methods Enzymol.* **463:** 631–645

Grundmann M & Kostenis E (2017) Temporal Bias: Time-Encoded Dynamic GPCR Signaling. *Trends Pharmacol. Sci.* **38:** 1110–1124

Guixà-González R, Albasanz JL, Rodriguez-Espigares I, Pastor M, Sanz F, Martí-Solano M, Manna M, Martinez-Seara H, Hildebrand PW, Martín M & Selent J (2017)

Membrane cholesterol access into a G-protein-coupled receptor. *Nat. Commun.* **8:** 14505

Gurevich V V. & Benovic JL (1995) Visual Arrestin Binding to Rhodopsin. *J. Biol. Chem.* **270:** 6010–6016

Hall SCL, Tognoloni C, Charlton J, Bragginton ÉC, Rothnie AJ, Sridhar P, Wheatley M, Knowles TJ, Arnold T, Edler KJ & Dafforn TR (2018) An acid-compatible co-polymer for the solubilization of membranes and proteins into lipid bilayer-containing nanoparticles. *Nanoscale* **10:** 10609–10619

Hanson MA, Cherezov V, Griffith MT, Roth CB, Jaakola VP, Chien EYT, Velasquez J, Kuhn P & Stevens RC (2008) A Specific Cholesterol Binding Site Is Established by the 2.8A Structure of the Human β2-Adrenergic Receptor. *Structure* **16:** 897–905

Harayama T & Riezman H (2018) Understanding the diversity of membrane lipid composition. *Nat. Rev. Mol. Cell Biol.* **19:** 281–296

Harding PJ, Attrill H, Boehringer J, Ross S, Wadhams GH, Smith E, Armitage JP & Watts A (2009) Constitutive dimerization of the G-Protein coupled receptor, neurotensin receptor 1, reconstituted into phospholipid bilayers. *Biophys. J.* **96:** 964–973

Harding PJ, Attrill H, Ross S, Koeppe JR, Kapanidis AN & Watts A (2007) Neurotensin receptor type 1: Escherichia coli expression, purification, characterization and biophysical study. *Biochem. Soc. Trans.* **35:** 760–763

Harikumar KG, Puri V, Singh RD, Hanada K, Pagano RE & Miller LJ (2005) Differential effects of modification of membrane cholesterol and sphingolipids on the conformation, function, and trafficking of the G protein-coupled cholecystokinin receptor. *J. Biol. Chem.* **280:** 2176–2185

Hauser AS, Attwood MM, Rask-Andersen M, Schiöth HB & Gloriam DE (2017) Trends in GPCR drug discovery: new agents, targets and indications. *Nat. Rev. Drug Discov.* **16:** 829–842

Heakal Y & Kester M (2009) Nanoliposomal short-chain ceramide inhibits agonist-dependent translocation of neurotensin receptor 1 to structured membrane microdomains in breast cancer cells. *Mol. Cancer Res.* **7:** 724–734

Heakal Y, Woll MP, Fox T, Seaton K, Levenson R & Kester M (2011) Neurotensin receptor-1 inducible palmitoylation is required for efficient receptor-mediated

mitogenic-signaling within structured membrane microdomains. *Cancer Biol. Ther.* **12:** 427–435

Heck M, Schädel SA, Maretzki D & Hofmann KP (2003) Secondary binding sites of retinoids in opsin: Characterization and role in regeneration. *Vision Res.* **43:** 3003–3010

Hedger G (2017) Characterisation of Lipid-Protein Interactions through Computational Modelling. DPhil Thesis, University of Oxford.

Hedin LE, Illergård K & Elofsson A (2011) An introduction to membrane proteins. *J. Proteome Res.* **10:** 3324–3331

Hendrickson WA (2016) Atomic-level analysis of membrane-protein structure. *Nat. Struct. Mol. Biol.* **23:** 464–467

Hessel E, Heck M, Müller P, Herrmann A & Hofmann KP (2003) Signal transduction in the visual cascade involves specific lipid-protein interactions. *J. Biol. Chem.* **278:** 22853–22860

Hessel E, Herrmann A, Müller P, Schnetkamp PPM & Hofmann KP (2000) The transbilayer distribution of phospholipids in disc membranes is a dynamic equilibrium: Evidence for rapid flip and flop movement. *Eur. J. Biochem.* **267:** 1473–1483

Hessel E, Müller P, Herrmann A & Hofmann KP (2001) Light-induced Reorganization of Phospholipids in Rod Disc Membranes. *J. Biol. Chem.* **276:** 2538–2543

Heydenreich FM, Vuckovic Z, Matkovic M & Scott DJ (2015) Stabilization of G protein-coupled receptors by point mutations. *Front. Pharmacol.* **6:** 1–15

Higashijima T, Ferguson KM, Smigel MD & Gilman AG (1987) The effect of GTP and Mg2+ on the GTPase activity and the fluorescent properties of G(o). *J. Biol. Chem.* **262:** 757–761

Higgins JB & Caseys PJ (1994) In Vitro Processing of Recombinant G Protein gamma Subunits. *J. Biol. Chem.* **12:** 9067–9073

Hirst DJ, Lee T, Pattenden LK & Thomas WG (2015) Helix 8 of the angiotensin- II type 1A receptor interacts with phosphatidylinositol phosphates and modulates membrane insertion. *Sci. Rep.* **5:** 09972

Ho JD, Chau B, Rodgers L, Lu F, Wilbur KL, Otto KA, Chen Y, Song M, Riley JP, Yang HC, Reynolds NA, Kahl SD, Lewis AP, Groshong C, Madsen RE, Conners K, Lineswala JP, Gheyi T, Saflor MBD, Lee MR, et al (2018) Structural basis for GPR40 allosteric agonism and incretin stimulation. *Nat. Commun.* **9:** 1645

Hom LG & Volkman LE (1998) Preventing proteolytic artifacts in the baculovirus expression system. *Biotechniques* **25:** 18–20

Hori T, Okuno T, Hirata K, Yamashita K, Kawano Y, Yamamoto M, Hato M, Nakamura M, Shimizu T, Yokomizo T, Miyano M & Yokoyama S (2018) Na+ -mimicking ligands stabilize the inactive state of leukotriene B4 receptor BLT1. *Nat. Chem. Biol.* **14:** 262–269

Hu J, Wang Y, Zhang X, Lloyd JR, Li JH, Karpiak J, Costanzi S & Wess J (2010) Structural basis of G protein-coupled receptor-G protein interactions. *Nat. Chem. Biol.* **6:** 541–548

Huang W, Manglik A, Venkatakrishnan AJ, Laeremans T, Feinberg EN, Sanborn AL, Gmeiner P, Kato HE, Livingston KE, Thorsen TS, Kling RC, Husbands SM, Traynor JR, Weis WI, Steyaert J, Dror RO & Kobilka BK (2015) Structural insights into μ-opioid receptor activation. *Nature* **524:** 315–321

Huang Y, Todd N & Thathiah A (2017) The role of GPCRs in neurodegenerative diseases: avenues for therapeutic intervention. *Curr. Opin. Pharmacol.* **32:** 96–110

Hubbell WL, Mchaourab HS, Altenbach C & Lietzow MA (1996) Watching proteins move using site-directed spin labeling. *Structure* **4:** 779–783

Ikonen E (2008) Cellular cholesterol trafficking and compartmentalization. *Nat. Rev. Mol. Cell Biol.* **9:** 125–138

Inagaki S, Ghirlando R, Vishnivetskiy SA, Homan KT, White JF, Tesmer JJG, Gurevich V V & Grisshammer R (2015) G Protein-Coupled Receptor Kinase 2 (GRK2) and 5 (GRK5) Exhibit Selective Phosphorylation of the Neurotensin Receptor in Vitro. *Biochemistry* **54:** 4320–4329

Inagaki S, Ghirlando R, White JF, Gvozdenovic-Jeremic J, Northup JK & Grisshammer R (2012) Modulation of the interaction between neurotensin receptor NTS1 and Gq protein by lipid. *J. Mol. Biol.* **417:** 95–111

Ingólfsson HI, Melo MN, Van Eerden FJ, Arnarez C, Lopez CA, Wassenaar TA, Periole

X, De Vries AH, Tieleman DP & Marrink SJ (2014) Lipid organization of the plasma membrane. *J. Am. Chem. Soc.* **136:** 14554–14559

Inoue A, Raimondi F, Kadji FMN, Singh G, Kishi T, Uwamizu A, Ono Y, Shinjo Y, Ishida S, Arang N, Kawakami K, Gutkind JS, Aoki J & Russell RB (2019) Illuminating G-Protein-Coupling Selectivity of GPCRs. *Cell* **177:** 1–15

Irannejad R, Pessino V, Mika D, Huang B, Wedegaertner PB, Conti M & Von Zastrow M (2017) Functional selectivity of GPCR-directed drug action through location bias. *Nat. Chem. Biol.* **13:** 799–806

Isberg V, Vroling B, van der Kant R, Li K, Vriend G & Gloriam D (2014) GPCRdb: an information system for G protein-coupled receptors. *Nucleic Acids Res.* **42:** D422-425

Jaakola V-P, Griffith M., Hanson M., Cherezov V, Chien EY., Lane J., Ijzerman A. & Stevens RC (2008) The 2.6 Angstrom Crystal Structure of a Human A2A Adenosine Receptor Bound to an Antagonist. *Science* **322:** 1211–1217

Jafurulla M, Aditya Kumar G, Rao BD & Chattopadhyay A (2019) A Critical Analysis of Molecular Mechanisms Underlying Membrane Cholesterol Sensitivity of GPCRs. In *Cholesterol Modulation of Protein Function* pp 21–52.

Jamshad M, Charlton J, Lin Y, Routledge SJ, Bawa Z, Knowles TJ, Overduin M, Dekker N, Dafforn TR, Bill RM, Poyner DR & Wheatley M (2015) G-protein coupled receptor solubilization and purification for biophysical analysis and functional studies, in the total absence of detergent. *Biosci. Rep.* **35:** 1–10

Jeschke G (2012) DEER Distance Measurements on Proteins. *Annu. Rev. Phys. Chem.* **63:** 419–446

Jeschke G (2013) Conformational dynamics and distribution of nitroxide spin labels. *Prog. Nucl. Magn. Reson. Spectrosc.* **72:** 42–60

Jesorka A & Orwar O (2008) Liposomes: Technologies and Analytical Applications. *Annu. Rev. Anal. Chem.* **1:** 801–832

Jian X, Clark WA, Kowalak J, Markey SP, Simonds WF & Northup JK (2001) Gβγ Affinity for Bovine Rhodopsin Is Determined by the Carboxyl-terminal Sequences of the γ Subunit. *J. Biol. Chem.* **276:** 48518–48525

Kang Y, Kuybeda O, De Waal PW, Mukherjee S, Van Eps N, Dutka P, Zhou XE,

Bartesaghi A, Erramilli S, Morizumi T, Gu X, Yin Y, Liu P, Jiang Y, Meng X, Zhao G, Melcher K, Ernst OP, Kossiakoff AA, Subramaniam S, et al (2018) Cryo-EM structure of human rhodopsin bound to an inhibitory G protein. *Nature* **558:** 553–558

Kang Y, Zhou XE, Gao X, He Y, Liu W, Ishchenko A, Barty A, White TA, Yefanov O, Han GW, Xu Q, de Waal PW, Ke J, Tan MHE, Zhang C, Moeller A, West GM, Pascal BD, Van Eps N, Caro LN, et al (2015) Crystal structure of rhodopsin bound to arrestin by femtosecond X-ray laser. *Nature* **523:** 561–567

Kato HE, Zhang Y, Hu H, Suomivuori C-M, Kadji FMN, Aoki J, Krishna Kumar K, Fonseca R, Hilger D, Huang W, Latorraca NR, Inoue A, Dror RO, Kobilka BK & Skiniotis G (2019) Conformational transitions of a neurotensin receptor 1–Gi1 complex. *Nature* **572:** 80–85

Katragadda M, MacIejewski MW & Yeagle PL (2004) Structural studies of the putative helix 8 in the human β2 adrenergic receptor: An NMR study. *Biochim. Biophys. Acta - Biomembr.* **1663:** 74–81

Katritch V, Fenalti G, Abola EE, Roth BL, Cherezov V & Stevens RC (2014) Allosteric sodium in class A GPCR signaling. *Trends Biochem. Sci.* **39:** 233–244

Kaye RG, Saldanha W, Lu Z & Hulme EC (2011) Helix 8 of the M1 Muscarinic Acetylcholine Receptor: Scanning Mutagenesis Delineates a G Protein Recognition Site. *Mol. Pharmacol.* **79:** 701–709

Kenakin T (2004) Efficacy as a vector: the relative prevalence and paucity of inverse agonism. *Mol. Pharmacol.* **65:** 2–11

Kinkead B & Nemeroff CB (2002) Neurotensin: An endogenous antipsychotic? *Curr. Opin. Pharmacol.* **2:** 99–103

Kirchberg K, Kim T, Möller M, Skegro D, Dasara G & Granzin J (2011) Conformational dynamics of helix 8 in the GPCR rhodopsin controls arrestin activation in the desensitization process. *Proc. Natl. Acad. Sci. U. S. A.* **108:** 18690–18695

Kitabgi P, Carraway R, Van Rietschoten J, Granier C, Morgat JL, Menez a, Leeman S & Freychet P (1977) Neurotensin: specific binding to synaptic membranes from rat brain. *Proc. Natl. Acad. Sci. U. S. A.* **74:** 1846–1850

Klenk HD (1996) Post-translational modifications in insect cells. *Cytotechnology* **20:** 139–144

Klug CS & Feix JB (2008) Methods and Applications of Site- Directed Spin Labeling EPR Spectroscopy. *Methods Cell Biol.* **84:** 617–658

Knowles TJ, Finka R, Smith C, Lin YP, Dafforn T & Overduin M (2009) Membrane proteins solubilized intact in lipid containing nanoparticles bounded by styrene maleic acid copolymer. *J. Am. Chem. Soc.* **131:** 7484–7485

Koehl A, Hu H, Maeda S, Zhang Y, Qu Q, Paggi JM, Latorraca NR, Hilger D, Dawson R, Matile H, Schertler GFX, Granier S, Weis WI, Dror RO, Manglik A, Skiniotis G & Kobilka BK (2018) Structure of the μ-opioid receptor-G i protein complex. *Nature* **558:** 547–552

Kofuku Y, Ueda T, Okude J, Shiraishi Y, Kondo K, Mizumura T, Suzuki S & Shimada I (2014) Functional Dynamics of Deuterated β2 -Adrenergic Receptor in Lipid Bilayers Revealed by NMR Spectroscopy. *Angew. Chemie Int. Ed.* **53:** 13376–13379

Konijnenberg A, Van Dyck JF, Kailing LL & Sobott F (2015) Extending native mass spectrometry approaches to integral membrane proteins. *Biol. Chem.* **396:** 991–1002

Krishna AG, Menon ST, Terry TJ & Sakmar TP (2002) Evidence that helix 8 of rhodopsin acts as a membrane-dependent conformational switch. *Biochemistry* **41:** 8298–8309

Krishna Kumar K, Shalev-Benami M, Robertson MJ, Hu H, Banister SD, Hollingsworth SA, Latorraca NR, Kato HE, Hilger D, Maeda S, Weis WI, Farrens DL, Dror RO, Malhotra S V, Kobilka BK & Skiniotis G (2019) Structure of a Signaling Cannabinoid Receptor 1-G Protein Complex. *Cell* **176:** 448–458

Krumm BE, Lee S, Bhattacharya S, Botos I, White CF, Du H, Vaidehi N & Grisshammer R (2016) Structure and dynamics of a constitutively active neurotensin receptor. *Sci. Rep.* **6:** 38564

Krumm BE, White JF, Shah P & Grisshammer R (2015) Structural prerequisites for G-protein activation by the neurotensin receptor. *Nat. Commun.* **6:** 7895

Kruse AC, Ring AM, Manglik A, Hu J, Hu K, Eitel K, Hubner H, Pardon E, Valant C, Sexton PM, Christopoulos A, Felder CC, Gmeiner P, Steyaert J, Weis WI, Garcia & Kobilka BK (2013) Activation and allosteric modulation of a muscarinic acetylcholine receptor. *Nature* **504:** 101–106

Kubota M, Tanaka T, Kohno T & Wakamatsu K (2009) GDP-GTP exchange processes of

Gαi1 protein are accelerated/ decelerated depending on the type and the concentration of added detergents. *J. Biochem.* **146:** 875–880

Kuhlbrandt W (2014) The Resolution Revolution. *Science* **343:** 1443–1444

Kumar A & Plückthun A (2019) In vivo assembly and large-scale purification of a GPCR - Gα fusion with Gβγ, and characterization of the active complex. *PLoS One* **14:** 1–25

Kumari P, Srivastava A, Banerjee R, Ghosh E, Gupta P, Ranjan R, Chen X, Gupta B, Gupta C, Jaiman D & Shukla AK (2016) Functional competence of a partially engaged GPCR–β-arrestin complex. *Nat. Commun.* **7:** 13416

Lally CCM, Bauer B, Selent J & Sommer ME (2017) C-edge loops of arrestin function as a membrane anchor. *Nat. Commun.* **8:** 1–12

Langen R, Cai K, Altenbach C, Gobind Khorana H & Hubbell WL (1999) Structural Features of the C-terminal Domain of Bovine Rhodopsin: A Site-Directed Spin-Labeling Study. *Biochemistry* **38:** 7918–7924

Latorraca NR, Venkatakrishnan AJ & Dror RO (2017) GPCR Dynamics: Structures in Motion. *Chem. Rev.* **117:** 139–155

Latorraca NR, Wang JK, Bauer B, Townshend RJL, Hollingsworth SA, Olivieri JE, Xu HE, Sommer ME & Dror RO (2018) Molecular mechanism of GPCR-mediated arrestin activation. *Nature* **557:** 452–456

Lebon G, Warne T, Edwards PC, Bennett K, Langmead CJ, Leslie AGW & Tate CG (2011) Agonist-bound adenosine A2A receptor structures reveal common features of GPCR activation. *Nature* **474:** 521–526

Lee S, Bhattacharya S, Tate CG, Grisshammer R & Vaidehi N (2015) Structural dynamics and thermostabilization of neurotensin receptor 1. *J. Phys. Chem. B* **119:** 4917–4928

Lee S, Mao A, Bhattacharya S, Robertson N, Grisshammer R, Tate CG & Vaidehi N (2016a) How Do Short Chain Nonionic Detergents Destabilize G-Protein-Coupled Receptors? *J. Am. Chem. Soc.* **138:** 15425–15433

Lee SC, Knowles TJ, Postis VLG, Jamshad M, Parslow RA, Lin Y, Goldman A, Sridhar P, Overduin M, Muench SP & Dafforn TR (2016b) A method for detergent-free isolation of membrane proteins in their local lipid environment. *Nat. Protoc.* **11:** 1149–1162

Leeman SE (1973) The Isolation of a New Hypotensive from Bovine Hypothalami. *J. Biol. Chem.* **248:** 6854–6861

Leney AC & Heck AJR (2017) Native Mass Spectrometry: What is in the Name? *J. Am. Soc. Mass Spectrom.* **28:** 5–13

Leventis PA & Grinstein S (2010) The Distribution and Function of Phosphatidylserine in Cellular Membranes. *Annu. Rev. Biophys.* **39:** 407–427

Li J, Song J, Zaytseva YY, Liu Y, Rychahou P, Jiang K, Starr ME, Yiannikouris FB, Katz WS, Nilsson PM, Kim JT, Jennifer W, Orho-Melander M, Chen J, Zhu H, Fahrenholz T, Higashi RM, Gao T, Weiss HL, Dobner PR, et al (2016) An obligatory role for neurotensin in high-fat-diet-induced obesity. *Nature* **533:** 411–415

Liu H, Kim HR, Deepak RNVK, Wang L, Chung KY, Fan H, Wei Z & Zhang C (2018) Orthosteric and allosteric action of the C5a receptor antagonists. *Nat. Struct. Mol. Biol.* **25:** 472–481

Liu JJ, Horst R, Katritch V, Stevens RC & Wuthrich K (2012a) Biased Signaling Pathways in β2-Adrenergic Receptor Characterized by 19F-NMR. *Science* **1106:** 1106–1111

Liu W, Chun E, Thompson AA, Chubukov P, Xu F, Katritch V, Han GW, Roth CB, Heitman LH, IJzerman AP, Cherezov V & Stevens RC (2012b) Structural Basis for Allosteric Regulation of GPCRs by Sodium Ions. *Science* **337:** 232–236

Liu X, Xu X, Hilger D, Aschauer P, Tiemann JKS, Du Y, Liu H, Hirata K, Sun X, Guixà-González R, Mathiesen JM, Hildebrand PW & Kobilka BK (2019) Structural Insights into the Process of GPCR-G Protein Complex Formation. *Cell* **177:** 1–19

Logez C, Damian M, Legros C, Dupré C, Guéry M, Mary S, Wagner R, M'Kadmi C, Nosjean O, Fould B, Marie J, Fehrentz J-A, Martinez J, Ferry G, Boutin JA & Banères J-L (2016) Detergent-free Isolation of Functional G Protein-Coupled Receptors into Nanometric Lipid Particles. *Biochemistry* **55:** 38–48

Lu J, Byrne N, Wang J, Bricogne G, Brown FK, Chobanian HR, Colletti SL, Di Salvo J, Thomas-Fowlkes B, Guo Y, Hall DL, Hadix J, Hastings NB, Hermes JD, Ho T, Howard AD, Josien H, Kornienko M, Lumb KJ, Miller MW, et al (2017) Structural basis for the cooperative allosteric activation of the free fatty acid receptor GPR40. *Nat. Struct. Mol. Biol.* **24:** 570–577

Luttrell LM & Lefkowitz RJ (2002) The role of β-arrestins in the termination and

transduction of G-protein-coupled receptor signals. *J. Cell Sci.* **115:** 455–465

Maeda S, Qu Q, Robertson MJ, Skiniotis G & Kobilka BK (2019) Structures of the M1 and M2 muscarinic acetylcholine receptor/G-protein complexes. *Science* **364:** 552–557

Maeda S & Schertler GFX (2013) Production of GPCR and GPCR complexes for structure determination. *Curr. Opin. Struct. Biol.* **23:** 381–392

Manglik A, Kim TH, Masureel M, Altenbach C, Yang Z, Hilger D, Lerch MT, Kobilka TS, Thian FS, Hubbell WL, Prosser RS & Kobilka BK (2015) Structural Insights into the Dynamic Process of β2-Adrenergic Receptor Signaling. *Cell* **161:** 1101–11

Manglik A & Kobilka B (2014) The role of protein dynamics in GPCR function: Insights from the B2AR and rhodopsin. *Curr. Opin. Cell Biol.* **27:** 136–143

Manglik A, Kobilka BK & Steyaert J (2016) Nanobodies to Study G Protein–Coupled Receptor Structure and Function. *Annu. Rev. Pharmacol. Toxicol.* **57:** 19–37

Manglik A & Kruse AC (2017) Structural Basis for G Protein-Coupled Receptor Activation. *Biochemistry* **56:** 5628–5634

Marin EP, Krishna AG, Zvyaga TA, Isele J, Siebert F & Sakmar TP (2000) The Amino Terminus of the Fourth Cytoplasmic Loop of Rhodopsin Modulates Rhodopsin-Transducin Interaction. *J. Biol. Chem.* **275:** 1930–1936

Martin S, Botto JM, Vincent JP & Mazella J (1999) Pivotal role of an aspartate residue in sodium sensitivity and coupling to G proteins of neurotensin receptors. *Mol. Pharmacol.* **55:** 210–215

Masiulis S, Desai R, Uchański T, Serna Martin I, Laverty D, Karia D, Malinauskas T, Zivanov J, Pardon E, Kotecha A, Steyaert J, Miller KW & Aricescu AR (2019) GABA A receptor signalling mechanisms revealed by structural pharmacology. *Nature* **565:** 454–459

Masuho I, Ostrovskaya O, Kramer GM, Jones CD, Xie K & Martemyanov KA (2015) Distinct profiles of functional discrimination among G proteins determine the actions of G protein–coupled receptors. *Sci. Signal.* **8:** ra123

Mazella J, Botto J-M, Guillemare E, Coppola T, Sarret P & Vincent J-P (1996) Structure, Functional Expression, and Cerebral Localization of the Levocabastine-Sensitive

Neurotensin/Neuromedin N Receptor from Mouse Brain. *J. Neurosci.* **16:** 5613–5620

Mazella J, Zsu N, Kaghad M, Caput D, Ferrara P, Vita N, Gully D, Maffrand J & Vincent J (1998) The 100-kDa Neurotensin Receptor Is gp95 / Sortilin, A Non-G-Protein-coupled Receptor. *J. Biol. Chem.* **5:** 26273–26277

McCorvy JD, Wacker D, Wang S, Agegnehu B, Liu J, Lansu K, Tribo AR, Olsen RHJ, Che T, Jin J & Roth BL (2018) Structural determinants of 5-HT2B receptor activation and biased agonism. *Nat. Struct. Mol. Biol.* **25:** 787–796

Van Meer G, Voelker DR & Feigenson GW (2008) Membrane lipids: Where they are and how they behave. *Nat. Rev. Mol. Cell Biol.* **9:** 112–124

Mehmood S, Allison TM & Robinson C V. (2015) Mass Spectrometry of Protein Complexes: From Origins to Applications. *Annu. Rev. Phys. Chem.* **66:** 453–474

Milic D & Veprintsev DB (2015) Large-scale production and protein engineering of G protein-coupled receptors for structural studies. *Front. Pharmacol.* **6:** 1–24

Milligan G & Kostenis E (2006) Heterotrimeric G-proteins: A short history. *Br. J. Pharmacol.* **147:** S46–S55

Mitchell DC, Niu SL & Litman BJ (2001) Optimization of receptor-G protein coupling by Bilayer lipid composition I: Kinetics of rhodopsin-transducin binding. *J. Biol. Chem.* **276:** 42801–42806

Mitra N, Liu Y, Liu J, Serebryany E, Mooney V, Devree BT, Sunahara RK & Yan ECYY (2013) Calcium-dependent ligand binding and g-protein signaling of family B GPCR parathyroid hormone 1 receptor purified in nanodiscs. *ACS Chem. Biol.* **8:** 617–625

Mondal S, Hsiao K & Goueli SA (2015) A Homogenous Bioluminescent System for Measuring GTPase, GTPase Activating Protein, and Guanine Nucleotide Exchange Factor Activities. *Assay Drug Dev. Technol.* **13:** 444–455

Morimoto K, Suno R, Hotta Y, Yamashita K, Hirata K, Yamamoto M, Narumiya S, Iwata S & Kobayashi T (2019) Crystal structure of the endogenous agonist-bound prostanoid receptor EP3. *Nat. Chem. Biol.* **15:** 8–10

Mumby SM & Linder ME (1994) Myristoylation of G-Protein alpha Subunits. *Methods Enzym.* **237:** 254–68

Munk C, Mutt E, Isberg V, Nikolajsen LF, Bibbe JM, Flock T, Hanson MA, Stevens RC,

Deupi X & Gloriam DE (2019) An online resource for GPCR structure determination and analysis. *Nat. Methods* **16:** 151–162

Mustain WC, Rychahou PG & Evers BM (2011) The role of neurotensin in physiologic and pathologic processes. *Curr. Opin. Endocrinol. Diabetes. Obes.* **18:** 75–82

Myung C, Lim WK, Defilippo JM, Yasuda H, Neubig RR & Garrison JC (2006) Regions in the G Protein γ Subunit Important for Interaction with Receptors and Effectors. *Mol. Pharmacol.* **69:** 877–887

Nagarajan S, Alkayed NJ, Kaul S & Barnes AP (2019) Effect of thermostable mutations on the neurotensin receptor 1 (NTSR 1) activation state. *J. Biomol. Struct. Dyn.* **0:** 1–14

Najimi M, Gailly P, Maloteaux J & Hermans E (2002) Distinct regions of C-terminus of the high affinity neurotensin receptor mediate the functional coupling with pertussis toxin sensitive and insensitive G-proteins. *FEBS Lett.* **512:** 329–333

Neale C, Herce HD, Pomès R & García AE (2015) Can Specific Protein-Lipid Interactions Stabilize an Active State of the Beta 2 Adrenergic Receptor? *Biophys. J.* **109:** 1652–1662

Neves SR, Ram PT & Iyengar R (2002) G Protein Pathways. *Science* **296:** 1636–1639

Nguyen NX, Armache JP, Lee C, Yang Y, Zeng W, Mootha VK, Cheng Y, Bai X & Jiang Y (2018) Cryo-EM structure of a fungal mitochondrial calcium uniporter. *Nature* **559:** 570–574

Nicolson GL (2014) The Fluid - Mosaic Model of Membrane Structure: Still relevant to understanding the structure, function and dynamics of biological membranes after more than 40 years. *Biochim. Biophys. Acta - Biomembr.* **1838:** 1451–1466

Niu S-L, Mitchell DC & Litman BJ (2001) Optimization of Receptor-G Protein Coupling by Bilayer Lipid Composition II. *J. Biol. Chem.* **276:** 42807–42811

Nygaard R, Zou Y, Dror RO, Mildorf TJ, Arlow DH, Manglik A, Pan AC, Bokoch MP, Thian FS, Kobilka TS, Shaw DE, Liu CW, Jose J, Mueller L, Prosser RS & Kobilka BK (2013) The Dynamic Process of β2 -Adrenergic Receptor Activation. *Cell* **152:** 532–542

Oates J, Faust B, Attrill H, Harding P, Orwick M & Watts a (2012) The role of cholesterol on the activity and stability of neurotensin receptor 1. *Biochim Biophys Acta* **1818:**

2228–2233

Oates J & Watts A (2011) Uncovering the intimate relationship between lipids, cholesterol and GPCR activation. *Curr. Opin. Struct. Biol.* **21:** 802–807

Okashah N, Wan Q, Ghosh S, Sandhu M, Inoue A, Vaidehi N & Lambert NA (2019) Variable G protein determinants of GPCR coupling selectivity. *Proc. Natl. Acad. Sci. U. S. A.* **116:** 12054–12059

Oluwole AO, Danielczak B, Meister A, Babalola JO, Vargas C & Keller S (2017) Solubilization of Membrane Proteins into Functional Lipid-Bilayer Nanodiscs Using a Diisobutylene/Maleic Acid Copolymer. *Angew. Chemie - Int. Ed.* **56:** 1919–1924

Orwick-Rydmark M, Lovett JE, Graziadei A, Lindholm L, Hicks MR & Watts A (2012) Detergent-free incorporation of a seven-transmembrane receptor protein into nanosized bilayer lipodisq particles for functional and biophysical studies. *Nano Lett.* **12:** 4687–4692

Orwick MC, Judge PJ, Procek J, Lindholm L, Graziadei A, Engel A, Gröbner G & Watts A (2012) Detergent-free formation and physicochemical characterization of nanosized lipid-polymer complexes: Lipodisq. *Angew. Chemie - Int. Ed.* **51:** 4653–4657

Ouyang Q, Zhou J, Yang W, Cui H, Xu M & Yi L (2017) Oncogenic role of neurotensin and neurotensin receptors in various cancers. *Clin. Exp. Pharmacol. Physiol.* **44:** 841–846

Overduin M & Esmaili M (2019) Memtein: The fundamental unit of membrane-protein structure and function. *Chem. Phys. Lipids* **218:** 73–84

Overington J. & Hopkins AL (2006) How many drug targets are there ? *Nat. Rev. Drug Discov.* **5:** 10

Palczewski K, Kumasaka T, Hori T, Behnke CA, Motoshima H, Fox BA, Le Trong I, Teller DC, Okada T, Stenkamp RE, Yamamoto M & Miyano M (2000) Crystal Structure of Rhodopsin: A G Protein-Coupled Receptor. *Science* **289:** 739–745

Pándy-Szekeres G, Munk C, Tsonkov TM, Mordalski S, Harpsøe K, Hauser AS, Bojarski AJ & Gloriam DE (2018) GPCRdb in 2018: Adding GPCR structure models and ligands. *Nucleic Acids Res.* **46:** D440–D446

Pardon E, Laeremans T, Triest S, Rasmussen SGF, Wohlkönig A, Ruf A, Muyldermans S,

Hol WGJ, Kobilka BK & Steyaert J (2014) A general protocol for the generation of Nanobodies for structural biology. *Nat. Protoc.* **9:** 674–693

Park JH, Scheerer P, Hofmann KP, Choe HW & Ernst OP (2008) Crystal structure of the ligand-free G-protein-coupled receptor opsin. *Nature* **454:** 183–187

Perozo E, Cortes DM, Sompornpisut P, Kloda A & Martinac B (2002) Open channel structure of MscL and the gating mechanism of mechanosensitive channels. *Nature* **418:** 942–8.

Pike LJ (2006) Rafts defined: A report on the Keystone symposium on lipid rafts and cell function. *J. Lipid Res.* **47:** 1597–1598

Preininger AM, Van Eps N, Yu NJ, Medkova M, Hubbell WL & Hamm HE (2003) The myristoylated amino terminus of Gαi1 plays a critical role in the structure and function of Gαi1 subunits in solution. *Biochemistry* **42:** 7931–7941

Qanbar R & Bouvier M (2003) Role of palmitoylation / depalmitoylation reactions in G-protein-coupled receptor function. *Pharmacol. Ther.* **97:** 1–33

Qin K, Dong C, Wu G & Lambert NA (2011) Inactive-state preassembly of Gq -coupled receptors and Gq heterotrimers. *Nat. Chem. Biol.* **7:** 740–747

Qiu W, Fu Z, Xu GG, Grassucci RA, Zhang Y, Frank J, Hendrickson WA & Guo Y (2018) Structure and activity of lipid bilayer within a membrane-protein transporter. *Proc. Natl. Acad. Sci. U. S. A.* **115:** 12985–12990

Raghupathy R, Anilkumar AA, Polley A, Singh PP, Yadav M, Johnson C, Suryawanshi S, Saikam V, Sawant SD, Panda A, Guo Z, Vishwakarma RA, Rao M & Mayor S (2015) Transbilayer lipid interactions mediate nanoclustering of lipid-anchored proteins. *Cell* **161:** 581–594

Rasmussen SGF, Choi HJ, Fung JJ, Pardon E, Casarosa P, Chae PS, Devree BT, Rosenbaum DM, Thian FS, Kobilka TS, Schnapp A, Konetzki I, Sunahara RK, Gellman SH, Pautsch A, Steyaert J, Weis WI & Kobilka BK (2011a) Structure of a nanobody-stabilized active state of the β2 adrenoceptor. *Nature* **469:** 175–181

Rasmussen SGF, DeVree BT, Zou Y, Kruse AC, Chung KY, Kobilka TS, Thian FS, Chae PS, Pardon E, Calinski D, Mathiesen JM, Shah ST a., Lyons J a., Caffrey M, Gellman SH, Steyaert J, Skiniotis G, Weis WI, Sunahara RK & Kobilka BK (2011b) Crystal structure of the β2 adrenergic receptor–Gs protein complex. *Nature* **477:** 549–

555

Ravula T, Hardin NZ, Ramadugu SK, Cox SJ & Ramamoorthy A (2018) Formation of pH-Resistant Monodispersed Polymer–Lipid Nanodiscs. *Angew. Chemie - Int. Ed.* **57:** 1342–1345

Ravula T, Ramadugu SK, Di Mauro G & Ramamoorthy A (2017) Bioinspired, Size-Tunable Self-Assembly of Polymer–Lipid Bilayer Nanodiscs. *Angew. Chemie - Int. Ed.* **56:** 11466–11470

Reis R & Moraes I (2018) Structural biology and structure–function relationships of membrane proteins. *Biochem. Soc. Trans.* **47:** 47–61

Reiter E, Ahn S, Shukla AK & Lefkowitz RJ (2012) Molecular mechanism of β-arrestin-biased agonism at seven-transmembrane receptors. *Annu. Rev. Pharmacol. Toxicol.* **52:** 179–97

Reiter E & Lefkowitz RJ (2006) GRKs and β-arrestins: roles in receptor silencing, trafficking and signaling. *Trends Endocrinol. Metab.* **17:** 159–165

Riddy DM, Delerive P, Summers RJ, Sexton PM & Langmead CJ (2018) G protein–coupled receptors targeting insulin resistance, obesity, and type 2 diabetes mellitus. *Pharmacol. Rev.* **70:** 39–67

Ring AM, Manglik A, Kruse AC, Enos MD, Weis WI, Garcia KC & Kobilka BK (2013) Adrenaline-activated structure of β 2-adrenoceptor stabilized by an engineered nanobody. *Nature* **502:** 575–579

Romani AMP (2011) Cellular magnesium homeostasis. *Arch. Biochem. Biophys.* **512:** 1–23

Rosenbaum DM, Cherezov V, Hanson M a, Rasmussen SGF, Thian FS, Kobilka TS, Choi H-J, Yao X-J, Weis WI, Stevens RC & Kobilka BK (2007) GPCR Engineering Yields High-Resolution Structural Insights into beta2-Adrenergic Receptor Function. *Science* **318:** 1266–1273

Rosenbaum DM, Zhang C, Lyons JA, Holl R, Aragao D, Arlow DH, Rasmussen SGF, Choi HJ, Devree BT, Sunahara RK, Chae PS, Gellman SH, Dror RO, Shaw DE, Weis WI, Caffrey M, Gmeiner P & Kobilka BK (2011) Structure and function of an irreversible agonist-β 2 adrenoceptor complex. *Nature* **469:** 236–242

Rostène WH & Alexander MJ (1997) Neurotensin and neuroendocrine regulation. *Front.*

Neuroendocrinol. **18:** 115–173

Roussy G, Dansereau MA, Doré-Savard L, Belleville K, Beaudet N, Richelson E & Sarret P (2008) Spinal NTS1 receptors regulate nociceptive signaling in a rat formalin tonic pain model. *J. Neurochem.* **105:** 1100–1114

Salas-Estrada LA, Leioatts N, Romo TD & Grossfield A (2018) Lipids Alter Rhodopsin Function via Ligand-like and Solvent-like Interactions. *Biophys. J.* **114:** 355–367

Sano T, Ohyama K, Yamano Y, Nakagomi Y, Nakazawa S, Kikyo M, Shirai H, Blank JS, Exton JH & Inagami T (1997) A Domain for G Protein Coupling in Carboxyl-terminal Tail of Rat Angiotensin II Receptor Type 1A. *J. Biol. Chem.* **272:** 23631–23636

Santos R, Ursu O, Gaulton A, Bento AP, Donadi RS, Bologa CG, Karlsson A, Al-Lazikani B, Hersey A, Oprea TI & Overington JP (2017) A comprehensive map of molecular drug targets. *Nat. Rev. Drug Discov.* **16:** 19–34

Sarkar CA, Dodevski I, Kenig M, Dudli S, Mohr A, Hermans E & Pluckthun A (2008) Directed evolution of a G protein-coupled receptor for expression, stability, and binding selectivity. *Proc. Natl. Acad. Sci. U. S. A.* **105:** 14808–14813

Sarvazyan NA, Remmers AE & Neubig RR (1998) Determinants of Gi1alpha and Beta Gamma Binding. Measuring High Affinity Interactions in a Lipid Environment Using Flow Cytometry. *J. Biol. Chem.* **273:** 7934–7940

Sastry PS (1985) Lipids of nervous tissue: Composition and metabolism. *Prog. Lipid Res.* **24:** 69–176

Scheerer P, Park JH, Hildebrand PW, Kim YJ, Krauß N, Choe HW, Hofmann KP & Ernst OP (2008) Crystal structure of opsin in its G-protein-interacting conformation. *Nature* **455:** 497–502

Scheidelaar S, Koorengevel MC, Pardo JD, Meeldijk JD, Breukink E & Killian JA (2015) Molecular Model for the solubilization of membranes into nanodisks by styrene maleic acid copolymers. *Biophys. J.* **108:** 279–290

Scheidelaar S, Koorengevel MC, van Walree CA, Dominguez JJ, Dörr JM & Killian JA (2016) Effect of Polymer Composition and pH on Membrane Solubilization by Styrene-Maleic Acid Copolymers. *Biophys. J.* **111:** 1974–1986

Schiöth HB & Fredriksson R (2005) The GRAFS classification system of G-protein coupled receptors in comparative perspective. *Gen. Comp. Endocrinol.* **142:** 94–101

Schlinkmann KM, Hillenbrand M, Rittner A, Künz M, Strohner R & Plückthun A (2012) Maximizing Detergent Stability and Functional Expression of a GPCR by Exhaustive Recombination and Evolution. *J. Mol. Biol.* **422:** 414–428

Schöppe J, Ehrenmann J, Klenk C, Rucktooa P, Schütz M, Doré AS & Plückthun A (2019) Crystal structures of the human neurokinin 1 receptor in complex with clinically used antagonists. *Nat. Commun.* **10:** 17

Sebastiani G, Ceccarelli E, Castagna MG & Dotta F (2018) G-protein-coupled receptors (GPCRs) in the treatment of diabetes: Current view and future perspectives. *Best Pract. Res. Clin. Endocrinol. Metab.* **32:** 201–213

Seddon AM, Curnow P & Booth PJ (2004) Membrane proteins, lipids and detergents: Not just a soap opera. *Biochim. Biophys. Acta - Biomembr.* **1666:** 105–117

Seidel SAI, Dijkman PM, Lea WA, van den Bogaart G, Jerabek-Willemsen M, Lazic A, Joseph JS, Srinivasan P, Baaske P, Simeonov A, Katritch I, Melo FA, Ladbury JE, Schreiber G, Watts A, Braun D & Duhr S (2013) Microscale thermophoresis quantifies biomolecular interactions under previously challenging conditions. *Methods* **59:** 301–315

Serebryany E, Zhu GA & Yan ECY (2012) Artificial membrane-like environments for in vitro studies of purified G-protein coupled receptors. *Biochim. Biophys. Acta - Biomembr.* **1818:** 225–233

Serrano-Vega MJ, Magnani F, Shibata Y & Tate CG (2008) Conformational thermostabilization of the beta1-adrenergic receptor in a detergent-resistant form. *Proc. Natl. Acad. Sci. U. S. A.* **105:** 877–882

Shibata Y, White JF, Serrano-Vega MJ, Magnani F, Aloia AL, Grisshammer R & Tate CG (2009) Thermostabilization of the Neurotensin Receptor NTS1. *J. Mol. Biol.* **390:** 262–277

Shukla AK, Manglik A, Kruse AC, Xiao K, Reis RI, Tseng WC, Staus DP, Hilger D, Uysal S, Huang LY, Paduch M, Tripathi-Shukla P, Koide A, Koide S, Weis WI, Kossiakoff AA, Kobilka BK & Lefkowitz RJ (2013) Structure of active β-arrestin-1 bound to a G-protein-coupled receptor phosphopeptide. *Nature* **497:** 137–141

Shukla AK, Westfield GH, Xiao K, Reis RI, Huang L-Y, Tripathi-Shukla P, Qian J, Li S, Blanc A, Oleskie AN, Dosey AM, Su M, Liang C-R, Gu L-L, Shan J-M, Chen X, Hanna R, Choi M, Yao XJ, Klink BU, et al (2014) Visualization of arrestin recruitment by a G-protein-coupled receptor. *Nature* **512:** 218–222

Singer SJ & Nicolson GL (1972) The Fluid Mosaic Model of the Structure of Cell Membranes. *Science* **175:** 720–731

Sixl F & Watts A (1983) Headgroup interactions in mixed phospholipid bilayers. *Proc. Natl. Acad. Sci. U. S. A.* **80:** 1613–1615

Skrzydelski D, Lhiaubet A, Lebeau A, Forgez P, Yamada M, Hermans E, Rostene W & Pelaprat D (2003) Differential Involvement of Intracellular Domains of the Rat NTS1 Neurotensin Receptor in Coupling to G Proteins : A Molecular Basis for Agonist-Directed Trafficking of Receptor Stimulus. **64:** 421–429

Smith JL, Fischetti RF & Yamamoto M (2012) Micro-crystallography comes of age. *Curr. Opin. Struct. Biol.* **22:** 602–612

Sommer ME, Hofmann KP & Heck M (2012) Distinct loops in arrestin differentially regulate ligand binding within the GPCR opsin. *Nat. Commun.* **3:** 995

Sommer ME, Smith WC & Farrens DL (2006) Dynamics of arrestin-rhodopsin interactions: Acidic phospholipids enable binding of arrestin to purified rhodopsin in detergent. *J. Biol. Chem.* **281:** 9407–9417

Soubias O, Teague WE & Gawrisch K (2006) Evidence for specificity in lipid-rhodopsin interactions. *J. Biol. Chem.* **281:** 33233–33241

Soubias O, Teague WE, Hines KG, Mitchell DC & Gawrisch K (2010) Contribution of membrane elastic energy to rhodopsin function. *Biophys. J.* **99:** 817–824

Sounier R, Mas C, Steyaert J, Laeremans T, Manglik A, Huang W, Kobilka BK, Demene H & Granier S (2015) Propagation of conformational changes during mu-opioid receptor activation. *Nature* **524:** 375–378

Spencer AG, Thuresson E, Otto JC, Song I, Smith T, DeWitt DL, Garavito RM & Smith WL (1999) The membrane binding domains of prostaglandin endoperoxide H synthases 1 and 2. *J. Biol. Chem.* **274:** 32936–32942

Srivastava A, Yano J, Hirozane Y, Kefala G, Gruswitz F, Snell G, Lane W, Ivetac A,

Aertgeerts K, Nguyen J, Jennings A & Okada K (2014) High-resolution structure of the human GPR40 receptor bound to allosteric agonist TAK-875. *Nature* **513:** 124–127

St-Pierre S, Lalonde JM, Gendreau M, Quirion R, Regoli D & Rioux F (1981) Synthesis of Peptides by the Solid-Phase Method. 6. Neurotensin, Fragments, and Analogues. *J. Med. Chem.* **24:** 370–376

Staus DP, Wingler LM, Pichugin D, Prosser RS & Lefkowitz RJ (2019) Detergent- and phospholipid-based reconstitution systems have differential effects on constitutive activity of G-protein–coupled receptors. *J. Biol. Chem.* **294:** 13218–13223

Stetsenko A & Guskov A (2017) An Overview of the Top Ten Detergents Used for Membrane Protein Crystallization. *Crystals* **7:** 197

Strathmann MP & Gautam N (1991) Diversity of G Proteins. *Science* **252:** 802–808

Strohman MJ, Maeda S, Hilger D, Masureel M, Du Y & Kobilka BK (2019) Local membrane charge regulates β2 adrenergic receptor coupling to Gi3. *Nat. Commun.* **10:** 2234

Stryer L (1991) Visual excitation and recovery. *J. Biol. Chem.* **266:** 10711–10714

Sun C, Benlekbir S, Venkatakrishnan P, Wang Y, Hong S, Hosler J, Tajkhorshid E, Rubinstein JL & Gennis RB (2018) Structure of the alternative complex III in a supercomplex with cytochrome oxidase. *Nature* **557:** 123–126

Swift S, Leger AJ, Talavera J, Zhang L, Bohm A & Kuliopulos A (2006) Role of the PAR1 Receptor 8th Helix in Signaling. **281:** 4109–4116

Szatmári D, Xue B, Kannan B, Burtnick LD, Bugyi B, Nyitrai M & Robinson RC (2018) ATP competes with PIP 2 for binding to gelsolin. *PLoS One* **13:** 1–17

Szczepek M, Beyrière F, Hofmann KP, Elgeti M, Kazmin R, Rose A, Bartl FJ, von Stetten D, Heck M, Sommer ME, Hildebrand PW & Scheerer P (2014) Crystal structure of a common GPCR-binding interface for G protein and arrestin. *Nat. Commun.* **5:** 4801

Takida S & Wedegaertner PB (2003) Heterotrimer formation, together with isoprenylation, is required for plasma membrane targeting of Gβγ. *J. Biol. Chem.* **278:** 17284–17290

Tanaka K, Masu M & Nakanishi S (1990) Structure and functional expression of the

cloned rat neurotensin receptor. *Neuron* **4:** 847–854

Taniguchi R, Inoue A, Sayama M, Uwamizu A, Yamashita K, Hirata K, Yoshida M, Tanaka Y, Kato HE, Nakada-nakura Y, Otani Y, Nishizawa T & Doi T (2017) Structural insights into ligand recognition by the lysophosphatidic acid receptor LPA6. *Nature* **548:** 356–360

Tate CG (2010) Practical Considerations of Membrane Protein Instability during Purification and Crystallisation. In *Heterologous Expression of Membrane Proteins* pp 187–203.

Tate CG & Schertler GF (2009) Engineering G protein-coupled receptors to facilitate their structure determination. *Curr. Opin. Struct. Biol.* **19:** 386–395

Toyoda Y, Morimoto K, Suno R, Horita S, Yamashita K, Hirata K, Sekiguchi Y, Yasuda S, Shiroishi M, Shimizu T, Urushibata Y, Kajiwara Y, Inazumi T, Hotta Y, Asada H, Nakane T, Shiimura Y, Nakagita T, Tsuge K, Yoshida S, et al (2019) Ligand binding to human prostaglandin E receptor EP 4 at the lipid-bilayer interface. *Nat. Chem. Biol.* **15:** 18–26

Tretter V, Altmann F & Marz L (1991) Peptide-N4-(N-acetyl-β-glucosaminyl)asparagine amidase F cannot release glycans with fucose attached α1 → 3 to the asparagine-linked N-acetylglucosamine residue. *Eur. J. Biochem.* **199:** 647–652

Tsai C-J, Marino J, Adaixo R, Pamula F, Muehle J, Maeda S, Flock T, Taylor NM, Mohammed I, Matile H, Dawson RJ, Deupi X, Stahlberg H & Schertler G (2019) Cryo-EM structure of the rhodopsin-Gαi-βγ complex reveals binding of the rhodopsin C-terminal tail to the gβ subunit. *Elife* **8:** e46041

Tsai C-J, Pamula F, Nehmé R, Mühle J, Weinert T, Flock T, Nogly P, Edwards PC, Carpenter B, Gruhl T, Ma P, Deupi X, Standfuss J, Tate CG & Schertler GFX (2018) Crystal structure of rhodopsin in complex with a mini-Go sheds light on the principles of G protein selectivity. *Sci. Adv.* **4:** eaat7052

Vaidehi N, Grisshammer R & Tate CG (2015) How Can Mutations Thermostabilize G-Protein-Coupled Receptors? *Trends Pharmacol. Sci.* **37:** 37–46

VanAken T, Foxall-VanAken S, Castleman S & Ferguson-Miller S (1986) Alkyl Glycoside Detergents: Synthesis and Applications to the Study of Membrane Proteins. *Methods* **125:** 27–35

Vandenbulcke F, Nouel D, Vincent JP, Mazella J & Beaudet A (2000) Ligand-induced internalization of neurotensin in transfected COS-7 cells: differential intracellular trafficking of ligand and receptor. *J. Cell Sci.* **113:** 2963–2975

Venkatakrishnan AJ, Deupi X, Lebon G, Heydenreich FM, Flock T, Miljus T, Balaji S, Bouvier M, Veprintsev DB, Tate CG, Schertler GFX & Babu MM (2016) Diverse activation pathways in class A GPCRs converge near the G-protein-coupling region. *Nature* **536:** 484–487

Vincent JP (1995) Neurotensin receptors: Binding properties, transduction pathways, and structure. *Cell. Mol. Neurobiol.* **15:** 501–512

Vincent JP, Mazella J & Kitabgi P (1999) Neurotensin and Receptors. *Trends Pharmacol. Sci.* **20:** 302–309

Violin JD, Crombie AL, Soergel DG & Lark MW (2014) Biased ligands at G-protein-coupled receptors: Promise and progress. *Trends Pharmacol. Sci.* **35:** 308–316

Vita N, Laurent P, Lefort S, Chalon P, Dumont X, Kaghad M, Gully D, Le Fur G, Ferrara P & Caput D (1993) Cloning and expression of a complementary DNA encoding a high affinity human neurotensin receptor. *FEBS Lett.* **317:** 139–142

Voss J, He MM, Hubbell WL & Ronald Kaback H (1996) Site-directed spin labeling demonstrates that transmembrane domain XII in the lactose permease of Escherichia coli is an α-helix. *Biochemistry* **35:** 12915–12918

Wacker D, Wang C, Katritch V, Han GW, Huang X-P, Vardy E, McCorvy JD, Jiang Y, Chu M, Siu FY, Liu W, Xu HE, Cherezov V, Roth BL & Stevens RC (2013) Structural features for functional selectivity at serotonin receptors. *Science* **340:** 615–9

Walski T, De Schutter K, Van Damme EJM & Smagghe G (2017) Diversity and functions of protein glycosylation in insects. *Insect Biochem. Mol. Biol.* **83:** 21–34

Warne T, Edwards PC, Dorfe AS, Leslie AGW & Tate CG (2019) Molecular basis for high-affinity agonist binding in GPCRs. *Science* **778:** 775–778

Warne T, Serrano-Vega MJ, Baker JG, Moukhametzianov R, Edwards PC, Henderson R, Leslie AGW, Tate CG & Schertler GFX (2008) Structure of a β1-adrenergic G-protein-coupled receptor. *Nature* **454:** 486–491

Warne T, Serrano-Vega MJ, Tate CG & Schertler GFX (2009) Development and

crystallization of a minimal thermostabilised G protein-coupled receptor. *Protein Expr. Purif.* **65:** 204–213

Warschawski DE, Arnold AA, Beaugrand M, Gravel A, Chartrand É & Marcotte I (2011) Choosing membrane mimetics for NMR structural studies of transmembrane proteins. *Biochim. Biophys. Acta - Biomembr.* **1808:** 1957–1974

Watts A, Volotovski ID & Volotovski ID (1979) Rhodopsin-Lipid Associations in Bovine Rod Outer Segment Membranes. Identification of Immobilized Lipid by Spin-Labels. *Biochemistry* **18:** 5006–5013

Wedegaertner PB, Chu DH, Wilson PT, Levis MJ & Bourne HR (1993) Palmitoylation is required for signaling functions and membrane attachment of G(q)α and G(s)α. *J. Biol. Chem.* **268:** 25001–25008

Weis WI & Kobilka BK (2018) The Molecular Basis of G Protein–Coupled Receptor Activation. *Annu. Rev. Biochem.* **87:** 897–919

White JF & Grisshammer R (2010) Stability of the Neurotensin Receptor NTS1 Free in Detergent Solution and Immobilized to Affinity Resin. *PLoS One* **5:** e12579

White JF, Noinaj N, Shibata Y, Love J, Kloss B, Xu F, Gvozdenovic-Jeremic J, Shah P, Shiloach J, Tate CG, Grisshammer R & Neurotensin (2012) Structure of the agonist-bound neurotensin receptor. *Nature* **490:** 508–515

White JF, Trinh LB, Shiloach J & Grisshammer R (2004) Automated large-scale purification of a G protein-coupled receptor for neurotensin. *FEBS Lett.* **564:** 289–293

Wingler LM, Elgeti M, Hilger D, Latorraca NR, Lerch MT, Staus DP, Dror RO, Kobilka BK, Hubbell WL & Lefkowitz RJ (2019a) Angiotensin Analogs with Divergent Bias Stabilize Distinct Receptor Conformations. *Cell* **176:** 468-478.e11

Wingler LM, Elgeti M, Hilger D, Latorraca NR, Lerch MT, Staus DP, Dror RO, Kobilka BK, Hubbell WL & Lefkowitz RJ (2019b) Angiotensin Analogs with Divergent Bias Stabilize Distinct Receptor Conformations. *Cell* **176:** 1–11

Wingler LM, McMahon C, Staus DP, Lefkowitz RJ & Kruse AC (2019c) Distinctive Activation Mechanism for Angiotensin Receptor Revealed by a Synthetic Nanobody. *Cell* **176:** 479–490

Woodfork KA, Lindorfer MA, Fletcher JE, Garrison JC & Yasuda H (2002) Role of the

Prenyl Group on the G Protein γ Subunit in Coupling Trimeric G Proteins to A1 Adenosine Receptors. *J. Biol. Chem.* **271:** 18588–18595

Wu B, Chien EYT, Mol CD, Fenalti G, Liu W, Katritch V, Abagyan R, Brooun A, Wells P, Bi FC, Hamel DJ, Kuhn P, Handel TM, Cherezov V & Stevens RC (2010) Structures of the CXCR4 Chemokine GPCR with Small-Molecular and Cyclic Peptide Antagonists. **330:** 1066–1071

Yang Z, Huang Z & Tao Y (2015) Functions of DPLIY motif and helix 8 of human melanocortin-3 receptor. *J. Mol. Endocrinol.* **55:** 107–117

Yasuhara K, Arakida J, Ravula T, Ramadugu SK, Sahoo B, Kikuchi JI & Ramamoorthy A (2017) Spontaneous Lipid Nanodisc Fomation by Amphiphilic Polymethacrylate Copolymers. *J. Am. Chem. Soc.* **139:** 18657–18663

Ye L, Eps N Van, Zimmer M & Oliver P (2016) Activation of the A2A adenosine G-protein-coupled receptor by conformational selection. *Nature* **533:** 265–268

Yen H-Y, Hoi KK, Liko I, Hedger G, Horrell MR, Song W, Wu D, Heine P, Warne T, Lee Y, Carpenter B, Plückthun A, Tate CG, Sansom MSP & Robinson C V. (2018) PtdIns(4,5)P2 stabilizes active states of GPCRs and enhances selectivity of G-protein coupling. *Nature* **559:** 423–427

Yen H-Y, Liko I, Allison TM, Robinson C V., Hopper JTS, Zhu Y, Wang D, Wu B, Mohammed S & Stegmann M (2017) Ligand binding to a G protein–coupled receptor captured in a mass spectrometer. *Sci. Adv.* **3:** e1701016

Zhang C, Srinivasan Y, Arlow DH, Fung JJ, Palmer D, Zheng Y, Green HF, Pandey A, Dror RO, Shaw DE, Weis WI, Coughlin SR & Kobilka BK (2012) High-resolution crystal structure of human protease-activated receptor 1. *Nature* **492:** 387–392

Zhang D, Gao Z-G, Zhang K, Kiselev E, Crane S, Wang J, Paoletta S, Yi C, Ma L, Zhang W, Han GW, Liu H, Cherezov V, Katritch V & Jiang H (2015a) Two disparate ligand-binding sites in the human P2Y1 receptor. *Nature* **520:** 317–321

Zhang H, Han GW, Batyuk A, Ishchenko A, White KL, Patel N, Sadybekov A, Zamlynny B, Rudd MT, Hollenstein K, Tolstikova A, White TA, Hunter MS, Weierstall U, Liu W, Babaoglu K, Moore EL, Katz RD, Shipman JM, Garcia-Calvo M, et al (2017a) Structural basis for selectivity and diversity in angiotensin II receptors. *Nature* **544:** 327–332

Zhang H, Qiao A, Yang D, Yang L, Dai A, De Graaf C, Reedtz-Runge S, Dharmarajan V, Zhang H, Han GW, Grant TD, Sierra RG, Weierstall U, Nelson G, Liu W, Wu Y, Ma L, Cai X, Lin G, Wu X, et al (2017b) Structure of the full-length glucagon class B G-protein-coupled receptor. *Nature* **546:** 259–264

Zhang H, Unal H, Desnoyer R, Han GW, Patel N, Katritch V, Karnik SS, Cherezov V & Stevens RC (2015b) Structural basis for ligand recognition and functional selectivity at angiotensin receptor. *J. Biol. Chem.* **290:** 29127–29139

Zhang H, Unal H, Gati C, Han GW, Liu W, Zatsepin NA, James D, Wang D, Nelson G, Weierstall U, Sawaya MR, Xu Q, Messerschmidt M, Williams GJ, Boutet S, Yefanov OM, White TA, Wang C, Ishchenko A, Tirupula KC, et al (2015c) Structure of the angiotensin receptor revealed by serial femtosecond crystallography. *Cell* **161:** 833–844

Zhang J, Zhang K, Gao ZG, Paoletta S, Zhang D, Han GW, Li T, Ma L, Zhang W, Müller CE, Yang H, Jiang H, Cherezov V, Katritch V, Jacobson KA, Stevens RC, Wu B & Zhao Q (2014a) Agonist-bound structure of the human P2Y12 receptor. *Nature* **508:** 119–122

Zhang K, Zhang J, Gao ZG, Zhang D, Zhu L, Han GW, Moss SM, Paoletta S, Kiselev E, Lu W, Fenalti G, Zhang W, Müller CE, Yang H, Jiang H, Cherezov V, Katritch V, Jacobson KA, Stevens RC, Wu B, et al (2014b) Structure of the human P2Y12 receptor in complex with an antithrombotic drug. *Nature* **508:** 115–118

Zhang Q & Cherezov V (2019) Chemical tools for membrane protein structural biology. *Curr. Opin. Struct. Biol.* **52:** 1–8

Zhang Y, Sun B, Feng D, Hu H, Chu M, Qu Q, Tarrasch JT, Li S, Sun Kobilka T, Kobilka BK & Skiniotis G (2017c) Cryo-EM structure of the activated GLP-1 receptor in complex with a G protein. *Nature* **546:** 248–253

Zhao C, Fenalti G, Wu H, Han GW & Cherezov V (2014) Crystal structure of the chemokine receptor CXCR4 in complex with a viral chemokine. *Science* **301:** 24322–24327

Zhou XE, He Y, de Waal PW, Gao X, Kang Y, Van Eps N, Yin Y, Pal K, Goswami D, White TA, Barty A, Latorraca NR, Chapman HN, Hubbell WL, Dror RO, Stevens RC, Cherezov V, Gurevich V V., Griffin PR, Ernst OP, et al (2017) Identification of

Phosphorylation Codes for Arrestin Recruitment by G Protein-Coupled Receptors. *Cell* **170:** 457–469

Zhu S, Zhang M, Davis JE, Wu WH, Surrao K, Wang H & Wu G (2015) A single mutation in helix 8 enhances the angiotensin II type 1a receptor transport and signaling. *Cell. Signal.* **27:** 2371–2379

Zick M, Stroupe C, Orr A, Douville D & Wickner WT (2014) Membranes linked by trans-SNARE complexes require lipids prone to non-bilayer structure for progression to fusion. *Elife* **3:** e01879